Improving the Stewart Platform Design of the Ampelmann System for Asymmetric Load Cases

G. Bresser

Master of Science Thesis

TU Delft Delft University of Technology

Hydraulic Engineering

Improving the Stewart Platform Design of the Ampelmann System for Asymmetric Load Cases

Master of Science Thesis

For the degree of Master of Science in Hydraulic Engineering at Delft University of Technology

G. Bresser

May 29, 2015

Faculty of Civil Engineering & Geoscience (CiTG) · Delft University of Technology

The work in this thesis is supported by the company Ampelmann Operations B.V.. Their coorporation is hereby gratefully acknowledged

Delft University of Technology
Department of
Hydraulic Structures

The undersigned hereby certify that they have read and recommend to the Faculty of Civil Engineering & Geoscience (CiTG) for acceptance a thesis entitled

Improving the Stewart Platform Design of the Ampelmann System for Asymmetric Load Cases

by

G. Bresser

in partial fulfillment of the requirements for the degree of

Master of Science Hydraulic Engineering

Dated: May 29, 2015

Supervisor(s):

prof.dr. A.V. Metrikine

ing. M. Paap

Reader(s):

ir. A. Van der Toorn

ir. J.S. Hoving

Abstract

The Ampelmann company produces a system, that makes easy and safe offshore transfer possible. The system makes use of a Stewart platform, which is widely used in flight simulators. With six cylinders the platform creates motions in six degrees of freedom (DoF). When placed on a vessel, it actively compensates all the motions of the hosting vessel, leaving the top frame of the platform nearly motionless. The platform is connected to an offshore platform by a telescoping bridge, the gangway. The use of larger gangways is desired, to reach higher platforms or reach platforms from a longer distance. The gangway creates a large asymmetric load case on top of the Stewart platform for which it is not primarily designed. The largest gangway of the company, the GangwayXXL (GXXL) can not be mounted on top of the currently most used A-type, because the cylinder forces exceed their maximum operation limit. When the push operation limit is exceeded, the cylinders are no longer able to extract and compensate the vessel motions. If the pull operation limit is exceeded, the rod of the cylinders can become disconnected with the cylinder barrel. This must be avoided at all times, since this can lead to a collapse of the total system. It is desired to use the A-type system for all type of gangways and make it possible to use the GXXL on small vessels, that do not have the space to accommodate the more powerful E-type system, which has a larger footprint than the A-type. The purpose of this study is to make the A-type operable for larger gangways by investigating the possibilities to reduce the cylinder forces by improving the Stewart platform for the large asymmetric load case.

In this report two optimisation directions of the Stewart platform are presented: (1) Improving the geometry of the Stewart platform for its loading capacity and (2) Reducing the loads on top of the Stewart platform by adding extra cylinders which add a counteracting force to the system. Before these two directions are investigated, the decision is made to relocate the slewing ring, which makes rotation of the gangway in the horizontal plane possible, to below the Stewart platform. This leads to a rotation of the total system in stead of only the gangway for which the external load case on top of the platform is orientated in the same direction during the whole operation.

The geometry of the Stewart platform can be optimised for the workspace, the dexterity (a controllability parameter) and the load capacity of the system. In this report the platform is optimised for the loading capacity with an allowable dexterity, by changing the size of the

top frame and the connection point of the cylinders. The new found geometry has a positive effect on the force distribution over the six cylinders. Eventhough the workspace decreases, it is assumed not to pose a problem as the size of the workspace is not directly linked to the workability of the system. The same workability can possibly be maintained by adapting the control limitations of the system. After improving the geometry of the system, the GXXL can be used for people transfer on top of the new A-type Stewart platform.

Alternatively, extra cylinders can be added to the design of the Stewart platform to reduce the load case. These cylinders do not compensate the vessel motions, but add an additional constant force to the system. These forces help reduce the load case for the Stewart platform cylinders. For this optimisation direction, different numbers of cylinders are considered. Each number of cylinders has a different configuration. With the use of a force optimisation criterion, the two and three cylinder configurations make it possible to use the GXXL on top of the A-type system for people transfer. When adding four cylinders to the system, the GXXL can also be used for cargo transfer. From both a construction and maintenance cost perspective, it is desired to keep the number of extra cylinders as low as possible. The possibility to use only three cylinders for cargo transfer is further investigated, by combining both optimisation directions. It is found that both directions complement each other as the cylinder forces of the Stewart platform become more evenly distributed in neutral position. However, cargo transfer is still not found possible, due to the force fluctuations that occur when the platform has to compensate large vessel motions.

A variable counteracting force is required to reach the lowest possible cylinder forces per position. For every position of the platform the required forces of the extra cylinders are determined to keep the forces of the Stewart platform cylinders below their operation limit. The suggested control method is using a Look-up table, where all the required pressures in the cylinder per position are stored. The combination of the active force control method of the three extra cylinders with the new geometry of the Stewart platform leads to cylinder forces below their pull operational limit for every position of the platform, making it possible to use the GXXL for people and cargo transfer during active compensation of the vessel motions.

Contents

List of Figures

List of Tables

Acknowledgements

This graduation thesis has been carried out under the supervision of prof. dr. A.V. Metrikine, ir. A. van der Toorn and ir. J.S. Hoving from the Delft University of Technology and ing. M. Paap from Ampelmann Operations B.V.. First of, I want to thank A.V. Metrikine for his guidance and feedback during this graduation period. Secondly, I want to thank M. Paap for his available time and the sharing of his knowledge and enthusiasm during our weekly meetings at the company. Third, I want to thank A. van der Toorn for his input during the time that my project needed some additional guidance. Last, I want to thank J.S. Hoving for challenging me during our meetings.

This project has been made possible by the guidance and shared knowledge of all the people of the company Ampelmann Operations B.V. and especially the people from the section Structural Engineering.

I had a great time during my graduation period and for that I have to thank my fellow graduation students for their joviality. Special thanks go to J. Wiegerink and G. Sprenger for their scientific support.

Finally, I want to thank my family and my girlfriend Marissa for all their love and support during this final stage of my master's degree.

Chapter 1

Introduction

The global offshore oil and gas industry is ever rising and over the past years there is a rapid growth in the number of offshore wind farms. Until a couple years ago offshore platforms and wind turbines were only accessible by helicopter or by vessel with a swinging rope or lifting basket. All these transportation services are highly susceptible to high waves, storms and fogs, resulting in only limited access.
In 2002 two Delft University of Technology PhD students came up with the Ampelmann idea. The Ampelmann is a system, which is installed on an offshore vessel, that makes safe and easy transfer possible to an offshore platform for personnel. The access system consists of a platform that compensates all the motions of the vessel in the Six Degrees of Freedom (6DoF). The gangway connected to this motion controlled platform stays (nearly) stationary with respect to the offshore platform, making *offshore access as easy as crossing the street.*

The system that can create motions in all the 6DoF is called a Stewart platform or hexapod, consisting of six cylinders. The Stewart platform is generally used for flight simulators, Figure 1-1. In these simulators the platform sets the cockpit and video screens in motion to recreate a real-life situation. In the Ampelmann system the Stewart platform is placed on a vessel and compensates the vessel motions that are measured by motion sensors. The gangway, located on top off the Stewart platform, makes the transfer to offshore structures possible.

Figure 1-1: Flight simulator with Stewart platform [1]

1-1 Problem statement

In the flight simulator the platform is loaded by the cockpit, which has a Centre of Gravity (CoG) in the middle of the platform. This is not the case with the Ampelmann system, as can be seen in Figure 1-2, the Stewart platform is loaded by the gangway. The gangway is the connection bridge between the Stewart platform and the offshore structure.

Figure 1-2: A-type Ampelmann [2]

The weight of the gangway creates a large tipping moment on top of the Stewart platform, however the current geometry is not designed to compensate this large tipping moment. The problem is partly solved by the use of a counterweight on the opposite side of gangway on the base frame. This solution however has some undesirable effects. The counterweight causes a large tipping moment in the other direction when the system is in Stowed Condition, meaning that the gangway rests on the deck of the vessel when it is not being used. This limits the use of a larger counterweight to counteract the moment of the gangway.

The large cylinder forces caused by the tipping moment and downward force, limits the possibility to use larger gangways on top of current A-type Ampelmann system. The A-type is the mid-size, most used Ampelmann system. At the moment, the largest gangway can only be used on top of the E-type system, which is 1.5 times larger than the A-type. This system has also a larger footprint, which limits the possibility to accommodate it on smaller vessels. The E-type system is also more expensive than the A-type, due to the larger parts. A new design of the Stewart platform can lead to the possibility to use larger gangways on the current A-type. The use of larger gangways is favourable to reach transfer points on a offshore platform, which have a large distance from the vessel.

1-2 Research objective

The main objective of this research is defined as follows:

> "Describe how the Stewart platform design of the A-type Ampelmann system can be improved for large asymmetric load cases, making it better suitable for higher loads"

This objective follows from the problem as stated in the previous section, that the Stewart platform system is implemented for off-centre load cases while the system is invented for loads with the CoG in the middle of the top platform. A solution has to be found in a new design of the Stewart platform which is able to handle this large tipping moment (as sketched in Figure 1-3) or in a way counteracts it within the system, without just enlarging the total system.

In this report two optimising directions for the Stewart platform are analysed:

1. Improve the geometry of the current Stewart platform to get a better force distribution over the six cylinders.
2. Make use of extra cylinders to reduce the force and moment on top of the Stewart platform, leading to lower cylinder forces.

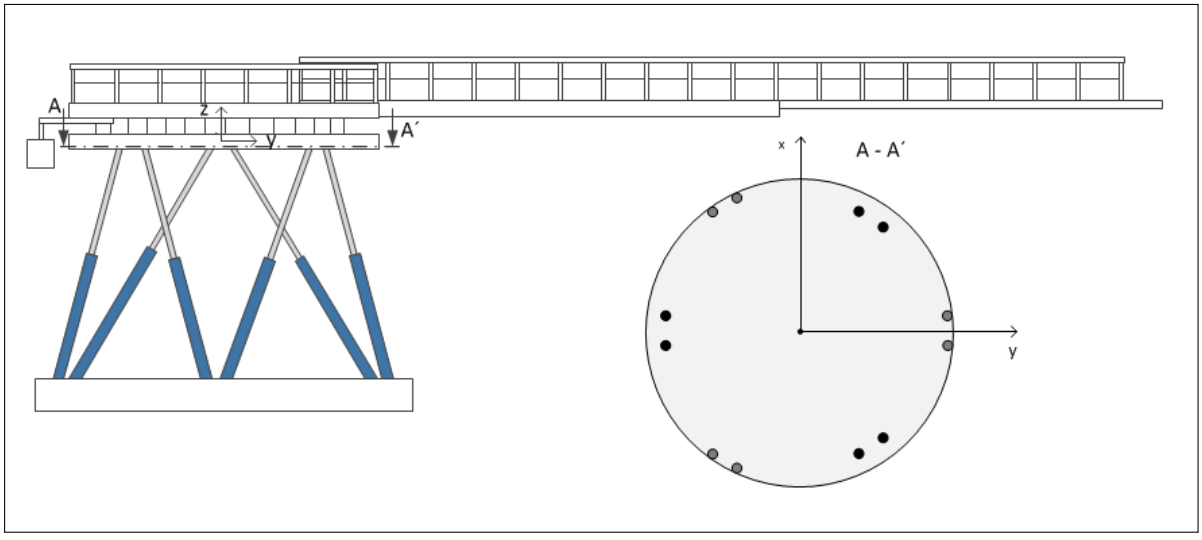

Figure 1-3: Side and top view Ampelmann system

For both optimising directions a model is generated which leads to a design of the Stewart platform with the lowest possible cylinder forces. A case study is used to determine the functionality of the optimising methods for new design of the Stewart platform of the Ampelmann system. The case study is the implication of the Gangway XXL (GXXL), the largest gangway Of Ampelmann, on the A-type system. Currently this gangway can only be used on top of an E-type system.

1-3 Content of thesis

The Ampelmann system consists of four main components, which are divided in smaller components. An overview is given in Figure 1-4. The focus of this thesis is on the components that are indicated with the red dashed line, which includes the complete Stewart platform. The new design of the Stewart platform should be applicable for all current gangways and also the GXXL. Currently the gangway and the Stewart platform are two separate components in the total Ampelmann system, with only one connection point. The connection point must remain at the current location and must be limited to one.

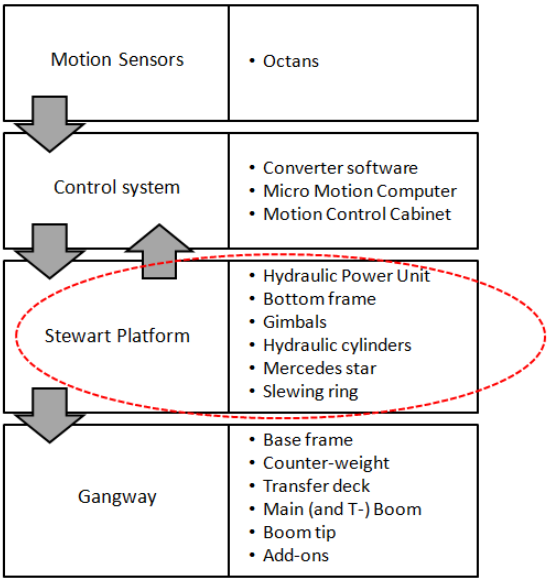

Figure 1-4: Diagram system components

To get a better understanding of the Ampelmann system and especially the Stewart platform, a literature survey was conducted. In this survey the following items were studied:

1. The overall Ampelmann system
2. The Stewart platform in the Ampelmann system
3. Different Stewart platform designs
4. Hydraulic actuators

With this acquired knowledge an approach was made for the study preformed in this report. This report consists of the following parts:

Chapter 2 - Stewart Platform in Ampelmann system The Ampelmann system consists of four components as stated in Figure 1-4. This chapter focusses on the Stewart platform, with all the calculation procedures for the dexterity, workspace and cylinder loads. Most attention is paid to the calculation of the cylinder load, both due to the external loads on top

of the Stewart platform as cylinder dynamics including the motion of the cylinders. These calculation methods are used in the remaining of this thesis for the optimisation of the Stewart platform.

Chapter 3 - External loads The components that contribute to the critical load cases of the GXXL system are described in this chapter. For these load cases, the Stewart platform is optimised. Describing of the loads leads to the first design step of relocating the slewing ring from above the top frame of the Stewart platform to below the bottom frame.

Chapter 4 - Optimisation of the geometry of the Stewart platform With the acquired knowledge of calculation procedures and the critical load cases, the geometry of the Stewart platform is optimised. The approach of this model is sketched, with (all) the variables and constraints. For every set of variables the local optimum is found. The different local optima lead to the global optimum for the cylinder force distribution of the Stewart platform. The coordinates, cylinder forces and workspace of the new geometry are presented.

Chapter 5 - Reducing loads on top of Stewart Platform The second optimisation method is to reduce the load case on top of the Stewart platform by implementing passive cylinders in the system. These extra cylinders have a certain force that is used to counteract a part of the tipping moment and reduce the loads of the cylinders of the Stewart platform. These cylinders are not used to control the motion of the platform as they only follow the trajectory of the Stewart platform cylinders. In this chapter the number and location of extra cylinders is determined in such a way that the forces of the Stewart platform cylinders of the current A-type are reduced as much as possible in neutral position. The chapter is concluded with the large fluctuations of the cylinder forces throughout the workspace of the system, leading to the next chapter.

Chapter 6 - Optimised geometry with active force control The two optimisation methods from the Chapter 4 and 5 were combined to see whether they are complementary to each other. This leads to the final design of the Stewart platform with a new geometry and passive cylinders. To reduce the remaining force fluctuations, Active Force Control (AFC) is introduced. For the AFC also two methods are investigated, which will reduce the forces for every position of the platform in the workspace of the system.

The approach and structure of this thesis is summarised in Figure 1-5. This shows the objective per chapter and the followed approach. Every chapter starts with a recap of this figure and the introduction of the associated objective.

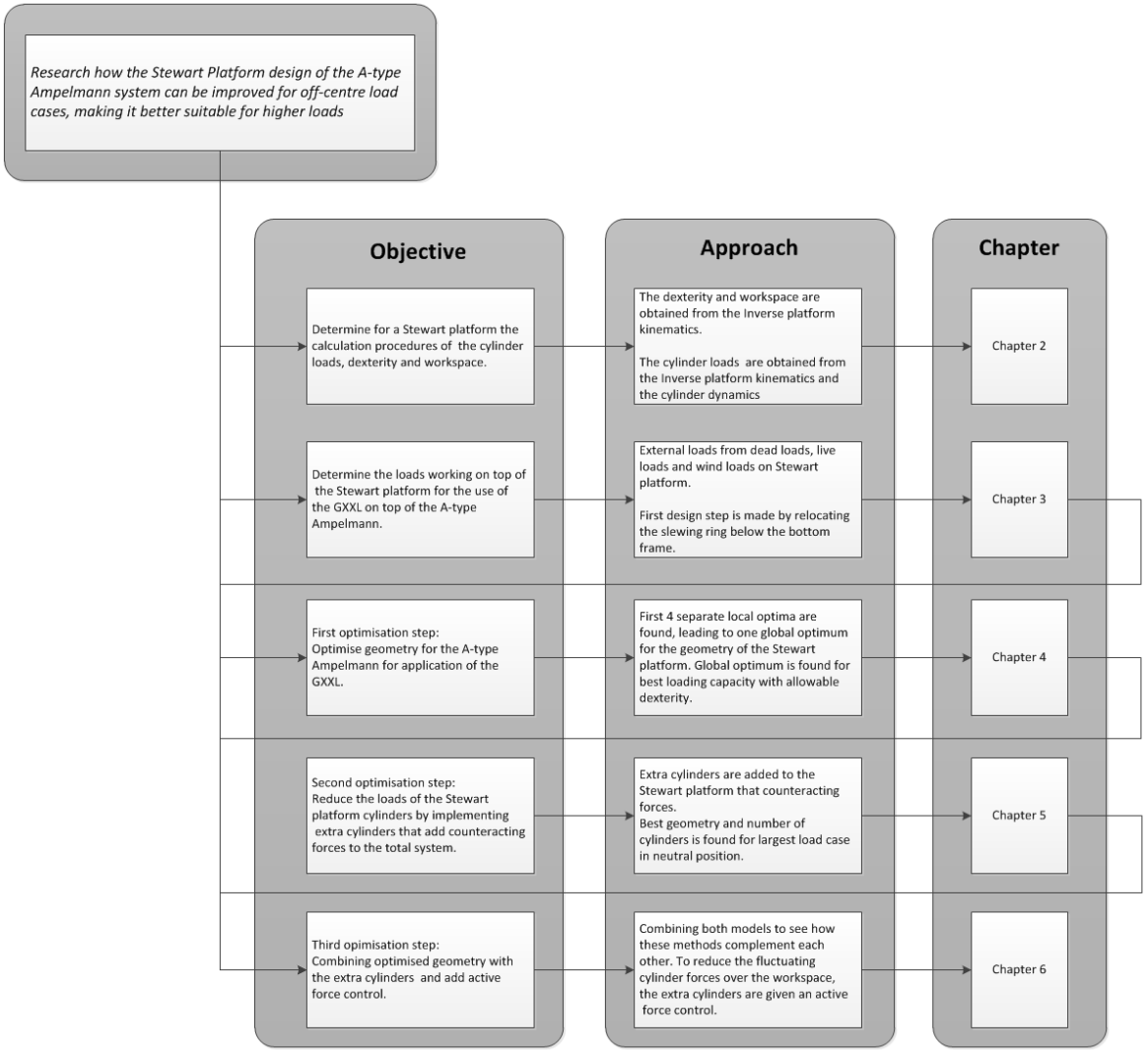

Figure 1-5: Approach and structure of this thesis

Chapter 2

Stewart Platform in Ampelmann system

2-1 Introduction

This chapter describes the Ampelmann system and especially the Stewart platform that is used in the system. The Stewart platform in the current Ampelmann system is optimised for the workspace with an minimum dexterity and a sufficient force distribution. Over the past years, the gangways that are used have grown causing larger load cases on top of the platform. These larger load cases led to a larger platform, the E-type. This system is 1.5 times larger than the A-type system. The question arises if the current system can be improved for the force distribution, making larger load cases possible on the current system, without the need to enlarge the total platform. To answer this question, the current system has to be investigated first. In this chapter the calculation procedures for the dexterity, workspace and cylinder forces are explained that are used in the remaining of this thesis.

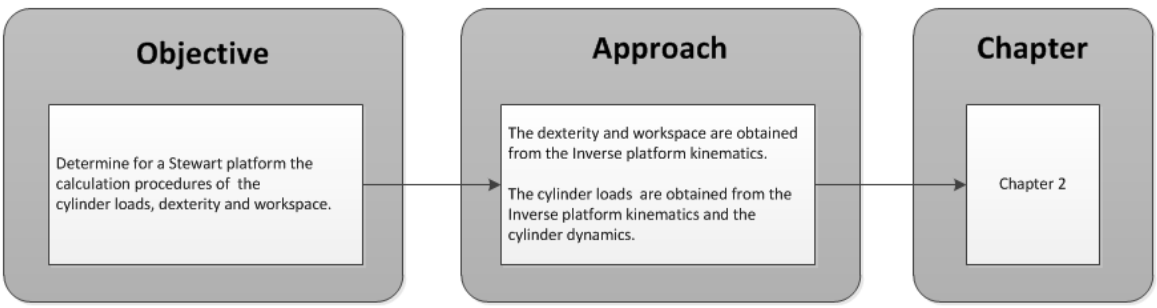

Figure 2-1: Approach Chapter 2

2-2 Ampelmann system

The Ampelmann system consists out of for main components as described in section 1-3. In this section the first two components (Motions sensors and Control system) are shortly described.

2-2-1 Motion sensors

Ampelmann system is placed on a vessel which has motions in all the 6DoF, three translations (surge, sway and heave) and three rotations (pitch, roll and yaw), as shown in Figure 2-2. These motions are measured with a motion sensor device that measures rotations and accelerations of the vessel using three gyroscopes and accelerometers. This motion sensor device is called the Octans System, which is placed in the middle of the bottom frame of the Stewart platform. These vessel motions are measured at a sampling rate of $f_m = 50$ [Hz].

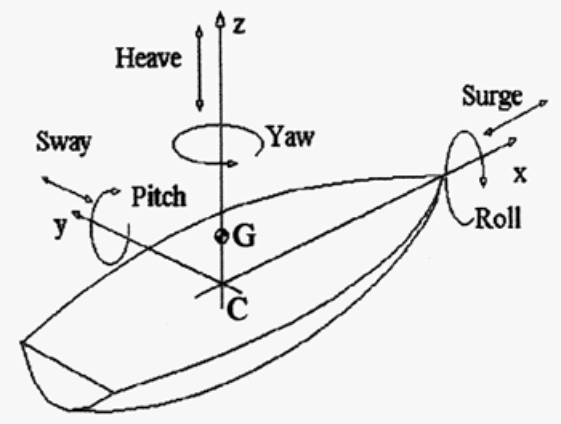

Figure 2-2: Three translations and three rotation of a sea vessel

First the three gyroscopes, Fibre Optic Gyroscopes (FOG), measure the rotational velocities of the vessel: $\dot{\phi}$, $\dot{\theta}$ and $\dot{\psi}$ [3]. The FOG consists out of a coil of optical fibre, which is injected by two beams from a laser at the same time. Both beams travel through the coil, which has a rotational velocity, which causes some delay in the travel time between the two beams. This difference is called the Sagnac effect and is used to determine the rotational velocity. With three FOG's, the three rotational velocities are determined in the inertial reference frame. Integrating these velocities, leads to the three rotation angles of the vessel.

The translations of the vessel are determined with the accelerometers, which measures the sum of the accelerations of the vessel and the gravity. The earth's rotation is eliminated from the sum of the acceleration by a real time Digital Signal Processing (DSP). Leaving only the vessel accelerations, which are integrated twice to get to the three translations of the vessel.

2-2-2 Control system

The measured motions are the input for the Motion Control Process. A High Speed Controller (HSC) first measures the current cylinder length, by determining the orientation of the bottom

frame in comparison with the top frame. This calculation process is called Inverse Kinematics, which is explained in section 2-3-3. After receiving the length of cylinders, the HSC assigns the Valve Control to acquire the desired cylinder length to compensate the vessel motions and leaving the top frame (nearly) motionless in the process.

2-3 Stewart Platform

The third component of the Ampelmann system is the Stewart platform, which consists out of a top and bottom frame that are connected by six actuators (cylinders). The position of the bottom frame is changed constantly due to the vessel motions. The actuators change in length making the top frame stay fixed. The sea vessel motions are in 6DoF, meaning that the Stewart platform has to be able to move in 6DoF. The functioning of the platform in these Degrees of Freedom is explained in section 2-3-1. After that the characteristics of the Stewart platform are elaborated in section 2-3-2 leading to the calculation procedure of the actuator length (section 2-3-3). The performance of the platform is described with the use of the Jacobian matrix (section 2-3-4). The performance of the Stewart platform is threefold: the loading capacity (section 2-4), the dexterity (section 2-5) and the workspace (section 2-6).

2-3-1 Degrees of Freedom

The Stewart platform compensates motions in 6DoF. The number of degrees of freedom of a mechanism has influence on the number of links and joints. This is shown in the following equation [4]:

$$F = \lambda(n_l - n_j - 1) + \sum_{i=1}^{n_j} f_i \tag{2-1}$$

Where,

F	Effective degrees of freedom in mechanism	[-]
λ	Degrees of freedom of the space in which mechanism can operate	[-]
	is 6 in Ampelmann system, where there are 3 translational and 3 rotational degrees	[-]
n_l	Number of links	[-]
n_j	Number of joints	[-]
f_i	Number of degrees of freedom of the i-th joint	[-]

The number of links and joints depend on the number of actuators used in the system. This links and joints are shown in Figure 2-3 can be written in the form of the number of actuators (n_a), where $n_l = 2n_a + 2 = 14$ and $n_j = 3n_a = 18$.

With the degrees of freedom and the number of links and joints known, the number of degrees of freedom of each joint can be calculated. To do this, f_i is first uncoupled:

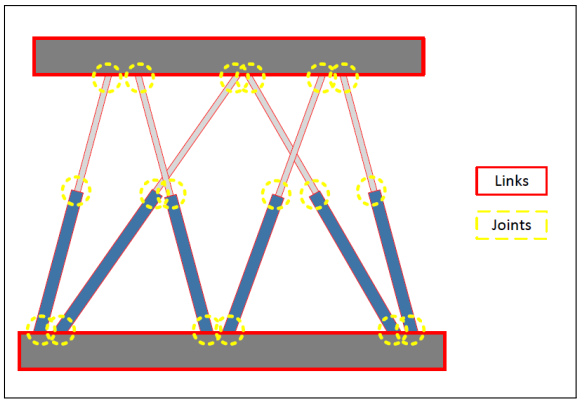

Figure 2-3: Links and joints in Stewart Platform

$$\sum_{i=1}^{n_j} f_i = n_a(f_b + f_c + f_t) \tag{2-2}$$

Where,

n_a	Number of actuators	[-]
f_b	Degrees of freedom at bottom frame level	[-]
f_c	Degrees of freedom at cylinder level	[-]
f_t	Degrees of freedom at top frame level	[-]

To substitute equation 2-2 in to equation 2-1, first equation 2-1 is rewritten with the number of actuators (n_a) implemented [5]:

$$\begin{aligned} F &= \lambda((2 + 2n_a) - 3n_a - 1) + \sum_{i=1}^{n_j} f_i \\ &= \lambda(1 - n_a) + \sum_{i=1}^{n_j} f_i \end{aligned} \tag{2-3}$$

Now the substitution will be:

$$F = 6(1 - n_a) + n_a(f_b + f_c + f_t) \tag{2-4}$$

With $n_a = 6$ and $F = 6$ gives:

$$f_b + f_c + f_t = 6 \tag{2-5}$$

This shows that six actuators in the system give a controllability in 6DoF, when the number of degrees of freedom in each joint is also six. However, equation 2-4 seems to show that the number of actuators in the system is irrelevant, as long as the $f_b + f_c + f_t$ is six.

The reason for the number of actuators to be six is that the system also has to be locked, meaning that it does not move. When the system is locked ($F = 0$), the actuators will no longer extend. The DoF of f_i is reduced from 6 to 5. Implementing this into equation 2-4 leads to the number of actuators to be 6.

Types of joints

Equation 2-5 shows that the number of DoF per actuater (including connection points) is six and is divided over actuator level and top and bottom frame level. Per level different types of joint exists with different number of degrees of freedom. The Ampelmann has cylindrical joints, with 2DoF, as cylinders and universal (or cardan) joints, with also 2DoF, at top and bottom frame. These type of joints are shown in Figure 2-4. The universal joints will be called gimbals from here on, as that is the name used by Ampelmann.

(a) Cylindrical joint: 2DoF **(b)** Universal joint: 2DoF

Figure 2-4: Types of joints at cylinder level

2-3-2 Characteristics of Stewart Platform

The Stewart platform consists of a bottom and top frame. The architecture is symmetric, which means that the gimbal pairs are separated 120 degrees from each other on the bottom and top frame. The symmetric design results in the use of six identical actuator. Each actuator and the gimbals at top and bottom level are referred to:

$$i = 1, 2, ..., 6 \tag{2-6}$$

The parameters of the platform that have to be determined are:

R_b	Radius bottom frame	[m]
R_t	Radius of top frame	[m]
γ_b	Half angle between gimbals at bottom level	[rad]
γ_t	Half angle between gimbals at top level	[rad]

With the radius and the half gimbal angle the coordinates of the gimbals in the top and bottom frame can be determined. The coordinates are in the x- and y-axis and are shown in the table below. The bottom frame is fixed and the z-coordinates of the top frame depend on the length of the six actuator.

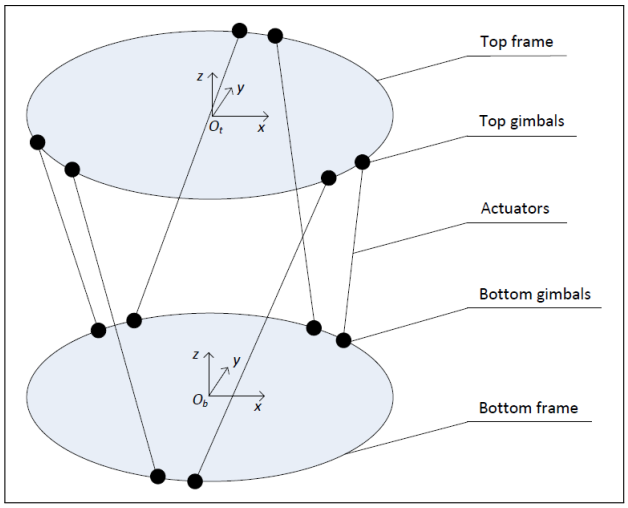

Figure 2-5: Coordinates of Stewart platform in Ampelmann system

b_i	x	y	t_i	x	y
1	$R_b \cdot \cos(\gamma_b)$	$R_b \cdot \sin(\gamma_b)$	1	$R_t \cdot \cos(\frac{1}{3}\pi - \gamma_t)$	$R_t \cdot \sin(\frac{1}{3}\pi - \gamma_t)$
2	$R_b \cdot \cos(\frac{2}{3}\pi - \gamma_b)$	$R_b \cdot \sin(\frac{2}{3}\pi - \gamma_b)$	2	$R_t \cdot \cos(\frac{1}{3}\pi + \gamma_t)$	$R_t \cdot \sin(\frac{1}{3}\pi + \gamma_t)$
3	$R_b \cdot \cos(\frac{2}{3}\pi + \gamma_b)$	$R_b \cdot \sin(\frac{2}{3}\pi + \gamma_b)$	3	$R_t \cdot \cos(\pi - \gamma_t)$	$R_t \cdot \sin(\pi - \gamma_t)$
4	$R_b \cdot \cos(\frac{4}{3}\pi - \gamma_b)$	$R_b \cdot \sin(\frac{4}{3}\pi - \gamma_b)$	4	$R_t \cdot \cos(\pi + \gamma_t)$	$R_t \cdot \sin(\pi + \gamma_t)$
5	$R_b \cdot \cos(\frac{4}{3}\pi + \gamma_b)$	$R_b \cdot \sin(\frac{4}{3}\pi + \gamma_b)$	5	$R_t \cdot \cos(\frac{5}{3}\pi - \gamma_t)$	$R_t \cdot \sin(\frac{5}{3}\pi - \gamma_t)$
6	$R_b \cdot \cos(-\gamma_b)$	$R_b \cdot \sin(-\gamma_b)$	6	$R_t \cdot \cos(\frac{5}{3}\pi + \gamma_t)$	$R_t \cdot \sin(\frac{5}{3}\pi + \gamma_t)$

Table 2-1: Coordinates top and bottom frame

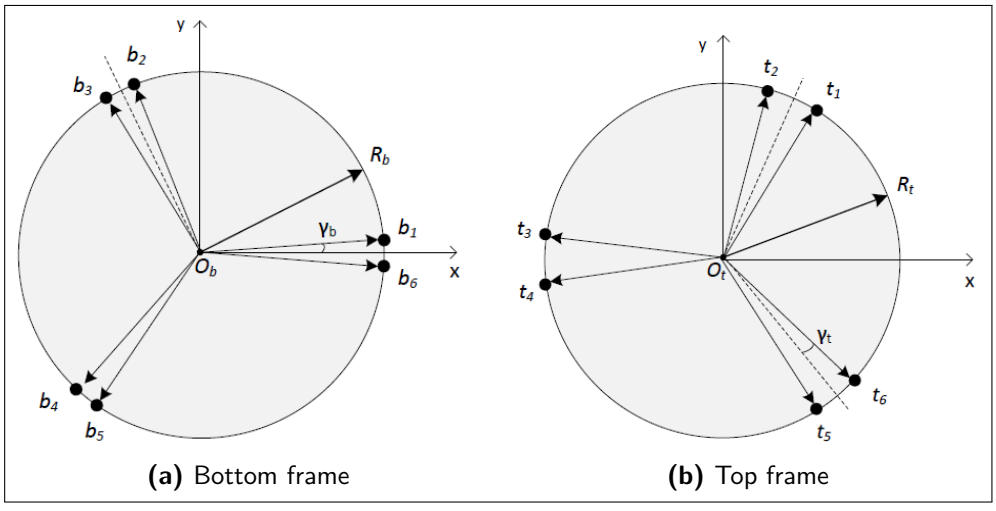

(a) Bottom frame **(b)** Top frame

Figure 2-6: Coordinates in Ampelmann system

2-3-3 Inverse platform Kinematics

With the variables R and γ the different coordinates of the top and bottom gimbals are determined and with that the geometry of the top and bottom frame. However, the coordinates obtained in Table 2-1 are only the x- and y-coordinates in a 2D plane. The z-coordinate still has to be determined, making the two frames in x-y plane connected with each other in a three dimensional space. The origin of the bottom frame is also the origin of the total system, making the z-coordinates of the fixed bottom frame zero. The z-coordinates of the fixed top frame follow from the neutral height of the system. The neutral height is the height for when the system is in neutral position. The neutral height depends on the length of the cylinders and the positions of the gimbals.

When the platform compensated the vessel motions, the bottom frame will rotate and translate along with the motions of the vessel. The coordinates of the rotated bottom frame of the platform are first calculated in the position kinematics. From this analysis the cylinder lengths are calculated. This is called the Inverse Kinematics approach, including position, velocity and acceleration of the platform. Another approach is the Forward Kinematics approach, where the cylinder lengths are fixed. For these fixed lengths all the possible positions of the bottom frame are determined. This approach has more than one outcome , namely 40 in complex domain for parallel manipulators such as the Stewart Platform. The Inverse Kinematics approach only has one real outcome, so this is used in the thesis.

Neutral height

For fixed position of both frames, the z-coordinate of the bottom frame is zero, but for the top frame this coordinate depends on the length of the cylinders and the location of the gimbal (the x- and y-coordinates). The z-coordinate is chosen as the neutral height of the top frame, which is in the middle of the maximum and minimum height of the frame. So first these two height are determined. This is done following the Pythagoras's Theorem in 3D.

The maximum and minimum height of the top frame becomes:

$$\begin{aligned} H_{max} &= \sqrt{l_{max}^2 - l_{xy}^2} \\ H_{min} &= \sqrt{l_{min}^2 - l_{xy}^2} \end{aligned} \tag{2-7}$$

With,

$$\begin{aligned} l_{xy} &= \sqrt{cyl_x^2 + cyl_y^2} \\ cyl_x &= b_{x1} - t_{x1} \\ cyl_y &= b_{y1} - t_{y1} \\ l_{min} &= l_{dead} + l_{stroke} \\ l_{max} &= l_{dead} + 2 \cdot l_{stroke} \end{aligned} \tag{2-8}$$

Where,

H_{max}	Maximum height of top frame	[m]
l_{dead}	Cylinder dead length is the part of cylinder that does not extend = 1.25	[m]
l_{stroke}	Cylinder stroke length is the part of cylinder that does extend = 2.00	[m]
l_{min}	Minimum cylinder length (= 3.25)	[m]
l_{max}	Maximum cylinder length (= 5.25)	[m]
l_{hor}	Distance between two gimbals in x-y plane	[m]
cyl_x	Distance in x-direction between two gimbals	[m]
cyl_y	Distance in y-direction between two gimbals	[m]

With these obtained maximum and minimum frame heights, the neutral height is determined:

$$H_{neutral} = \frac{1}{2}(H_{max} + H_{min}) = t_{zi} \tag{2-9}$$

The neutral height of the system represents the height of the top frame in z-direction. With the origin of the global system in the middle of the bottom frame (O_b), as shown in Figure 2-6.

Position kinematics

Now the coordinates of the fixed top and bottom frame are known in the three dimensional Cartesian space. The Stewart platform's main function is to compensate vessel motions, so the bottom frame is not fixed but translates and rotates around the x-y- and z-axis, respectively: roll (ϕ_b), pitch (θ_b) and yaw (ψ_b). The following vectors are used for translation and for the Euler angles [6]:

$$\underline{c}^b = \begin{bmatrix} x_b \\ y_b \\ z_b \end{bmatrix} \qquad \underline{\Theta}_b = \begin{bmatrix} \phi_b \\ \theta_b \\ \psi_b \end{bmatrix} \tag{2-10}$$

In practice the Stewart platform moves in the same 6DoF as the vessel motions. For the optimisation of the geometry, the vessel motions are not used, but the whole workspace of the system itself is used as an input.

From the Euler angles, the Euler transformation matrix can be derived. For each rotation, the tranformation matrix is:

$$= \begin{bmatrix} 1 & 0 & 0 \\ 0 & cos\phi & -sin\phi \\ 0 & sin\phi & cos\phi \end{bmatrix} \quad \underline{\underline{R}}_{y,\theta} = \begin{bmatrix} cos\theta & 0 & sin\theta \\ 0 & 1 & 0 \\ -sin\theta & 0 & cos\theta \end{bmatrix} \quad \underline{\underline{R}}_{z,\psi} = \begin{bmatrix} cos\psi & sin\psi & 0 \\ -sin\psi & cos\psi & 0 \\ 0 & 0 & 1 \end{bmatrix} \tag{2-11}$$

And with these three matrices the complete Euler transformation matrix can be derived. The sequence of the rotations to fixed top frame O_t that is chosen is: yaw-pitch-roll:

$$\underline{\underline{R}}_b = \begin{bmatrix} c\psi \cdot c\theta & -s\psi \cdot c\phi + c\psi \cdot s\theta \cdot s\phi & s\psi \cdot s\phi + c\psi \cdot c\phi \cdot s\theta \\ s\psi \cdot c\theta & c\psi \cdot c\phi + s\phi \cdot s\theta \cdot s\psi & -c\psi \cdot s\phi + s\psi \cdot c\phi \cdot s\theta \\ -s\theta & c\theta \cdot s\phi & c\theta \cdot c\phi \end{bmatrix} \tag{2-12}$$

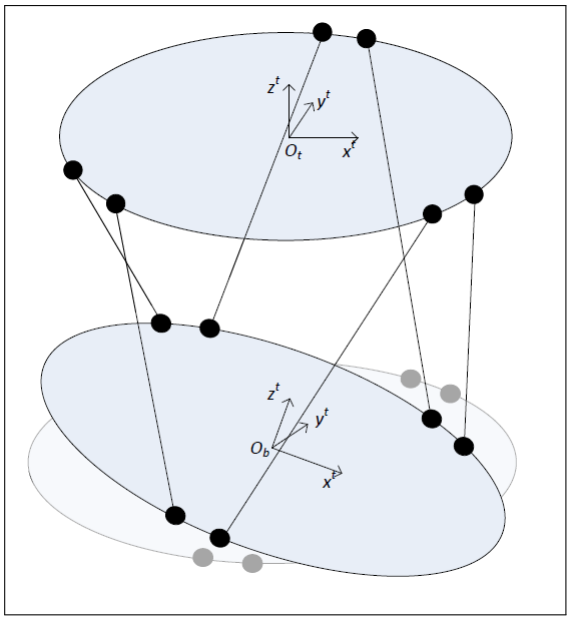

Figure 2-7: Rotation of bottom frame in contrast to fixed top frame

With, $c\phi = cos\phi$ and $s\psi = sin\psi$

For the coordinates of the rotated bottom frame, the fixed bottom frame coordinates have to be multiplied with Euler transformation matrix ($\underline{\underline{R}}_b$). The translations are added to the rotated bottom frame by using the translation vector ($\underline{c}^b$):

$$\underline{b}'_i = \underline{\underline{R}}_b \cdot \underline{b}_i + \underline{c}^b \tag{2-13}$$

Where,

$\underline{b}'_i$	Coordinates rotated bottom frame	[-]
$\underline{\underline{R}}_b$	Euler transformation matrix	[-]
$\underline{b}_i$	Coordinates fixed bottom frame	[-]
$\underline{c}^b$	Translation vector	[-]

Cylinder lengths

With the obtained coordinates in the three dimensional Cartesian space of the fixed top frame and rotated bottom frame, the corresponding cylinder lengths can be calculated. The cylinder length follows from the cylinder vector. This vector of one cylinder is in the 3d space, between a top and a bottom gimbal point and is obtained as follows:

$$\underline{l}_i = \underline{t}_i - \underline{b}'_i \tag{2-14}$$

The cylinder vector is used to calculated the cylinder lengths of the system. The relation between the cylinder length and the cylinder vector is again the Pythagoras's Theorem in 3D:

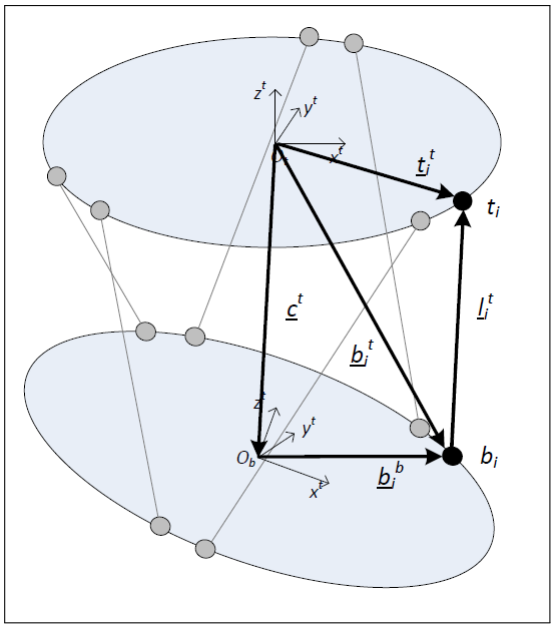

Figure 2-8: Vector in bottom and top reference frame

$$||l_i|| = \sqrt{\underline{l}_{ix}^2 + \underline{l}_{iy}^2 + \underline{l}_{iz}^2} \tag{2-15}$$

All the values of the parameters of the A-type Ampelmann system are summarised in Table 2-2.

Parameter	Value	Unit
R_b	3.00	[m]
R_t	2.75	[m]
γ_b	$\pi/36$	[rad]
γ_t	$\pi/36$	[rad]
l_{dead}	1.25	[m]
l_{stroke}	2.00	[m]

Table 2-2: Parameters of Ampelmann system

Velocity kinematics

When the Ampelmann system is operational on a sea vessel, the bottom platform of the Stewart platform translates and rotates along with the vessel motions while the top platform stays fixed. The velocities of the bottom platform can be obtained by taking the time derivative of the equation 2-13:

$$\dot{b_i'} = \dot{c^b} + \omega \times \underline{\underline{R}}_{bt} b_i \tag{2-16}$$

With,

$$\dot{c^b} = \begin{bmatrix} v_x \\ v_y \\ v_z \end{bmatrix} \qquad \omega = \begin{bmatrix} \omega_x \\ \omega_y \\ \omega_z \end{bmatrix} = \begin{bmatrix} 0 & cos\phi & sin\phi \sin\theta \\ 0 & sin\phi & -cos\phi sin\theta \\ 1 & 0 & cos\theta \end{bmatrix} \begin{bmatrix} \dot{\phi} \\ \dot{\theta} \\ \dot{\psi} \end{bmatrix} \tag{2-17}$$

Acceleration kinematics

The acceleration of the bottom frame can be obtained by differentiating the equation 2-16:

$$\ddot{b_i}' = \ddot{c^b} + \alpha \times \underline{\underline{R}}_b b_i + \omega \times (\omega \times \underline{\underline{R}}_b b_i) \tag{2-18}$$

With,

$$\ddot{c^b} = \begin{bmatrix} a_x \\ a_y \\ a_z \end{bmatrix} \tag{2-19}$$

$$\alpha = \begin{bmatrix} \alpha_x \\ \alpha_y \\ \alpha_z \end{bmatrix} = \begin{bmatrix} 0 & cos\phi & sin\phi \sin theta \\ 0 & sin\phi & -cos\phi sin\theta \\ 1 & 0 & cos\theta \end{bmatrix} \begin{bmatrix} \ddot{\phi} \\ \ddot{\theta} \\ \ddot{\psi} \end{bmatrix} + \begin{bmatrix} 0 & -\dot{\phi}sin\phi & \dot{\phi}cos\phi sin(\theta) + \dot{\theta}sin\phi cos\theta \\ 0 & \dot{\phi}cos\phi & \dot{\phi}sin\phi sin\theta + \dot{\theta}cos\phi cos\theta \\ 0 & 0 & -\dot{\theta}sin\theta \end{bmatrix} \begin{bmatrix} \phi \\ \theta \\ \psi \end{bmatrix} \tag{2-20}$$

2-3-4 Jacobian Matrix

For all type of manipulators, including the parallel manipulator, the Jacobian Matrix maps the linear transformation of the change of the position of the platform to the change of the joints. It represents the relative kinematic efficiency from the actuator motions to platform motions. The Jacobian Matrix is used to measure the performance of the platform, such as the actuator velocity, actuator forces and the dexterity. First the derivation of the matrix is elaborated and after that the application for the actuator forces and dexterity is presented.

The ratio between the change of the actuator length and the change of the position of the platform can be described as:

$$\delta l_i = \underline{\underline{J}} \delta q_i \tag{2-21}$$

With,

$$\begin{aligned} q_i &= \begin{bmatrix} x & y & z & \phi & \theta & \psi \end{bmatrix}^T \\ l_i &= \begin{bmatrix} l_1 & l_2 & l_3 & l_4 & l_5 & l_6 \end{bmatrix}^T \end{aligned} \tag{2-22}$$

Where,

q_i	Generalised coordinates of bottom platform	[m]
l_i	Actuator length	[m]

Rewriting equation 2-21 and 2-22, the Jacobian Matrix is defined as [4]:

$$\underline{\underline{J}} = \begin{bmatrix} \frac{\delta l_1}{\delta x} & \frac{\delta l_1}{\delta y} & \frac{\delta l_1}{\delta z} & \frac{\delta l_1}{\delta \phi} & \frac{\delta l_1}{\delta \theta} & \frac{\delta l_1}{\delta \psi} \\ \frac{\delta l_2}{\delta x} & \frac{\delta l_2}{\delta y} & \frac{\delta l_2}{\delta z} & \frac{\delta l_2}{\delta \phi} & \frac{\delta l_2}{\delta \theta} & \frac{\delta l_2}{\delta \psi} \\ \frac{\delta l_3}{\delta x} & \frac{\delta l_3}{\delta y} & \frac{\delta l_3}{\delta z} & \frac{\delta l_3}{\delta \phi} & \frac{\delta l_3}{\delta \theta} & \frac{\delta l_3}{\delta \psi} \\ \frac{\delta l_4}{\delta x} & \frac{\delta l_4}{\delta y} & \frac{\delta l_4}{\delta z} & \frac{\delta l_4}{\delta \phi} & \frac{\delta l_4}{\delta \theta} & \frac{\delta l_4}{\delta \psi} \\ \frac{\delta l_5}{\delta x} & \frac{\delta l_5}{\delta y} & \frac{\delta l_5}{\delta z} & \frac{\delta l_5}{\delta \phi} & \frac{\delta l_5}{\delta \theta} & \frac{\delta l_5}{\delta \psi} \\ \frac{\delta l_6}{\delta x} & \frac{\delta l_6}{\delta y} & \frac{\delta l_6}{\delta z} & \frac{\delta l_6}{\delta \phi} & \frac{\delta l_6}{\delta \theta} & \frac{\delta l_6}{\delta \psi} \end{bmatrix} \tag{2-23}$$

This change of length has to be determined for all the different poses of the platform. For every change in 1DoF the length of all the six cylinders have to be determined with this matrix. Combining equation 2-13 and 2-14 gives the length of the actuator vector:

$$\underline{l_i} = t_i - (\underline{\underline{R}}_b \cdot \underline{b}_i + \underline{c}^b) \tag{2-24}$$

The direction of each actuator is obtained with the use of the unit vector. A unit vector ($\underline{\hat{l}_i}$) is derived as:

$$\underline{\hat{l}_i} = \frac{\underline{l_i}}{l_i} \tag{2-25}$$

The new equation for the vector length becomes:

$$\begin{aligned} l_i &= \underline{\hat{l}_i}^T \cdot \underline{l_i} \\ &= \underline{\hat{l}_i}^T \cdot t_i - \underline{\hat{l}_i}^T \cdot (\underline{\underline{R}}_b \cdot \underline{b}_i - \underline{c}^b) \end{aligned} \tag{2-26}$$

The Jacobian matrix can be obtained from the time derivative of the actuator length and the platform pose.As the top frame stays fixed, the time derivative of the top frame is zero ($\underline{\dot{t}_i} = 0$). The velocities of the bottom frame are divided in the linear velocities and angular velocities:

$$\begin{aligned} \underline{\dot{q}}_i &= \underline{\dot{c}} + \underline{\omega} \times (\underline{\underline{R}}_b \cdot \underline{b}_i) \\ &= \underline{\dot{c}} + \underline{\omega} \times \underline{f}_r \end{aligned} \tag{2-27}$$

With,

$$\underline{\dot{c}} = \begin{bmatrix} v_x \\ v_y \\ v_z \end{bmatrix} \qquad \underline{\omega} = \begin{bmatrix} \omega_x \\ \omega_y \\ \omega_z \end{bmatrix} \tag{2-28}$$

Where,

$\underline{\dot{c}}$	Linear platform velocities
ω	Angular platform velocities
$\underline{f}_r$	Position vector of top/bottom frame with respect to the rotating reference frame

Taking the time derivative of the actuator length from equation 2-26 and implementing the velocities of the bottom frame leads to:

$$\dot{l}_i = \underline{\hat{l}_i}^T \cdot \underline{\dot{c}} + \underline{\hat{l}_i}^T \cdot (\underline{\omega} \times \underline{f}_r) \tag{2-29}$$

With the use the properties of scalar triple products, equation 2-29 can be written as:

$$\dot{l}_i = \underline{\hat{l}_i}^T \cdot \underline{\dot{c}} + (\underline{\hat{l}_i} \times \underline{f}_r)^T \cdot \underline{\omega} \tag{2-30}$$

Putting equation 2-30 with all the six actuator lengths and 6DoF of the Stewart platform into a matrix, leads to the Jacobian Matrix:

$$\begin{bmatrix} \dot{l}_1 \\ \dot{l}_2 \\ \vdots \\ \dot{l}_6 \end{bmatrix} = \begin{bmatrix} \widehat{\underline{l}}_{x1} & \widehat{\underline{l}}_{y1} & \widehat{\underline{l}}_{z1} & (\widehat{\underline{l}}_1 \times \underline{f}_{r1})^T \\ \widehat{\underline{l}}_{x2} & \widehat{\underline{l}}_{y2} & \widehat{\underline{l}}_{z2} & (\widehat{\underline{l}}_2 \times \underline{f}_{r2})^T \\ \vdots & \vdots & \vdots & \vdots \\ \widehat{\underline{l}}_{x6} & \widehat{\underline{l}}_{y6} & \widehat{\underline{l}}_{z6} & (\widehat{\underline{l}_6} \times \underline{f}_{r6})^T \end{bmatrix} \begin{Bmatrix} \underline{\dot{c}} \\ \underline{\omega} \end{Bmatrix} = \underline{\underline{J}} \begin{Bmatrix} \underline{\dot{c}} \\ \underline{\omega} \end{Bmatrix} \tag{2-31}$$

The obtained Jacobian Matrix will be used in the following sections to obtain the dexterity and the actuator forces of the Stewart platform used in the Ampelmann system.

2-4 Cylinder forces

The cylinder forces in the Stewart platform are dependent on the external loads and on the internal loads of the cylinders. With the external loads, the required axial reaction forces of the cylinders can be obtained for every position of the Stewart platform. This can be done with a static equilibrium around the CoG of the fixed top platform. The axial reaction forces are first derived in this section. This method assumes that half of the weight of the cylinders is distributed to the top of the cylinder and the other have to the bottom of the cylinder.

The lateral forces are obtained from the internal loads of the cylinders, following from the cylinder dynamics. This is first done by including the position and length of the of the cylinders to determine the distribution of the mass. The second part includes not only the position and mass of the cylinder as well as the motion of the cylinders. Leading to a total cylinder force, distributed over a axial and a lateral forces.

2-4-1 Axial cylinder forces

The Jacobian Matrix as derived in section 2-3-4 is used to determine the dexterity, but is also used for force mapping to obtain the actuator forces of the Stewart platform. The actuator forces and the external loads all work on the top platform, making the top frame the frame of reference:

$$W = \begin{Bmatrix} \underline{F} \\ \underline{M} \end{Bmatrix} = \begin{bmatrix} \widehat{\underline{l}}_{x1} & \widehat{\underline{l}}_{x1} & \cdots & \widehat{\underline{l}}_{x6} \\ \widehat{\underline{l}}_{y1} & \widehat{\underline{l}}_{y1} & \cdots & \widehat{\underline{l}}_{y6} \\ \widehat{\underline{l}}_{z1} & \widehat{\underline{l}}_{z1} & \cdots & \widehat{\underline{l}}_{z6} \\ (\widehat{\underline{l}}_1 \times \underline{t}_1) & (\widehat{\underline{l}}_2 \times \underline{t}_2) & \cdots & (\widehat{\underline{l}}_6 \times \underline{t}_6) \end{bmatrix} \begin{bmatrix} N_1^a \\ N_2^a \\ \vdots \\ N_6^a \end{bmatrix} = \underline{\underline{J}}^T \cdot N_i \tag{2-32}$$

Where,

W	External wrench, generalised force	[-]
$\underline{F}$	External force	[kN]
$\underline{M}$	Effective external moment with respect to origin of top frame	[kNm]
N_i	Actuator force	[kN]

When looking at this matrix from equation 2-32, it can be seen as a force equilibrium around the origin of the top frame (O_t):

$$\begin{aligned} \sum F_x &= \sum F_y &= \sum F_z &= 0 \quad [\text{kN}] \\ \sum M_x &= \sum M_y &= \sum M_z &= 0 \quad [\text{kNm}] \end{aligned} \tag{2-33}$$

Each columns of Jacobian Matrix from equation 2-32 contains a cross product. The Jacobian Matrix can be divided into two 3-by-6 matrices:

$$\underline{\underline{J}}^T = \left\{ \begin{array}{c} \underline{\underline{J}}_f^T \\ \underline{\underline{J}}_m^T \end{array} \right\} \tag{2-34}$$

The new defined matrix $\underline{\underline{J}}_m$ can be expanded by expanding the cross product:

$$\underline{\underline{J}}_m = \begin{bmatrix} y_{t1} \cdot \widehat{z}_{t1} - z_{t1} \cdot \widehat{y}_{t1} & \cdots & y_{t6} \cdot \widehat{z}_{t6} - z_{t6} \cdot \widehat{y}_{t6} \\ z_{t1} \cdot \widehat{x}_{t1} - x_{t1} \cdot \widehat{z}_{t1} & \cdots & z_{t6} \cdot \widehat{x}_{t6} - x_{t6} \cdot \widehat{z}_{t6} \\ x_{t1} \cdot \widehat{y}_{t1} - y_{t1} \cdot \widehat{x}_{t1} & \cdots & x_{t6} \cdot \widehat{y}_{t6} - y_{t6} \cdot \widehat{x}_{t6} \end{bmatrix} \tag{2-35}$$

The matrix defined in equation 2-35 contains all the six x-y and z-coordinates and unit vectors. The reference frame for the Jacobian Matrix for the actuator forces is the top frame and as this frame is fixed, the z-coordinates are zero. When cancelling these out of the equation the matrix $\underline{\underline{J}}_m$ becomes:

$$\begin{bmatrix} -y_{t1} \cdot \widehat{z}_{l1} & -y_{t2} \cdot \widehat{z}_{l2} & \cdots & -y_{t6} \cdot \widehat{z}_{l6} \\ x_{t1} \cdot \widehat{z}_{l1} & x_{t2} \cdot \widehat{z}_{l2} & \cdots & x_{t6} \cdot \widehat{z}_{l6} \\ x_{t1} \cdot \widehat{y}_{l1} - y_{t1} \cdot \widehat{x}_{l1} & x_{t2} \cdot \widehat{y}_{l2} - y_{t2} \cdot \widehat{x}_{l2} & \cdots & x_{t6} \cdot \widehat{y}_{l6} - y_{t6} \cdot \widehat{x}_{l6} \end{bmatrix} \tag{2-36}$$

Implementing equation 2-36 into the equation 2-32 gives the total Jacobian matrix which is use to obtain the actuator forces. The forces on the right hand side are the external loads that influence the actuator forces.

$$\begin{bmatrix} \widehat{x}_{l1} & \widehat{x}_{l2} & \widehat{x}_{l3} & \widehat{x}_{l4} & \widehat{x}_{l5} & \widehat{x}_{l6} \\ \widehat{y}_{l1} & \widehat{y}_{l2} & \widehat{y}_{l3} & \widehat{y}_{l4} & \widehat{y}_{l5} & \widehat{y}_{l6} \\ \widehat{z}_{l1} & \widehat{z}_{l2} & \widehat{z}_{l3} & \widehat{z}_{l4} & \widehat{z}_{l5} & \widehat{z}_{l6} \\ -y_{t1} \cdot \widehat{z}_{l1} & -y_{t2} \cdot \widehat{z}_{l2} & -y_{t3} \cdot \widehat{z}_{l3} & -y_{t4} \cdot \widehat{z}_{l4} & -y_{t5} \cdot \widehat{z}_{l5} & -y_{t6} \cdot \widehat{z}_{l6} \\ x_{t1} \cdot \widehat{z}_{l1} & x_{t2} \cdot \widehat{z}_{l2} & x_{t3} \cdot \widehat{z}_{l3} & x_{t4} \cdot \widehat{z}_{l4} & x_{t5} \cdot \widehat{z}_{l5} & x_{t6} \cdot \widehat{z}_{l6} \\ x_{t1} \cdot \widehat{y}_{l1} - y_{t1} \cdot \widehat{x}_{l1} & x_{t2} \cdot \widehat{y}_{l2} - y_{t2} \cdot \widehat{x}_{l2} & x_{t3} \cdot \widehat{y}_{l3} - y_{t3} \cdot \widehat{x}_{l3} & x_{t4} \cdot \widehat{y}_{l4} - y_{t4} \cdot \widehat{x}_{l4} & x_{t5} \cdot \widehat{y}_{l5} - y_{t5} \cdot \widehat{x}_{l5} & x_{t6} \cdot \widehat{y}_{l6} - y_{t6} \cdot \widehat{x}_{l6} \end{bmatrix} \begin{bmatrix} N_1^a \\ N_2^a \\ N_3^a \\ N_4^a \\ N_5^a \\ N_6^a \end{bmatrix} = - \begin{bmatrix} F_x \\ F_y \\ F_z \\ M_x \\ M_y \\ M_z \end{bmatrix} \tag{2-37}$$

The axial cylinders forces are now derived from the external loads. The next step is to determine te lateral forces from the cylinder dynamics. With these two forces, the total cylinders forces can be obtained.

2-4-2 Lateral reaction forces

In the previous section the Jacobian matrix is derived to determine the axial cylinder forces with the use of an static equilibrium. The lateral forces can be obtained with the use of the

weight of the cylinders and the be more precise the cylinder dynamics.

This leads to two different cylinder forces. (1) Forces which are obtained for every position of the workspace of the system. For this only the external loads and the weight of the cylinders is used. (2) The cylinder forces from the cylinder dynamics. Here the forces are obtained by also including the motion of the cylinders between the positions. This method is used to see whether the motion of the cylinders contributes to the total cylinder force during operation and compensation of the vessel motions.

Internal loads from cylinder weight

The important parameters of an A-type cylinder are shown in Table 2-3.

Parameter	Value	Unit
m_{cyl}	890	[kg]
m_b	490	[kg]
m_r	400	[kg]
l_b	2.930	[m]
l_r	2.675	[m]

Table 2-3: Parameters of an A-type cylinder

When adding the mass (the internal loads) of the cylinder to the external loads in equation 2-37, the number of loads is expanded with internal moments in x- and y-direction created by the mass of every cylinder ($M^{in}_{x,yi}$). Including this in equation 2-32 ,the total number of loads becomes eighteen:

$$W = [F^{ex} \quad M^{ex} \quad F^{in}_{x,i} \quad F^{in}_{y,i}]^T \tag{2-38}$$

The right hand side of equation 2-37 now has eighteen components, this means that the Jacobian matrix has to be expanded tot a 18-by-18 matrix to be able to calculate the cylinder reaction forces. The internal forces can not be included into the 6-by-6 matrix, as every cylinder has its own angle and direction, leading to different forces. The matrix no longer has unit vectors, as the reaction forces are divided into an x-, y- and z-component. The entire equation becomes:

$$\begin{bmatrix}
1 & 0 & 0 & 1 & 0 & 0 & \cdots & 1 & 0 & 0 \\
0 & 1 & 0 & 0 & 1 & 0 & \cdots & 0 & 1 & 0 \\
0 & 0 & 1 & 0 & 0 & 1 & \cdots & 0 & 0 & 1 \\
0 & 0 & -y_{t1} & 0 & 0 & -y_{t2} & \cdots & 0 & 0 & -y_{t6} \\
0 & 0 & x_{t1} & 0 & 0 & x_{t2} & \cdots & 0 & 0 & x_{t6} \\
y_{t1} & -x_{t1} & 0 & y_{t2} & -x_{t2} & 0 & \cdots & y_{t6} & -x_{t6} & 0 \\
\hdashline
0 & z_{t1}-z_{b1} & -(y_{t1}-y_{b1}) & 0 & 0 & 0 & \cdots & 0 & 0 & 0 \\
0 & 0 & 0 & 0 & z_{t2}-z_{b2} & -(y_{t2}-y_{b2}) & \cdots & 0 & 0 & 0 \\
 & \vdots & & & \vdots & & \ddots & & \vdots & \\
0 & 0 & 0 & 0 & 0 & 0 & \cdots & 0 & z_{t6}-z_{b6} & -(y_{t6}-y_{b6}) \\
\hdashline
z_{t1}-z_{b1} & 0 & -(x_{t1}-x_{b1}) & 0 & 0 & 0 & \cdots & 0 & 0 & 0 \\
0 & 0 & 0 & z_{t2}-z_{b2} & 0 & -(x_{t2}-x_{b2}) & \cdots & 0 & 0 & 0 \\
 & \vdots & & & \vdots & & \ddots & & \vdots & \\
0 & 0 & 0 & 0 & 0 & 0 & \cdots & z_{t6}-z_{b6} & 0 & -(x_{t6}-x_{b6})
\end{bmatrix}
\begin{bmatrix} N_{1x} \\ N_{1y} \\ N_{1z} \\ N_{2x} \\ N_{2y} \\ N_{2z} \\ \vdots \\ N_{6x} \\ N_{6y} \\ N_{6z} \end{bmatrix}
= -
\begin{bmatrix} F^{ex} \\ M^{ex} \\ M^{in}_{x,i} \\ M^{in}_{y,i} \end{bmatrix} \tag{2-39}$$

The internal forces due to the mass of the cylinder still have to be calculated. To obtain the reaction forces, the external and internal loads are multiplied with the inverse of the matrix. The reaction forces of the six cylinders are now in x-, y- and z-direction. To obtain the axial reaction force, all three direction have to multiplied with its unit vector. The lateral forces follow from the difference between the total reaction forces and the axial forces:

$$\begin{aligned} N_i^a &= N_{ix} \cdot \widehat{x}_i + N_{iy} \cdot \widehat{y}_i + N_{iz} \cdot \widehat{z}_i \\ N_i^{lat} &= \sqrt{(N_i^{tot})^2 - (N_i^a)^2} \end{aligned} \tag{2-40}$$

With,

$$N_i^{tot} = \sqrt{\left(N_{ix}^2 + N_{iy}^2 + N_{iz}^2\right)} \tag{2-41}$$

Now the complete derivation is found for the axial and lateral reaction forces of the hydraulic cylinder of the A-type Ampelmann. The contribution of the cylinder weight on the axial force will be used to calculate the optimised geometry of the Stewart platform. The cylinder forces of the A-type system in neutral position and over the entire workspace are plotted in Figure 2-9 and 2-10. The red dashed line represents the operation limit of the A-type cylinder, which will be elaborated in section 3-4-2.

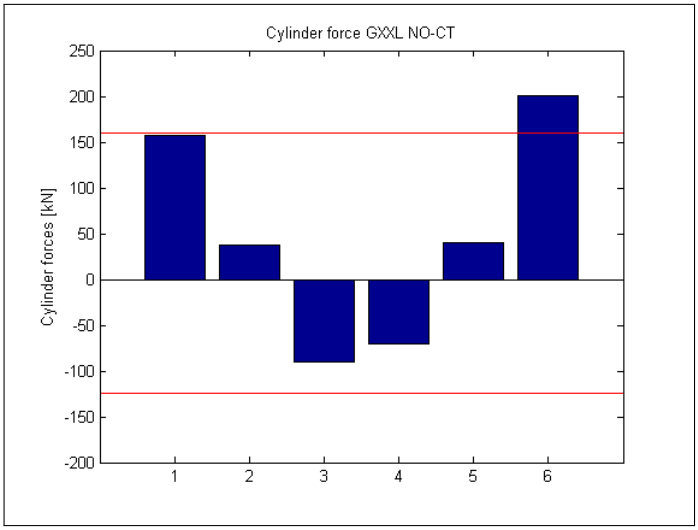

Figure 2-9: Axial cylinder forces in neutral position

Cylinder dynamics

One cylinder is considered in this part. The cylinder and the two universal joints at the end as the gimbals give the schematic drawing as shown in Figure 2-11.

To create the rotational equilibrium of the entire cylinder around bottom gimbal (point A), the mass of the upper and lower chamber are taken into account with the corresponding (angular) velocity, accelerations and gravity. It is assumed that the universal joints of the Ampelmann are frictionless at both ends. Euler's equation of the cylinder consists of external forces on the left hand side and inertial moments on the right hand side [7]:

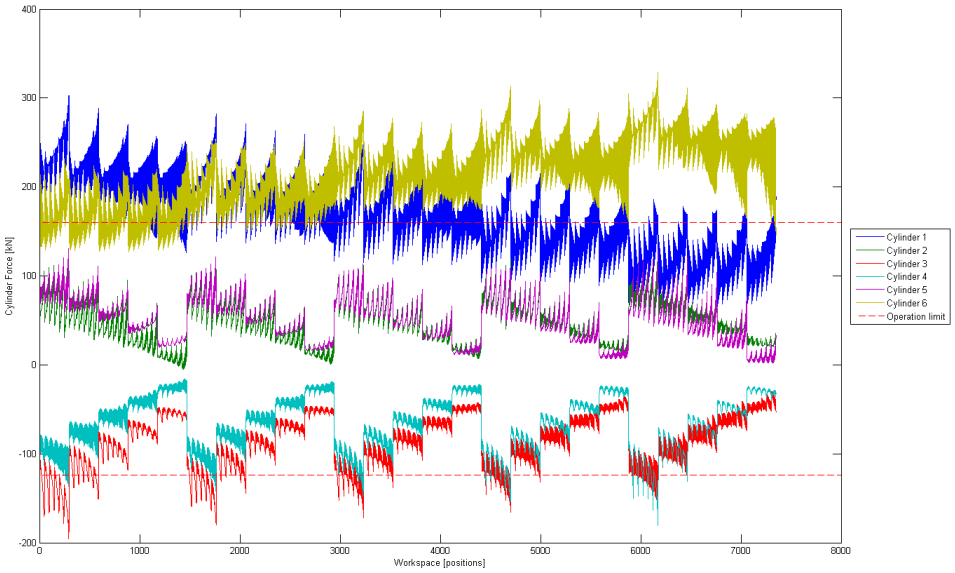

Figure 2-10: Axial cylinder forces over workspace

$$\begin{aligned} &m_1 l_1 \widehat{l_i} \times g + m_2 (l_i - l_2) \widehat{l_i} \times g + l_i \widehat{l_i} N_i^L + M_i \\ &\quad = (I_1^R + I_2^R)\omega_i \times \omega_i + (I_1^R + I_2^R)\alpha_i + m_1 l_1 \widehat{l_i} \times a_{i,1} + m_2 (l_i - l_2)\widehat{l_i} \times a_{i,2} \end{aligned} \tag{2-42}$$

Where,

m_1	Mass of cylinder barrel	[kg]
m_2	Mass of cylinder rod	[kg]
F_i^L	Lateral force at top of cylinder	[kN]
M_i	Moment around the cylinder normal axis transmitted by the universal link	[-]
I_1^R	Mass moment of inertia of lower cylinder chamber	[kgm^2]
I_2^R	Mass moment of inertia of upper cylinder chamber	[kgm^2]
α_i	Angular acceleration of the cylinder	
$a_{i,1}$	Acceleration of lower cylinder chamber	[m/s^2]
$a_{i,2}$	Acceleration of upper cylinder chamber	[m/s^2]

All the unknown from equation 2-42 have to be determined one by one. The mass of the cylinders are already obtained in the previous section. It is assumed that the cylinder does not rotate around its own axes. The angular velocity will be perpendicular to the the unit vector ($\hat{l}_i$). The angular velocity and acceleration of the cylinder can be derived from the velocity and acceleration of the bottom platform, equation 2-16 and 2-18, as described in [8] and [9]:

$$\omega_i = (\hat{l}_i \times \dot{b}_i)/l_i \tag{2-43}$$

$$\alpha_i = (\hat{l}_i \times \ddot{a}_i - 2\dot{l}_i\omega_i)/l_i \tag{2-44}$$

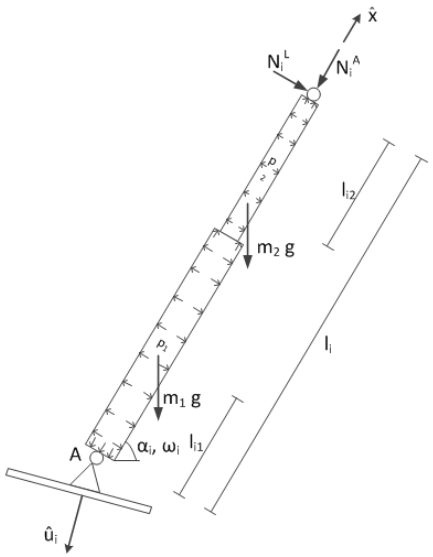

Figure 2-11: Schematic drawing of hydraulic cylinder

Both the barrel and the moving rod of each cylinder have an acceleration vectors due to the rotation, respectively a_{i1} and a_{i2}:

$$a_{i1} = l_1\omega_i \times (\omega_i \times \hat{l}_i) + l_1\alpha_i \times \hat{l}_i \tag{2-45}$$

$$a_{i2} = (l_i - l_2)\omega_i \times (\omega_i \times \hat{l}_i) + (l_i - l_2)\alpha_i \times \hat{l}_i + 2\omega_i \times \dot{l}_i\hat{l}_i + \ddot{l}\hat{l}_i \tag{2-46}$$

The moment of inertia of the upper and lower part of the cylinder still have to be determined with reference to the rotating bottom (I_i^R) frame. This is done with the use of a transformation matrix ($\underline{\underline{T}}$). Due to the rotation of the bottom frame, a new axis for the cylinder has to be determined. The x vector is along the line of the cylinder, the y vector is perpendicular to the horizontal plane of the cylinder and the z vector follows from the other two vectors:

$$\begin{aligned} \hat{x}_{ci} &= \hat{l}_i \\ \hat{y}_{ci} &= \begin{bmatrix} -\dfrac{l_{iy}}{\sqrt{l_{ix}^2 + l_{iy}^2}} & \dfrac{l_{ix}}{\sqrt{l_{ix}^2 + l_{iy}^2}} & 0 \end{bmatrix}^T \\ \hat{z}_{ci} &= \hat{x_{ci}} \times \hat{y_{ci}} \end{aligned} \tag{2-47}$$

Where,

$$\underline{\underline{T}} = \begin{bmatrix} \hat{x}_{ci} & \hat{y}_{ci} & \hat{z}_{ci} \end{bmatrix} \tag{2-48}$$

The moment of inertia along these three axis can be obtained from the inner and outer dimensions of the cylinders, leading to the inertia matrices of the cylinder (with j=1,2 for the two parts of the cylinder):

$$\overline{I}_{j,i} = \text{diag}(\begin{bmatrix} I_{xx} & I_{yy} & I_{zz} \end{bmatrix}) \tag{2-49}$$

Combining the transformation matrix from equation 2-48 and the moment of inertia of the cylinder parts from equation 2-49, the mass moment of inertia can be obtained that is required

for the cylinder dynamic equation 2-42:

$$I_{j,i}^{R} = \underline{\underline{T}}\overline{I}_{j,i}\underline{\underline{T}}^{T} \tag{2-50}$$

The revolting gimbals will transmit a moment from the moving bottom platform to the cylinders. This moment can be described as:

$$M_i = m_i \hat{u}_i \tag{2-51}$$

Where,

m_i	Magnitude of reaction moment	[kNm]
$\hat{u}_i$	Unit vector normal to bottom platform	[-]

The magnitude of the reaction moment is derived by rewriting equation 2-42:

$$l_i \hat{l}_i \times N_i^L + m_i \hat{u}_i = N_i \tag{2-52}$$

With,

$$\begin{aligned} N_i = &-m_1 l_1 \widehat{l}_i \times g - m_2 (l_i - l_2)\widehat{l}_i \times g + (I_1^R + I_2^R)\alpha_i \\ &- (I_1^R + I_2^R)\omega_i \times \omega_i + + m_1 l_1 \widehat{l}_i \times a_{i,1} + m_2 (l_i - l_2)\widehat{l}_i \times a_{i,2} \end{aligned} \tag{2-53}$$

By taking the dot product of equation 2-52 with $\hat{l}_i$, the lateral force drops out of the equation, as it is normal to the unit vector. The magnitude of the reaction moment becomes:

$$m_i = \frac{N_i \cdot \hat{l}_i}{\hat{u}_i \cdot \hat{l}_i} \tag{2-54}$$

All the unknowns from equation 2-42 are solved and now the lateral forces can be calculated that follow from the vessel motions.

Total cylinder forces

The total cylinder force can be derived by combining the axial cylinder force obtained from the external loads and the lateral cylinder force obtained from the internal cylinder dynamics. The lateral cylinder force is included in equation 2-32:

$$\left(N_i^a\right)^2 + \left(N_i^L\right)^2 = \left(\left(\underline{\underline{J}}^T\right)^{-1} W\right)^2 \tag{2-55}$$

The lateral forces are subtracted from the external loads, and with that the axial reaction forces are obtained that the cylinders of the Stewart Platform have to deliver during operation with certain vessel motions.

Example of axial and combined cylinder forces are given in Figure 2-13. The run contains vessel motions of 1 minute in time steps of 0.2 seconds, Figure 2-12. The loads on top of the Stewart platform are during normal operation of cargo transfer with use of the GXXL.

During the run of 1 minute is can be seen that the total cylinder forces are only a few kN's higher for every cylinder, when calculated with the cylinder dynamics. This change is almost only due to the weight of the cylinders. The motion of the cylinders can be assumed to be negligible. The forces due to the gangway and transfer deck are much higher than the forces due to the motion and weight of the cylinders.

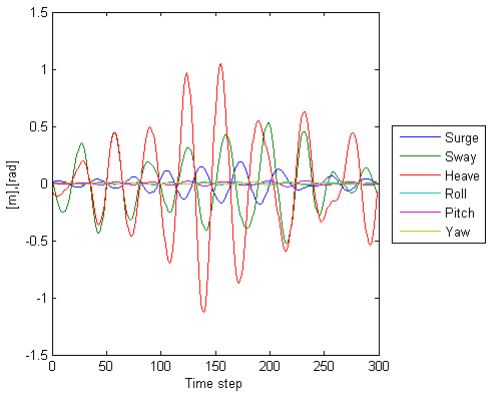

Figure 2-12: Vessel motions over 1 min. with time step of 0.2 sec.

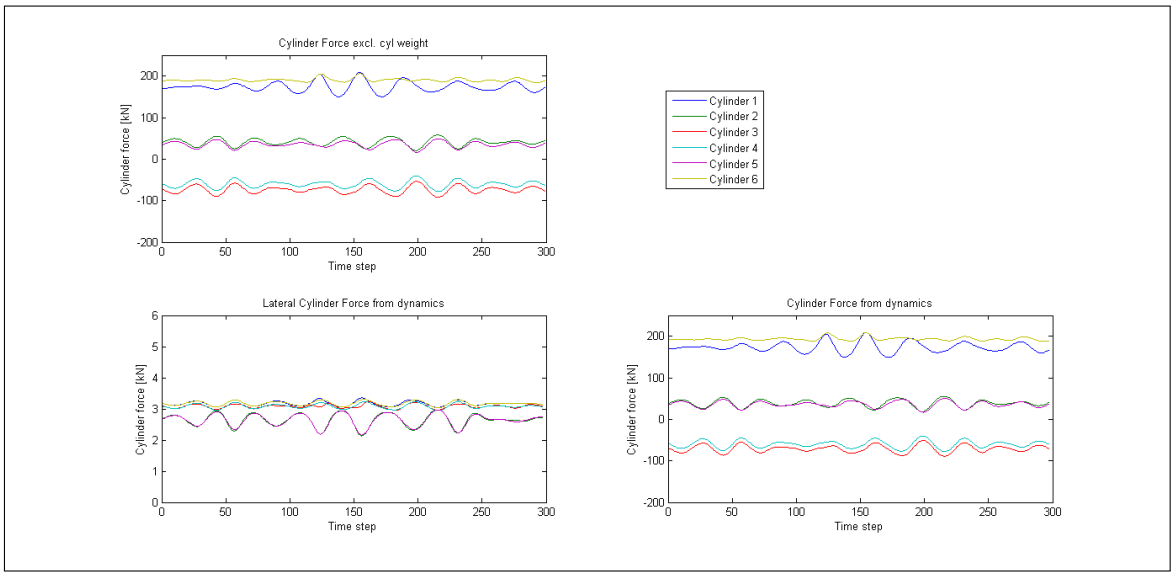

Figure 2-13: Cylinder forces over vessel motions

2-5 Dexterity

With the cylinder length known from 2-3-3, the functioning of the system has to be checked. This is done by looking at the singularities and the dexterity. `Singularities` in a system represent how well the position and orientation of the platform can be controlled. Or in other words, how a system 'behaves'. A good functioning of the Stewart platform requires low

singularities as the system may not show unpredictable behaviour at a certain configuration. Singularity can cause more degrees of freedom to occur in the system and/or lead to high actuator forces.

The `dexterity` is a measurement tool for the singularity. It measures the kinematic performance of the parallel manipulator. This can be seen as the ability of the system to change its position and orientation. The dexterity has a characteristic value between zero and one for a every position of the platform. A value of zero means that the singularities will occur and a high value means that the system operates in good manner and the actuator lengths will change efficiently relative to the platform [10]. With the dexterity the actuator forces and velocities can be kept within reasonable limits, to prevent it of becoming unstable. The dexterity of the system has to be checked for all possible positions, through the entire workspace of the system. This is checked with the use of the Jacobian Matrix described in the previous section.

The `Jacobian Matrix` is described to a frame of reference. To determine the dexterity, the frame of reference is the rotating frame. In this study, the top frame is presumed fixed and the bottom frame rotates and translates with the vessel motion. However, the bottom frame is fixed in the Stewart platform and the top frame moves. Only it moves with the same motions as the vessel, making it stay 'fixed' (see Figure 2-14). For the dexterity check, the frame of reference is the rotating top frame, the Jacobian matrix becomes:

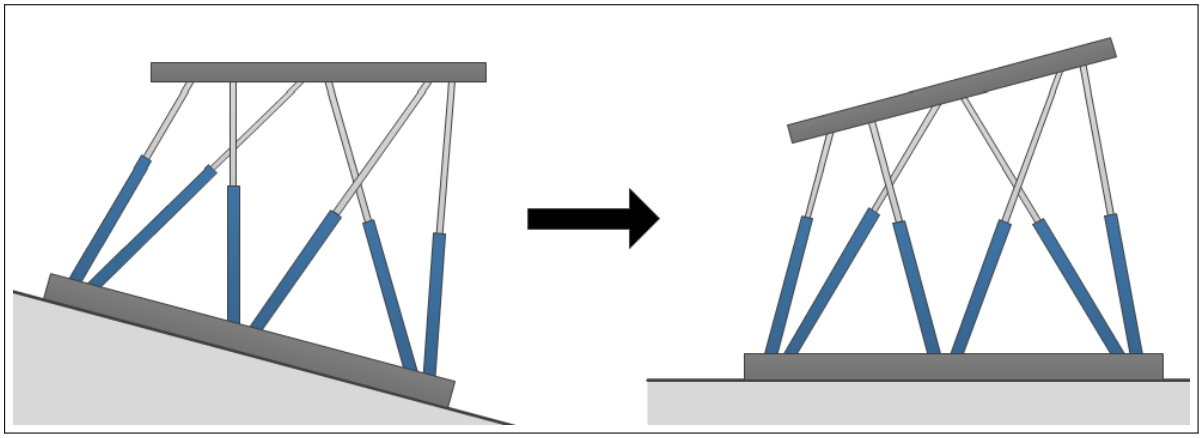

Figure 2-14: Rotating frame of reference

$$\underline{\underline{J}} = \begin{bmatrix} \widehat{\underline{l}}_{x1} & \widehat{\underline{l}}_{y1} & \widehat{\underline{l}}_{z1} & (\widehat{\underline{l}}_1 \times \underline{y}_{r1})^T \\ \widehat{\underline{l}}_{x2} & \widehat{\underline{l}}_{y2} & \widehat{\underline{l}}_{z2} & (\widehat{\underline{l}}_2 \times \underline{y}_{r2})^T \\ \vdots & \vdots & \vdots & \vdots \\ \widehat{\underline{l}}_{x6} & \widehat{\underline{l}}_{y6} & \widehat{\underline{l}}_{z6} & (\widehat{\underline{l}}_6 \times \underline{y}_{r6})^T \end{bmatrix} \tag{2-56}$$

The condition number (κ) gives the effort that the actuator has to deliver in order to achieve the velocities in the coordinates of the moving platform. It is also called the amplification factor, which shows the gain of the Jacobian matrix and can be written as:

$$\kappa = ||\underline{\underline{J}}||\ \ ||\underline{\underline{J}}^{-1}|| \tag{2-57}$$

To come to the dexterity of the platform only the eigenvalues have to be determined. The eigenvalues can be found with the use of singular value decomposition. The non-zero elements in a singular value composition are the square root of the non-zero eigenvalues of the Jacobian matrix:

$$\underline{\underline{J}}_s = \begin{bmatrix} \sigma_1 & 0 & 0 & 0 & 0 & 0 \\ 0 & \sigma_2 & 0 & 0 & 0 & 0 \\ 0 & 0 & \sigma_3 & 0 & 0 & 0 \\ 0 & 0 & 0 & \sigma_4 & 0 & 0 \\ 0 & 0 & 0 & 0 & \sigma_5 & 0 \\ 0 & 0 & 0 & 0 & 0 & \sigma_6 \end{bmatrix} \tag{2-58}$$

The condition number is now determined with the maximum and minimum singular values from the matrix [11]:

$$\kappa = \frac{\sigma_{max}(||\underline{\underline{J}})||}{\sigma_{min}(||\underline{\underline{J}})||} \tag{2-59}$$

Where a condition number of one gives the best possible condition of the system. When κ becomes infinite, the system is in a singularity condition.

The inverse of the condition number, with a value between zero and one, represents the dexterity (D). And the a value of zero shows that the inverse Jacobian matrix is singular.

$$D = \frac{1}{\kappa} = \frac{\sigma_{min}(||\underline{\underline{J}})||}{\sigma_{max}(||\underline{\underline{J}})||} \tag{2-60}$$

As is showed above, the Jacobian and the dexterity both depend on the architecture and pose of the system. The best pose and architecture of the system can be chosen by minimizing κ. For the Ampelmann system a minimum allowable dexterity of 0.12 is chosen, based on many researches of the system in the flight simulator motion bases [4] and on testing of the Ampelmann Demonstrator [12]. For all position of the platform, the dexterity should not be below the minimum value. This value is used in Chapter 4, where the geometry of the Stewart platform is optimised for the best cylinder force distribution

2-6 Workspace

The vessel motions are measured by the Octans and the Control system determines the required cylinder lengths to counteract these motions. The transfer deck of the Ampelmann system should stay fixed with respect to the offshore structure. The workspace of a Stewart platform is highly non-linear and the physical interpretation is not straight forward. The movement of the platform has boundaries, which form the workspace of the Ampelmann system. The boundaries are the length of the cylinders, which are:

$$l_{min} \leq l_i \leq l_{max} \tag{2-61}$$

The length of each cylinder influences each other, as all the six cylinders are all connected to the top and bottom frame. In other words, the displacement in one degree of freedom

depends in the displacement in the other five degrees of freedom. For example, the heave compensation will increase if the yaw angle decreases. For each degree of freedom a part of the cylinder stroke needs to be conserved.

The workspace for the entire Stewart platform can be determined by imposing a lot of different poses of the platform and checking it for the criterion of equation 2-61. To be able to control the workspace and avoid high forces in the system due to extreme platform poses, the workspace of the Ampelmann is given some limitations by the control software. The limitations are shown in Table 2-4. The sway and surge motions are coupled in the control system, reducing the workspace in the x-y-plane to a circle ($x^2 + y^2 \leq 1.00$ [m]). The yaw rotation is set to zero as this motion can be compensated by the slewing motion of the gangway 3-2-3.

Translation			Rotation		
Sway	$-1.00 \leq x \leq 1.00$	[m]	Roll	$-15 \leq \phi \leq 15$	[°]
Surge	$-1.00 \leq y \leq 1.00$	[m]	Pitch	$-15 \leq \theta \leq 15$	[°]
Heave	$-1.20 \leq z \leq 1.20$	[m]	Yaw	$0 \leq \psi \leq 0$	[°]

Table 2-4: Workspace limitations

Next to these limitations, the control system also uses a asymptote function, to avoid extreme platform motions. Each DoF is smoothly limited towards its maximum value.

The workspace of the current A-type can be plotted in fifteen sub-plots of two DoF. These plots are used in Chapter 4, where the workspace of the optimised geometry can be compared with the current workspace. The red squares are the positions what the cylinder can reach and the blue squares are the positions where at least one of the cylinders has exceeded the minimum or maximum value.

2-6-1 Workability

The workspace of the system influences the workability of the Ampelmann system. The `workability` is the percentage that the system can be used at sea. When the sea is too rough and the vessel motions become too large, the system can not compensate these motions any more. This means that the system does not function any more.

The workspace shows all the positions that the platform can reach, but some DoF are more important than others. The sway motion for example is not important to compensate, but the heave motion is important for the workability. At the moment their are certain studies preformed at the company Ampelmann, where the workability of the system is optimised. In these studies the workspace is reduced in certain DoF to increase the workability. It can already be concluded from these studies that a sufficient workspace for system is required, but a smaller workspace does not necessary mean a reduction of the workability. This knowledge will also be used in Chapter 4.

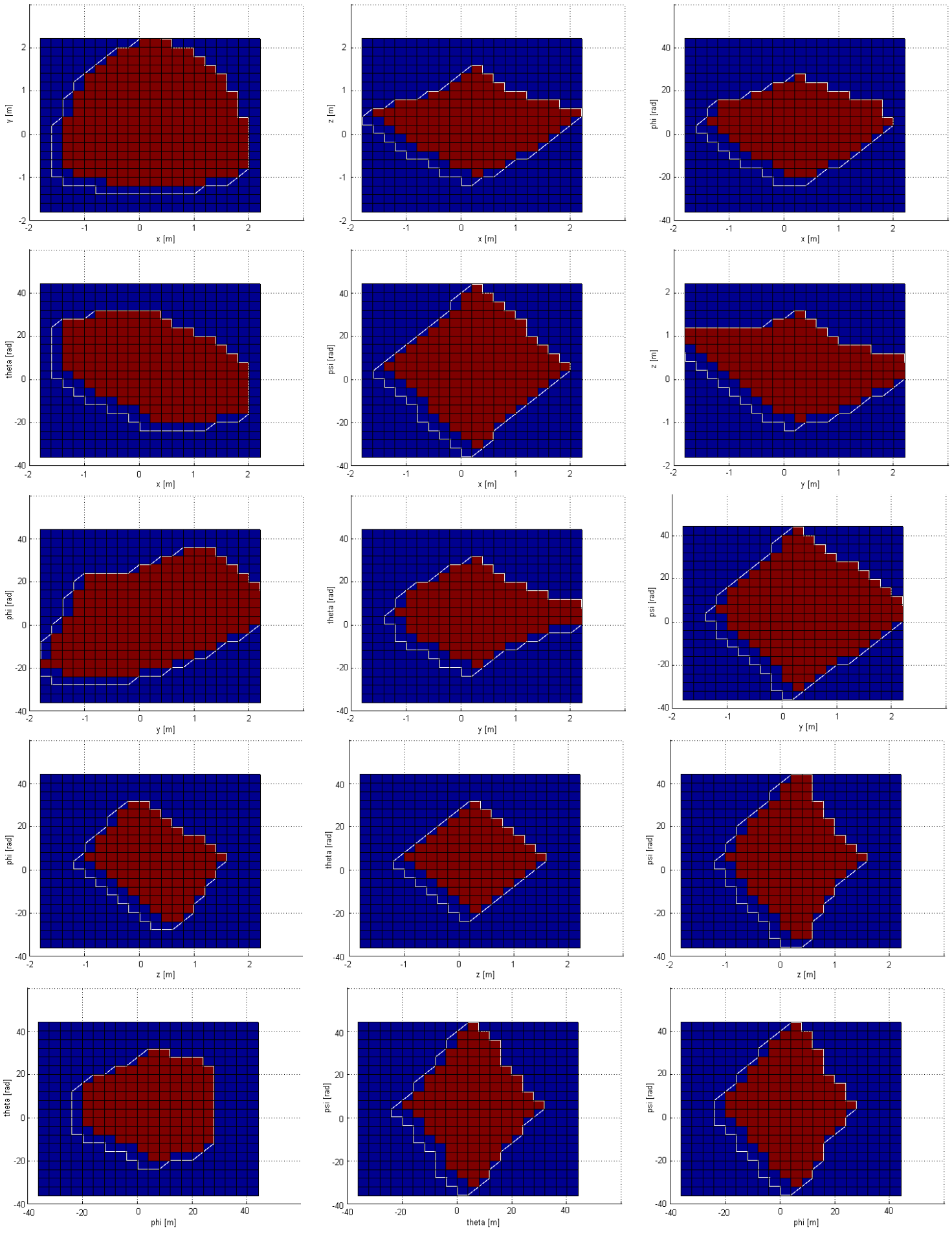

Workspace current A-type

2-7 Concluding remarks

In this chapter the functioning of the Ampelmann system is explained and all the knowledge and required calculation methods for the cylinder force distribution, dexterity and the workspace of the Stewart platform are found.

Cylinder forces In this chapter the cylinder forces are first derived from the external loads only with the use of the Jacobian matrix. This led to the axial reaction forces. After that the lateral forces were included by also using the weight of the cylinders and their position. This method is used to determine the cylinder forces at every position in the workspace. The third method was the cylinder dynamic approach, which also included the motion of the cylinders. This method was used to see whether the motions of the cylinders would contribute to higher cylinder forces during operation. It can be concluded that the motion of the cylinders does not contribute to significant larger cylinder forces. For the rest of this research the second method will be used, which included the weight and the position of the cylinders.

Dexterity From different researches ([4] among other) the minimum dexterity is suggested at 0.2 for good controllability of the system. In the current Ampelmann system, the minimum dexterity is 0.12 is used. As the controllability of the current system is good, the constraint for the minimum dexterity for this research is also set at 0.12. This means that geometries with a lower dexterity will not be used.

Workspace The workspace of the Stewart platform represents all the position the platform can reach before one cylinder reaches its minimum or maximum length. Of the current A-type, the workspace is shown in fifteen sub-plots in Figure XX in section 2-6. The workability of the system shows the percentage that the system can be used in a sea state. This workability is coupled to the workspace of the system, but does not fully depend on it. The control method of the Ampelmann system has also an influence on the workability. A maximum allowable displacement in one DoF depends on the displacements in the other five DoF. By limiting one DoF, a larger displacement in other DoF is possible. For the optimisation of the geometry in Chapter 4 it is possible that the workspace will be reduced, but this does not have to affect the workability of the system.

These calculation methods will be used in during the optimisation of the Stewart platform in Chapter 4 to 6.

Chapter 3

Loads on Stewart platform by GXXL

3-1 Introduction

In previous chapter, the first three components of the Ampelmann system are elaborated with the focus on the Stewart platform. The cylinder forces of the platform are derived from the mass and position of the cylinders (internal forces) and from the load case caused by the gangway on top of the platform (external load). The latter has the largest influence on the cylinder forces. In this chapter the load cases are obtained that will be used in the remaining of this report. The largest gangway (the GXXL) can not be placed on top of the current A-type system, because the cylinder forces exceed the operation limit. This means that the cylinders are not able to extract and with that compensate the vessel motions. To be able to optimise the Stewart platform for the GXXL, the corresponding load cases are determined in this chapter.

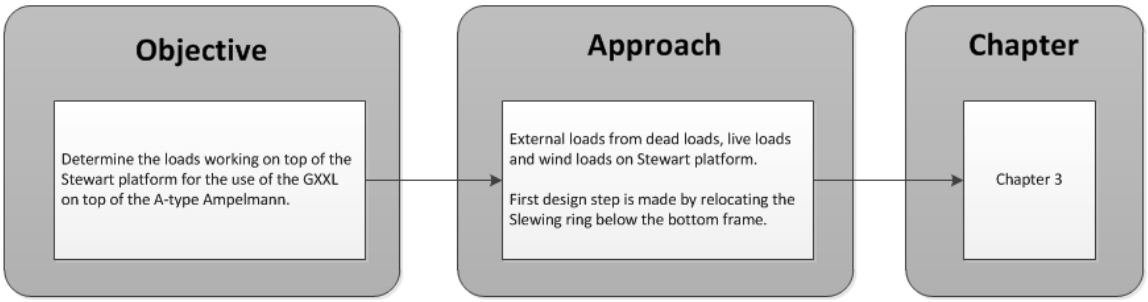

Figure 3-1: Approach Chapter 3

3-2 GXXL loadcase

The load case of the gangway is divided in the dead load and the live load of the system. The dead load contains the mass of all the elements and the associated forces and moments. The live load consists out of the forces and moments due to motions and extra added weight (people or cargo), during operation. This difference is relevant for the optimisation of the Stewart platform. The dead load of the system is always present, but the live load may vary during operation.

3-2-1 Dead loads

All the components of the GXXL contribute to the load case on top of the Stewart platform. In Table 3-1 the main components are summarised with their masses and their CoG with respect to the middle point of the top frame. These distances cause the downward force of the components to create a moment on top of the platform. The critical loads are needed for the new designs of the Stewart platform, for this reason the gangway is fully extracted for all the loads calculations.

Elements	mass [kg]	CoG x [m]	CoG y [m]	CoG z [m]
(1) T-Boom	1585	0.00	23.33	1.78
(2) Main Boom	4562	0.00	9.57	1.68
(3) Transfer deck	1907	-0.18	-1.68	2.08
(4) Base Frame	3443	0.00	-1.52	1.03
(5) Star Frame	2091	0.00	-2.42	0.59
(6) Luffing cylinders	1160	0.00	-1.935	2.03
(7) Slewing ring	866	0.00	0.00	0.53
(8) Counter Weight	4253	0.00	-2.42	0.59
(9) Star Frame	2091	0.00	0.00	0.18
(10) Upper Gimbals	534	0.00	0.00	0.00

Table 3-1: Mass elements of Ampelmann system

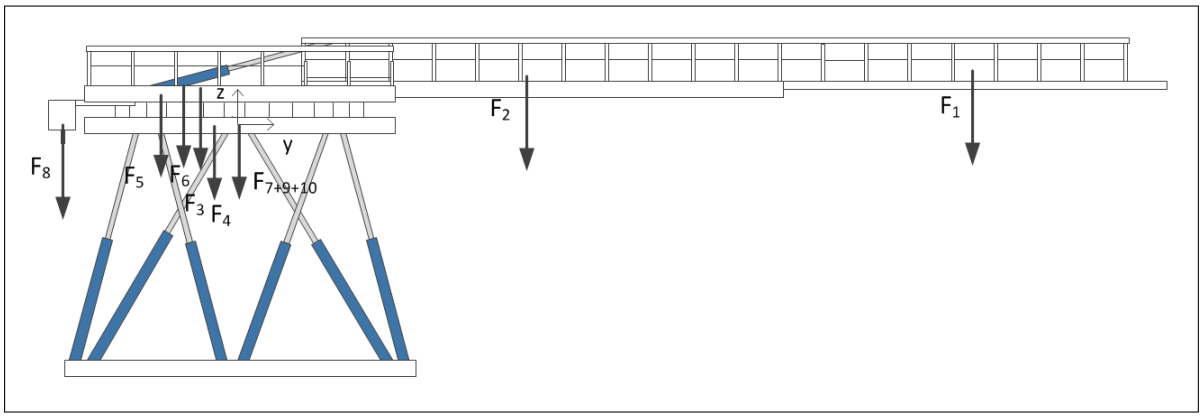

Figure 3-2: Dead loads

With the masses of every element and the position of their CoG with respect to the CoG of the top platform, the forces and moments can be calculated. These static loads are shown in Table 3-2.

	Dead loads	
F_x	0	[kN]
F_y	0	[kN]
F_z	-221	[kN]
M_x	-497	[kNm]
M_y	-12	[kNm]
M_z	0	[kNm]

Table 3-2: Dead loads at Upper Gimbal Level

3-2-2 Live loads

Next to the static forces that work on the platform due to the dead load of the components above the Stewart platform, their are also live loads present on the system for the people standing on the Ampelmann or cargo which is transferred. These operations are done separately, so the external loads are from now on divided into people transfer operation and cargo transfer operation (Figure 3-3 and 3-4). The person on the transfer deck is the operator who controls the motions of the gangway.

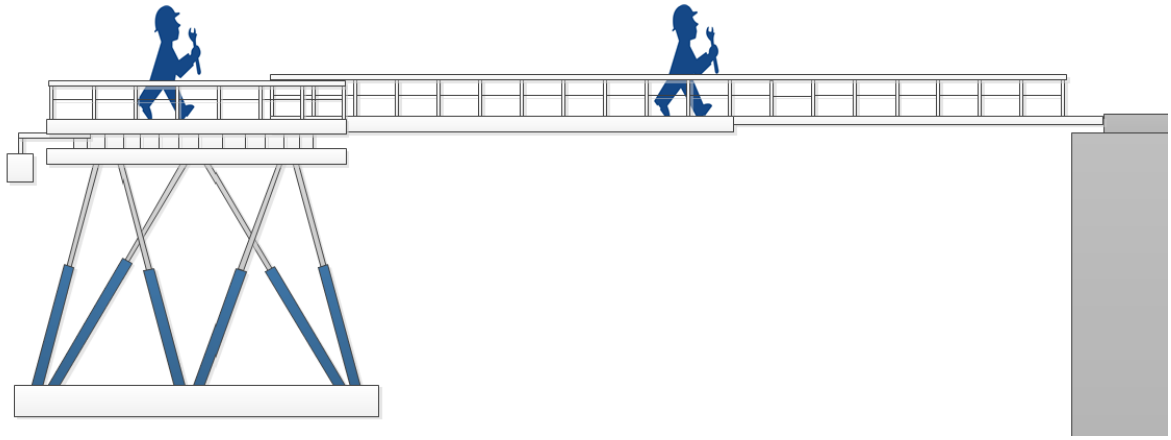

Figure 3-3: People transfer

People on Ampelmann The number of people on the Ampelmann depends on the operation mode as described above. It is assumed that people walk slowly over the gangway and stand still on the transfer deck. The live load due to personnel is seen as a static force.

Cargo transfer Cargo is transferred on the tip of the gangway. When the GXXL is used in a lifting crane manner, the cargo is subjected to wind loading. In this report it is assumed that the cargo transfer is only preformed by placing cargo on the tip of the gangway. The maximum cargo that is allowed to be transferred is 1000 kg.

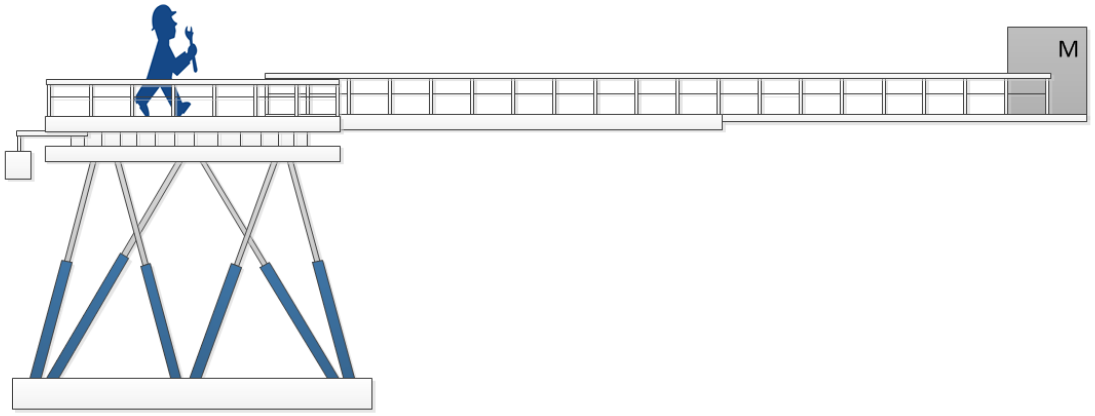

Figure 3-4: Cargo transfer

3-2-3 Other conditions

Next to the different factors that influence the loading case, their are also some other rules and conditions of the Ampelmann system such as [13]:

People on Transfer deck A maximum of 21 people (of 100 kg pp) is allowed on the transfer deck during motion compensation.

People on Gangway For the GXXL two people (of 100 kg pp) are allowed on the gangway at the same time, one on the main boom and one on the t-boom.

Cargo transfer Cargo can be lifted at the tip of the GXL. The maximum weight of the cargo is M = 1000 kg.

Platform accelerations When the Ampelmann system is in Stowed Condition or during Emergency Case, in the worst case scenario, the Stewart platform does not compensate the vessel motions. The maximum vessel accelerations are set at 2 m/s^2 in every direction.

During normal procedure, the Stewart platform compensates the vessel motions. However, when the wave conditions are more severe than the design conditions (H_s = 2.5 m), the Stewart platform is not able to compensate all the vessel motions and residual motions of the transfer deck occur. The residual motions in the system are set for accelerations of 0.5 m/s^2 in x- and y-direction and 0.5 m/s^2 in z-direction.

Gangway motions The Stewart platform can translate and rotate in 3 directions, leading to the 6DoF. Next to the platform, the gangway has three types of motions: telescoping, slewing and luffing (Figure 3-5). All three motions also create a force on top of the Stewart platform. The maximum force due to telescoping during normal people transfer procedure is 10 kN in y-direction, when the gangway is pushed against the offshore platform. The luffing

motion does not create forces onto the platform, it only changes the angle of the gangway. The largest load case is when the gangway is in horizontal position and fully extracted. The force due to the slewing motion is set at 1 kN in x-direction to take into account friction.

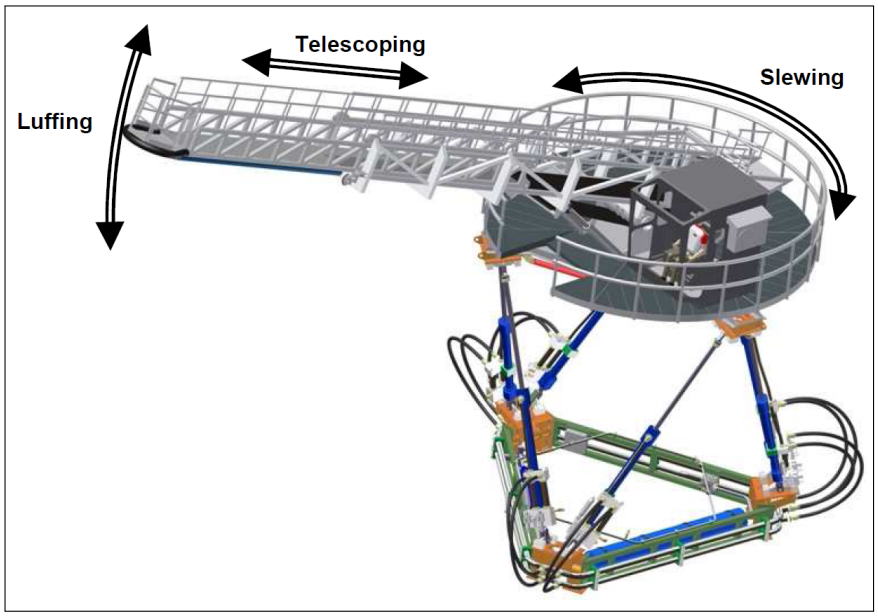

Figure 3-5: Residual motions of gangway

Slewing accelerations The slewing motion of the gangway around the z-axis of the Stewart platform has a maximum tangential acceleration (a_T) of 0.6 m/s^2. The angular acceleration is calculated by dividing the tangential acceleration with the total length of the gangway in the horizontal direction. The angle of the gangway with the x-y-plane (α_{GXL}) is also has to be taken into account:

$$a_{slewing} = \frac{a_T}{(l_{MB} + l_{TB,re} + \Delta l_{TB,ex}) \cdot \cos\alpha_{GXL}} = 0.021 \quad [\text{rad/s}^2] \tag{3-1}$$

Where,

l_{MB}	Length main boom = 17.75	[m]
$l_{TB,re}$	Extension T-boom when retracted	[m]
$l_{TB,ex}$	Extension T-boom when extracted ($l_{TB,re} + \Delta l_{TB,ex}$ = max 10.82)	[m]

3-2-4 Loads from dead and live loads

The live loads from the Ampelmann system can be added to the dead loads from Table 3-2. The new loads are obtained with the use of the load case factors and accelerations from the platform and the slewing motion. The forces in x- and y-direction are calculated with the following equation:

$$F_{x,y} = (a_{x,y} + a_{slew,x,y}) \cdot F_{dead} + (a_{x,y} + a_{slew,x,y}) \cdot F_{live} \tag{3-2}$$

		NO-PT	NO-CT
F_x	[kN]	-13	-14
F_y	[kN]	12	13
F_z	[kN]	-248	-258
M_x	[kNm]	-551	-853
M_y	[kNm]	-42	-49
M_z	[kNm]	53	50

Table 3-3: Dead and live loads at Upper Gimbal Level

The difference in loads can be explained by the cargo of 1000 kg that is located at the tip during cargo transfer.

3-3 Wind load

The Ampelmann system operates offshore where high wind speeds can occur. The GXXL is designed to be functional up to 16 m/s wind speed for people transfer and 13 m/s for cargo transfer. The wind creates a static and a dynamic load on the system. In current use, no flutter has occurred. For this research it is assumed that no flutter of the gangway occurs, which has an impact on the load case on top of the Stewart platform.

The critical wind direction is perpendicular to the gangway. The static load is obtained with the use of the frontal area of the system. This load will be added to the loads from Table 3-3. For normal operation, the moment created by wind load on the gangway is compensated by the slewing motion of the gangway for the current Ampelmann. The wind load on the transfer deck and base frame are compensated by the cylinders of the Stewart platform.

3-3-1 Static wind load on transfer deck

The static wind load depends on the frontal area of the gangway and Stewart platform, wind pressure, force coefficient (C_f) and shielding factor (η). The shielding factor is taken into account because the transfer deck consists out of elements that are behind each other. The total expression of the wind force is from section 2.12.4 of the CLAME [14]:

$$\begin{aligned} F_{w,TD} &= A_e \cdot p \cdot C_f(1+\eta) \cdot \frac{A}{A_e} \\ F_{w,BF,ST} &= A_e \cdot p \cdot C_f \cdot \frac{A}{A_e} \end{aligned} \tag{3-3}$$

Where,

A	Effective area of the structure	[m^2]
p	Wind pressure	[N/m^2]
C_f	Force coefficient in the direction of the wind	[-]
η	Shielding factor	[-]
A_e	Enclosed area	[m^2]

Frontal area The frontal area of the Ampelmann is divided into the frontal area of the transfer deck, base frame and star frame. From [13] the enclosed frontal area are: $A_{TD} = 9.00$ m^2, $A_{BF} = 3.30$ m^2 and $A_{SF} = 3.18$ m^2.

Wind pressure The wind pressure on the Ampelmann system follows from this expression:

$$p = 0.613 \cdot v_{wind}^2 \tag{3-4}$$

From equation 3-4 follows that for people transfer $p_{PT} = 157$ N/m^2 and for cargo transfer $p_{CT} = 104$ N/m^2.

Force coefficient C_f This coefficient is determined with the aerodynamic slenderness of the system, which is the length width ratio. The coefficient for all three elements are: $C_{f,TD} = 1.35$, $C_{f,TD} = 1.70$ and $C_{f,TD} = 1.35$. [13]

Shielding factor The shielding factor follows from the solidity ratio and the spacing ratio of the framework the elements. The solidity ratio is area of solid parts divided by the total enclosed area. The base and star frame both exist out of a solid frame, so the ratio is 1.00. This gives a shielding factor of 1.00. For the transfer deck the solidity ratio is 0.60. The spacing ratio is the width of the transfer deck divided by the height and is 4.00. This gives a shielding ratio of 0.45.

Distance to centre top platform The moment created by the wind force depends on distance from the centroid of the element to the centre of the top frame. These are:

Elements	x [m]	y [m]	z [m]
Transfer deck	-0.38	-0.92	1.23
Base Frame	0.08	-0.64	0.87
Star Frame	0.00	0.00	0.2

Table 3-4: Centroid element to centre top platform

3-3-2 Static wind load on gangway

The gangway consists out of the main boom and the T-boom. These two parts partly overlap and consist multiple lattice elements. The total wind load is calculated following the steps section 2.12.7 of the CLAME [14]:

$$F_w = A_e \cdot p \cdot C_f \left(\frac{1 - \eta^n}{1 - \eta} \right) \cdot \frac{A}{A_e} \tag{3-5}$$

Where,

n	Number of frames = 2	[-]

The gangway also has banners that cashes wind. For the total force of the wind is the summation of the force on the gangway and the force on the banners:

$$F_{w,tot} = F_{w,GW} + F_{w,banner} \tag{3-6}$$

Frontal area For both the fully extracted and retracted case, the frontal area of the gangway is determined. Following from [13] the enclosed frontal area of the retracted gangway is 20.9 $\cdot$ 2 = 41.8 m^2 and the extracted gangway is 29.9 $\cdot$ 2 = 59.8 m^2. For conservative reason it is assumed that there is no overlap in the lattice elements of the main and T-Boom. For the same conservative reason is the surface area of the banner on the gangway determined for the open area it is placed in front. This surface are for the main boom is $A_{banner,MB}$ = 19.88 m^2 and for the T-boom is $A_{banner,TB}$ = 11.45 m^2.

Wind pressure The banner on the gangway is of the material Air mesh and has a permeability of v_{perm} = 11000 l/m^2s. The effective wind velocity that works on the banner is:

$$v_{eff,PT} = v_{wind} - v_{perm} \cdot 10^{-3} \tag{3-7}$$

From expression 3-7 follows that the effective speed for people transfer is: $v_{eff,PT}$ = 5 m/s, with a pressure of 15.325 N/m^2. For cargo transfer $v_{eff,CT}$ = 2 m/s, with a pressure of 2.452 N/m^2.

Force coefficient C_f The smallest ratio for the aerodynamic slenderness of the gangway is for the diagonal element of the T-boom of the GXXL. This ratio is 1214/40 = 30 [-]. For hollow sections, from CLAME Table 4.2.4 [14], this ratio leads to C_f = 1.65 [-].

For the banner on the main boom of the GXXL the aerodynamic slenderness is 1775/112 = 15.8 [-] and for the banner on the T-boom the ratio is 14145/83 = 17 [-]. This leads to a C_f of 1.48 and 1.50.

Shielding factor The shielding factor follows from the solidity ratio and the spacing ratio of the framework of the gangway.

$$\begin{aligned}
\text{Solidity ratio}_{retr} &= \frac{A}{A_e} = \frac{13.4}{41.8} &&= 0.32 \quad [-] \\
\text{Solidity ratio}_{extr} &= \frac{A}{A_e} = \frac{13.4}{59.8} &&= 0.22 \quad [-] \\
\text{Spacing ratio} &= \frac{w}{h} = \frac{0.77}{0.9} &&= 0.9 \quad [-] \\
\eta_{retr} & &&= 0.56 \quad [-] \\
\eta_{extr} & &&= 0.72 \quad [-]
\end{aligned} \tag{3-8}$$

For the banner on the GXXL the following applies:

$$\begin{aligned}
\text{Solidity ratio} &= 0.35 \quad [-] \\
\text{Spacing ratio} &= 0.9 \quad [-] \\
\eta_{banner} &= 0.51 \quad [-]
\end{aligned} \tag{3-9}$$

Wind force on gangway When including all the parameters in equation 3-5, the force on the extracted gangway is:

$$\begin{aligned} F_{GW,PT} &= 5.86 \quad [\text{kN}] \\ F_{GW,CT} &= 3.88 \quad [\text{kN}] \\ F_{MB,banner,PT} &= 0.68 \quad [\text{kN}] \\ F_{TB,banner,PT} &= 0.39 \quad [\text{kN}] \\ F_{MB,banner,CT} &= 0.11 \quad [\text{kN}] \\ F_{TB,banner,CT} &= 0.06 \quad [\text{kN}] \end{aligned} \tag{3-10}$$

It can be concluded that the banners have an effect negligible effect on the horizontal loads.

Total loads on platform When including all above determined parameters in equation 3-3, this lead to a total static wind load on the Stewart platform. When adding these forces to the dead and live load forces from Table 3-3, the total forces on the top will be:

		NO-PT	NO-CT
F_x	[kN]	-23	-22
F_y	[kN]	12	13
F_z	[kN]	-248	-258
M_x	[kNm]	-551	-853
M_y	[kNm]	-44	-51
M_z	[kNm]	54	51

Table 3-5: Dead and live loads at Upper Gimbal Level

3-4 Operation modes

The Stewart platform in the Ampelmann system has three operation modes as can be seen in Figure 3-6, from left to right: settled, neutral, engaged. To ensure safe operation of the system, also a safe mode is implemented.

Safe mode The hydraulic pressure is turned on, but the cylinders are not actively controlled. The cylinders remain in retracted condition.

Settled The cylinders are actively controlled, but do not compensate the vessel motions. The cylinders are all retracted: $l_{min} = l_{dead} + l_{stroke} = 1.25 + 2.00 = 3.25m$

Neutral The cylinders are brought to neutral position, but do not compensate yet. The cylinders are at half stroke length: $l_{neutral} = l_{dead} + \frac{3}{2} \cdot l_{stroke} = 4.25m$

Figure 3-6: Operation modes

Engaged Cylinders are actively compensating the vessel motions, where the cylinder length has a maximum of: $l_{max} = l_{dead} + 2 \cdot l_{stroke} = 5.25m$

During the engaged mode, the cylinders can go from l_{min} to l_{max}. If one cylinder of the Stewart platform reaches one of these lengths, the limit of the workspace is found. The workspace of the Stewart platform is already elaborated in section 2-6.

3-4-1 Operation modes platform

The total operation procedure of the Ampelmann system contains different loading conditions, which can be summarised as follows:

1. Normal operation mode
    - Normal operation mode - Start / Ending (NO-SE)
    - Normal operation mode - Motion compensation (NO-MC)
    - Normal Operation - People transfer (NO-PT)
    - Normal Operation - Cargo Transfer (NO-CT)
    - Normal Operation - 2 People transfer (NO-2P)
2. Emergency Case
   These modes are for the emergency case, meaning that the Stewart platform no longer compensates the vessel motions.
    - Emergency Case - Three People transfer (EC-3P)
    - Emergency Case - Cargo Transfer (EC-CT)
    - Emergency Case - 2 People transfer (EC-2P)
    - Emergency Case - KIB Operation (EC-KO)
    - Emergency Case - Extra Length (EC-EL)
3. Stowed Condition (SC)
   This is when the Ampelmann is not in use and the gangway rests on the deck of the sea vessel.

The operation cases are used to check whether the occurring cylinder forces stay below the maximum operation forces (section 3-4-2). The emergency cases are used to check whether the cylinder forces stay below the other failure modes. For the emergency cases, when the platform does not compensate the vessel motions any more, the external loads have to be rotated as the top frame is not fixed any more and rotated along with the bottom frame. In this thesis the focus will be on the operation mode. The goal is to implement the GXXL on the A-type and make it suitable for operation, meaning that the occurring cylinders forces have stay below their operation limit.

3-4-2 Operation limit cylinders

These forces should be kept below the limiting values of the hydraulic cylinders, which are per motion for the A-type:

Motion	Failure mode	Limit value	Unit
Push	Buckling	220	kN
	Stress	445	kN
	Seals	382	kN
	Max operation force	160	kN
Pull	Stress	346	kN
	Seals	291	kN
	Max operation force	124	kN

Table 3-6: Limit values A-type cylinders
[13]

The maximum operation force is obtained from the capacity of the A-type cylinders and the corresponding maximum pressure that the HPU delivers in the Ampelmann system. This limit represents the the maximum forces that the cylinders can counteract and still extract and retract. The A-type cylinders have a inner diameter of the chamber ($d_{b,i}$) of 120 [mm] and a outer diameter of the rod ($d_{r,o}$) of 90 [mm] (Figure 3-7). The pressure (p) in the upper chamber is constant at 250 [bar](=25 [N/mm^2]). For larger lower chamber has a variable pressure. The maximum working load of the cylinders can be calculated with the following formula [15]:

$$\begin{aligned} F_{push} &= \frac{d_{b,i}^2}{4}\pi \cdot p - \left(\frac{d_{b,i}^2 - d_{r,o}^2}{4}\pi\right) \cdot p \quad = 160 \quad [\text{kN}] \\ F_{pull} &= \left(\frac{d_{b,i}^2 - d_{r,o}^2}{4}\pi\right) \cdot p \qquad\qquad\qquad\quad = 124 \quad [\text{kN}] \end{aligned} \tag{3-11}$$

The critical loading condition which will be looked at in the next chapter is during operation mode, so the limiting cylinder forces will also be for operation mode ($F_{max} = 160$ [kN] and $F_{min} = -124$ [kN]).

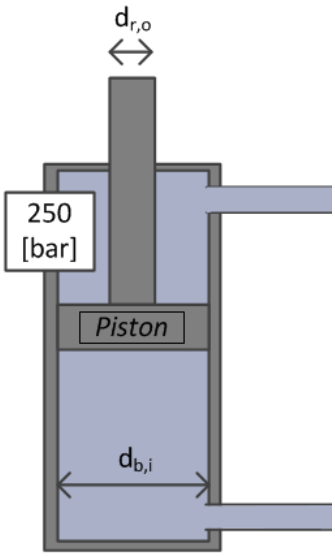

Figure 3-7: Hydraulic cylinder: A-type

3-5 Design A-type with GXXL

In previous sections the last component, the gangway, of the Ampelmann system is elaborated. The external loads caused by the GXXL are derived and implemented in the cylinder force calculation from section 2-4. This leads to cylinder forces that exceed their operation limit,due to the large tipping moment and downward force of the GXXL. There are different methods to improve the Stewart platform, making it better suitable for the large asymmetric load cases. However, before optimising the platform it must be stated that the load case caused by the GXXL is not always orientated in the same direction. In section 3-2-3 is explained that the gangway on top of the Stewart platform can make a slewing motion. This motion is necessary for the gangway to turn from the Stowed Condition, when the gangway is resting on the deck of the vessel, to the offshore platform. Due to this slewing motion, the loading of the platform also rotates around its vertical axis. Leading to cylinders that are sometimes loaded under pressure and other times under tension. Also the angle in which the system is used depends per project. This makes it difficult the optimise the platform.

This problem can be solved by relocating the slewing ring, which makes the slewing motion of the gangway possible, from above the platform to below the platform (Figure 3-8). This has several consequences:

+ The platform rotates along with the loading of the gangway
+ The same cylinders are loaded under tension and pressure
+ Less components above the platform, lowering the total mass of the system
- Larger loads on top of the slewing ring
- The ring has to rotated the whole system in stead of just the gangway
- Moment created by wind load on the gangway is no longer compensated by the slewing ring

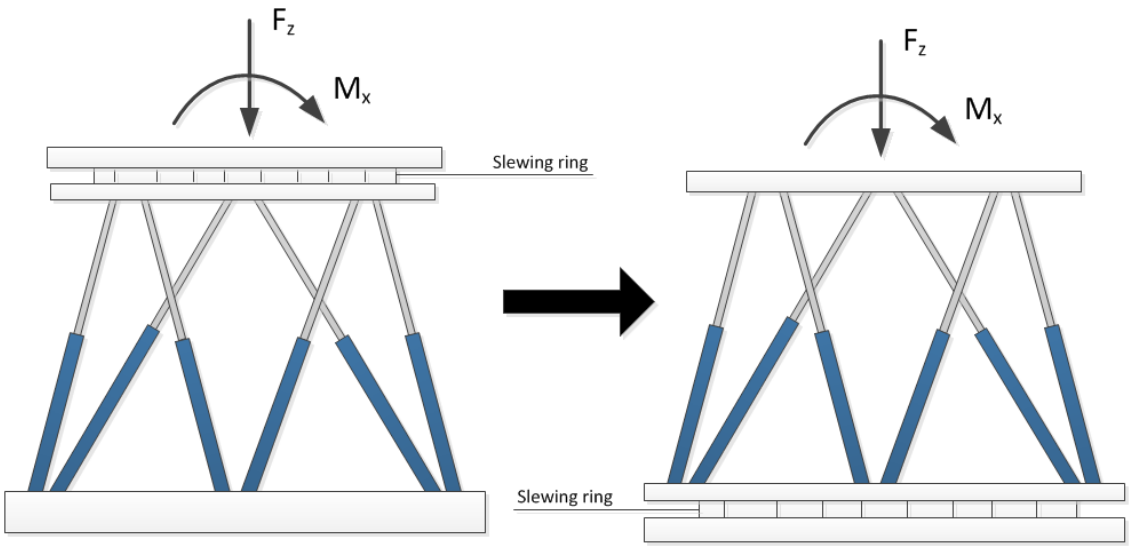

Figure 3-8: Tipping moment by GXXL

Comparing the advantages and disadvantages of this new design of the A-type, the positive effects outweigh the (possible) negative effects. The relocation of the slewing ring has a great positive influence on the possibilities to optimise the Ampelmann system for the asymmetric load cases. The only downside is only that the slewing ring should possibly be redesigned.

The new design of the Stewart platform with the GXXL can be seen in Figure 3-9. The base frame is now connected to the star frame.

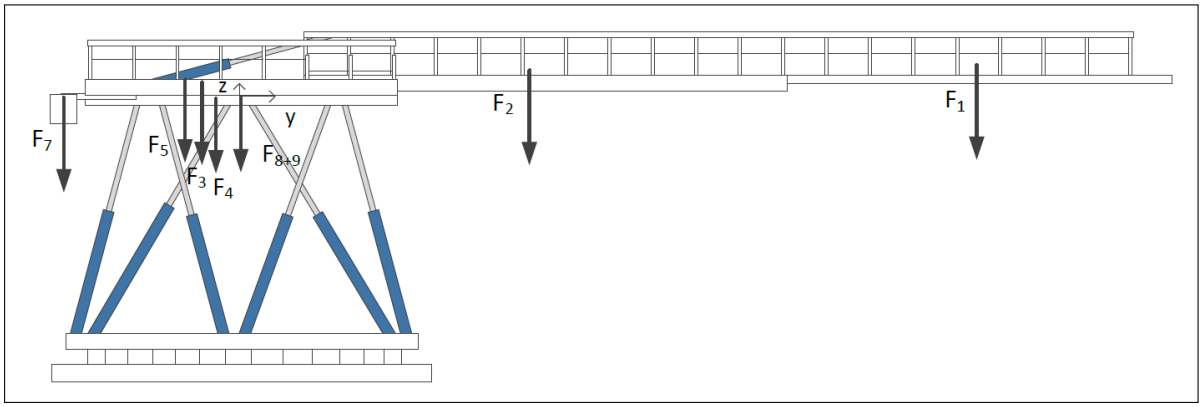

Figure 3-9: Redesign A-type GXXL

The external forces as shown in Table 3-5 have to be altered for the new design. This is done in the next section.

3-5-1 Redefined loads GXXL

The load case for the GXXL is redefined for the design where the slewing ring is below the bottom frame.

Dead and live loads

The loads from the dead and live loads from Table 3-3 are reduced to the following loads.

		NO-PT	NO-CT
F_x	[kN]	-20	-19
F_y	[kN]	11	12
F_z	[kN]	-235	-245
M_x	[kNm]	-550	-851
M_y	[kNm]	-39	-46
M_z	[kNm]	53	85

Table 3-7: Dead and live loads at Upper Gimbal Level for redefined A-type

The relocation of the slewing ring has an influence on the wind load distribution over the system. The moment created by the wind load on the gangway is no longer compensated by the slewing motion of the gangway as in the current A-type. The wind load on the gangway calculated in the section 3-3-2, is recalculated.

3-5-2 Static wind load on gangway

Distance to centre top platform The wind load on the gangway is calculated to the centre of the top platform. The distance depends on the angle of the gangway and is the largest when the gangway is fully extracted in horizontal position.

$$\begin{aligned} y &= \overline{y}_{MB} \cdot A_{MB} + \overline{y}_{TB} \cdot A_{TB}/(A_{MB} + A_{TB}) = 12.77 \quad [\text{m}] \\ z &= \overline{z}_{MB} \cdot A_{MB} + \overline{z}_{TB} \cdot A_{TB}/(A_{MB} + A_{TB}) = 1.78 \quad [\text{m}] \end{aligned} \tag{3-12}$$

Where from [13],

$\overline{y}_{MB}$	Distance centroid$_{MB}$ to centre top platform in y-direction = 8.9	[m]
$\overline{y}_{TB}$	Distance centroid$_{TB}$ to centre top platform in y-direction = 22.7	[m]
$\overline{z}_{MB}$	Distance centroid$_{MB}$ to centre top platform in z-direction = 1.75	[m]
$\overline{z}_{TB}$	Distance centroid$_{TB}$ to centre top platform in z-direction = 1.84	[m]
A_{MB}	Area main boom = 9.66	[m^2]
A_{TB}	Area T-boom = 3.76	[m^2]

For the banners, the following values hold:

$y_{MB,banner}$	Distance from centroid$_{MB,banner}$ to centre top platform in y = 9.3	[m]
$y_{TB,banner}$	Distance from centroid$_{TB,banner}$ to centre top platform in y = 22.9	[m]
$z_{MB,banner}$	Distance from centroid$_{MB,banner}$ to centre top platform in z = 1.85	[m]
$z_{TB,banner}$	Distance from centroid$_{TB,banner}$ to centre top platform in z = 1.93	[m]

Total loads on platform When including all above determined parameters in equation 3-3, this lead to a total static wind load on the Stewart platform. When adding these forces to the dead and live load forces from Table 3-3, the total forces on the top will be:

		NO-PT	NO-CT
F_x	[kN]	-23	-24
F_y	[kN]	12	13
F_z	[kN]	-248	-258
M_x	[kNm]	-553	-855
M_y	[kNm]	-56	-63
M_z	[kNm]	144	141

Table 3-8: Dead and live loads at Upper Gimbal Level for redefined A-type

Especially the moment in z-direction has increased. However, it is still relatively small in comparison with the moment in x-direction. This moment remains the critical load on the Stewart platform.

3-6 Concluding remarks

The external loads from the GXXL have been elaborated in this chapter. The loads are divided into dead load and live loads. The dead load contribute to the downward force and the tipping moment. The live load increase the downward force and tipping moment and also creates forces and moments in other directions. The loads created by the wind are static and dynamic, only the static loads are taken into account in this research. Another study is recommended to investigate the effect of the dynamic wind loading on the gangway and the Stewart platform. The static part of the force is the most negative when it is perpendicular to the gangway. This force is now calculated in one direction, but can also occur in the other direction. This has to be kept in mind when optimising the geometry of the platform and adding passive cylinders to the system.

The gangway on top of the platform rotates during the whole operation procedure, by a slewing motion made possible by the slewing ring. This slewing ring is currently located above the platform and below the gangway. Due to this slewing motion, the load case rotates along with the gangway while the orientation of the platform stays fixed. To be able to optimise the platform for this asymmetric external load case caused by the gangway, the platform should rotate along with the gangway. In this way the load case due to the dead load remain the same during the whole operation. The platform can rotate with the gangway when the slewing ring is relocated to below the platform, which results in the fact that the platform is loaded in the same manner during operation. The slewing motion can no longer counteract the moment caused by the wind on the gangway. This moment now reaches the cylinders of the Stewart platform. The wind load case is reduced for the slewing ring, but the design still has to be checked whether it is able to handle the larger forces due to the weight of the gangway. Also the rotation speed and control of the slewing motion have to be checked.

For the remaining of this thesis it is assumed that a slewing ring is below the Stewart platform and is able to handle both the weight of the gangway and the platform and has to can be controlled in the same manner as the current slewing motion. With this first redesign, the corresponding load case and the operation limits of the A-type cylinders the Stewart platform will be optimised.

Chapter 4

Geometry optimisation

4-1 Introduction

The first way of optimising the Ampelmann for large external asymmetric load cases is to optimise the geometry of the Stewart platform, meaning the location of the top and bottom gimbals. In general, the geometry of the Stewart platform can be optimised for an (1) improved dexterity, (2) enlarged workspace or (3) increased loading capacity. As formulated in the problem statement in Chapter 1, the Stewart platform in this research will be optimised in such a way that it can handle larger external loads than the current Ampelmann system. For this thesis, the case study of placing an GXXL on the A-type system is used. The minimum dexterity will be used as a constraint. As the platform should be able to handle the most critical load cases, the dead and live loads are taken into account, with the slewing ring below the platform.

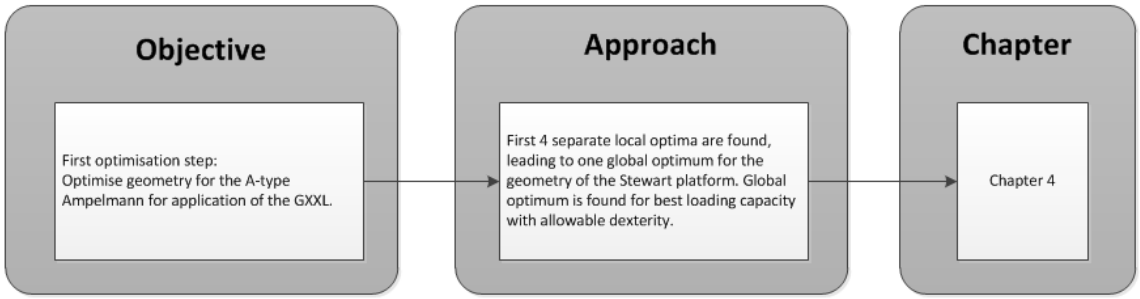

Figure 4-1: Approach Chapter 4

Free body diagram

Before looking at the 3d Stewart platform with all the calculations from Chapter 2, first the idea behind optimisation of the geometry is given. When a platform is loaded symmetrical, like by the flight simulator from Figure 1-1, it is logical that the platform itself is also symmetrical. Because no moments are created due to asymmetry. However, when the platform is loaded asymmetrical, like by the gangway, a symmetrical geometry is only logical for the workspace of the system and no longer for the loading capacity. A solution has to be found for a new geometry with a better loading capacity for the asymmetric loads and a comparable workspace. Their are two aspects of the geometry that can be improved for the loading capacity. First the top frame can be enlarged, creating larger arms for the cylinder forces to counteract the tipping moment. And second, enlarging the distance between the gimbals. This will create a larger vertical force component for the cylinder forces to counteract the tipping moment M_x and downward force F_z. These two aspects are shown in Figure 4-2.

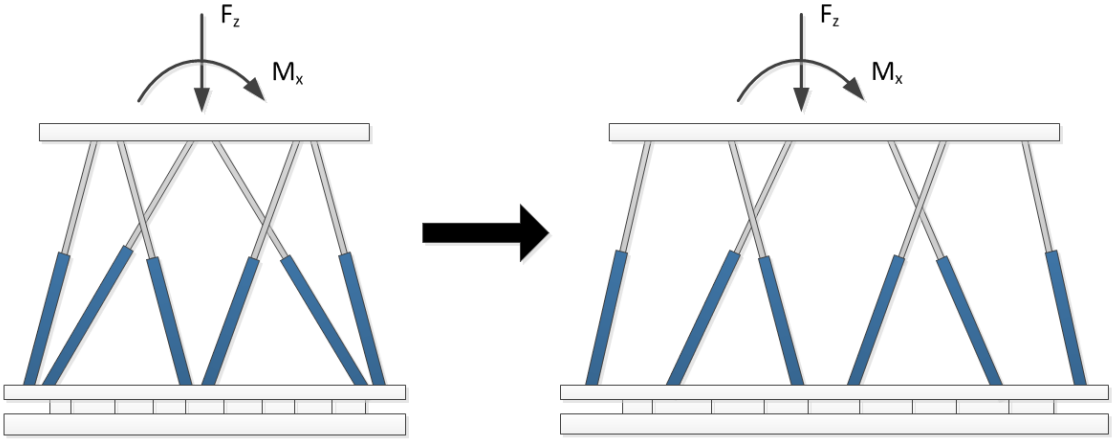

Figure 4-2: Optimising geometry for large asymmetric load case

4-2 Geometry optimisation model

The 2d free body diagram of Figure 4-2, will be adapted to the 3d representation of the Stewart platform in this chapter. To optimise the platform, a model is created including all the calculation methods of Chapter 2 and the variables such as the gimbal angle and radius of the top and bottom frame. The optimisation model used in this study is made in `Matlab`. A flow diagram of this model is presented in Figure 4-3. The steps are further elaborated throughout this chapter.

The Stewart platform will be loaded with the critical loading case from Chapter 3, Table 3-8. For the 3d model, the geometry can be adapted according to ten parameters of the Stewart platform. To get a better understanding of the influences of these parameters, first local optima have been found. This can already lead to some conclusions for which the input variables of the total model can be reduced. Once there is a better understanding of these

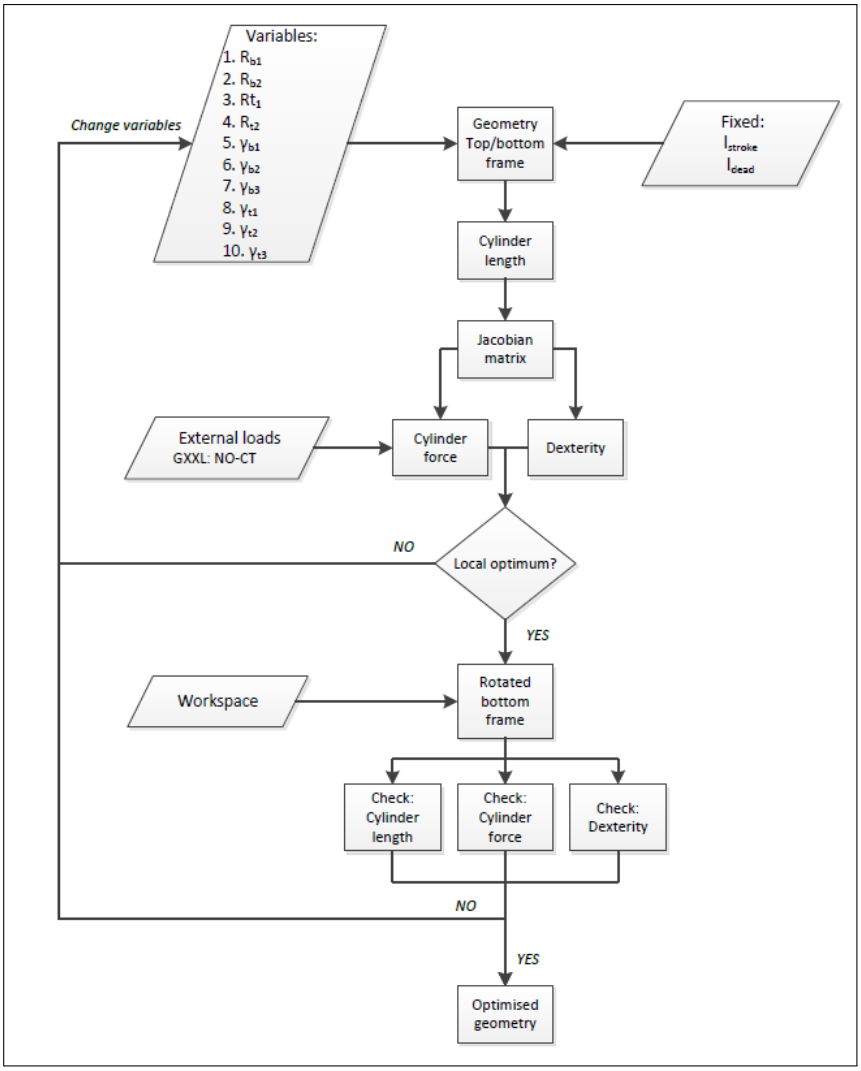

Figure 4-3: Flow diagram: Optimisation geometry

parameters, the global optimum can be found for the geometry with the best loading capacity with an allowable dexterity and workspace.

The model as described in Figure 4-3 is, divided into three parts: (1) input: geometry parameters, (2) calculations and (3) output. These are all further elaborated in this section.

4-2-1 Input: Geometry variables

The Stewart platform consists out of a rigid top and bottom frame, which are connected with six linear hydraulic actuators. To make the rotational capacity of the bottom frame in contrast to the top frame possible, the actuators are connected to the frames with the use of gimbals.

The parameters that can be adapted of the Stewart platform are the radius of the top, the bottom frame, the actuator length and the gimbal angles. These parameters can be divided

in a number of twenty variables:

Radius	Top gimbal angle	Bottom gimbal angle	Cylinder length
1. R_{t1}	7. γ_{t1}	13. γ_{b1}	19. l_{stroke}
2. R_{t2}	8. γ_{t2}	14. γ_{b2}	20. l_{dead}
3. R_{t3}	9. γ_{t3}	15. γ_{b3}	
4. R_{b1}	10. γ_{t4}	16. γ_{b4}	
5. R_{b2}	11. γ_{t5}	17. γ_{b5}	
6. R_{b3}	12. γ_{t6}	18. γ_{b6}	

Table 4-1: Total number of optimisation variables

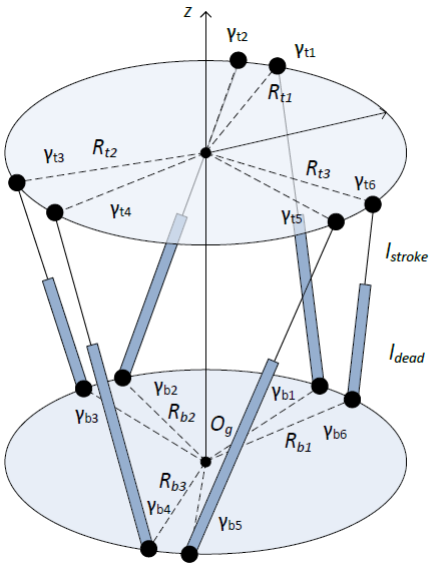

Figure 4-4: Parameters Stewart Platform

This is quite a large number of variables, which is undesirable when preforming an optimisation. In the next two paragraphs this number will be reduced as much as possible, without compromising the outcome of this study.

Assumptions

The number of variables can be reduced by introducing symmetry. As stated before, the slewing ring will be relocated to below the bottom frame. This leads to always the same load distribution of the gangway onto the platform. The largest contribution to the force is the dead load of the gangway (F_z and M_y). The other two forces and moments are mostly due to live loads, like wind on the gangway. One has to take into account the live loads, but the optimisation of the geometry will be based on the dead load. Following from this is that symmetry around the x-axis, reducing the gimbal angles from twelve to six. The radii variables is reduced from six to four. The symmetry axis is shown in Figure 4-5.

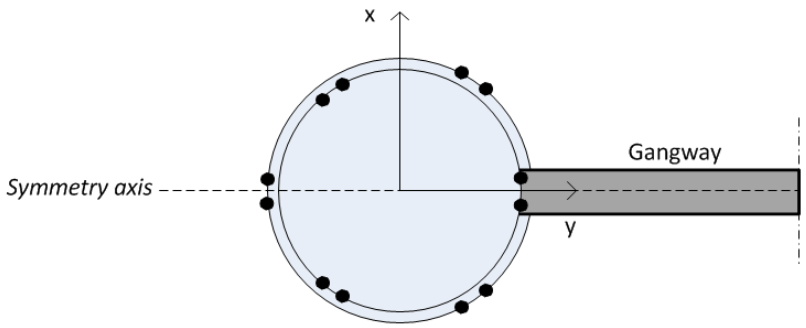

Figure 4-5: Gangway configuration

Constraints

A number of constraints are used in this research, which are summarised below:

- In this thesis the geometry of the A-type is optimised, so that the GXXL can be placed on top of this Stewart platform. The same cylinders will be used as for the current A-type. This reduces the number of variables, as the minimum and maximum length of the cylinders are known, due to the fixed dead and stroke length:

$$l_{min} = l_{dead} + l_{stroke} \qquad = 1.25 + 2.00 = 3.25 \qquad \text{[m]} \qquad (4\text{-}1)$$
$$l_{max} = l_{dead} + 2 \cdot l_{stroke} \qquad = 1.25 + 4.00 = 5.25 \qquad \text{[m]} \qquad (4\text{-}2)$$

- As the same cylinders are used, the minimum and maximum operation limit of the cylinders are also known:

$$F_{min} = -124 \qquad \text{[kN]} \qquad (4\text{-}3)$$
$$F_{max} = 160 \qquad \text{[kN]} \qquad (4\text{-}4)$$

- The minimum radius of a platform is chosen at one meter, as top frame should be usable to transfer people from sea vessel to a offshore platform. The maximum radius of 3 meter is set as the bottom frame has a maximum footprint. This makes it possible for the A-type system to be installed on small sea vessels. Larger footprint will cause problems on ships that do not have to space to accommodate the Ampelmann:

$$1.00 \leq R_{ti,bi} \leq 3.00 \qquad \text{[m]} \qquad (4\text{-}5)$$

- The cylinders of the Stewart platform may not cross each other. This will increase the torsion capacity, but will not have a positive effect on the loading capacity of the platform as shown in [16]. Also the gimbals should have a minimum separation angle of each other of $\pi/36$. The gimbal angles can be varied between:

$$\frac{\pi}{36} \leq \gamma_{ti,bi} \leq (\frac{\pi}{3} - \frac{\pi}{36}) \qquad \text{[m]} \qquad (4\text{-}6)$$

- The dexterity of the Stewart platform can have a value between zero and one. A value of zero means that singularities will occur meaning that the system becomes unstable and extensively high actuator forces may occur. From different studies,[4], a minimum suggested value for the dexterity is 0.2. The current A-type has a minimum value lower than this, namely of 0.12. This value is assumed to be the minimum value for the dexterity of the Stewart platform:

$$\text{dexterity} \geq 0.12 \qquad [\text{-}] \tag{4-7}$$

Variables

With these assumptions and boundaries some variables can be left out. The reduced number of variables on which the geometry will optimised are shown in the Table below.

Radius	Top gimbal angle	Bottom gimbal angle
1. R_{t1}	5. γ_{t1}	8. γ_{b1}
2. R_{t2}	6. γ_{t2}	9. γ_{b2}
3. R_{b1}	7. γ_{t3}	10. γ_{b3}
4. R_{b2}		

Table 4-2: Reduced number of optimisation variables

These parameters will be varied between the following values:

$$1.00 \leq R \leq 3.00 \quad [\text{m}] \qquad \frac{\pi}{36} \leq \gamma \leq (\frac{\pi}{3} - \frac{\pi}{36}) \quad [\text{rad}] \tag{4-8}$$

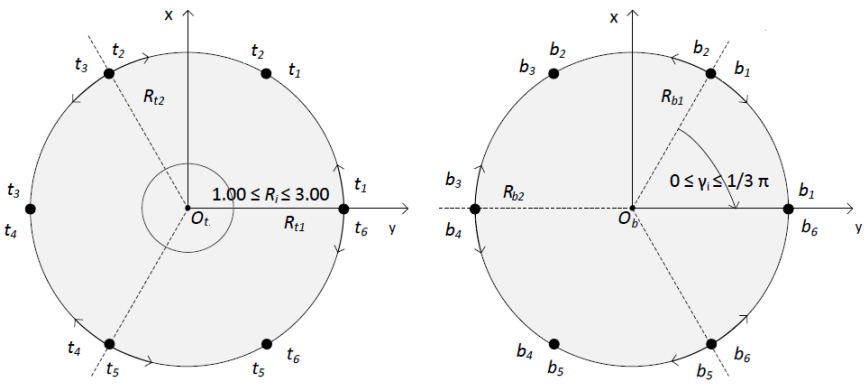

Figure 4-6: Variable radii and gimbal angles

4-2-2 Model: calculation steps

In the model the following calculation steps have been done. A majority of these steps have already been elaborated in Chapter 2:

1. Geometry parameters
2. Inverse Kinematics
3. Jacobian Matrix
4. Dexterity
5. Inverse Dynamics

Geometry parameters

With the following formulas the coordinates of the top and bottom gimbals will be calculated. Note that the coordinates of the Stewart platform are used when located on a ship with the gangway towards the offshore platform. For this reason the y-axis is horizontal and the x-axis is vertical. These parameters are valid for the all the local optima.

b_i	x	y	t_i	x	y
1	$R_{b1} \cdot \sin(\frac{1}{3}\pi - \gamma_{b1})$	$R_{b2} \cdot \cos(\frac{1}{3}\pi - \gamma_{b1})$	1	$R_{t1} \cdot \sin(\gamma_{t1})$	$R_{t2} \cdot \cos(\gamma_{t1})$
2	$R_{b1} \cdot \sin(\frac{1}{3}\pi + \gamma_{b2})$	$R_{b2} \cdot \cos(\frac{1}{3}\pi + \gamma_{b2})$	2	$R_{t1} \cdot \sin(\frac{2}{3}\pi - \gamma_{t2})$	$R_{t2} \cdot \cos(\frac{2}{3}\pi - \gamma_{t2})$
3	$R_{b1} \cdot \sin(\pi - \gamma_{b3})$	$R_{b2} \cdot \cos(\pi - \gamma_{b3})$	3	$R_{t1} \cdot \sin(\frac{2}{3}\pi + \gamma_{t3})$	$R_{t2} \cdot \cos(\frac{2}{3}\pi + \gamma_{t3})$
4	$R_{b1} \cdot \sin(\pi + \gamma_{b3})$	$R_{b2} \cdot \cos(\pi + \gamma_{b3})$	4	$R_{t1} \cdot \sin(\frac{4}{3}\pi - \gamma_{t3})$	$R_{t2} \cdot \cos(\frac{4}{3}\pi - \gamma_{t3})$
5	$R_{b1} \cdot \sin(\frac{5}{3}\pi - \gamma_{b2})$	$R_{b2} \cdot \cos(\frac{5}{3}\pi - \gamma_{b2})$	5	$R_{t1} \cdot \sin(\frac{4}{3}\pi + \gamma_{t2})$	$R_{t2} \cdot \cos(\frac{4}{3}\pi + \gamma_{t2})$
6	$R_{b1} \cdot \sin(\frac{5}{3}\pi + \gamma_{b1})$	$R_{b2} \cdot \cos(\frac{5}{3}\pi + \gamma_{b1})$	6	$R_{t1} \cdot \sin(-\gamma_{t1})$	$R_{t2} \cdot \cos(-\gamma_{t1})$

Table 4-3: Gimbal coordinates top and bottom frame

Inverse kinematics

Following the Inverse kinematics with the obtained geometry parameters, the rotated bottom frame, cylinder lengths and cylinder vectors can be calculated. As stated before, the bottom frame stays fixed for the first part of the optimisation study, to solely optimise the geometry for the external loading capacities. However, once the optimised geometry is found the workspace of the system had to be checked. For this reason the rotation of the bottom frame is already included in the model.

Jacobian Matrix

The cylinder length and cylinder vectors are used to obtain the Jacobian Matrix of the system. The Jacobian Matrix is calculated with reference to the rotating top frame for the dexterity and to the fixed top frame for the inverse dynamics.

Dexterity

With the Jacobian matrix the dexterity of the Stewart platform will be determined. The optimised geometry should have a minimum dexterity of 0.12, so all geometries with a lower value will not be used.

Inverse dynamics

The Jacobian matrix is also used to obtain the actuator forces. The external loading condition used in this research are obtained in Chapter 3. The critical load case is the GXXL:NO-CT, as this loading case has the largest forces and moments in every direction.

4-2-3 Output: Optimisation

To find the geometry that can withstand the largest load case, the loads should be even distributed over the six cylinders. The optimised geometry is chosen according to the following criteria:

$$\min\{\max\{|N_i^a|\}\} \tag{4-9}$$

Where,

i	Number of the actuator (1, 2 .. 6)	[-]
N^a	Axial actuator force	[kN]

With this criteria, the geometry is chosen with the lowest maximum forces over the six cylinders. The geometry should have a dexterity of at least 0.12.

4-3 Verification and validation

The model which is described in the previous section is created in Matlab. Before this model is used for the optimisation of the geometry, it should be verified and validated.

4-3-1 Verification

The model is first verified to see whether the output variables are calculated correctly. The output dexterity is checked with different input parameters and the cylinder forces are checked with a constant external load in one direction.

Geometry variables and dexterity

The dexterity is a parameter with a value between zero and one. For the dimensions of the current A-type, the dexterity is around 0.2. When changing the radius of the top or bottom frame will have to lead to varying value of the dexterity around 0.2. In this verification step, both radii are varied between 1 and 6 while the other frame is fixed at 3 meters. All the gimbal angles are fixed at $\frac{\pi}{36}$. The dexterity for these radii are plotted in Figure 4-7.

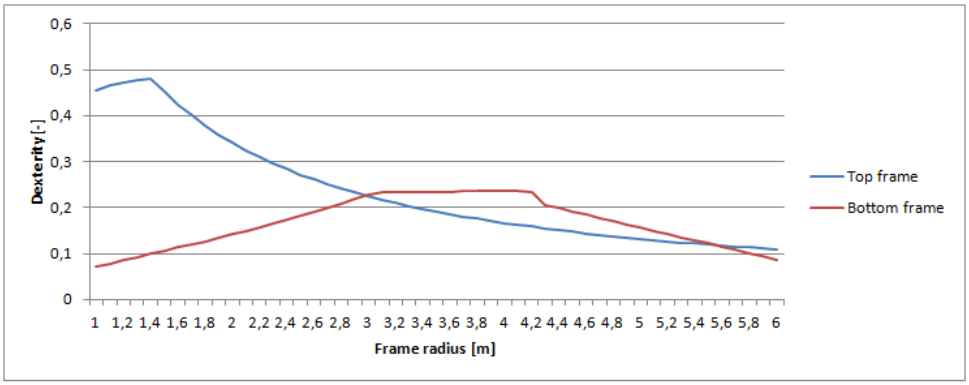

Figure 4-7: Dexterity vs variable radius

The dexterity is indeed around 0.2 with higher values for a small top frame and low values for a small bottom frame. This has been found reasonable as a small bottom frame makes the controllability of a larger top frame difficult, leading to a smaller dexterity.

Cylinder force distribution

The second verification step is to check the cylinder force distribution within the Stewart platform. This step is performed by applying one external load at the time, and looking at the forces per actuator. It can be seen that when applying the loads and the moments one by one on the Stewart platform, the counteracting cylinder forces are all in the opposite direction. From this can be concluded that the force distribution over the cylinders is correct.

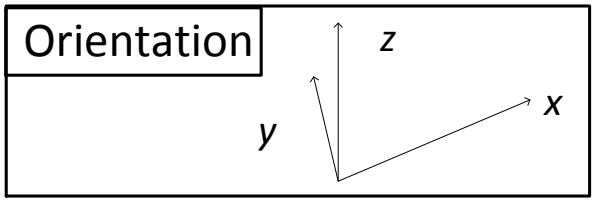

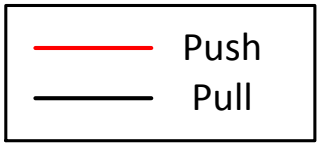

$F_x = 100$ kN

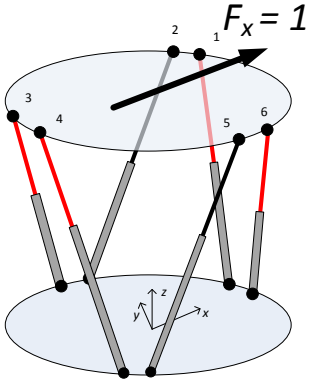

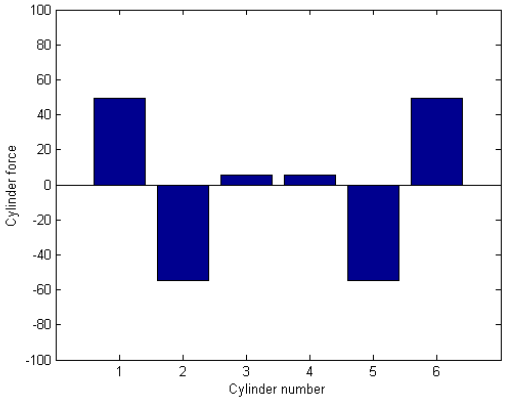

$F_y = 100$ kN

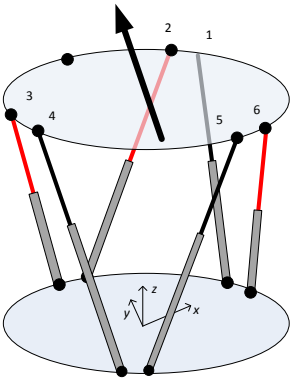

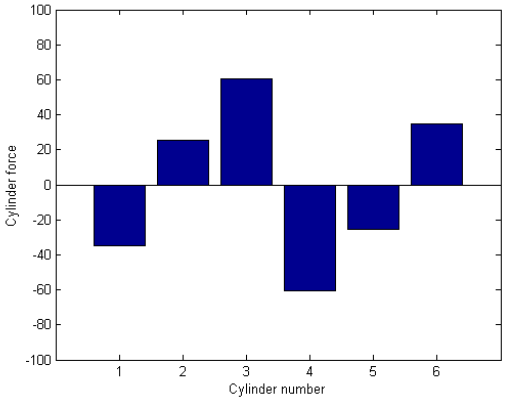

$F_z = 100$ kN

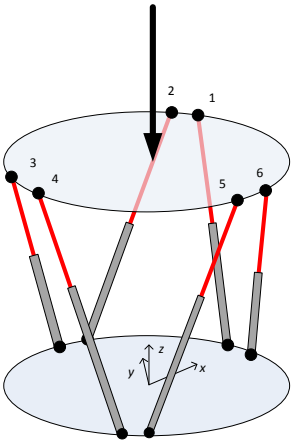

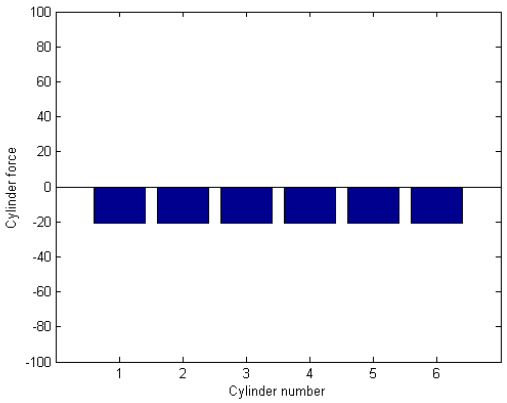

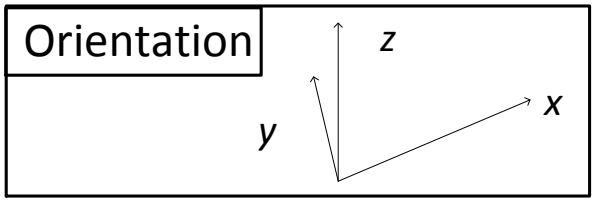

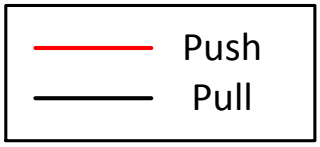

M_x = 200 kNm

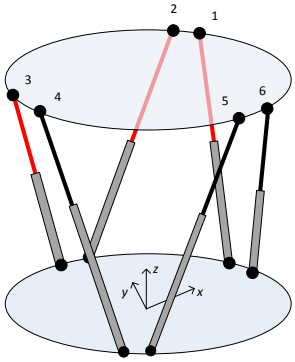

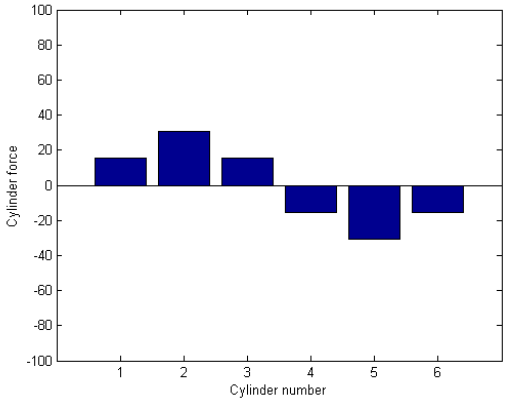

M_y = 200 kNm

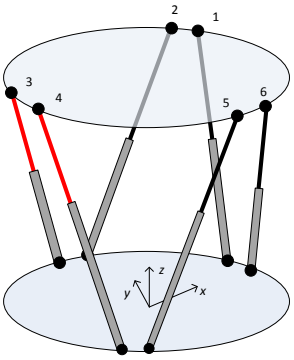

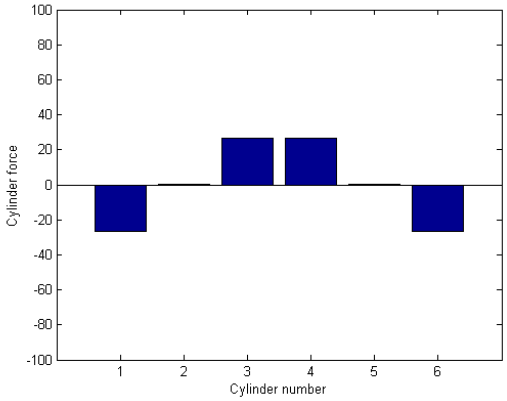

M_z = 200 kNm

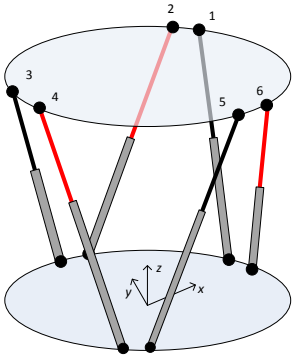

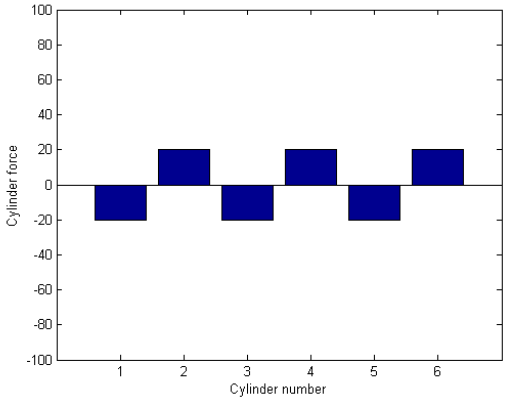

4-3-2 Validation

The validation step is to see whether the model resembles the reality. The results of this model are compared with results found in other papers and studies of the Stewart platform. The output of the dexterity over the workspace of the system is checked and also the results found in the verification of the dexterity are also compared with other studies.

Dexterity vs workspace

Over the entire workspace the dexterity of the current Stewart platform used in the Ampelmann system can be plotted. The only limitations taken into account are the relation between surge and sway ($x^2 + y^2 = 1.00$ [m]) and the minimum and maximum cylinder length ($l_{min} \leq l_i \leq l_{max}$).

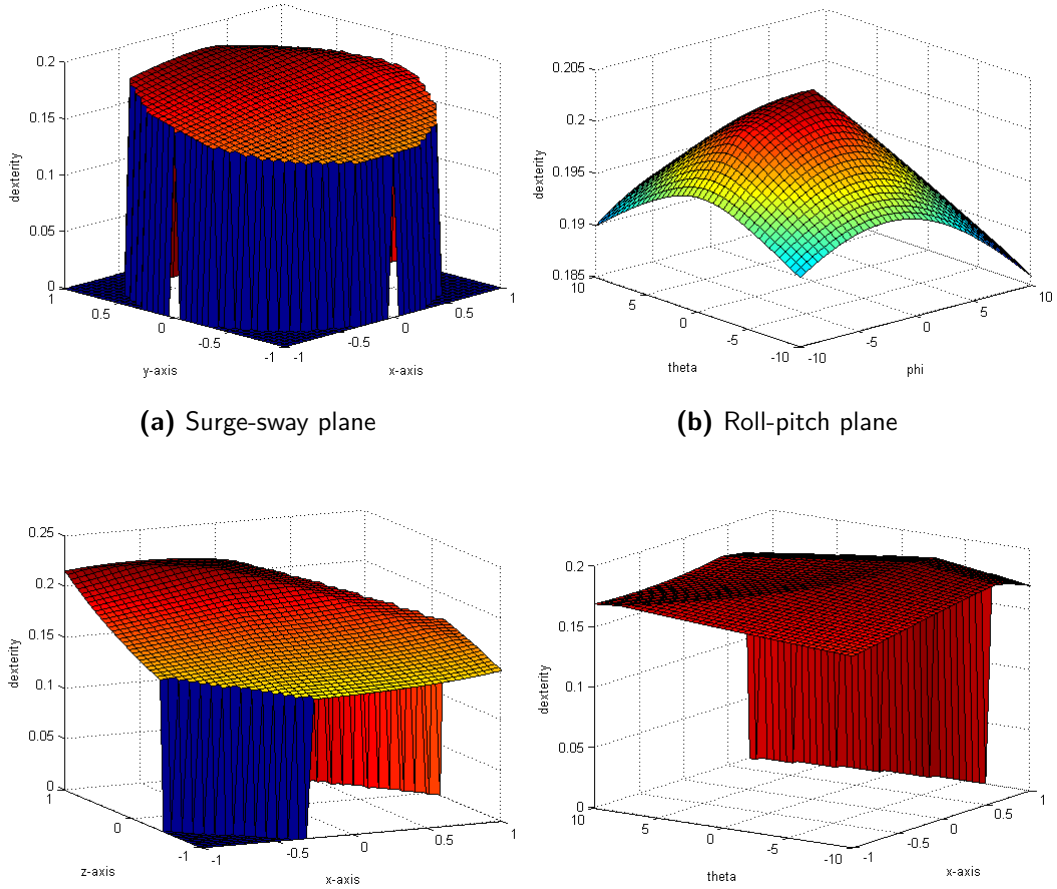

(a) Surge-sway plane

(b) Roll-pitch plane

(c) Surge-heave plane

(d) Surge-pitch plane

Figure 4-8: Dexterity in 2D plane

The mapped dexterity in Figure 4-8a resembles the limitation between surge and sway, as the dexterity is is circular in the 2D plane. These outcomes are found reliable is they are comparable with outcomes from other performed studies like [4] and [17].

Geometry variables and dexterity

The input variables of the geometry and the dexterity are checked in the verification step in section 4-3-1. These results are in compliance with the results from the study [4]. The optimum dexterity is obtained when the ratio between the two frames is approximately: $R_b = \sqrt{2}R_t$. Once the bottom frame becomes larger than this, the dexterity goes down again. This is the same conclusion as found by Advandi [4].

4-3-3 Outcome verification and validation

The model created in Matlab of the Steward platform is verified and validated in this section. First the dexterity are plotted for different radii of the top and bottom frame. The dexterity is around 0.2 what is as expected. Second the cylinder force distribution is investigated by applying one force at the time on the Stewart platform. The distribution of these forces are all counteracting the external load. With these two steps the output is found reliable and the model is verified. For the validation the dexterity is plotted over the workspace and compared with results from other studies. The input parameters, workspace and dexterity are checked and are all results resemble results from studies like [4] and [17]. The model is found to be reliable and will be used in the next section to optimise the geometry of the Stewart platform.

4-4 Optimisation of geometry: Local optimum

The geometry of the A-type Ampelmann system will be optimised with the variables from previous sections. The first step of running the model for the different geometries is in neutral position with one load case (GXXL:NO-CT).

The critical load case is used to determine the local optimum. To find the geometry that can withstand the largest load case, the loads should be even distributed over the six cylinders. The optimised geometry is chosen according criteria from section 4-2-3. Each local optimum is a optimisation of one type of variables. The following four local optima are investigated in this section:

1. Circular top and bottom frames
2. Linked gimbal angles
3. Separate gimbal angles
4. Elliptical top and bottom frames

4-4-1 Circular top and bottom frames

The first local optimum that is found is for the top and bottom radius of the Stewart Platform. In this first local optimum both frame are circular, meaning that $R_1 = R_2$ (from Figure 4-6). The gimbal angles are all fixed at $\frac{\pi}{36}$. This step is divided into three sub local optima (1) a

variable top radius, (2) a variable bottom radius and (3) a variable top and bottom radius. This is schematised in Figure 4-9.

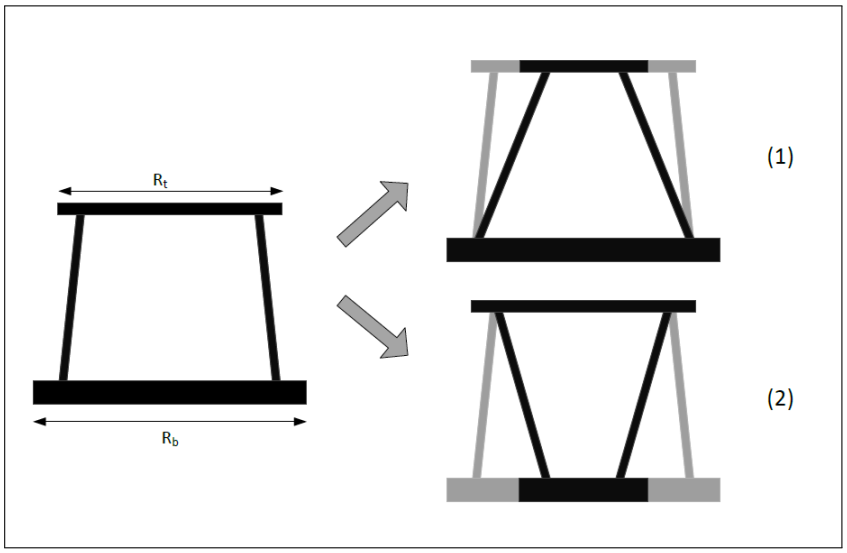

Figure 4-9: Variable top and bottom radius

Top radius

The top radius is varied between 1.00 and 3.00 meter while all the other parameters are kept fixed. The parameter values and coordinates can be seen in Table 4-4 and Figure 4-10

Variable		Fixed	
$1.00 \leq R_{t,i} \leq 3.00$	[m]	$R_{b,i} = 3.00$	[m]
		$\gamma_{t,i} = \gamma_{b,i} = \frac{\pi}{36}$	[rad]

Table 4-4: Variable and fixed parameters 1.1

For these variable top radius, the forces and dexterity are plotted in Figure 4-11. The dexterity for a variable top radius was already elaborated in section 4-3. The forces of all the cylinders converge when the top radius is increased. The reason for this is that the lever arm which creates a counteracting moment also increases. The best force distribution is for a top radius of $R_t = 3.00$ meter.

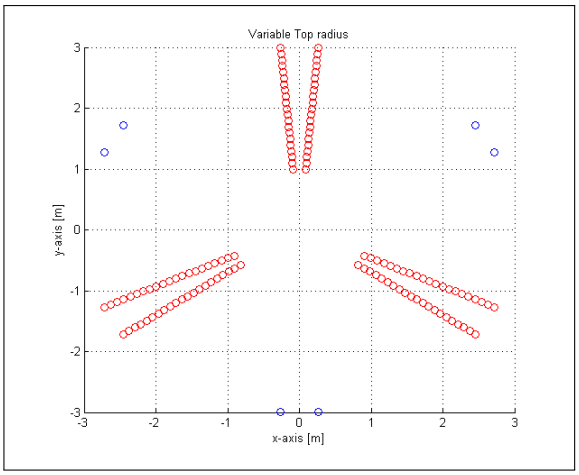

Figure 4-10: Variable top radius

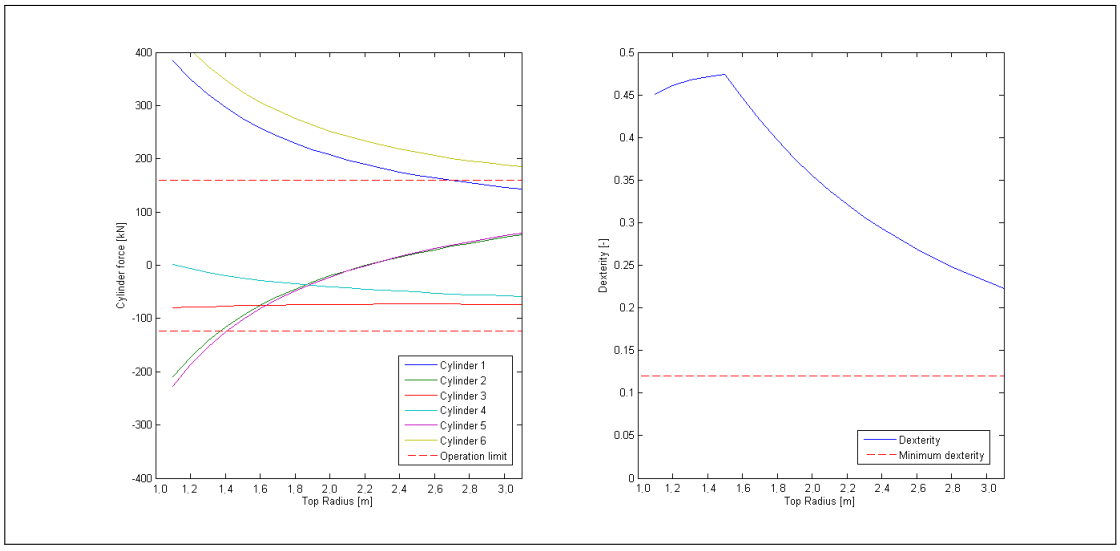

Figure 4-11: Forces and dexterity: Variable top radius

Bottom radius

The bottom radius is varied between 1.00 and 3.00 meter while all the other parameters are kept fixed. The parameter values and coordinates can be seen in Table 4-5 and Figure 4-12

Variable		Fixed	
$1.00 \leq R_{b,i} \leq 3.00$	[m]	$R_{t,i} = 2.75$	[m]
		$\gamma_{t,i} = \gamma_{b,i} = \frac{\pi}{36}$	[rad]

Table 4-5: Variable and Fixed parameters 1.2

The second sub local optimum is the bottom radius. The forces and dexterity are plotted in

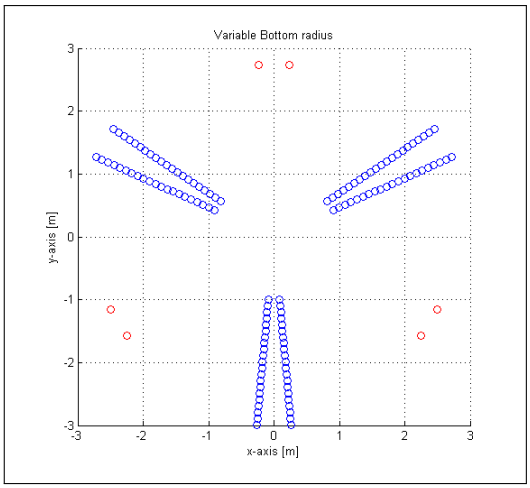

Figure 4-12: Variable bottom radius

Figure 4-13. For both the forces and the dexterity a large bottom frame is favourable. The lower force for an increasing bottom frame can be explained by the fact that the cylinder vector increases with the radius. This leads to a larger unit vector, larger Jacobian Matrix and in the end smaller cylinder forces, meaning that the vertical force component becomes larger in comparison with the horizontal force component.

For the dexterity, the larger Jacobian matrix leads to a smaller condition number κ and so an increasing dexterity.

It can be concluded that this sub local optimum is a bottom radius of $R_b = 3.00$ meter.

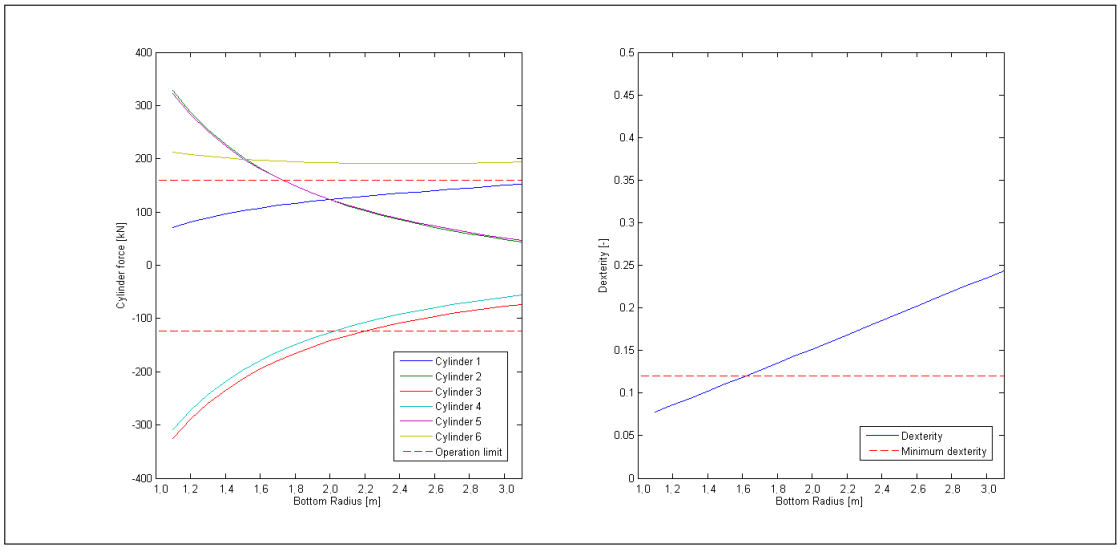

Figure 4-13: Forces and dexterity: Variable bottom radius

Top and bottom radius

The local optimum for both the top and bottom radius can already be expected from the previous two sub local optima. But a check is preformed by also including both variables in the model. The parameters are again given in Table 4-6

Variable		Fixed	
$1.00 \leq R_{b,i} \leq 3.00$	[m]	$\gamma_{t,i} = \gamma_{b,i} = \frac{\pi}{36}$	[rad]
$1.00 \leq R_{t,i} \leq 3.00$	[m]		

Table 4-6: Variable and Fixed parameters 1.3

This leads to the distribution of the cylinder forces as plotted per cylinder in Figure 4-14. It must be stated that the cylinder forces on the z-axis varies over the six figures. The best distributed cylinder forces are still found for both a top and bottom radius of 3.00 meter. As two parameters are variables, the cylinder forces and the dexterity have to be plotted in 3D.

For the dexterity the influence of both variables can be seen more clearly (Figure 4-15). As the bottom radius is enlarged, the dexterity increases, but the dexterity decreases when enlarging the top radius. The dexterity is 0.2227 when both radii are 3.00 meter, which is well above the minimum of 0.12.

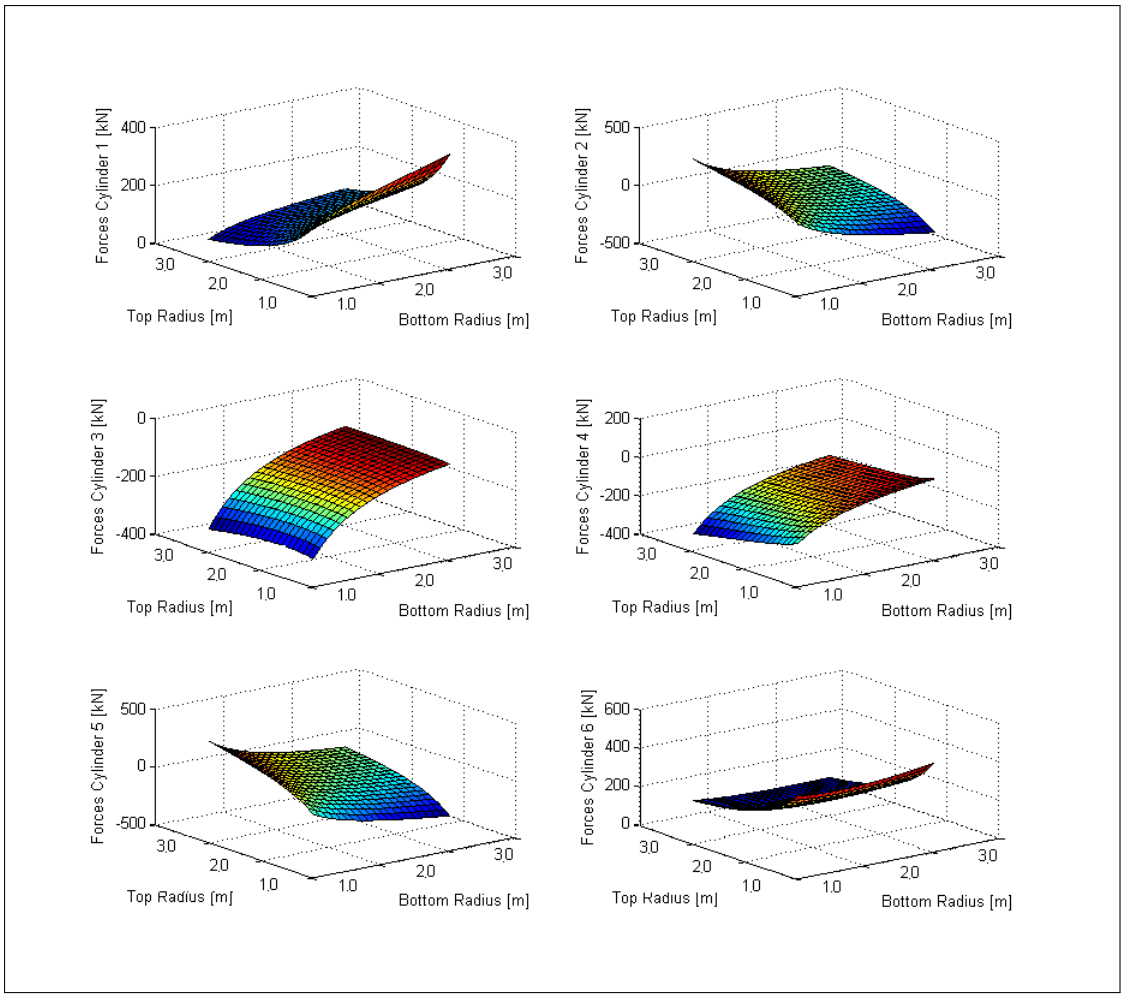

Figure 4-14: Forces: Variable top and bottom radius

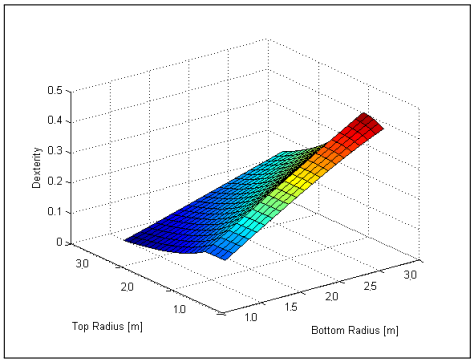

Figure 4-15: Dexterity: Variable top and bottom radius

Local optimum 1

For the first parameter set of the variable circular top and bottom radii can be concluded that the most optimal cylinder force distribution is found for $R_{b,i} = R_{t,i} = 3.00$ meter. The largest top frame creates the largest distance to the centre of the top frame, which leads to the largest lever arm for the cylinder forces to counteract the external loads. The largest bottom frame creates the largest vertical component of the cylinder forces.

The forces of the first local optimum are displayed in Figure 4-16a. Over the six cylinders the forces are reduced with a few percent. However, the two highest forces are reduced with 10 [kN], which is favourable. The dexterity for this configuration is 0.2227 [-]. The geometry of the first local optimum of the Stewart platform with both top and bottom gimbals is plotted in Figure 4-16b.

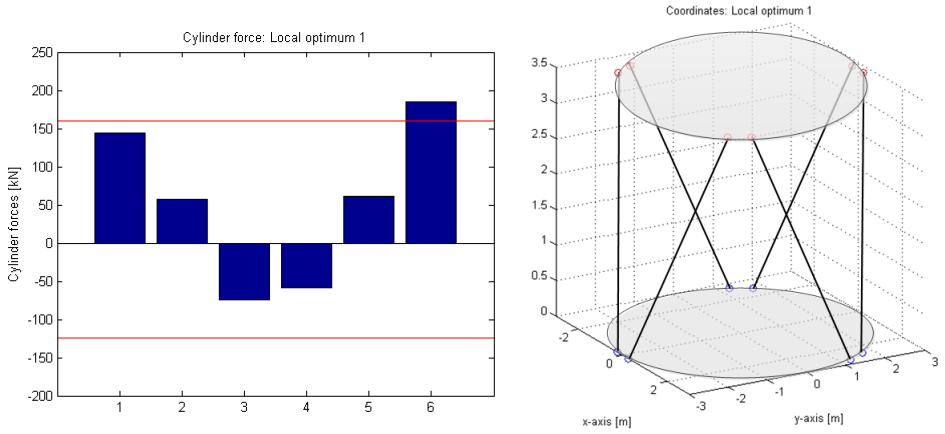

(a) Forces: Local optimum 1 **(b)** Coordinates: Local optimum 1

Figure 4-16: Local optimum 1

4-4-2 Linked gimbal angles

The second local optimum is found for the linked gimbal angles, meaning that all the gimbal angles in one frame are varied with the same value at the same time ($\gamma_{t1} = \gamma_{t2} = \gamma_{t3}$ and $\gamma_{b1} = \gamma_{b2} = \gamma_{b3}$). The radius of both frames is remained the same as for the current A-type. As with the previous local optimum, this one is also divide into three sub local optima: (1) a variable top gimbal angle, (2) a variable bottom gimbal angle and (3) a variable top and bottom gimbal angle.

Top gimbal angle

The top gimbal angle is varied over the radius of the top frame. The rest of the parameters will remain fixed as shown in Table 4-7. The coordinates of all variables are plotted in Figure 4-17.

Variable		Fixed	
$\frac{\pi}{36} \leq \gamma_{t,i} \leq (\frac{\pi}{3} - \frac{\pi}{36})$	[rad]	$R_{b,i} = 3.00$	[m]
		$R_{t,i} = 2.75$	[m]
		$\gamma_{b,i} = \frac{\pi}{36}$	[rad]

Table 4-7: Variable and fixed parameters 2.1

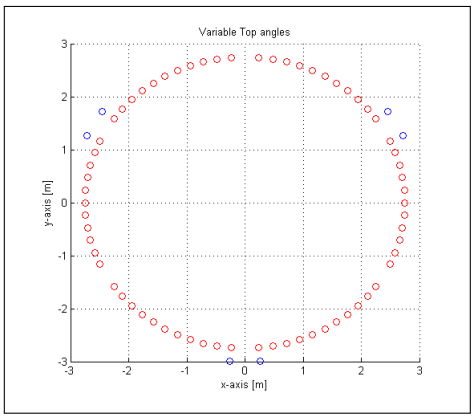

Figure 4-17: Variable top angle

The forces and dexterity for all the variables are plotted in Figure 4-18. At one point the top gimbals are located above the bottom gimbals, the leads to high cylinder forces (above 400 kN) and a dexterity that reaches zero. The system is then singular. When the top angles become larger, the figuration of the cylinders becomes more vertical. This has a positive effect on the force distribution as the forces can counteract the bending moment and downward force in a more efficient matter.

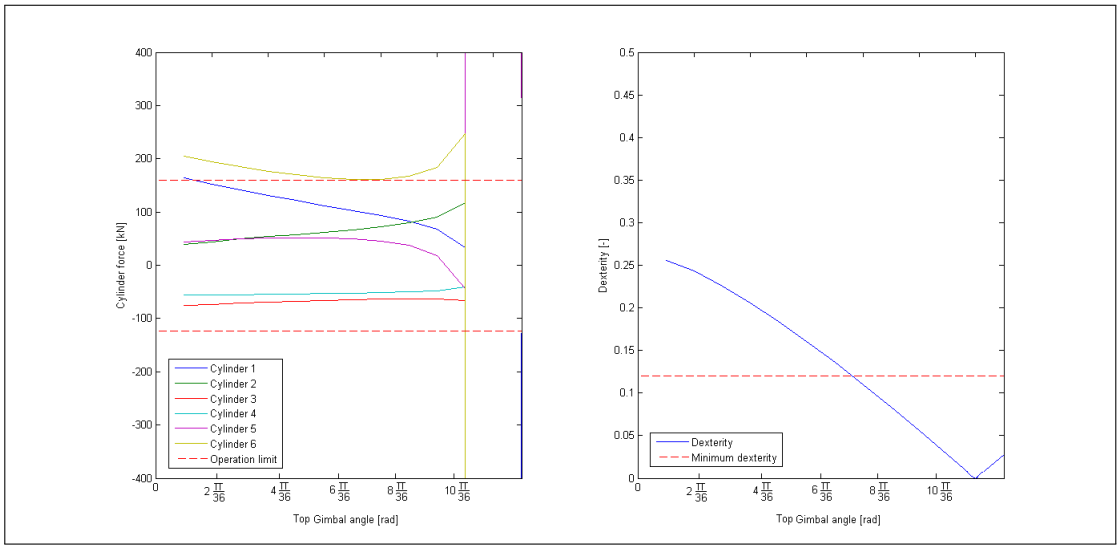

Figure 4-18: Forces and dexterity: Variable top angle

Bottom angle

Next to the top angle, also the bottom angle can be varied. The variables and the according coordinates are shown in Table 4-8 and Figure 4-19

Variable		Fixed	
$\frac{\pi}{36} \leq \gamma_{b,i} \leq (\frac{\pi}{3} - \frac{\pi}{36})$	[rad]	$R_{b,i} = 3.00$	[m]
		$R_{t,i} = 2.75$	[m]
		$\gamma_{t,i} = \frac{\pi}{36}$	[rad]

Table 4-8: Variable and fixed parameters 2.2

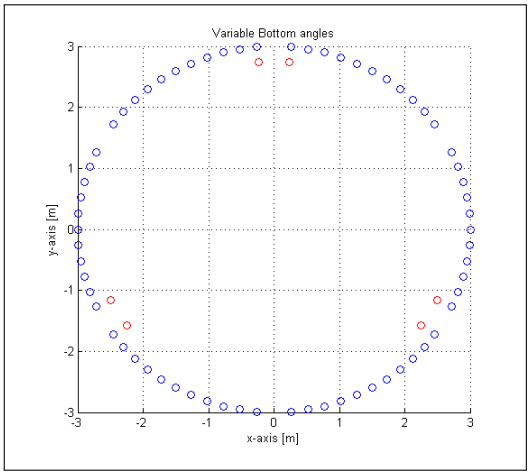

Figure 4-19: Variable bottom angle

The forces and dexterity distribution for the variable bottom angle are comparable with the top angle. For the both the force and dexterity the same explanations are valid as given in for the top gimbal angles.

Top and bottom gimbal angles

The first two sub local optima had comparable results. The results when combining sub local optima can not be estimated as easily as for the radius. First the parameters are again given in Table 4-9.

Variable		Fixed	
$\frac{\pi}{36} \leq \gamma_{t,i} \leq (\frac{\pi}{3} - \frac{\pi}{36})$	[rad]	$R_{b,i} = 3.00$	[m]
		$R_{t,i} = 2.75$	[m]
$\frac{\pi}{36} \leq \gamma_{b,i} \leq (\frac{\pi}{3} - \frac{\pi}{36})$	[rad]		

Table 4-9: Variable and Fixed parameters 2.3

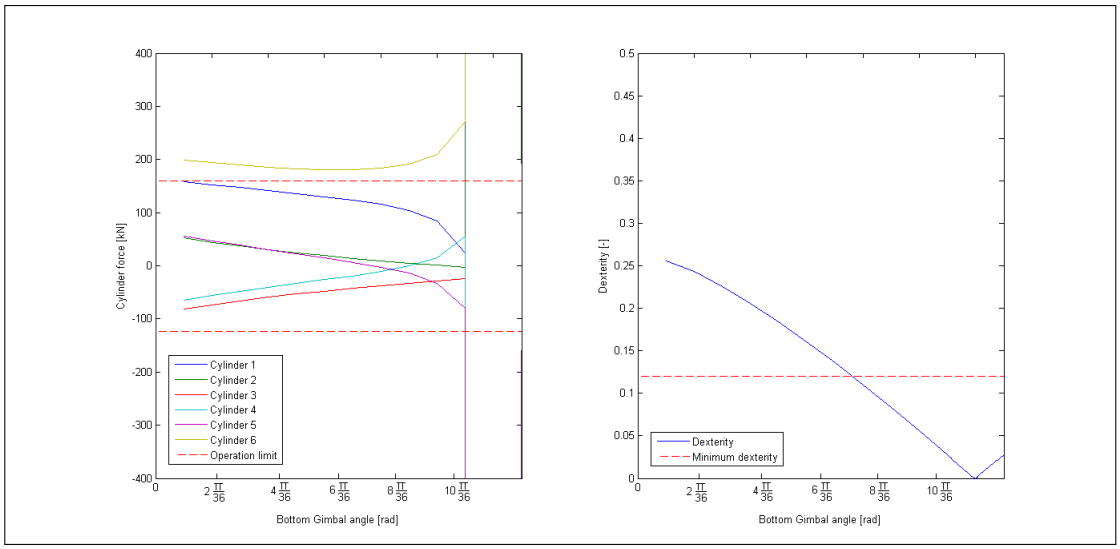

Figure 4-20: Forces and dexterity: Variable bottom angle

For the sub local optima 2.1 and 2.2, singularity occurred when the top and bottom gimbals where located above each other. For configurations where the top and bottom gimbals are located near each other in the horizontal plane, the dexterity is below the minimum of 0.12. When combining these two sub local optima, the forces are only obtained for the configurations that had a dexterity of above 0.12, the other forces have been made zero. The following forces and dexterity can be plotted in 3D (Figure 4-21 and 4-22), as there are again two variables.

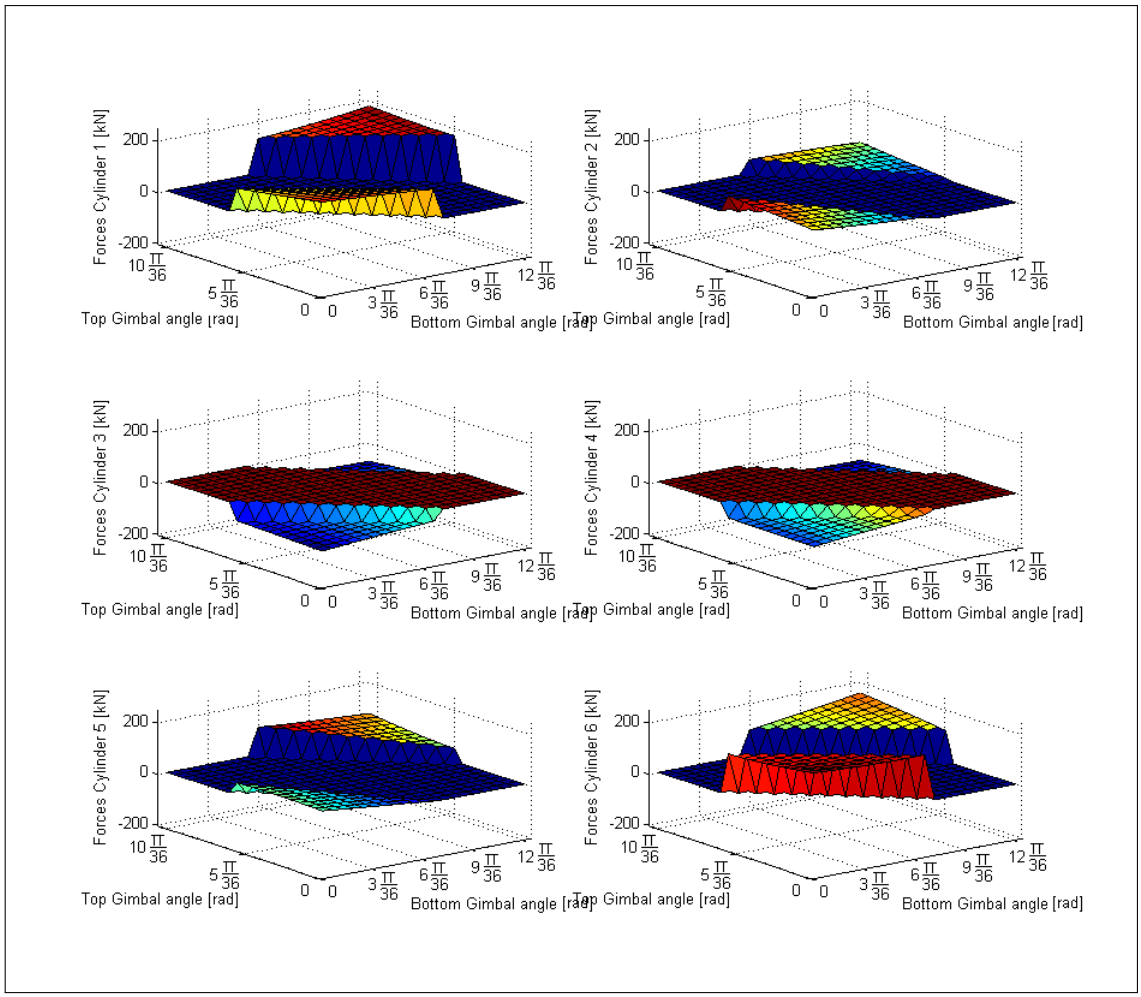

Figure 4-21: Forces: Variable top and bottom angles

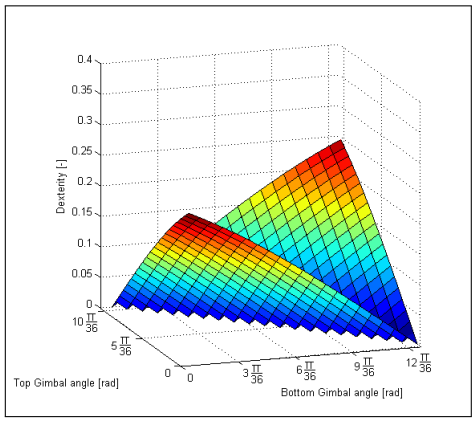

Figure 4-22: Dexterity: Variable top and bottom angles

From Figures 4-21 and 4-22, it is clear that for a large part the dexterity is below 0.12 and the forces are made zero. It is however difficult to see what the best configuration is for the

linked top and bottom angles. To obtain the optimum configuration, the optimisation criteria is applied in the next section.

Local optimum 2

The optimised geometry for the linked top and bottom gimbal angle follows from the optimisation criteria. The coordinates and corresponding cylinder forces are shown in Figure 4-23b and 4-23a. It can be concluded that the cylinder forces are optimised when the top and bottom gimbal angle are $\gamma_t = \left(\frac{\pi}{3} - \frac{\pi}{36} \right)$ and $\gamma_b = \frac{\pi}{6}$. This means that the top angle is maximum, placing the cylinders from under the gangway to besides the gangway on either side. The bottom angle locates the cylinders on a more vertical configuration, making them better suitable for counteracting the external loads. The forces over the cylinders are more even distributed, with all the forces under their operation limit. The maximum force of cylinder 6 is reduced with 95 [kN]. As compensation the force of cylinder 5 has increased, however this is only to reach a better force distribution.

The dexterity for this geometry is 0.1356 [-]. It has to be stated that this dexterity is near the minimum, meaning that when the bottom frame is rotated and translated the dexterity will become lower and possibly below the minimum value of 0.12 [-]. This will further be investigated in section 4-5.

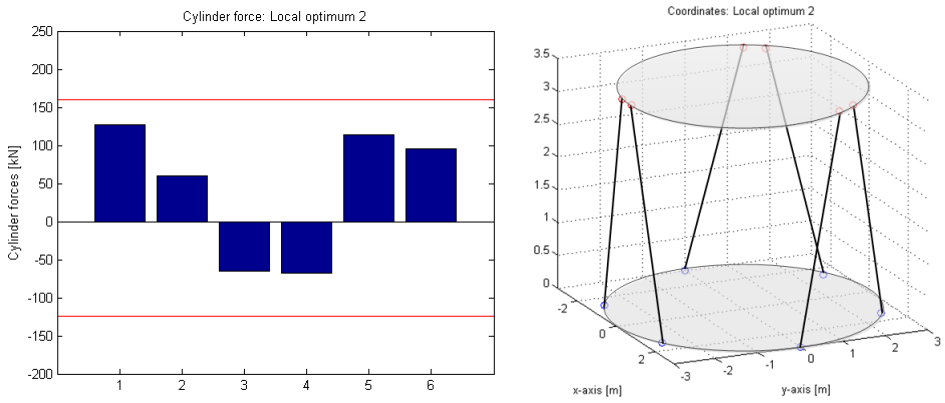

(a) Forces: Local optimum 2 **(b)** Coordinates: Local optimum 2

Figure 4-23: Local optimum 2

4-4-3 Separate gimbal angles

The third local optimum is a continuation of the second local optimum. Instead of varying all the gimbal angles at the same time, the angles are now varied separately. Again this local optimum in divided into three sub local optima: (1) a variable top gimbal angles, (2) a variable bottom gimbal angles and (3) a variable top and bottom gimbal angles.

Top angles

The variable and fixed parameters are shown in Table 4-10. The coordinates of these variables are the same as for sub local optimum 2.1 (Figure 4-17), only this time these locations are reached independently of each other.

Variable		Fixed	
$\frac{\pi}{36} \leq \gamma_{t,1} \leq \frac{\pi}{3}$	[rad]	$R_{b,i} = 3.00$	[m]
$\frac{\pi}{36} \leq \gamma_{t,2} \leq \frac{\pi}{3}$	[rad]	$R_{t,i} = 2.75$	[m]
$\frac{\pi}{36} \leq \gamma_{t,3} \leq \frac{\pi}{3}$	[rad]	$\gamma_{b,i} = \frac{\pi}{36}$	[rad]

Table 4-10: Variable and fixed parameters 3.1

The forces and dexterity are plotted in Figure 4-24. All the configuration where the dexterity is below the minimum of 0.12 are already been crossed out. The same as for the previous local optima can be concluded. When the angles become to large and the configuration of the cylinders becomes too vertical orientated, the dexterity drops below its minimum value. The forces tend to decrease for the larger angles, but most of the time the force of cylinder 6 is above its operation limit.

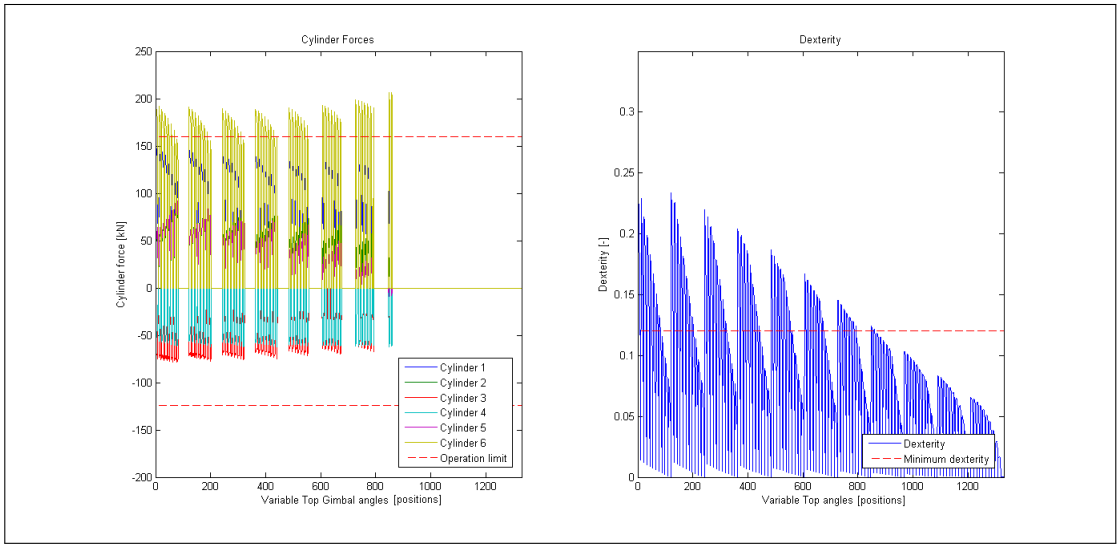

Figure 4-24: Forces and dexterity: Variable top angles

Bottom angles

As for the top angles, the orientation of the variable bottom angles is the same as Figure 4-19. The fixed and variable parameters are again given in Table 4-11.

Variable		Fixed	
$\frac{\pi}{36} \leq \gamma_{b,1} \leq \frac{\pi}{3}$	[rad]	$R_{b,i} = 3.00$	[m]
$\frac{\pi}{36} \leq \gamma_{b,2} \leq \frac{\pi}{3}$	[rad]	$R_{t,i} = 2.75$	[m]
$\frac{\pi}{36} \leq \gamma_{b,3} \leq \frac{\pi}{3}$	[rad]	$\gamma_{t,i} = \frac{\pi}{36}$	[rad]

Table 4-11: Variable and fixed parameters 3.2

The forces and dexterity are plotted in the same manner as previous sub local optimum. The dexterity shows a big resemblance, the dropping of the dexterity for the larger angles. The pull forces tend to decrease when enlarging the bottom angles. The force of cylinder 6 still remains above the operation for most of the time as for the sub local optima for the top angles.

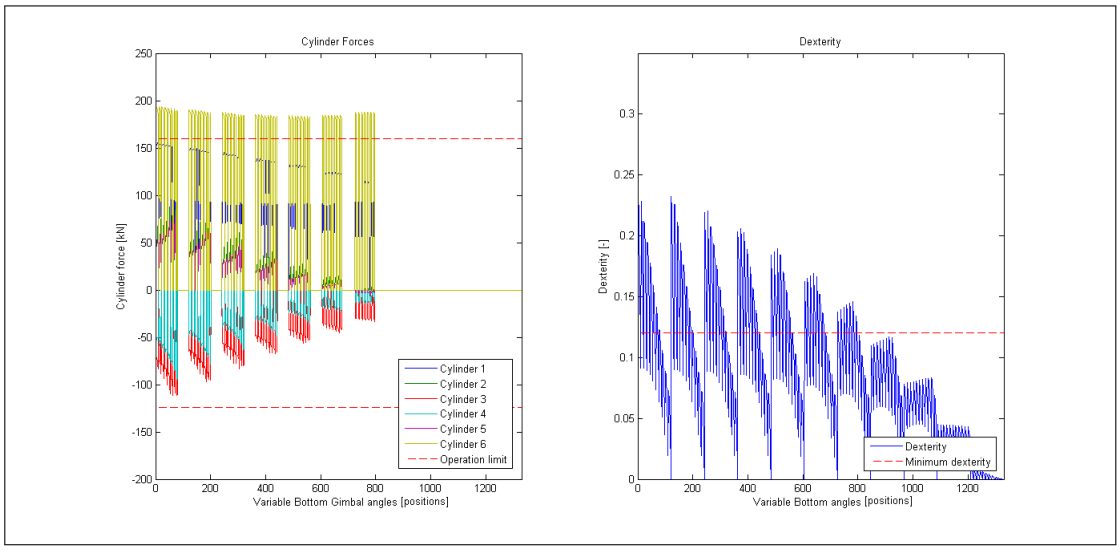

Figure 4-25: Forces and dexterity: Variable bottom angles

Top and bottom angles

The last sub local optima is the combination of the previous two. The variable and fixed parameters are shown in Table 4-12.

Variable		Fixed	
$\frac{\pi}{36} \leq \gamma_{t,1} \leq \frac{\pi}{3}$	[rad]	$R_{b,i} = 3.00$	[m]
$\frac{\pi}{36} \leq \gamma_{t,2} \leq \frac{\pi}{3}$	[rad]	$R_{t,i} = 2.75$	[m]
$\frac{\pi}{36} \leq \gamma_{t,3} \leq \frac{\pi}{3}$	[rad]		
$\frac{\pi}{36} \leq \gamma_{b,1} \leq \frac{\pi}{3}$	[rad]		
$\frac{\pi}{36} \leq \gamma_{b,2} \leq \frac{\pi}{3}$	[rad]		
$\frac{\pi}{36} \leq \gamma_{b,3} \leq \frac{\pi}{3}$	[rad]		

Table 4-12: Variable and fixed parameters 3.3

The dexterity and forces can no longer be plotted in a clear fashion due to the large number of variables. The conclusion of this sub local optima can be found in the next paragraph (local optimum 3), where the optimised configuration is found with the use of the optimisation criteria.

Local optimum 3

With the use of the optimisation criteria, the coordinates and force distribution of this local optimum is found (Figure 4-26a and 4-26b). It can be stated that the outcome of this local optimum is almost the same as for the second local optimum. The angle of the top gimbals remain maximum, $\gamma_{t1} = \gamma_{t2} = \gamma_{t3} = \left(\frac{\pi}{3} - \frac{\pi}{36} \right)$. The angle of the bottom gimbals becomes asymmetric, $\gamma_{b1} = \frac{9\pi}{36}$, $\gamma_{b2} = \frac{5\pi}{36}$ and $\gamma_{b3} = \frac{7\pi}{36}$.
The coordinates of the bottom gimbals differ from the previous local optimum, as they are more concentrated towards the y-axis. Forming a more elliptical shape. This asymmetric shape is as expected as the external loads are also asymmetric.

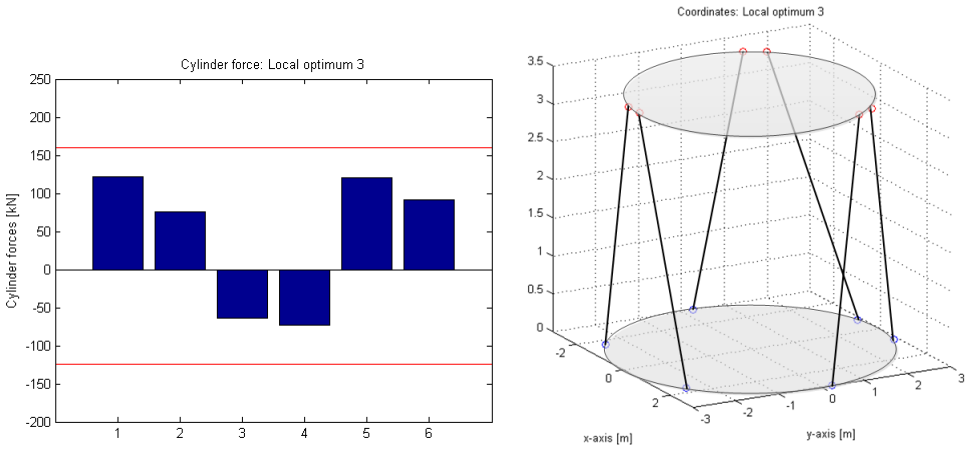

(a) Forces: Local optimum 3 **(b)** Coordinates: Local optimum 3

Figure 4-26: Local optimum 3

4-4-4 Elliptical top and bottom frames

The critical loading condition on top of the Stewart platform is the tipping moment caused by the gangway. For the platform being able to withstand this moment, it is not required to be symmetrical. In previous local optimum already a elliptical shape was found. It is possible that the radius of different gimbal pairs, have different radii, making the Stewart platform elliptical. To withstand the large tipping moment it can be assumed that the radius in y-direction will be as large as possible, but in x-direction the radius may be smaller.

To make such an elliptical shape possible, two radius variables per frame should be used, these are already shown in Table 4-1. The influence of these variable radii can be seen in Figure 4-27. This local optimum is also divided into the three sub local optima: (1) variable top radii, (2) a variable bottom radii and (3) a variable of top and bottom radii.

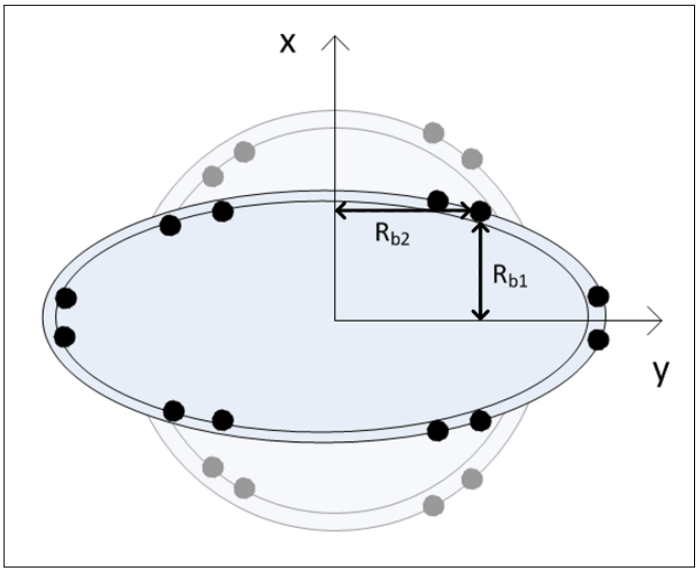

Figure 4-27: Elliptical frames

Top radii

The first sub local optima is varying both top radii from 1.00 to 3.00 meter. The parameters and the variables are shown in Table 4-13 and Figure 4-28.

Variable		Fixed	
$1.00 \leq R_{t,1} \leq 3.00$	[m]	$R_{b,i} = 3.00$	[m]
		$R_{t,2} = 3.00$	[m]
		$\gamma_{t,i} = \gamma_{b,i} = \frac{\pi}{36}$	[rad]

Table 4-13: Variable and fixed parameters 4.1

The elliptical shape can be seen in the coordinates of the variables. The forces and dexterity that follow from this shape are plotted in Figure 4-29. The maximum push forces decrease

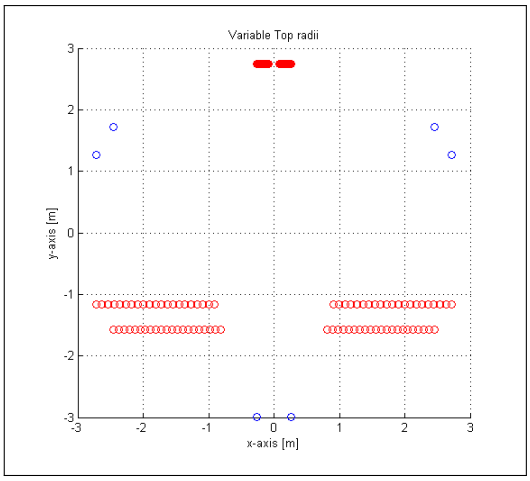

Figure 4-28: Coordinates: Variable top radii

while the elliptical shape becomes more circular. The dexterity is far above the minimum value for every configuration.

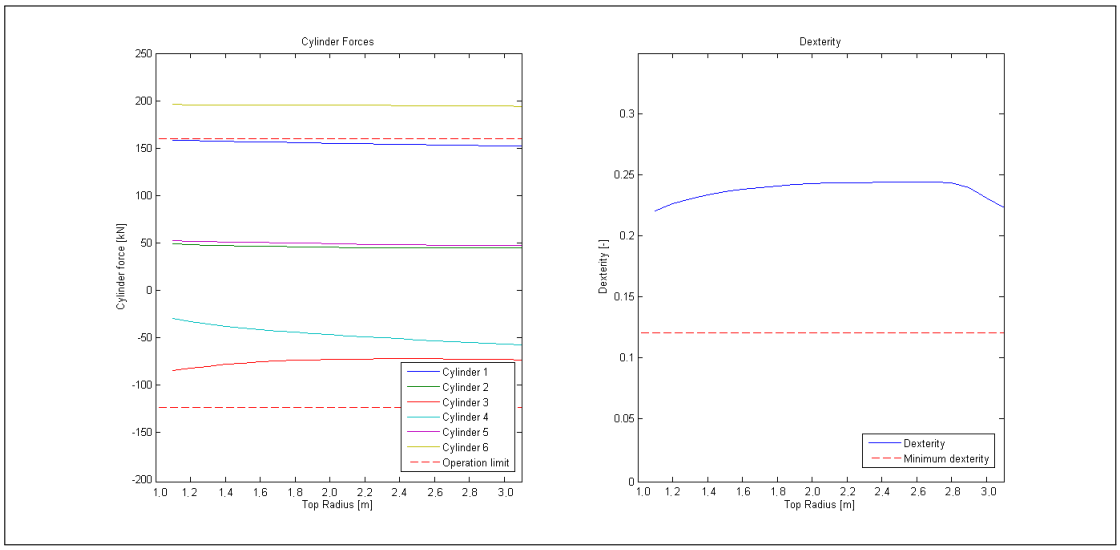

Figure 4-29: Forces and dexterity: Variable top radii

Bottom radii

The second sub local optimum is the elliptical shape of the bottom frame. The fixed and variable parameters can be seen in Table 4-14 and Figure 4-31.

Variable		Fixed	
$1.00 \leq R_{b,1} \leq 3.00$	[m]	$R_{t,i} = 2.75$	[m]
		$R_{b,2} = 3.00$	[m]
		$\gamma_{t,i} = \gamma_{b,i} = \frac{\pi}{36}$	[rad]

Table 4-14: Variable and Fixed parameters 4.2

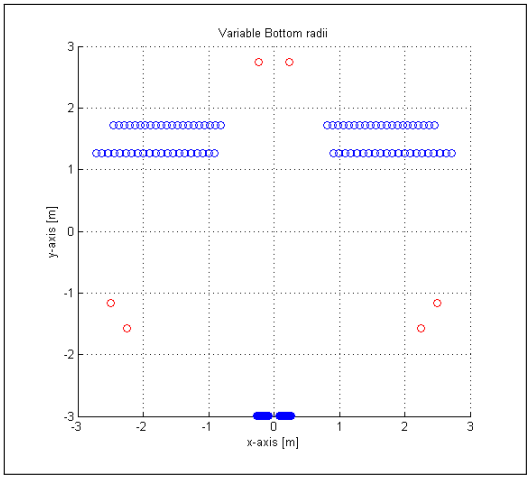

Figure 4-30: Coordinates: Variable bottom radii

The cylinder forces that follow from the elliptical bottom frame are shown in Figure 4-30. Two cylinder forces increase when the shape is changed from elliptical to circular. However, the elliptical shape with the smallest R_{b1} has a dexterity of below the minimum value. The system becomes more stable while the radius increases. For a good indication of the force distribution over an elliptical shaped Stewart platform, both frames are varied in the next section.

Top and bottom radii

The last local sub optimum is the combination of both previous sub local optima. The parameters are again given in Table 4-15.

Variable		Fixed	
$1.00 \leq R_{b,1} \leq 3.00$	[m]	$\gamma_{t,i} = \gamma_{b,i} = \frac{\pi}{36}$	[rad]
$1.00 \leq R_{t,1} \leq 3.00$	[m]	$R_{b,2} = 3.00$	[m]
		$R_{t,2} = 3.00$	[m]

Table 4-15: Variable and Fixed parameters 4.3

As shown in the previous sub local optimum, the small bottom radii cause a dexterity below 0.12 (Figure 4-33). This can also be seen in this sub local optimum, the forces for these

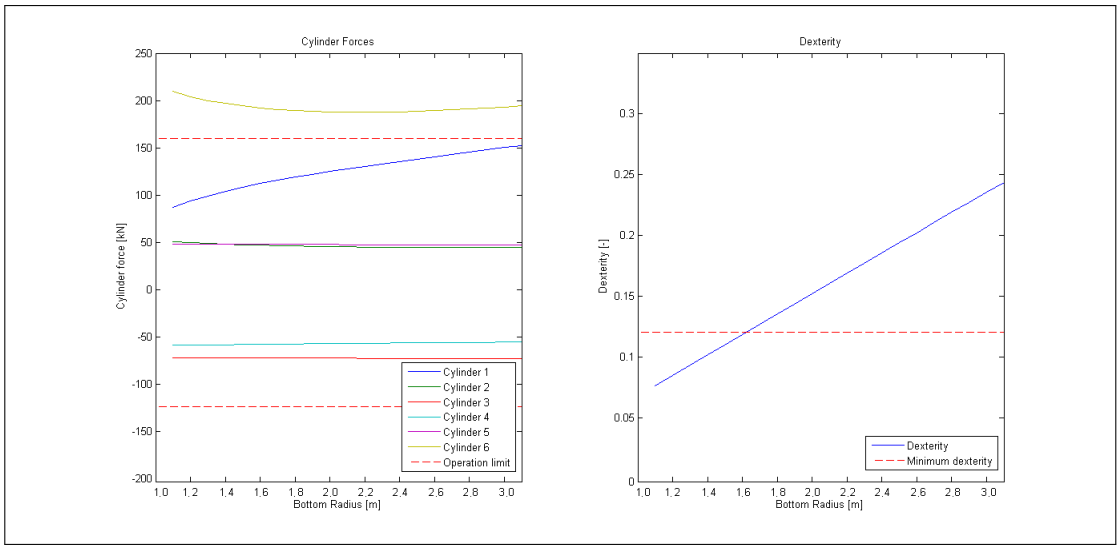

Figure 4-31: Forces and dexterity: Variable bottom radii

configurations are set to zero (see Figure 4-32). The small variation of the forces from the previous two sub local optima can also be seen in this combination.

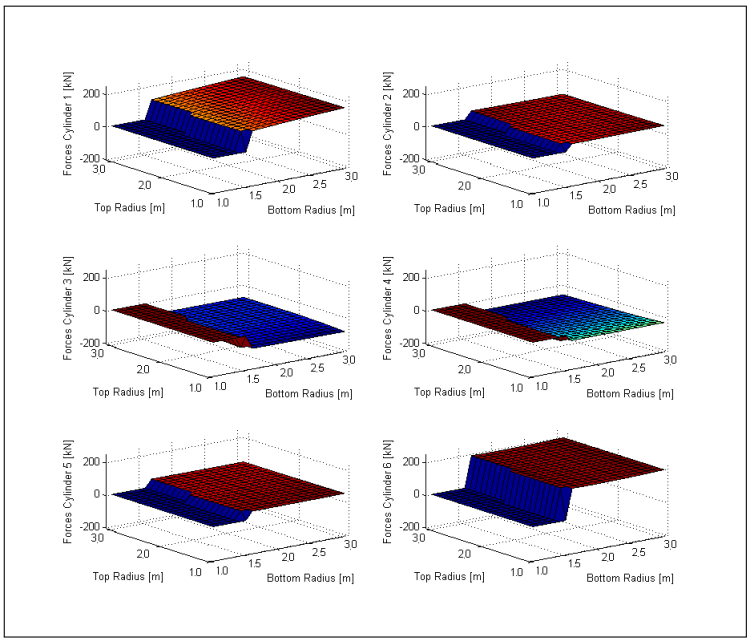

Figure 4-32: Forces: Variable top and bottom radii

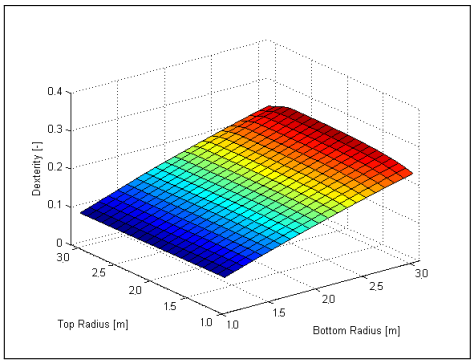

Figure 4-33: Dexterity: Variable top and bottom radii

Local optimum 4

The elliptical top and bottom frame has a small influence on the cylinder force distribution. The best configuration can not be seen from the forces from Figure 4-32. The optimum criteria is again applied which gives the best configuration of the elliptical local optimum. The force distribution and coordinates are given in Figure 4-34a and 4-34b. The bottom radius $R_{b1} = 1.90$ meter and the top radius is $R_{t1} = 1.00$ meter. The forces are reduced with a maximum of 10 kN.

It can be concluded that making the frames elliptical has a small advantage for the force distribution over the circular frames. For this local optimum the radius in x-direction have been made smaller, due to the restriction of the bottom frame of 3.00 meters. Without this restriction the shape can be elongated along the y-axis, which could lead to more favourable results for the force distribution. This will only lead to a platform which exceeds its maximum footprint.

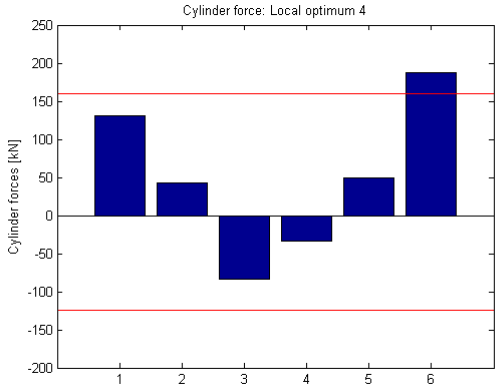

(a) Forces: Local optimum 4

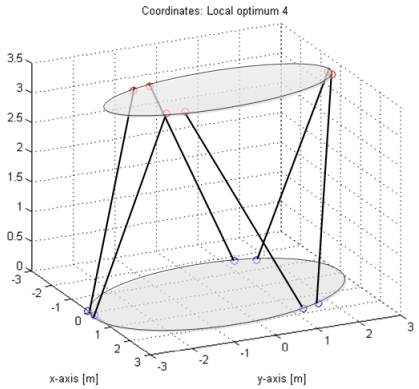

(b) Coordinates: Local optimum 4

Figure 4-34: Local optimum 4

4-5 Global optimum

The influence of all the different parameters have been established by the four local optima from the previous section. Per local optimum the following points where concluded:

1. The larger the radius of the top and bottom frame, the lower the cylinder forces. This was due to the more vertical configuration of the cylinders and the larger distance to the centre of the top frame. The local optimum was found for a top and bottom frame with a radius of 3.00 meter. The dexterity is also far above the minimum value.
2. From the linked top and bottom gimbal angle followed that the bottom gimbals are located below the gangway instead of the top gimbals as first assumed. The four cylinders are now located on the side of the gangway, giving a better support for the weight of the gangway. The bottom gimbals are as far away from each other as possible, again to increase the vertical position. The dexterity at this point is above the minimum value, but it has to be checked whether this will hold for the whole workspace of the system.
3. The separate gimbal angles had equivalent results for the linked top gimbals. The bottom gimbals are still located further away from each other, only this time they have become asymmetric. This is found reasonable as the external loading of the platform is also asymmetric.
4. The elliptical shape of the top and bottom frame has a minor advantage over the circular frames. The advantage of the elliptical shape is limited by the constraint that the frames can not be made larger than 3.00 meter. Without this constraint.

With the variables and constraints from the beginning of this chapter, the global optimum for the Stewart platform will be found. This means that all four local optima will be combined in the model. First the geometry for the best force distribution with allowable dexterity is found and after that the geometry is tested for the workspace of the system.

4-5-1 Cylinder force distribution

When combining all the different variables in one model, the optimum geometry for the force distribution with an allowable dexterity (in neutral) is as shown in Figure 4-35b. The parameters of the geometry are given in Table 4-16. The corresponding cylinder forces are plotted in Figure 4-35a, with the cylinder forces of the current A-type faded behind it. The dexterity of the global optimum in neutral position is 0.1264.

Radius [m]	Top gimbal angle [rad]	Bottom gimbal angle [rad]
1. $R_{t1} = 2.00$	5. $\gamma_{t1} = \frac{11\pi}{36}$	8. $\gamma_{b1} = \frac{9\pi}{36}$
2. $R_{t2} = 3.00$	6. $\gamma_{t2} = \frac{11\pi}{36}$	9. $\gamma_{b2} = \frac{5\pi}{36}$
3. $R_{b1} = 3.00$	7. $\gamma_{t3} = \frac{11\pi}{36}$	10. $\gamma_{b3} = \frac{7\pi}{36}$
4. $R_{b2} = 3.00$		

Table 4-16: Parameters first global optimum

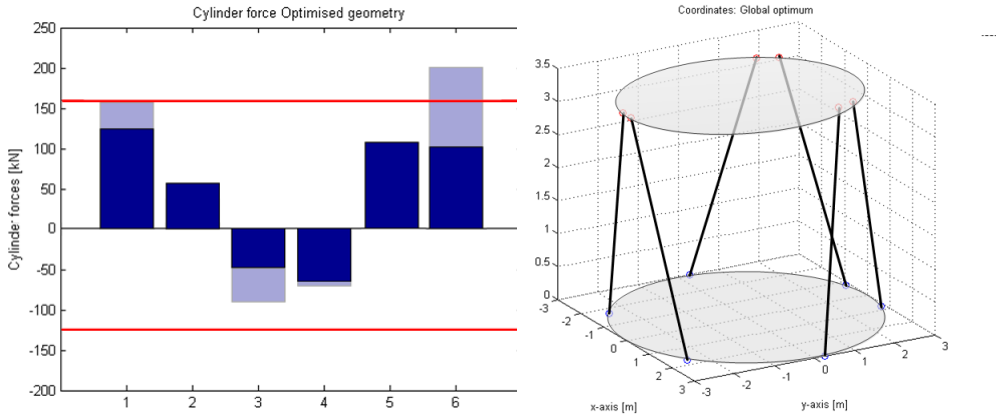

(a) Forces: Global optimum **(b)** Coordinates: Global optimum

Figure 4-35: Global optimum

4-5-2 Workspace

The workspace has to be checked for the global optimum of the geometry. The workspace of the system is derived with the use of the Inverse Kinematics. For every position the cylinder length is determined and then set to zero if one of the cylinders reached its minimum or maximum. The workspace of the global optimum in plotted in fifteen cross-sectional planes on the next page and can be compared to the workspace of the current A-type (already shown in Chapter 2). The red squares are within the reach of the Stewart platform and the blue squares are for when one of the cylinders has reached its minimum or maximum.

The workspace is plotted from -2.00 to 2.00 meter for al the translations and -40 to 40 degrees for the rotations. From the two plots of the A-type and the geometry of the global optimum, it can be concluded that the workspace of the global optimum is smaller in multiple DoF. In two DoF the workspace is enlarged, in x and ψ. In x-dirction is a result of the elliptical shape of the top platform. The larger bottom gimbal angles lead to more vertical configuration of the cylinders, which results in a larger angle ψ. The motion in ψ direction is not compensated by the Ampelmann system, however with this angle is not used more stroke length can be reserved for the other directions.

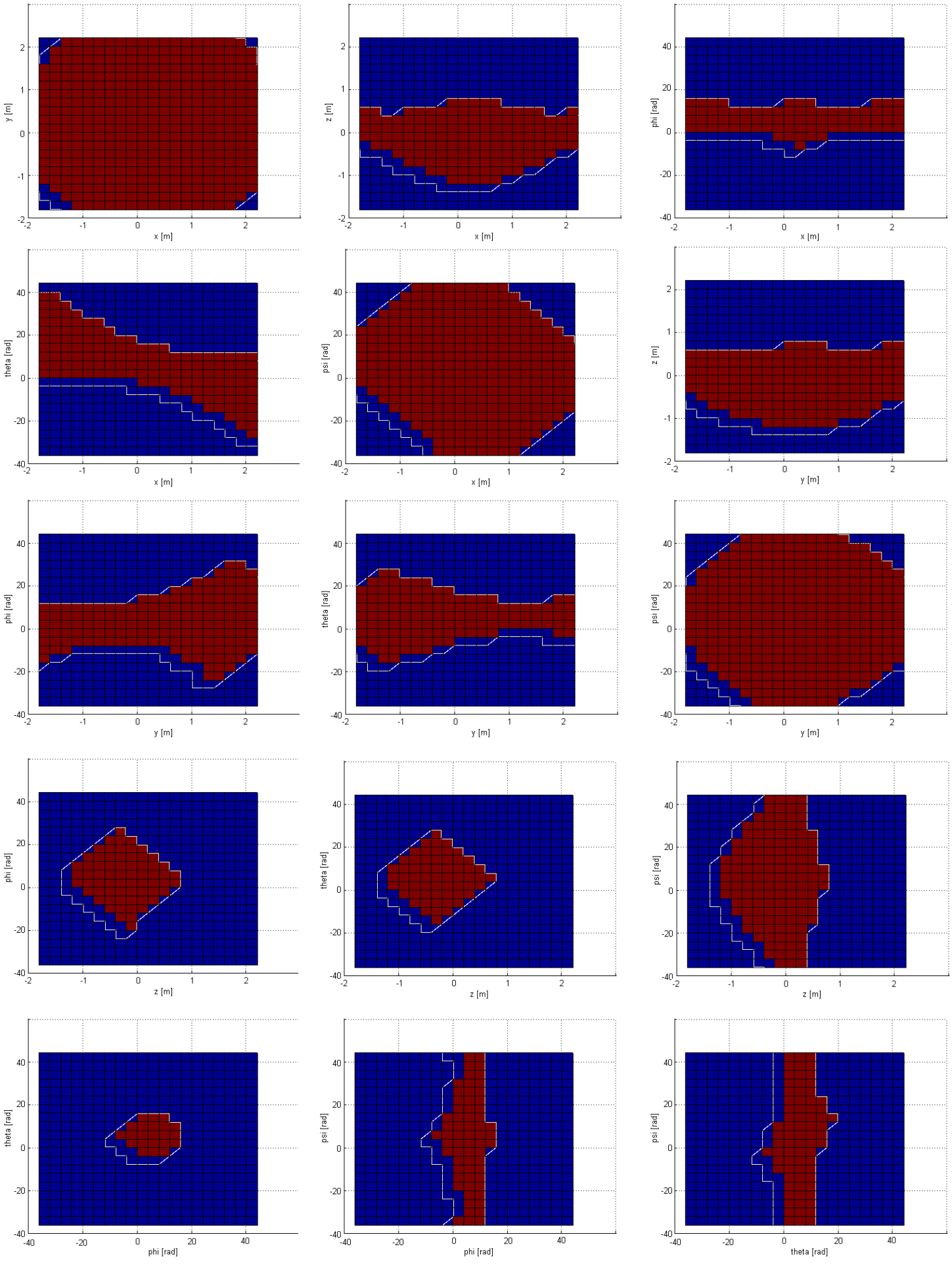

Workspace Global optimum

4-5-3 Dexterity

Next to the cylinder length check, also the dexterity has to be checked throughout the whole workspace. In every position, that is in reach of the new geometry, the dexterity should be above the minimum value of 0.12. The following criteria should hold:

$$P(n_{dex}|n_{cyl}) = \frac{P(n_{dex} \bigcap n_{cyl})}{P(n_{cyl})} = 100\% \tag{4-10}$$

Where,

P	Probability	[-]
n_{dex}	Number of times dexterity ≥ 0.12	[-]
n_{cyl}	Number of times $l_{min} \leq l_i \leq l_{max}$	[-]

This percentage is checked for the current global optimum and appeared to be only 83.17 %. A geometry of a Stewart platform that reaches below the minimum dexterity value in certain positions can lead to an uncontrollable platform. This is not accepted as it can lead to malfunctioning of the system. To reach a percentage of 100%, the parameters should be changed. From the local optima it can be seen that the elliptical top frame has a minor influence on the dexterity, but the large angles between the bottom gimbals has.

4-5-4 Final global optimum

To obtain the geometry of the final global optimum the bottom gimbal angle is reduced to satisfy the dexterity criteria. The new geometry with a dexterity above 0.12 for all positions is:

Radius [m]	Top gimbal angle [rad]	Bottom gimbal angle [rad]
1. $R_{t1} = 2.00$	5. $\gamma_{t1} = \frac{11\pi}{36}$	8. $\gamma_{b1} = \frac{9.7 \cdot \pi}{36}$
2. $R_{t2} = 3.00$	6. $\gamma_{t2} = \frac{11\pi}{36}$	9. $\gamma_{b2} = \frac{9.3 \cdot \pi}{36}$
3. $R_{b1} = 3.00$	7. $\gamma_{t3} = \frac{11\pi}{36}$	10. $\gamma_{b3} = \frac{9.5 \cdot \pi}{36}$
4. $R_{b2} = 3.00$		

Table 4-17: Parameters final global optimum

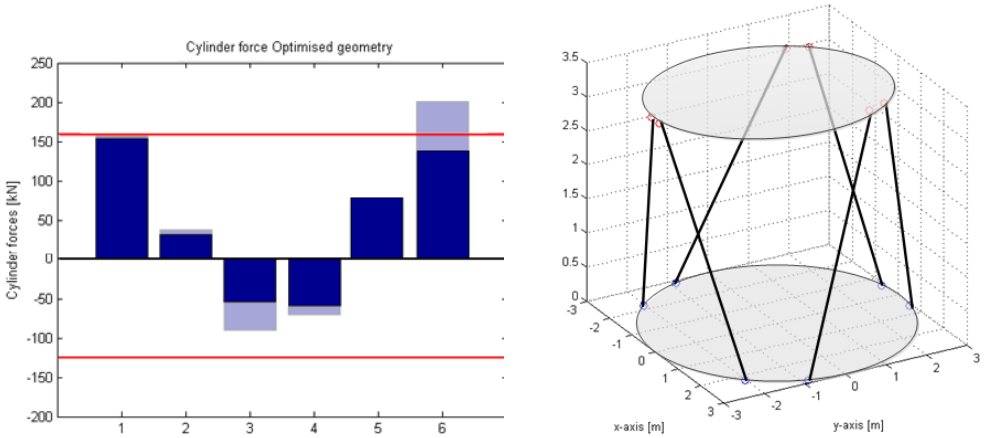

(a) Forces: Final Global optimum **(b)** Coordinates: Final Global optimum

Figure 4-36: Final Global optimum

The coordinates of the new geometry are plotted in Figure 4-36, with the corresponding cylinder forces in neutral position. It can be concluded that the cylinder forces have increased in this last optimisation step, however they are still below operation limit. When this geometry is moved though its workspace, the cylinder forces will fluctuate and exceed their operation limit as shown in Figure 4-37 for cargo transfer with 1000 [kg]. A solution for this problem is introduced in Chapter 6. For people transfer, the forces only exceed their limit at certain extreme positions of the platform (Figure 4-39). This is assumed to be acceptable as it is only the case for certain positions and it is only the push force which is exceeded.

The new workspace for this final global optimum of the geometry of the Stewart platform is plotted on the next page. The workspace of the system has increased with this latest adaptation, especially the rotation angles ϕ and θ.

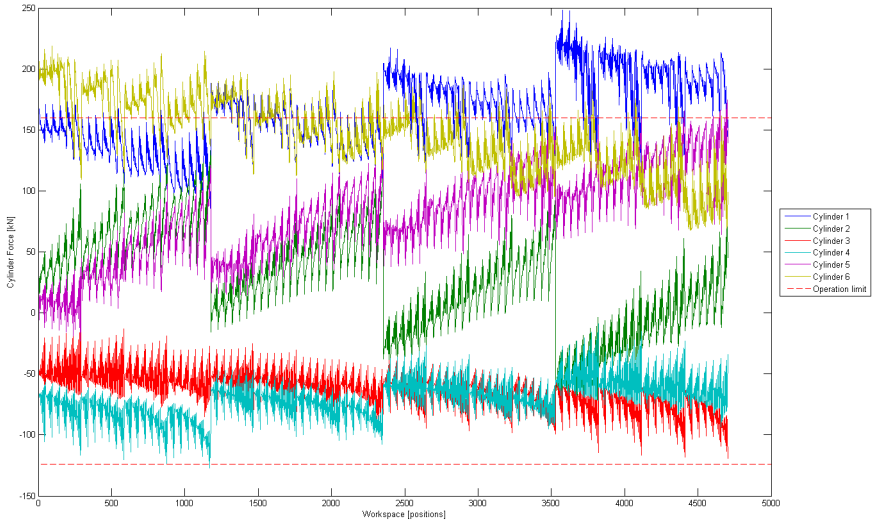

Figure 4-37: Forces Global optimum over workspace: GXXL-NO-CT1000kg

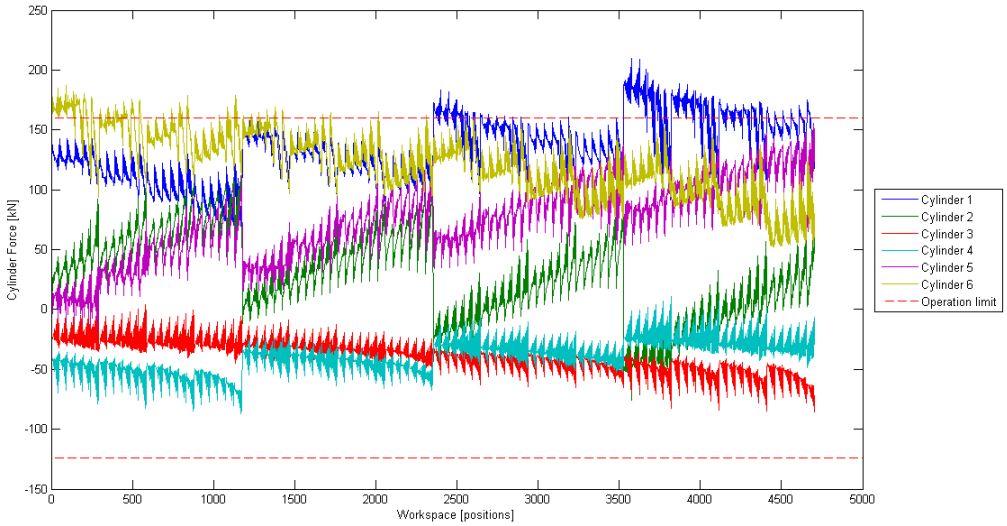

Figure 4-38: Forces Global optimum over workspace: GXXL-NO-CT500kg

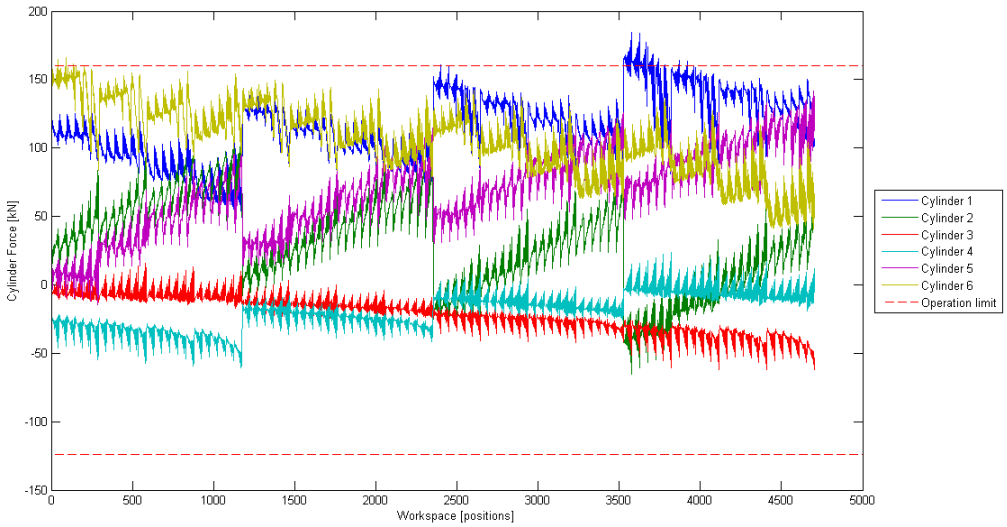

Figure 4-39: Forces Global optimum over workspace: GXXL-NO-PT

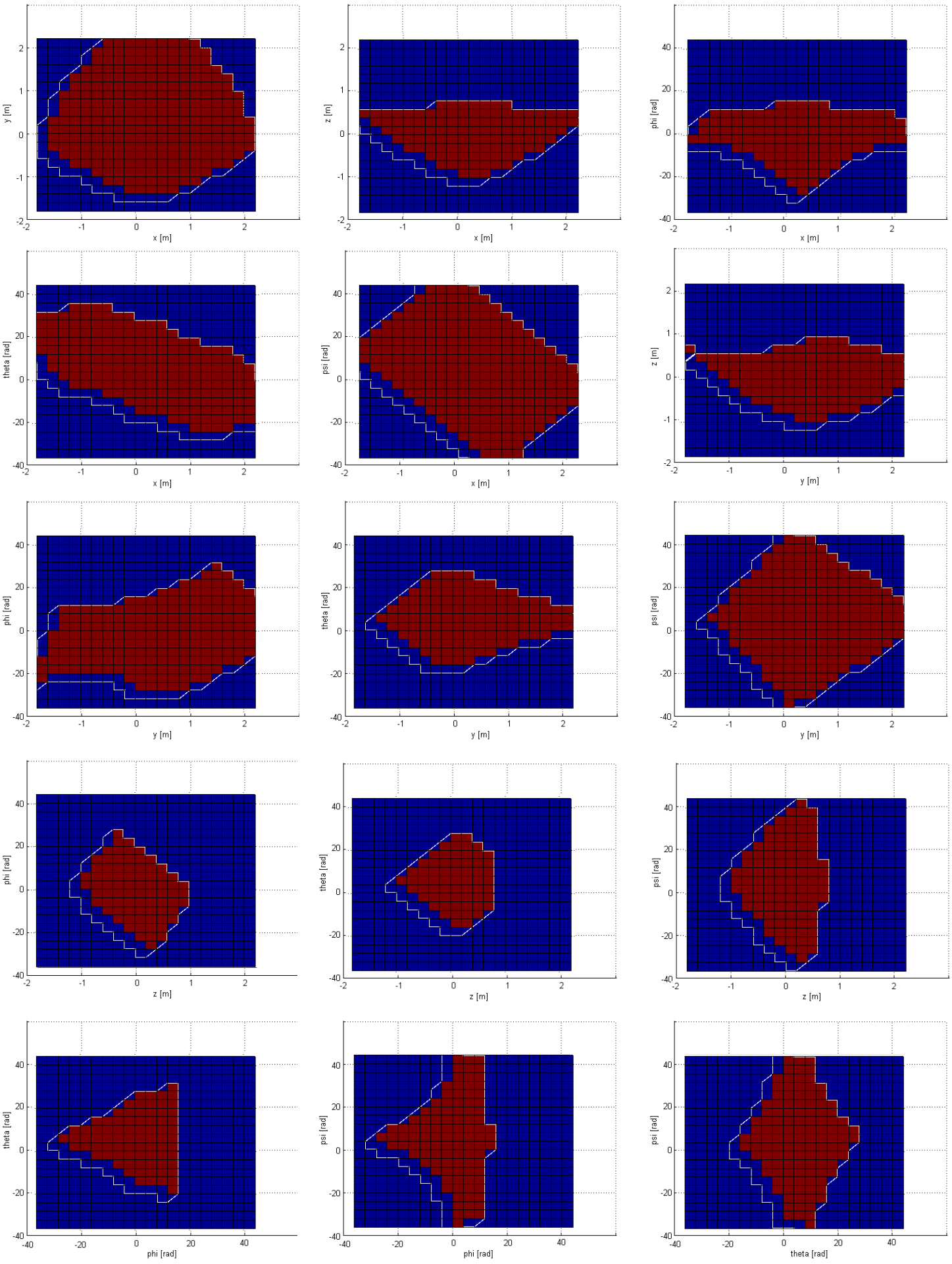

Workspace Final Global optimum

4-6 Concluding remarks

In this chapter the Stewart platform of the A-type has been optimised for the asymmetric load cases caused by the GXXL. The optimisation is preformed with the use of a Matlab model. The optimisation criteria was a minimisation of the absolute maximum cylinder force. First four local optima where found:

1. Variable radius of a circular frame
2. Variable linked gimbal angle
3. Variable separate gimbal angle
4. Variable radius of a elliptical frame

For all four local optima the results are discussed and compared, to see the influence of each parameter. This led to the global optimum for the geometry of the system, with a maximum circular bottom frame with large gimbal angles and a elliptical top frame with small gimbal angles. The workspace of this geometry was tested and compared with the workspace of the current A-type. The workspace is reduced in most DoF, except for the x-direction and ψ angle. As stated before, the Stewart platform can be optimised for the workspace, dexterity of loading capacity. This reduced workspace is a result of the optimisation of the geometry for the loading capacity of the large asymmetric load cases. The workspace of the system was used to determine the dexterity for all position that the new geometry could reach. It was concluded that at some position, the dexterity was below the minimum value. This is not acceptable, as this can lead to unpredictable behaviour. The geometry is changed, so that the for every position the dexterity is above the minimum value. The new geometry has a minor increase in cylinder forces. The workspace of the new geometry has increased for the rotation angles ϕ and θ.

The optimised geometry has a better force distribution within the six cylinders than the current A-type and has a dexterity of above 0.12 for every position. To accomplish this optimisation, there is a minor decrease of the workspace of the system, but as stated in Chapter 2 this does not mean that the workability of the system should decrease. The cylinder forces in neutral position are all below their operation limit. However, when moving the platform through its workspace, the forces fluctuate and become larger than their operation limit. A second optimisation method is introduced in Chapter 5 to reduce the forces even further. The fluctuations are reduced in Chapter 6.

Chapter 5

Reducing external loads

5-1 Introduction

The optimisation of the geometry of the Stewart platform in Chapter 4 led to a reduction of the cylinder forces. However, when moving the platform through the workspace, the forces fluctuate and exceed their operation limit. A second optimisation method is needed to make it possible to place a GXXL on top of a Stewart platform. Passive cylinders are added with a constant force which counteracts the loads from gangway. First the functioning of the cylinders is explained. After that the geometry of these cylinders is elaborated starting with a 2D sketch and concluding with a 3d representation of the geometry. In the third part the model is described which is used to determine the required force from the passive cylinders, including the optimisation criteria.

The forces of the passive cylinders are assumed to be constant in this chapter, so to be able place a GXXL on top of the platform, these forces have to counteract the most critical load case (dead load + live load). To see the effect of the passive cylinders, they are included in the A-type system in this chapter. In Chapter 6 the passive cylinders are added to the optimised geometry.

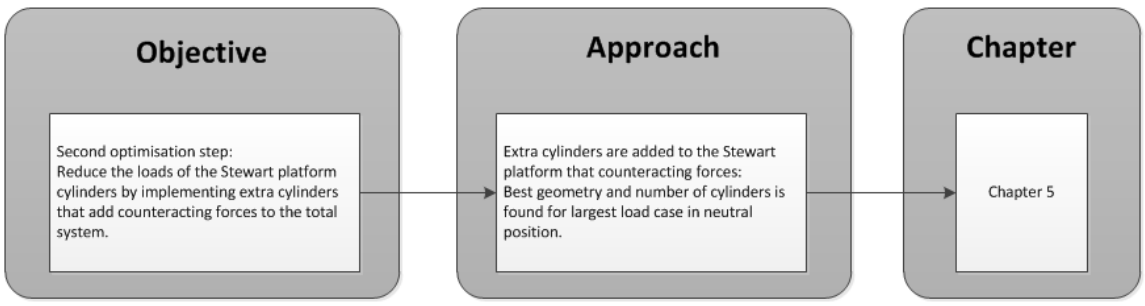

Figure 5-1: Approach Chapter 5

5-2 Functioning of passive cylinders

As stated in section 2-3-1, the number of cylinder in the Stewart platform is six. Cylinders can not be added that also control the motion of the platform. However, it is possible to add passive cylinders to the system. Passive cylinders move along with the current six cylinders, but also add a force to the system.

Before implementing passive cylinders in the Ampelmann system, first the functioning of these cylinders is elaborated. In this chapter a constant pressure is used when the passive cylinders counteract the load in neutral position. For the distinction between these extra cylinders and the Stewart platform cylinders, they are called passive cylinders in this chapter.

5-2-1 Motion control

Passive cylinders are connected to the top and bottom platform with the use of gimbals (the same as for the Stewart platform cylinders). The passive cylinders follow the trajectory of the other cylinders.

The motion of Stewart platform cylinders is determined with a motion control method [12]. First the vessel motions are obtained with the use of Octans. These motions are the input for the Reference generator that calculated the cylinder length with Inverse Kinematics. The set point of the cylinders (r_i) are transmitted to the cylinders valve control. This valve control also receives information from the position transduces, which determines the actual length of each cylinder. With the required and actual cylinder length, the control error is determined. This error is multiplied with the gain factor that leads to the proportional part of the total control signal. This process is called the `Proportional control method`. To reach the length that is calculated with the Inverse Kinematics, each cylinder should re- or extract with a certain velocity, which is calculated with the Jacobian matrix. This velocity is multiplied with the feed forward gain factor, leading to the feed forward part of the total control signal. This process is called the `Feed forwards contol method`. Signals from both processes are combined to the preliminary control signal. To cancel non-linearities of the valve, the control signal is determined with the use of a Look-up table. Here the calculated cylinder velocity ($\dot{l}_i$) are compared with the required control input (u_i). These signal are transmitted to the valve of each cylinder. The Hydraulic Power Unit (HPU) determines the hydraulic pressure that is required for the cylinders to reach their correct cylinder length. This control method is schematised in Figure 5-2.

With this motion control method the Stewart platform can compensate the vessel motions. The passive cylinders do not have such a motion control method, as they move along with other six cylinders. By adding the passive cylinder, the motion control of the Stewart platform cylinders does not have to be changed. The passive cylinders can cause friction, which can lead to larger pressures needed for the Stewart platform cylinders to move the platform. With respect to the external loads, this extra pressure assumed negligible, but should be investigated in further researches. The passive motion is made possible with the use of an accumulator, as schematised in Figure 5-3. The fluid moves through the accumulator to make it possible for fluid to flow from the top chamber to the bottom chamber of the cylinder. The accumulator is filled with compressible gas, nitrogen (N_2).

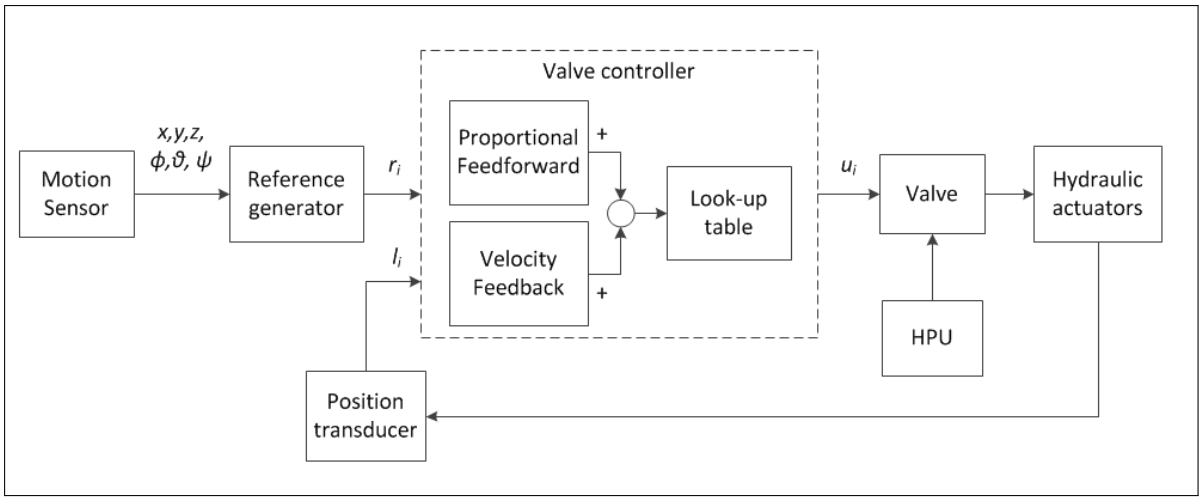

Figure 5-2: Motion control

5-2-2 Force control

The passive cylinders will have to maintain a certain pressure to deliver a force to the total system. The pressure in the cylinders can be controlled with a pressure controller, connected with to a valve. The force controller and the valve are both shown in Figure 5-3. In this chapter, only a constant force is used for the passive cylinders, counteracting the loads in neutral position. In the next chapter the possibility is investigated to make the force control active, counteracting the external loads over the entire workspace.

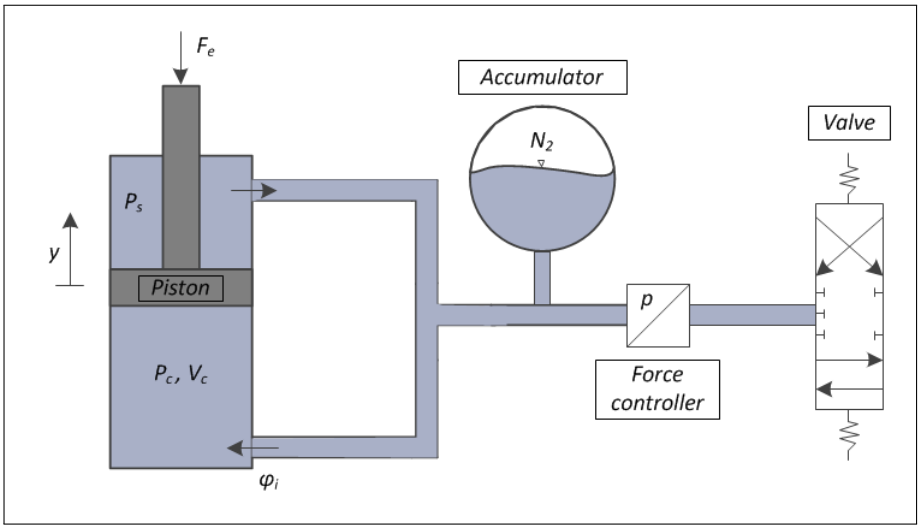

Figure 5-3: Force control

5-3 Passive force optimisation model

Free body diagram

The goal of the use of passive cylinders is to counteract the external loads on the Stewart platform, leading to the lowest possible Stewart platform cylinder forces. The free body diagram of this concept is shown in Figure 5-4.

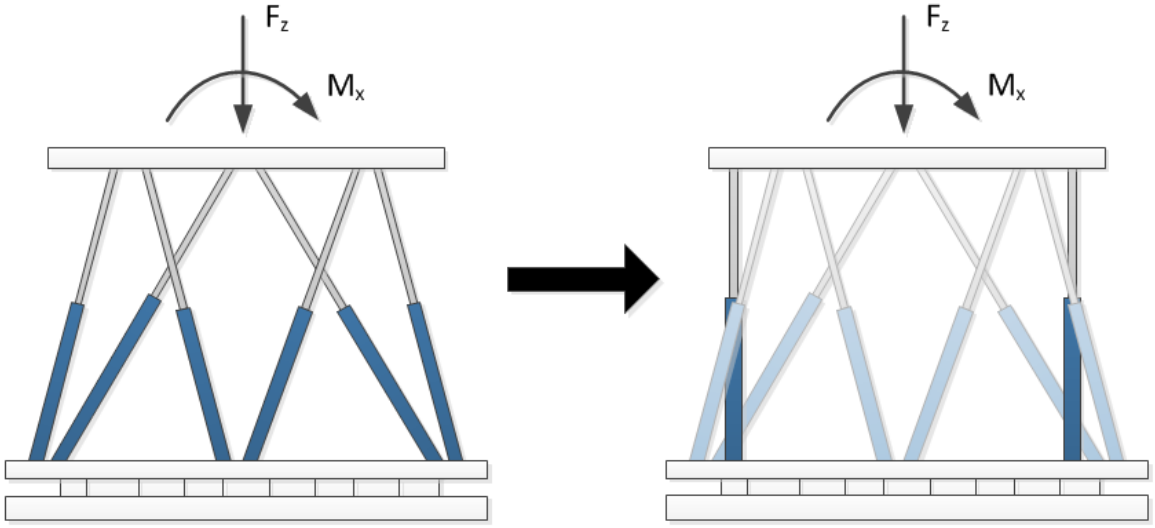

Figure 5-4: Reduction of load case with use of passive cylinders

In the same manner as Chapter 4, the 2d free body diagram is adapted to a 3d representation of the total Stewart platform in `Matlab`, containing both the Stewart platform cylinders as the passive cylinders. This time the geometry of the Stewart platform is known (the A-type system), but the model for passive cylinders has to be determined.

The platform will be loaded again with the critical loading condition from Chapter 3, Table 3-8. In this chapter first only the neutral position is considered. A passive force in chosen in the model, which will lead to a load case on top of the platform. This load case is subtracted from the external load case caused by the GXXL leading to a new reduced load case. For this reduced load case, the cylinder forces of the Stewart platform are derived. An optimisation criteria is used to achieve the lowest possible Stewart platform cylinder forces. The model of the passive cylinders depends on three parameters: (1) the number of cylinders, (2) the geometry of the cylinders and (3) the cylinder force optimisation. These three parameters are elaborated in the following sections. Only single stroke cylinders are used, which lengths are calculated with the equation 2-8 and 2-61. Double stroke cylinders have a larger reach, but this has a negative effect on the cylinder force and buckling strength, which is undesirable for the purpose of the passive cylinders.

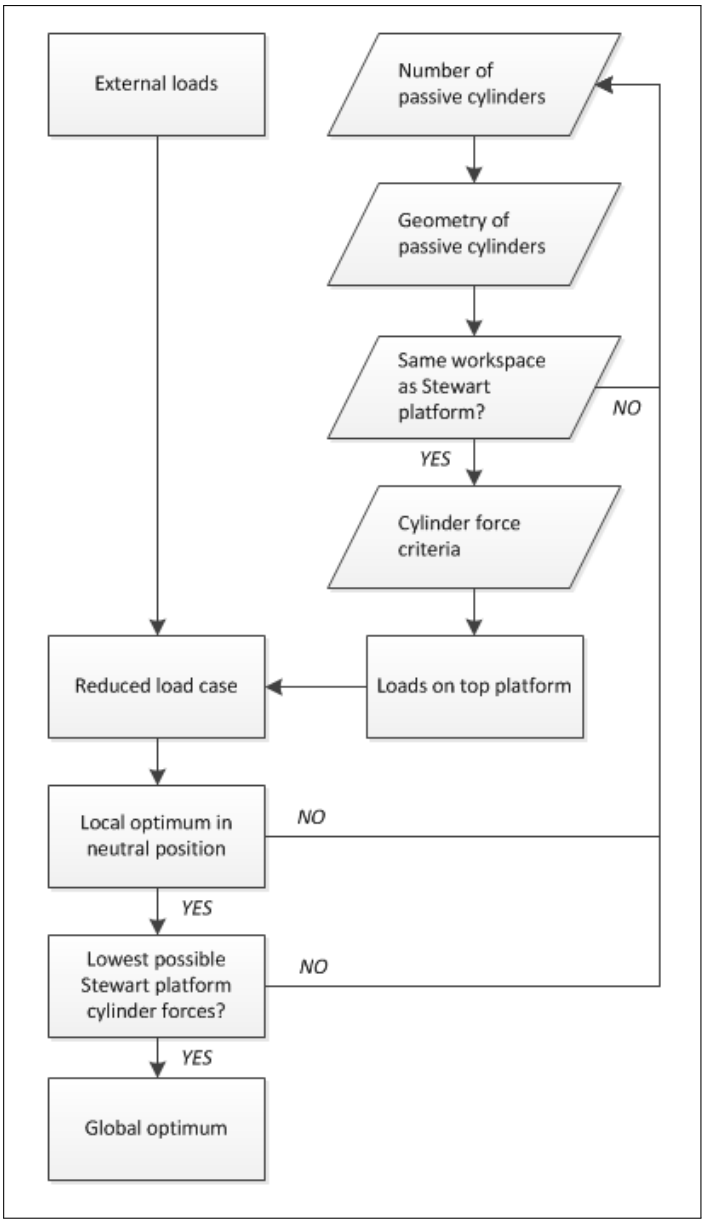

Figure 5-5: Flow diagram: Required passive forces

Geometry Stewart platform The geometry of the current A-type Stewart platform is used in this optimisation model. The direction of the load case with respect to the coordinates of the cylinders follows from Chapter 4. The cylinder force distribution is favourable for 4 cylinders located at the top on the gangway side and two at the backside, see Figure 5-6a. However, the effect of the passive cylinders on the Stewart platform cylinder forces is not yet determined. For a complete understanding of the passive cylinders, also a rotated load case of 60 degrees in the horizontal plane is taken into account (Figure 5-6b). In the following sections a distinction is made between these two configurations of the Stewart platform.

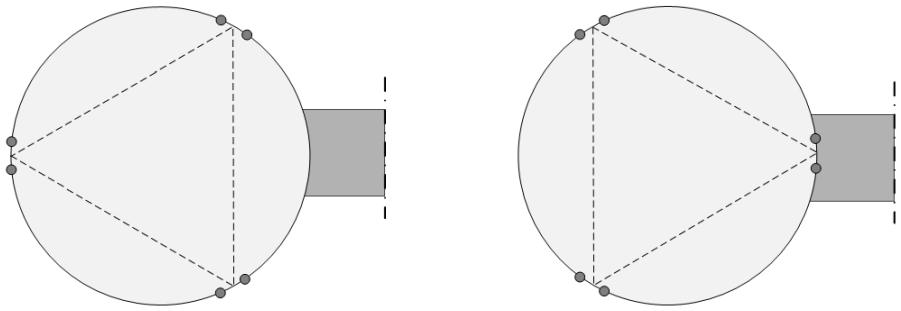

(a) Stewart platform configuration 1 **(b)** Stewart platform configuration 2

Figure 5-6: Top frame Stewart platform A-type

5-3-1 Number of cylinders

In this report the number of passive cylinders that is considered is from one to six. More than six cylinders will be redundant, because all cylinders of the Stewart platform will have their own slave cylinder. It is evident that a large number of passive cylinders will lead to the lowest cylinder forces. However, from a cost perspective it is desired that the number is as low as possible. Taken both points into consideration leads to the lowest number of passive cylinders with a sufficient load reduction. The configurations for 1 to 6 cylinders are given in Figure 5-7.

One cylinder When adding one cylinder to the platform, the downward force and tipping moment can be counteracted. The cylinder should be placed below the gangway to create the largest counteracting moment. For the first assumption the workspace of the cylinders is not taken into account. This means that the passive cylinder is located vertical to be able to create the largest force in vertical direction.

Two cylinders Two cylinders can complement each other as the cylinder under the gangway (the right cylinder in Figure 5-7b) has a push force and the cylinder on the left has a pull force. This only contributes to counteracting the tipping moment and less for the downward force.

Three cylinders With three cylinders, the tipping moment and the downward force can be counteracted when two cylinders are placed on the right of Figure 5-7c and one is on the left side. There are multiple alternatives for the configuration of the three cylinder model, which depend on the location of the top and bottom gimbals. These alternatives are investigated in section 5-3-3.

Four cylinders When applying four cylinder to the system, the four cylinders can be used as next to the four cylinders with the largest forces (cylinder 1, 3, 5 and 6). The passive cylinders become 'slaves' of the Stewart platform cylinders.

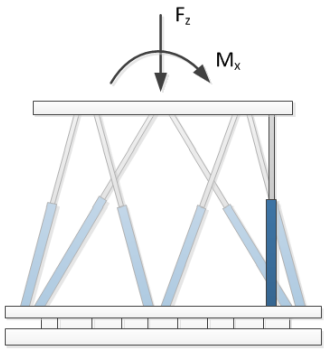

(a) One passive cylinder

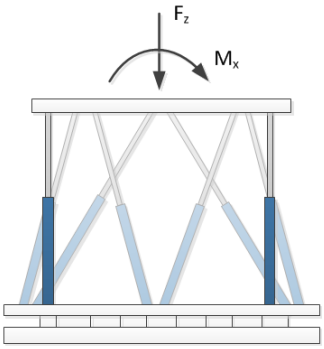

(b) Two passive cylinders

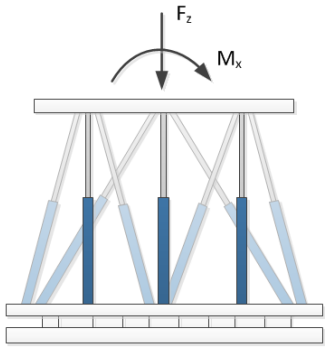

(c) Three passive cylinders

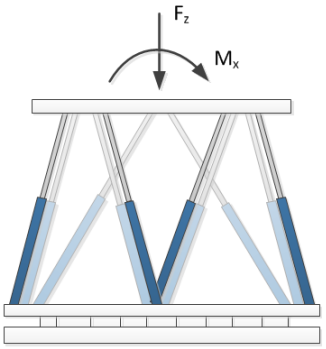

(d) Four passive cylinders

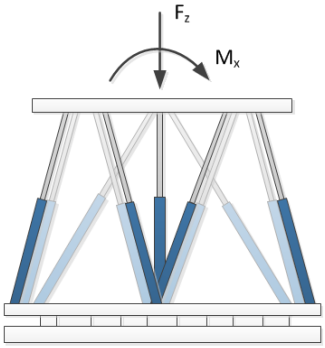

(e) Five passive cylinders

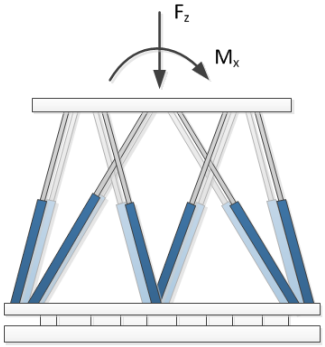

(f) Six passive cylinders

Figure 5-7: Number of passive cylinders

Five cylinders With five cylinders, the same 'slave' method can be used as for the four cylinder configuration. The fifth cylinder can only be used counteract the downward force, in the middle of the platform as shown in Figure 5-7e. The cylinder can also be used to counteract the tipping moment by placing the fifth cylinder in the same location as the one cylinder configuration (Figure 5-7a).

Six cylinders The configuration of six passive cylinders, all the cylinders act as slaves of the six Stewart platform cylinders.

For the first three configurations (Figure 5-7a to 5-7c), the passive cylinders are used to reduce the load case on top of the Stewart platform. For the last three configurations (Figure 5-7d to 5-7f), the passive cylinders can reduce the forces for the specific cylinders they are the slaves of. This is taken into consideration for the passive cylinder force optimisation.

5-3-2 Geometry passive cylinder models

The geometry of the passive cylinders depends on the number of cylinders that is used. In this section the geometry per number of cylinders will be elaborated. The geometry of the passive cylinders has an influence on the counteracting force due to the angle of the axial force and the distance to the centre of the platform and also on the workspace of the system. The passive cylinders should be able to reach every position of the current platform. Otherwise the workspace of the Stewart platform would be limited. The workspace of the passive cylinders depend on the cylinder lengths. The dexterity of the passive cylinders does not have to be checked, because the cylinders do not control the motion of the platform. First the location of the top gimbals is investigated and after that the bottom gimbals. The section is concluded with the geometry of the 3 cylinder model, because this configuration is less straight forward than the other models.

Top gimbals

For optimising of the geometry of the Stewart platform, the largest top frame in y-direction led to the lowest cylinder forces. The location of the top gimbal of the passive cylinders is also assumed to be on the edge of the platform. This theory is checked with a 2d (in y-z plane) 2 cylinder model of the top platform with only F_z and a M_x as external loads (as shown on the left part in Figure 5-8).

Both N_1 and N_2 can be determined with the use of a static equilibrium around respectively support 1 and 2. To see the influence of the distance from the centre of the supports, the external loads F_z and M_x are set at a half of their actual load as determined in Chapter 3. A half of the load is assumed reasonable for the first sketch as the remaining of the forces are distributed over the other cylinders. The reaction forces are obtained for a variable $0.1 \leq y_{1,2} \leq 2.75$ and are shown in the right part of Figure 5-8.

It can be concluded from Figure 5-8 that the smallest reaction forces occur for the largest y_1 and y_2. The reason for this is that the tipping moment is far greater than the downward force. To counteract this moment, the passive cylinders should be placed as far from the centre as possible. This theory can be used for all the models described in section 5-3-1.

Bottom gimbals

With the knowledge that the top gimbals should be placed as far from the centre as possible to create the largest counteracting moment, the location of the bottom gimbals should be

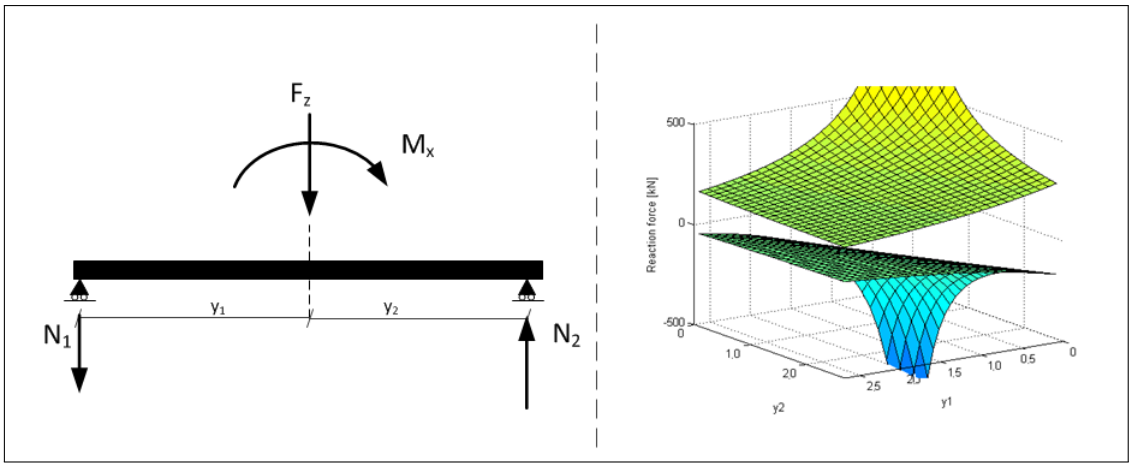

Figure 5-8: Reaction forces 2D sketch

investigated. The location of the bottom gimbals influence the angle of the cylinders and with that the angle of the force. The required length of the passive cylinders is calculated for the configuration of Figure 5-7b, where the cylinders are vertical orientated. For the Stewart platform the heave motion is limiting DoF [12], so this DoF is also used to determine the passive cylinder lengths. The minimum and maximum height of the platform, as shown in Figure 5-9, gives the lengths of the cylinders from the following criteria:

$$\begin{aligned} l_{stroke} &= l_{max} - l_{min} = 2.00 \quad [\text{m}] \\ l_{min} - l_{stroke} &\leq l_{dead} \end{aligned} \tag{5-1}$$

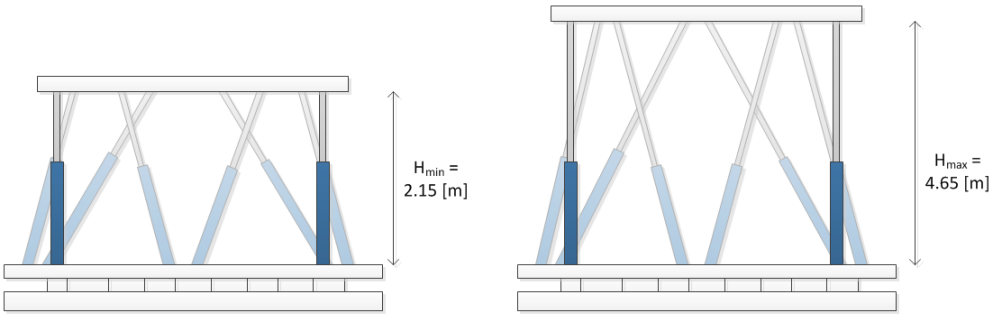

Figure 5-9: Minimum and maximum height Stewart platform

This gives a negative dead length which is impossible, meaning that the passive cylinders should be placed under an angle, with a to be determined length in the horizontal plane. A decision is made to use the same lengths of the A-type cylinders for the passive cylinders. In Chapter 7, this decision is further elaborated. For a 2 cylinder model, with a fixed dead and stroke length and minimum and maximum height of the platform, the length in the horizontal plane becomes 2.45 [m] ($\sqrt{5.25^2 - 4.65^2} = 2.45$ [m] and $\sqrt{3.25^2 - 2.15^2} = 2.45$ [m]). The angle of the passive cylinders reduces the vertical force component of the axial passive force. To obtain the same vertical force component, the axial passive forces will become larger. A

larger axial force under an angle, creates force components in x- and y-direction which is undesirable. The consequences of these force components are elaborated in section 5-3-4.

For the 1, 2 and 3 cylinder model, the obtained length in horizontal plane is used. The 1 and 2 cylinder model, the cylinders are placed in the plane of the tipping moment (Figure 5-10a and 5-10b). For the 4 to 6 cylinder model, the top and bottom gimbals are located next to the Stewart platform cylinders (Figure 5-7d to 5-7f).

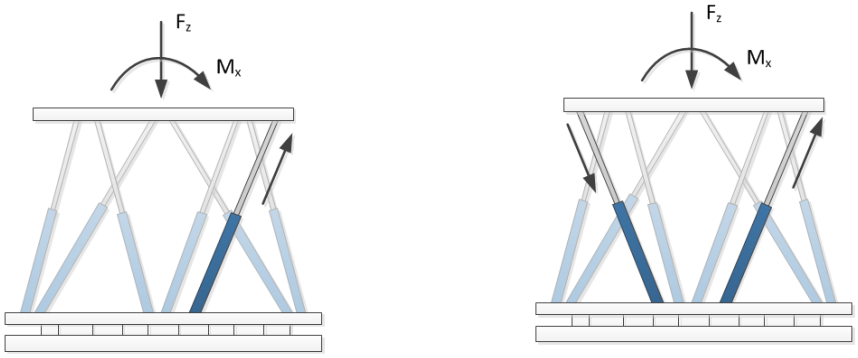

(a) One passive cylinder **(b)** Two passive cylinders

Figure 5-10: Location passive cylinders

5-3-3 Geometry 3 cylinder model

For the 3 cylinder model, the geometry is not as straight forward as for the other 5 models. Both the location of the top and bottom gimbals is investigated in this section. The only constraint is that the cylinders should have a length in the horizontal plane of 2.45 [m] as established in previous section. The three passive cylinders can be placed as an equilateral triangle with 120 degrees from each other at the top frame, or symmetrical around the y-axis (axis of the gangway) as shown in Figure 5-11b. The second configuration means that not all cylinders are located 120 degrees from each other at the top frame. This configuration also contains two cylinders below the gangway and one on the back side. Only, the two cylinders at the front can be located closer to each other. Figure 5-11b shows one possible asymmetrical configuration. The two push cylinders remain symmetric around the y-axis, to counteract each others horizontal force component in x-direction.

The passive cylinders in the equilateral triangle model are used as extra reaction forces for the Stewart platform cylinders in the entire top frame. In the other model the passive cylinders are used to counter act the tipping moment, in the same manner as for the 2 cylinder model. In total ten possible configurations of the total 3 passive cylinder model are researched, divided in two possible configurations for the Stewart platform cylinders and five for the passive cylinders. These models are all shown in 3d in Appendix A.

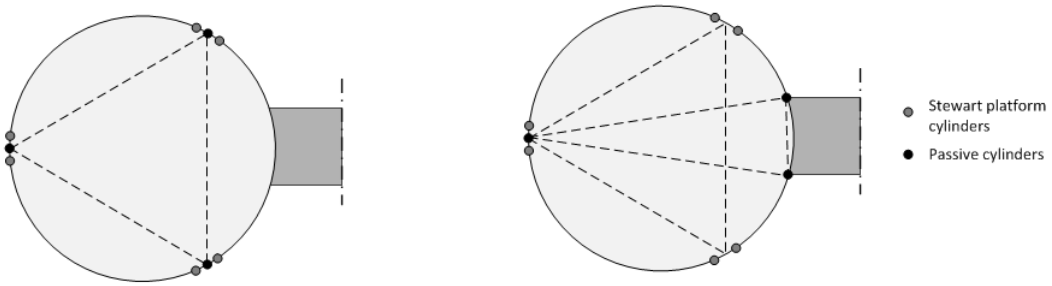

(a) Equilateral triangle configurations three cylinders mode

(b) Possible symmetrical configurations three cylinders model

Figure 5-11: Possible 3 cylinder model configurations

5-3-4 Stewart platform cylinders force reduction

The influence of each passive cylinder model on the force distribution over the Stewart platform cylinders is determined by applying a force of 100 [kN] to the passive cylinders. For every i-th cylinder model there are two configurations. Except for the 3 cylinder model, which has ten configuration. A total of twenty configurations is plotted from Figure A-2 to A-11 in Appendix A. The following conclusions are drawn from the plots of each configuration.

1. For an increasing number of passive cylinders the forces of the Stewart platform cylinders are reduced. For the 4 cylinder model, all the forces are below their optimum and are also all push forces. The configuration of the Stewart platform with respect to the direction of the gangway is of minor importance for this model as can be seen in Figure A-9, as long as the four passive cylinders act as slave cylinders of the two Stewart platform cylinders in the front and the two in the back. The gain that is achieved by adding a fifth or a sixth cylinder is minimal. The forces for the 6 cylinder model are even larger than of the 4 and 5 cylinder model. This is due to the arbitrary chosen axial force of the passive cylinders of 100 [kN]. For the two middle cylinders this force is too high, leading to larger forces in the Stewart platform cylinders.

2. The configurations of the 3 cylinder model lead to different cylinder force distributions as can be seen in Figure A-4 to A-8. It is evident that the configuration of the Stewart platform with respect to the load also has a large influence on the force distribution in the 3 cylinder model. The configuration of two Stewart platform cylinders below the gangway (Figure 5-6b) has a more even force distribution over the six cylinders.

3. Two configurations (Figure A-4b and A-7b) of the 3 cylinder model have the most even force distribution over the Stewart platform cylinders. The reason for this is that the vertical force component of all the cylinder models is equal due to the length in the horizontal plane as described in section 5-3-2. The remaining force components in x- and y-direction are different per configuration. In x-direction, these forces are in opposite direction which gives a netto force in x-direction of 0 [kN]. If the distance of the top gimbals from the gangway is increased, the horizontal force component in y-direction is decreased. However, the arm of the vertical force to counteract external load M_x is

also reduced. The smaller force component in y-direction has a larger influence on the even force distribution over the Stewart platform cylinder than the smaller arm length.

4. A decision is made for the number of cylinders based on the force reduction. For all the models and configurations the cylinder forces are below their operation limit. The 1 cylinder model is in neutral position already near the maximum value, so this model is not used. The 2 cylinder model has forces further away from the limit value, so this model will be used for force optimisation in section 5-4. For the 3 cylinder model configuration I and IV will be used, due to the best force distribution. The last model is the 4 cylinder model, which has only small push forces. The 5 and 6 cylinder do not have an advantage over the 4 cylinder model, and will only be more expensive due to the extra cylinders. These models will no longer be used.

The 3d representation of the four models is shown in Figure 5-12.

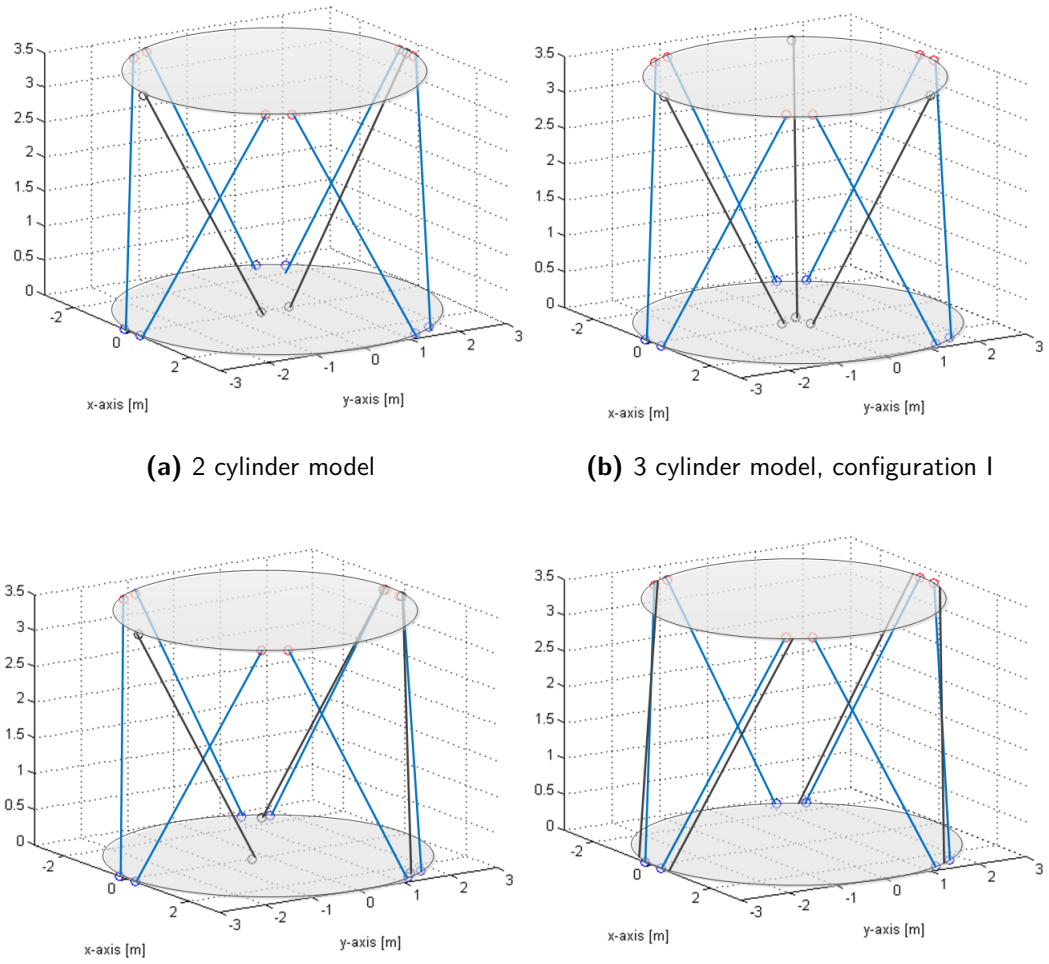

(a) 2 cylinder model

(b) 3 cylinder model, configuration I

(c) 3 cylinder model, configuration IV

(d) 4 cylinder model

Figure 5-12: Selected models and configurations

5-4 Force optimisation criteria

The next step of the optimisation model is the determination of the passive cylinder forces. For the selected models and configurations the passive forces will be obtained that lead to the lowest and even distributed forces of the Stewart platform cylinders. This optimisation step is preformed for the neutral position of the platform, because the passive cylinders contribute a constant force to the system. The used load case is the GXXL:NO-CT load case, without wind. Wind is a variable load in both magnitude and direction and can not be used in this optimisation step. The chosen configuration and passive force should be checked for the load case with wind and including the motions of the platform through the workspace.

For the 4 cylinder model, the passive forces follow from the forces of the Stewart platform cylinders. The slave cylinders counteract the forces of the cylinders next to them. For the 2 and 3 cylinder model an optimise criteria is chosen which reduces the forces of the cylinders to below the maximum operation force. The following criteria are investigated:

1. Minimise absolute maximum forces
2. Minimise pull forces
3. Combination of both criteria

These 3 criteria are tested for the 3 cylinder model with configuration I.

1. Minimise absolute maximum forces The first optimise criteria is to minimise the absolute maximum forces. With this the forces of cylinder 1 and 6 will be reduced due to the forces delivered by the passive cylinders. This criteria is uses the following equation:

$$\min\{\max\{|N_i^a|\}\} \tag{5-2}$$

When implementing this equation in the model described in section 5-3 the forces of the Stewart platform cylinders are reduced. The new cylinder forces are shown in Figure 5-13. The forces are indeed reduced, however the pull forces of cylinder 3 and 4 have increased. This is not a desired effect. When the pull forces exceed their maximum operating limit the rod of the cylinder can be pulled out of the rod. This will is very dangerous for people on and around the Ampelmann system as it will most likely collapse. Concluding, this criteria is not sufficient.

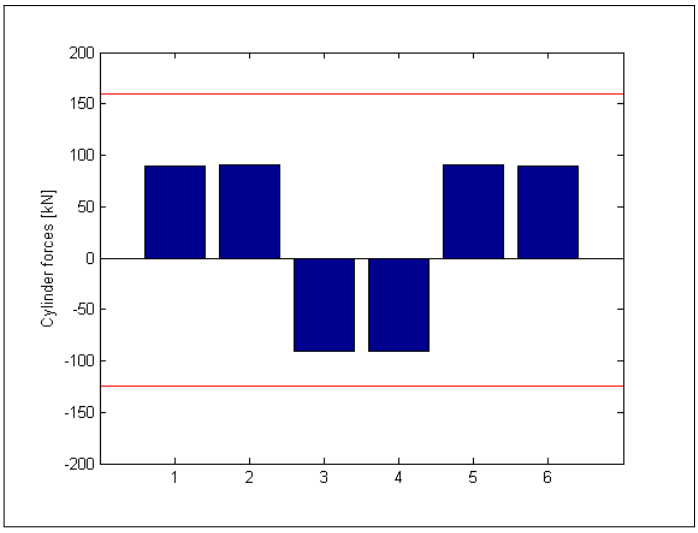

Figure 5-13: Absolute maximum forces minimised

2. Minimise pull forces As shown in previous section, it is desired to reduce the pull forces of the cylinders. This leads to the second optimisation criteria; maximising the minimum forces:

$$\max\{\min\{N_i^a\}\} \tag{5-3}$$

Implementing equation 5-3 in the model, the pull forces of the are reduced as is shown in Figure 5-14. Only this time the maximum push forces exceed the maximum operating forces. Concluding, this criteria is also not sufficient.

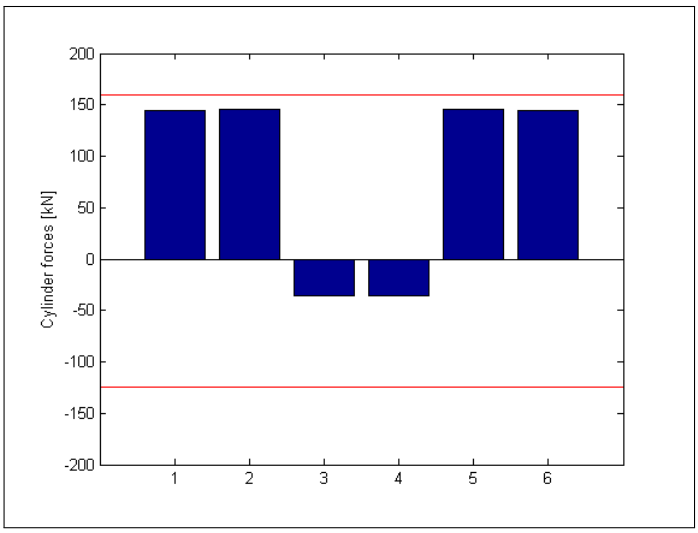

Figure 5-14: Maximum pull forces minimised

3. Combining both criteria The third optimisation criteria is a combination of the first two. Namely, the pull forces are reduced as much as possible, with a constraint that the push

forces may not be higher then 75% of the maximum operation limit:

$$\begin{aligned} &\max\{\min\{N_i^a\}\} \\ \text{With,} \quad &N_i^a \leq 0.75 \cdot F_{max.push.} \end{aligned} \tag{5-4}$$

Where,

$F_{max.op}$	Maximum operation push force = 160	[kN]

This criteria leads to the reduction of the pull forces with still acceptable push forces. The cylinders forces obtained with this criteria are shown in Figure 5-15. The criteria of 75% is derived from the varying cylinder forces from the mean over the workspace as plotted in Figure 2-10. The maximum force over the workspace for the two critical cylinders (1 and 6) exceed the mean with 88% respectively 105%. However, no passive forces can contribute to this kind of load reduction. Hence, the percentage is lowered to workable value of 25%, meaning 75% of the maximum operating force.

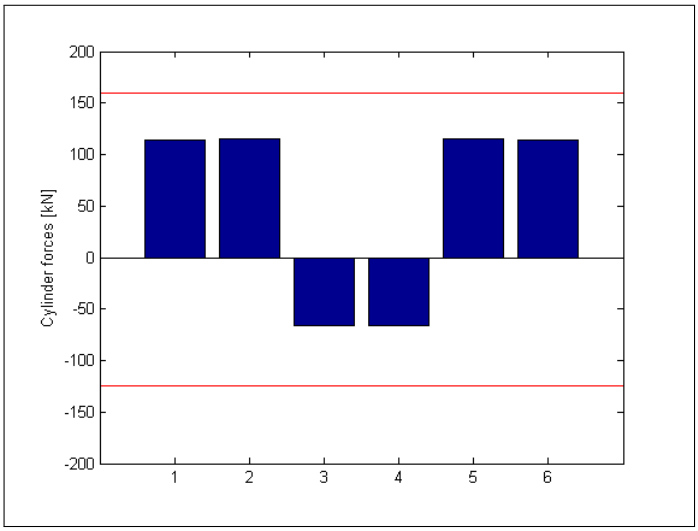

Figure 5-15: Maximum push and pull forces minimised

For a lower percentage the pull forces increase significantly. This percentage differs per model and configuration. For the 3 cylinder model configuration I it is 75% and for configuration 55%. For the 2 cylinder model it is also 75%. Another optimisation criteria for the 4 cylinder model is used, as this model has multiple force distributions with only push forces. The first optimisation criteria will be used for the 4 cylinder model.

5-5 Global optimum passive cylinders

For the four the models and configuration from previous section, the required passive force in neutral position can be derived by using the passive force optimisation criteria. When applying this force to the system and then moving the platform through the workspace,

the Stewart platform cylinder forces for extreme positions are obtained. In this section the platform is loaded with a wind load as described in Chapter 3 and three types of live load: (1) GXXL:NO-CT1000kg, (2) GXXL:NO-CT500kg and (3) GXXL:NO-PT. This distinction is made due to the fact that the cargo transfer load case is the most extreme load case, but not the most used. The GXXL is primary used for people transfer. The influence of the three different load cases is examined in this section. This last step is preformed to see the effect of the constant passive forces to the workability of the total system and obtain the global optimum for the passive cylinders optimisation model. All the twelve Stewart platform cylinder force plots are shown in Figure B-2 to B-16 in Appendix B. In this section the following conclusions are drawn from these plots.

1. For all the models and configurations, the smaller load cases lead to a more favourable and even force distribution of the six Stewart platform cylinders. For people transfer all the models and configurations have only forces below their operation limit.

2. The 4 cylinder model has the lowest cylinder forces for all three the load cases. This is evident as this model has the most cylinders. However, when the load cases are reduced, the pull forces increase. For certain positions of the platform, these pull forces almost reach their maximum value. As stated before, exceeding of the pull force limit can cause hazardous situations where the total system may collapse. It is recommended for the four cylinder model to decrease the passive forces, leading to lower pull forces of the Stewart platform cylinders during people transfer.

3. Both the 2 and 3 cylinder model contain forces above the operation push limit for the load case of cargo transfer with 1000 [kg] cargo. The difference between both models is minor, where the forces for the 3 cylinder model are only slightly lower. For both cargo transfer with 500 [kg] cargo and people transfer, both models have only a small number op positions where the push forces exceed their maximum. Because these extreme positions will only occur for a maximum of a few seconds during compensation, this is found acceptable.

4. For all the models and configurations, the force fluctuations are significant. Different options are presented to reduce these fluctuations and keep the forces below their maximum:

    - Reduction of the workspace of the system
    - Increase the operation limits
    - Use active force control

Reduction of the workspace For both the 2 and 3 cylinder model, the positions can be derived for which the cylinder forces exceed their operation limit. The system can be programmed that these positions can not be reached. This option has multiple disadvantages: (1) If the control system is not programmed correctly the platform can collapse as a cylinder will exceed its operation limit and (2) A large reduction of the workspace is not favourable and the solution will exceed its purpose.

Increase the operation limits A second option is to enlarge the Stewart platform cylinders and with increasing the operation limit. When this option is considered, the whole optimisation goal is exceeded. Because this would create an E-type system. This option will not be looked into further in this research.

Active force control The third option is to use active force control of the passive cylinders. With active force control, the fluctuations of the Stewart platform cylinders can be counteracted with varying forces. This option does not affect the workspace and does not require other cylinders for the A-type. The active force control is only possible for the 3 cylinder model. In the next chapter this force control method is further elaborated.

5-6 Concluding remarks

In this chapter passive cylinders are used to reduce the total load case on top of the Stewart platform. The motion of the passive cylinders is not controlled, they move along with the six Stewart platform cylinders. The reduction of the load case is made possible by the use of a force controller, which keeps a constant pressure in these passive cylinders. Following the flow diagram for this optimisation method, three parameters are determined in this chapter: (1) the number of passive cylinders, (2) the geometry of these cylinders and (3) the force optimisation criteria for these cylinders.

The number of cylinders is investigated between one and six. One cylinder is found not to be sufficient to counteract the large external loads on top of the Stewart platform. Two, three and four passive cylinders lead to a favourable and even distributed Stewart platform cylinder forces. For this reason the number of five and six cylinders have been found redundant. The geometry for the 2, 3 and 4 cylinder model is obtained for the dead and stroke cylinder lengths of the current A-type cylinders. These lengths are used as they are able to reach the same positions in the workspace of the system as the Stewart platform cylinders. Due to these lengths, the cylinders are located under an angle with a length in the horizontal plane of 2.45 [m]. This horizontal length leads to one configuration for the 2 cylinder model, ten for the 3 cylinder model and one for the 4 cylinder model. Due to the angle of the passive cylinders, the axial force of the cylinders contains force components in all directions. The vertical force component is equal for all configurations with a length in the horizontal plane of 2.45 [m]. The force components in x- and y-direction are undesirable as these forces will lead to larger Stewart platform cylinder forces. Due to symmetry of the configurations, the force components in x-direction are in opposite directions. Two configurations for the 3 cylinder model are selected with the criteria that these configurations have a small force component in y-direction. The 4 cylinder model contains four passive cylinders that are located next to the Stewart platform cylinders with the largest forces, leading to the passive cylinders acting as 'slaves. With use of the force optimisation criteria, the lowest possible and even distributed Stewart platform cylinders are obtained for all the different models and configurations.

The obtained passive forces per model and configuration are used to determine the Stewart platform cylinder forces through the workspace of the system. Three different load cases are used, GXXL:NO-CT1000kg, GXXL:NO-CT500kg and GXXL:NO-PT. The 4 cylinder model is the only model which has cylinder forces below the maximum operation limit for all

three load cases. This model is recommended when cargo transfer is the decisive load case. However, the cargo transfer is the most extreme load case, but not the primary function of the gangway. For people transfer both the 2 and 3 cylinder model can be used. Cargo transfer can be made possible for the 2 and 3 cylinder model by reducing the force fluctuations of the Stewart platform. The suggested method to reduce these forces us by using Active force control. With the use of active force control, the fluctuations can be reduced by applying a variable force. This option is only valid for a 3 cylinder model, as this model can counteract all three of the forces and moments. In the Chapter 6 this option is further investigated.

Chapter 6

Optimised geometry with active force control

6-1 Introduction

In Chapter 4 the geometry of the Stewart platform was optimised for the large off-centre load-case caused by the GXXL. This led to an elliptical top frame and larger bottom gimbal angles then the current A-type design. Next to this optimisation step are in Chapter 5 passive cylinders added to the current A-type system. With these cylinders, an extra constant force could be delivered to top platform which counteracted the external loads. Hence, the forces of the Stewart platform cylinders are reduced. In this section these two methods are combined to see whether they are complementary or not.

For the optimised geometry with extra cylinders, the Active Force Control method is used to counteract the dead load of the system for every position in the workspace. This means that the force control of the extra cylinders becomes active and differs per position. Two methods are used to determine the required forces of the extra cylinders.

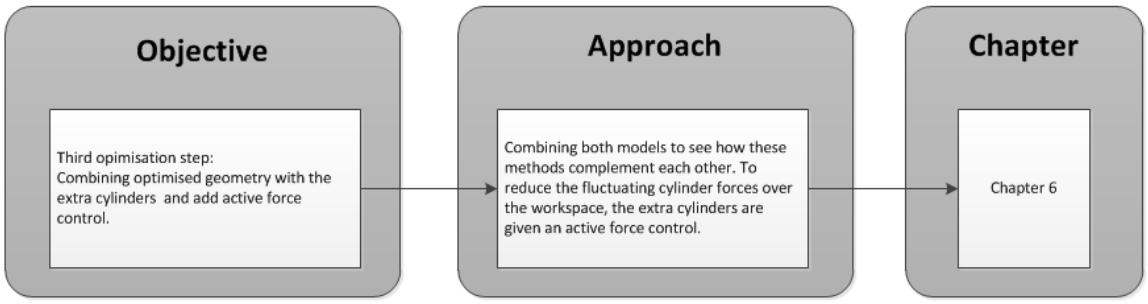

Figure 6-1: Approach Chapter 6

6-2 Optimised geometry with passive cylinders

Two optimisation directions have been performed in the previous 2 chapters. First the geometry of the Stewart platform was optimised for the large asymmetric load case and second passive cylinders were added to the platform to counteract the load case. Both directions gave a positive outcome for the the use of the GXXL for people transfer. However, for cargo transfer the cylinder loads still exceeded the operation limit for a large number of positions. A combination of both directions is performed to see whether the two directions are complementary to each other.

When including the passive cylinders from Chapter 5 in the optimised geometry of the Stewart platform from Chapter 4, first the configuration of all the cylinders is chosen. Second, the workspace of the passive cylinders is checked.

6-2-1 Configuration cylinders

The optimisation of the geometry and implementation of extra cylinders resulted in two different configurations of the Stewart platform cylinders. For the combination of both directions, these two configurations are compared in this section. Second, from Chapter 5 followed that two configuration for the 3 cylinder model can be used. The 2 cylinder model will not be used, as Active force control will be added to this new geometry of the system (sections 6-3). The two different configurations of the 3 cylinder model had comparable Stewart platform cylinder forces. The decision is made to use configuration I (Figure 5-12b) based on the fact that configuration IV has passive and Stewart platform cylinders close to each other. This has a possible risk of collision of the cylinders, which must be avoided at all times.

For the optimisation of the geometry followed that the four top gimbals are located on the side of the gangway, for the passive only two top gimbals are located on this side. When combining both methods, a decision is made for the location of all the cylinders. Two configurations are considered, Figure 6-2 and **??**, for which the force optimisation from section 5-4 is applied. Both configurations the force criteria of 60% of the maximum operation push force is used. With this criteria the Stewart platform cylinder forces in neutral position are obtained. These passive forces are again applied to the system when it is moved through the workspace and is loaded with a wind load in x-direction.

Configuration 1 The first configuration follows from the geometry of the Stewart platform as obtained in Chapter 4. The passive cylinders are located between the top gimbals of the Stewart platform cylinders as shown in Figure 6-2. This configuration results in two push forces and four pull forces in neutral position, due to the large push forces of the passive cylinders.

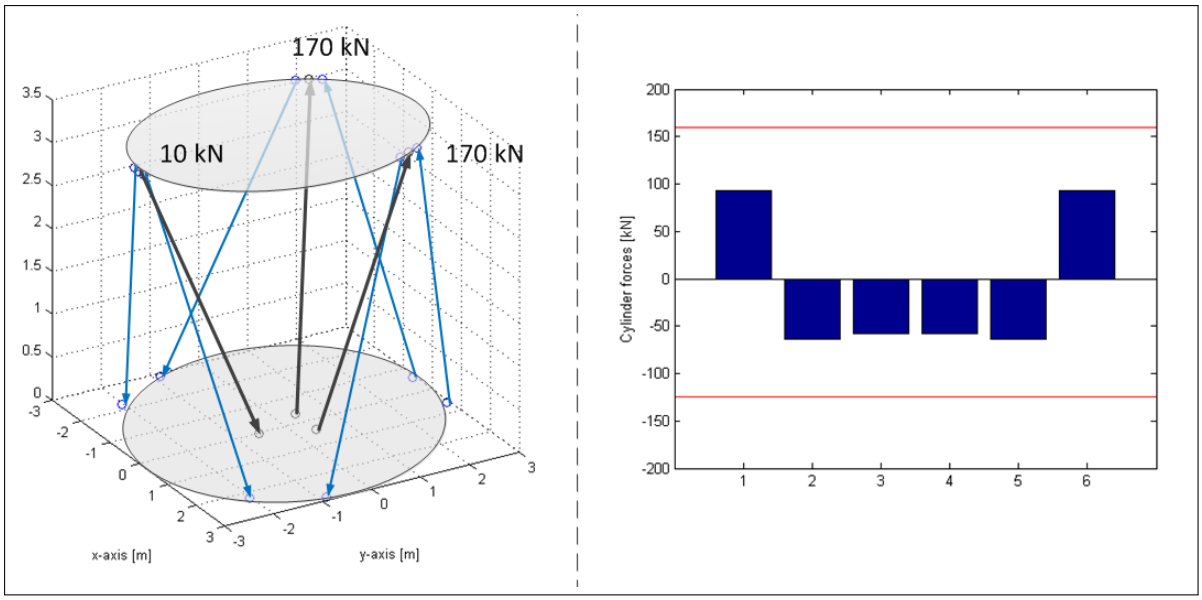

Figure 6-2: Optimised geometry including passive cylinders: Configuration 1

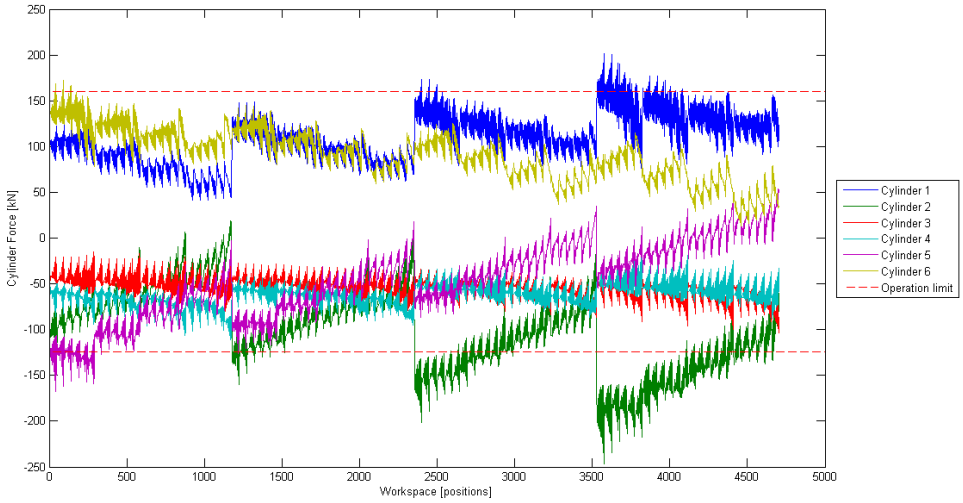

Figure 6-3: Cylinder forces over workspace: Configuration 1

Configuration 2 The second configuration of the Stewart platform follows from Chapter 5, where the top gimbals of the Stewart platform are located below the gangway. This configuration has four push forces and two pull forces. The passive forces for this configuration are more even distributed than for the first configuration.

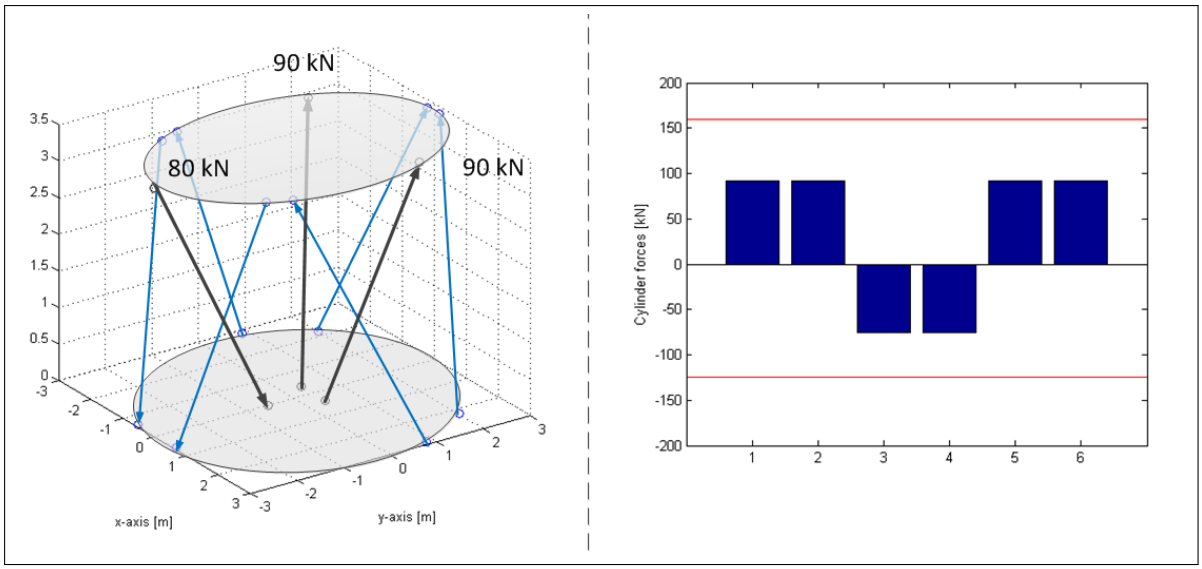

Figure 6-4: Optimised geometry including passive cylinders: Configuration 2

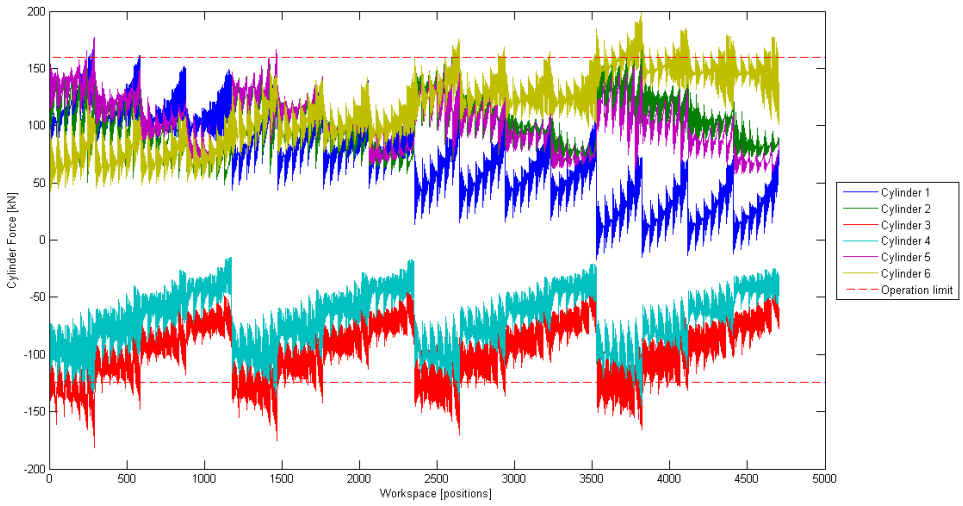

Figure 6-5: Cylinder forces over workspace: Configuration 2

Evaluation two configurations From the two configurations, some conclusions are drawn. But first the two are evaluated. A noticeable difference between the two is that the first configuration has two push forces and the second configuration has four. This is explained by the fact that the second configuration has top gimbals below the gangway. The vertical force components of these two cylinders have the largest possible distance to the centre of the top frame in y-direction. This creates the largest possible counter moment. To reach a force equilibrium in z-direction, the other four cylinder forces are divided into two push forces and two pull forces.

The push Stewart platform cylinders in the first configuration have a smaller length to the

centre of the top platform in y-direction. To counteract the external tipping moment, the passive forces are divided into two large push forces and one small pull force. To reach a force equilibrium in z-direction, the Stewart platform cylinders have two push forces and four pull forces.

The force distribution over the six Stewart platform cylinders leads to the decision for the configuration of the cylinders. The decision is based on the following items:

1. The second configuration has less pull forces, which is favourable, because exceeding of the pull limit force is more hazardous than exceeding of the push limit force.
2. Comparing the cylinder forces over the workspace of Figure 6-3 and 6-5 it is concluded that the forces of the configuration 2 are more even distributed and closer to each other than configuration 1.
3. The distribution of the passive forces are more extreme for the first configuration. It is favourable for these forces to be more even distributed over the top platform. This leads to lower required forces which leads to a more cost efficient design.
4. It can be concluded that the two optimisation directions from Chapter 4 and 5 complement each other. To reduce the maximum occurring cylinder force to below the operation limit, the active force control method will be used in section 6-3. At some positions in the workspace the cylinder forces still exceed the operation limit. The number of times that this happens has decreased compared to the current A-type and the current A-type with passive cylinders, due to the combination of passive cylinders and the new geometry of the Stewart platform.

6-2-2 Workspace extra cylinders

In the previous chapter, section 5-3-2, the location of the top and bottom gimbals was determined with a horizontal distance of 2.45 [m], to maintain the workspace of the system. When applying the extra cylinders to the optimised geometry model, the horizontal distance is reduced due to the elliptical top shape. Before introducing the active force method, the workspace of the extra cylinders is checked, whether it is the same as for the optimised geomtery. On the next page, the fifteen sub-plots of the 2DoF planes are given (The green sub-plots mean that the whole workspace can be reached). When comparing these with the workspace sub-plots of the optimised geometry it can be concluded that the workspace of the extra cylinders is smaller in three sub-plots: y-ϕ, y-ψ and y-z. The first two, are smaller, but are in the programmed workspace from the system. The only 2DoF that are smaller and not in the programmed workspace of the system is the y-z plot. Due to the elliptical shape of the top frame some combinations of sway and heave motion could not be reached. The pull cylinders exceeds its maximum value and/or the push cylinders exceed their minimum.

To solve this problem, the workspace of the Stewart platform can be reduced or the location of the cylinders can be adjusted. The heave motion is a important DoF during vessel compensation, so it is not favourable to reduce this workspace. This means that the location of the extra cylinders will be adjusted. The bottom gimbal of the pull cylinder will located 0.3 m higher and the bottom gimbals of the other 2 cylinders are put in the x-axis and 0.1 m lower.

This adjusted geometry of the extra cylinders leads to a workspace that is the same size as the workspace of the Stewart platform. The new geometry of the extra cylinders is shown in Figure 6-6 and the coordinates in Table 6-1.

b_i	x	y	z	t_i	x	y
1	0	-0.55	0.3	1	0	-3.0
2	$0.55 \cdot \sin(\pi/4.28)$	0	-0.1	2	$2.0 \cdot \sin(2\pi/3)$	$3.0 \cdot -\cos(2\pi/3)$
3	$-0.55 \cdot \sin(\pi/4.28)$	0	-0.1	3	$2.0 \cdot \sin(4\pi/3)$	$3.0 \cdot -\cos(4\pi/3)$

Table 6-1: Gimbal coordinates top and bottom frame of extra cylinders

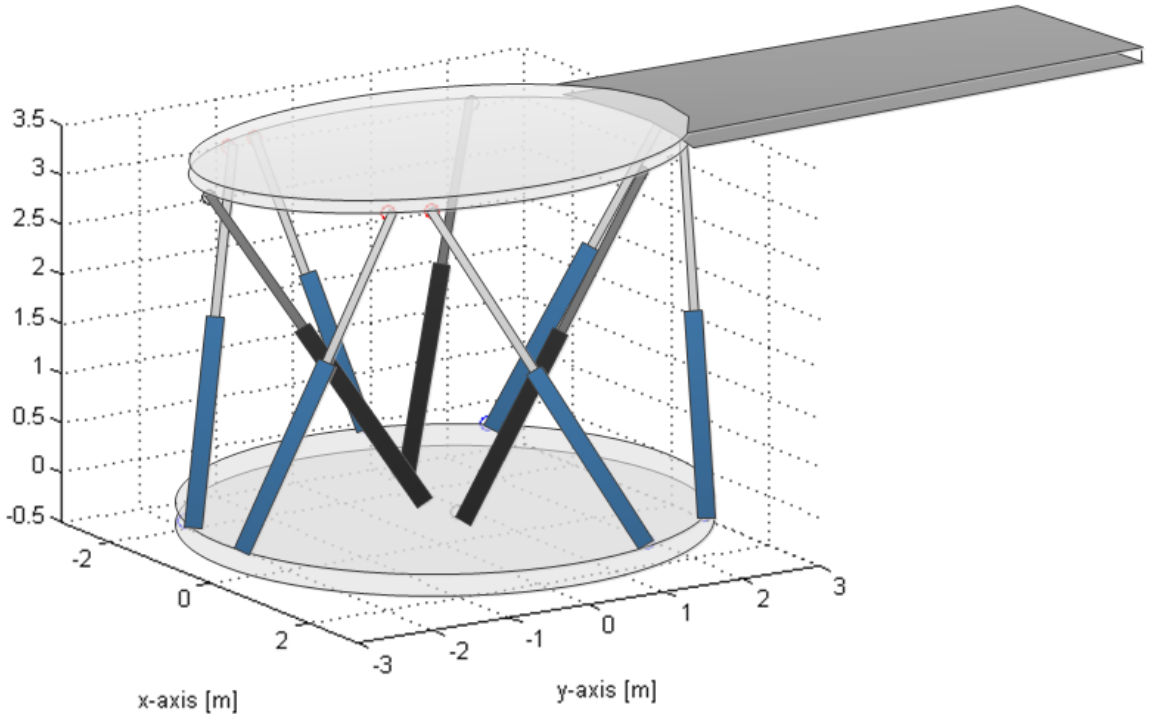

Figure 6-6: Final system model: Optimised Stewart platform with extra cylinders

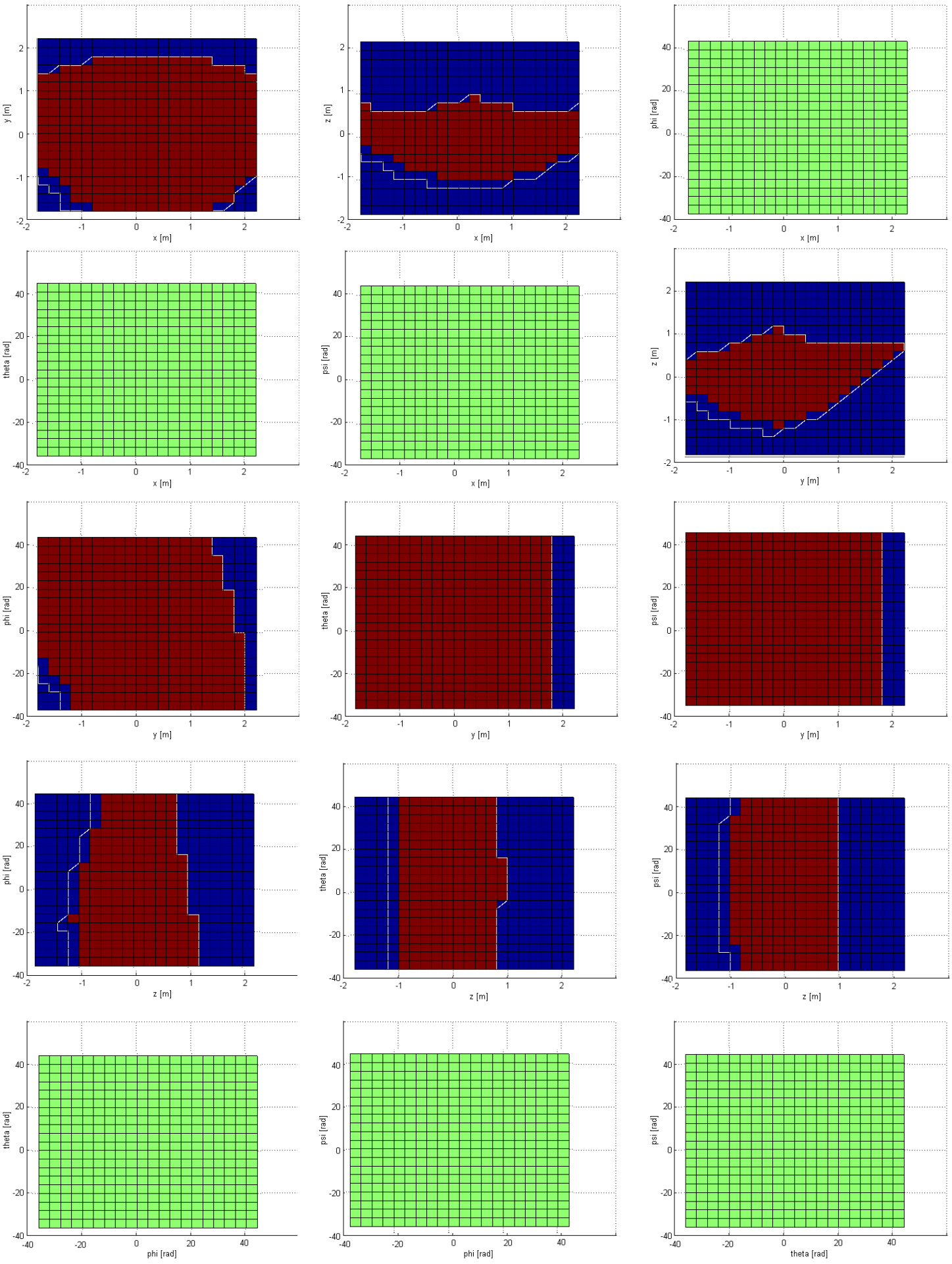

Workspace Extra Cylinders

6-3 Active force control

The geometry of the Stewart platform as the extra cylinders are now known. In Chapter 5 a constant force of the extra cylinders was used to counteract the largest load case (GXXL-NO-CT). For neutral position a force distribution of the extra cylinders was obtained that kept the forces of the Stewart platform cylinders below their operation limits. However, when the platform was moved through its workspace, the cylinder forces still exceeded their maximum. In this section Active Force Control (AFC) is used for the extra cylinders. When applying a dynamic force to the system, the extra cylinders become `active` in force control and `passive` in motion control. The required forces of the extra cylinders are determined in this section. In Appendix C, the pressure dynamics of a cylinder are given that have to be used for the AFC system.

Free body diagram The goal of the AFC is to reduce the force fluctuations, which are caused by (1) the position within the workspace and (2) the different load cases on top of the Stewart platform. A variable counteracting force of the extra cylinders can lead to lower Stewart platform cylinder forces. In Figure 6-7 is shown that when the platform is moved in y-direction, the extra cylinder forces also change direction. To achieve the same counteracting load case (for only the tipping moment in this case), the forces have to change with the position of the platform. In the shown right free body diagram the pull force becomes more vertical. This force can counteract the tipping moment with a smaller remaining horizontal force component. This pull force will become larger, while the push force becomes smaller to counteract the tipping moment.

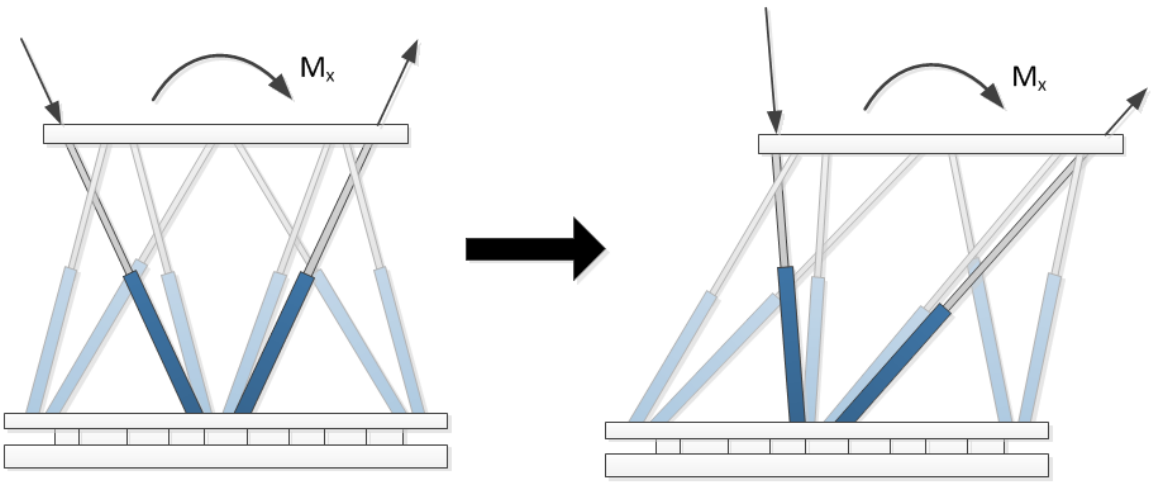

Figure 6-7: Active force control

6-3-1 Goal AFC

The ultimate goal of using AFC is to make the forces in the Stewart platform cylinders constant over the entire workspace per load case. Force fluctuations will only occur when the load case on top of the platform is changed. To see whether this is possible is investigated

in the first method by counteracting the dead load of the gangway with the extra cylinders. If this does not work as predicted, then a second method will be introduced. This second method will reduce the fluctuations by looking at the required forces of the extra cylinders that is necessary to keep the Stewart platform cylinders below their operation limit. This approach is shown in Figure 6-8.

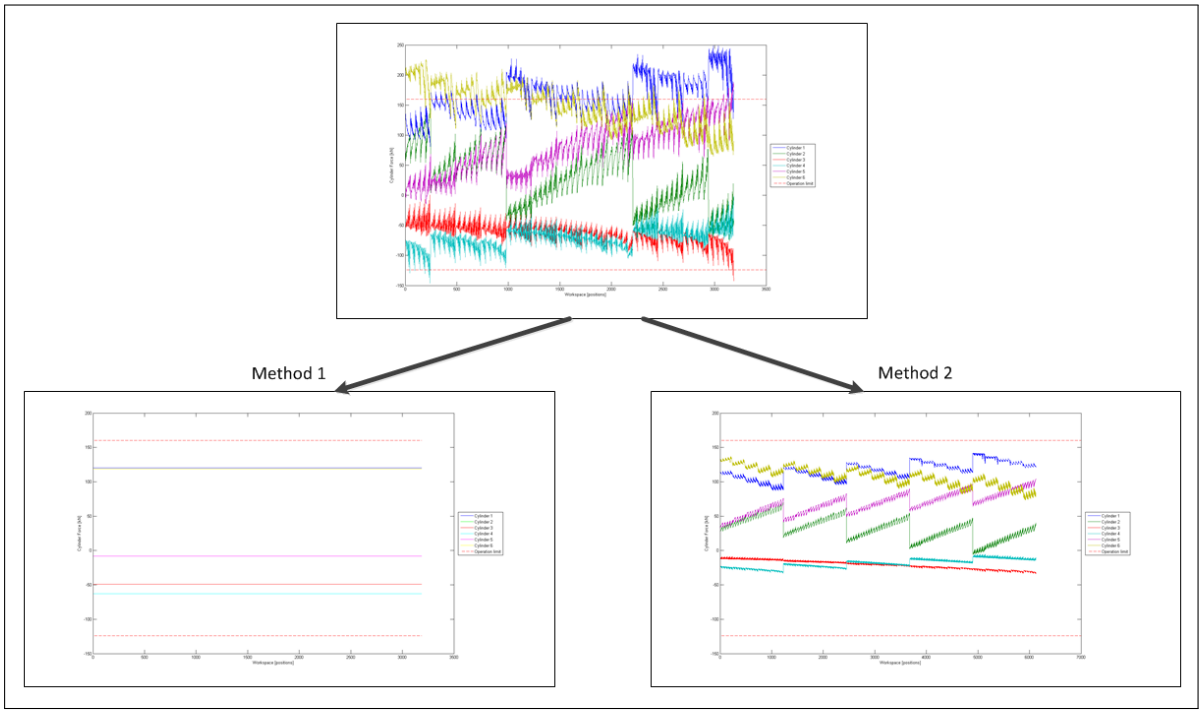

Figure 6-8: Approach AFC

6-3-2 Method 1: 3DoF model

Three extra cylinders are used to counteract the dead load of the GXXL. These 3 cylinders have a 3DoF model: z, ϕ and θ. Three cylinders can not control a platform in 6DoF. But as these cylinders are not used to control the motion of the system, they can be implemented and follow the trajectory of the 6DoF model. For the 3DoF model of the extra cylinders, the same Inverse Kinematics approach can be used as described in section 2-3-3. Only the Euler transformation matrix from equation 2-12 has to be reduced, as only z, ϕ and θ are used. The matrix is reduced to:

$$\underline{\underline{R}}_b = \begin{bmatrix} c\theta & s\theta \cdot s\phi & c\psi \cdot s\theta \\ 0 & c\phi & -s\phi \\ -s\theta & c\theta \cdot s\phi & c\theta \cdot c\phi \end{bmatrix} \tag{6-1}$$

Forces extra cylinders 3DoF The three cylinders are used to statically compensate the dead load of the GXXL for all the positions in the workspace:

$$\dot{F_{ref}} \equiv 0 \tag{6-2}$$

With,

$$F_{ref} = \begin{bmatrix} N_1^a \\ N_2^a \\ N_3^a \end{bmatrix} = - \begin{bmatrix} F_z \\ M_x \\ M_y \end{bmatrix} \tag{6-3}$$

To calculate the required forces of the extra cylinders to counteract the dead load of the gangway, the Jacobian matrix of section 2-3-4 also has to be reduced to a 3x3 matrix. To calculate the cylinder forces, the inverse Jacobian Matrix is multiplied with the external loads. Because the inverse of a matrix is used, the Jacobian matrix must be squared. This reduced matrix is implemented in the equation for the axial cylinder forces:

$$\begin{bmatrix} \widehat{z}_{l1} & \widehat{z}_{l2} & \widehat{z}_{l3} \\ -y_{t1} \cdot \widehat{z}_{l1} & -y_{t2} \cdot \widehat{z}_{l2} & -y_{t3} \cdot \widehat{z}_{l3} \\ x_{t1} \cdot \widehat{z}_{l1} & x_{t2} \cdot \widehat{z}_{l2} & x_{t3} \cdot \widehat{z}_{l3} \end{bmatrix} \begin{bmatrix} N_1^a \\ N_2^a \\ N_3^a \end{bmatrix} = - \begin{bmatrix} F_z \\ M_x \\ M_y \end{bmatrix} \tag{6-4}$$

A 3DoF model can only counteract the loads F_z, M_x and M_y. This is convenient, as these loads are the same for the dead load of the GXXL. When adding the dead load of the GXXL in equation 6-4, the forces of the extra cylinders can be calculated over the entire workspace of the system. These forces are shown in Figure 6-9.

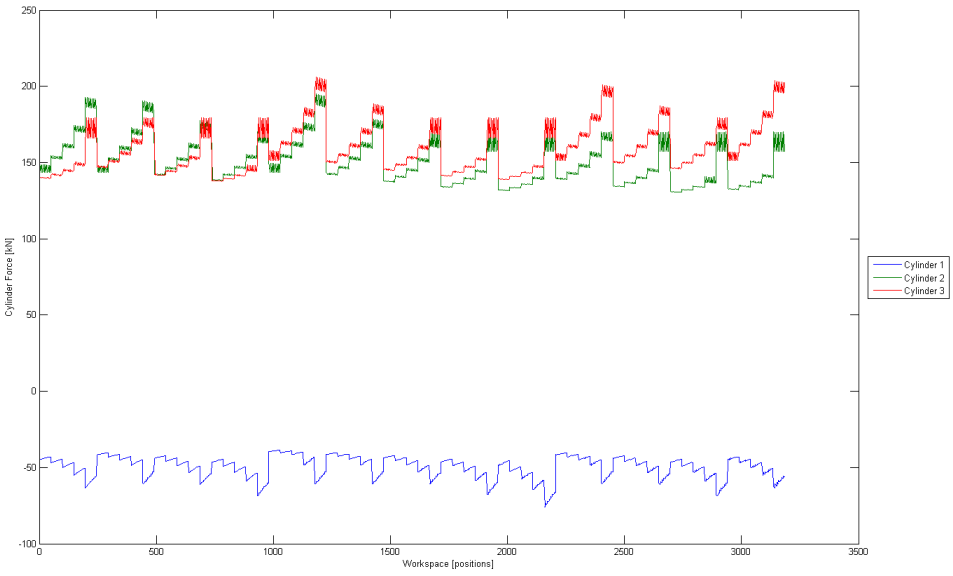

Figure 6-9: Axial forces extra cylinders 3DoF

6DoF load case extra cylinder The forces of the extra cylinders needed to counteract the dead load of the GXXL through the entire workspace are now known. However, these forces are used in a 6DoF model of the Stewart platform. To see the load case caused by the extra cylinders, equation 6-4 has to be expended to a 6DoF model for the 3 extra cylinders:

$$\begin{bmatrix} \widehat{x}_{l1} & \widehat{x}_{l2} & \widehat{x}_{l3} \\ \widehat{y}_{l1} & \widehat{y}_{l2} & \widehat{y}_{l3} \\ \widehat{z}_{l1} & \widehat{z}_{l2} & \widehat{z}_{l3} \\ -y_{t1} \cdot \widehat{z}_{l1} & -y_{t2} \cdot \widehat{z}_{l2} & -y_{t3} \cdot \widehat{z}_{l3} \\ x_{t1} \cdot \widehat{z}_{l1} & x_{t2} \cdot \widehat{z}_{l2} & x_{t3} \cdot \widehat{z}_{l3} \\ x_{t1} \cdot \widehat{y}_{l1} - y_{t1} \cdot \widehat{x}_{l1} & x_{t2} \cdot \widehat{y}_{l2} - y_{t2} \cdot \widehat{x}_{l2} & x_{t3} \cdot \widehat{y}_{l3} - y_{t3} \cdot \widehat{x}_{l3} \end{bmatrix} \begin{bmatrix} N_1^a \\ N_2^a \\ N_3^a \end{bmatrix} = - \begin{bmatrix} F_x \\ F_y \\ F_z \\ M_x \\ M_y \\ M_z \end{bmatrix} \tag{6-5}$$

When adding the obtained forces, from equation 6-4, of the extra cylinders in equation 6-5 The load case caused by the extra cylinders is obtained, see Figure 6-10. It can be seen loads caused by the extra cylinders are indeed constant for F_z, M_x and M_y. Only the forces also create large loads in the other 3 DoF, especially F_y.

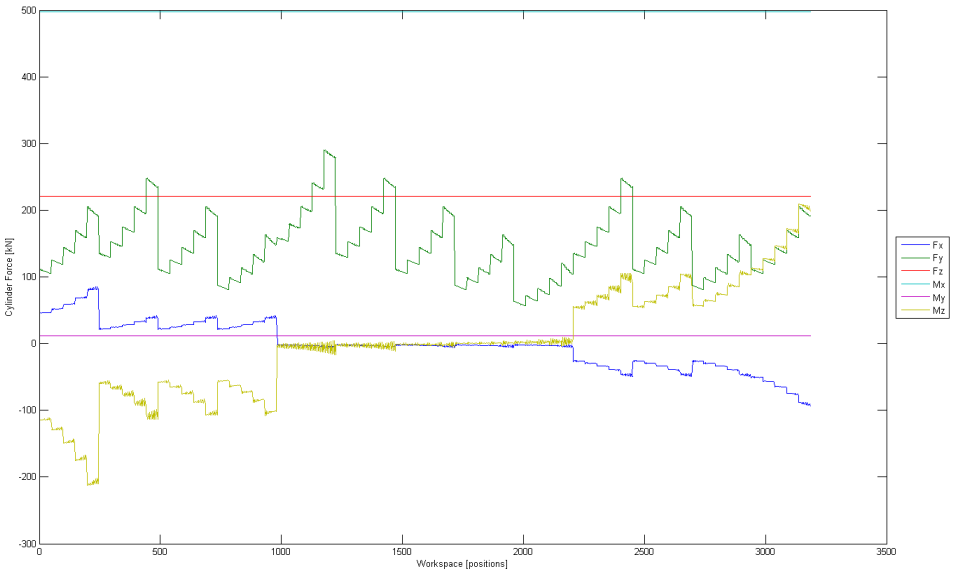

Figure 6-10: 6DoF load case by extra cylinders

Reduced 6DoF load case When subtracting this load case from the load case of the GXXL-CT, the load case remains that has to be counteracted by the cylinders of the Stewart platform. In Figure 6-11 this new reduced load case can be seen.

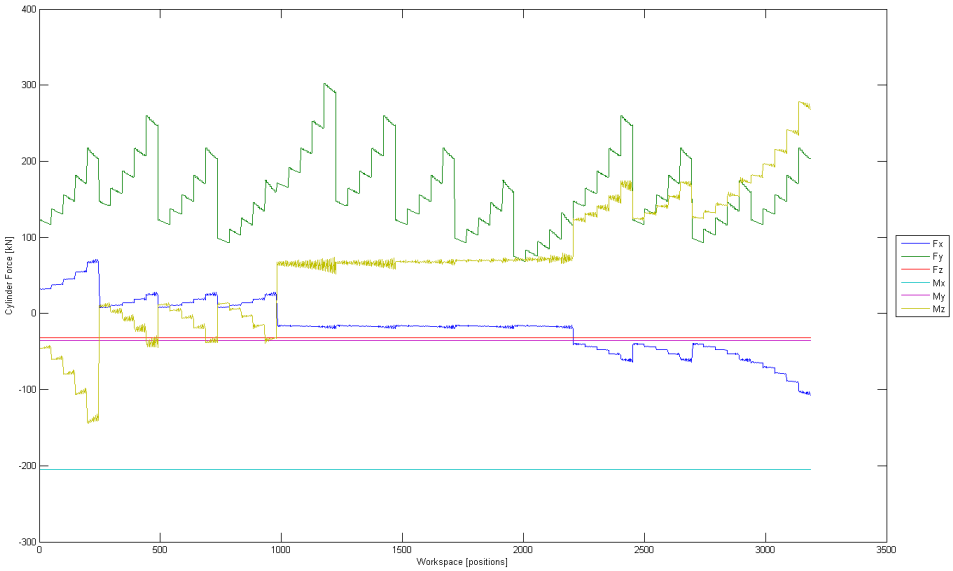

Figure 6-11: Reduced load case GXXL-CT

Stewart platform cylinder forces In the reduced load case, the loads F_z, M_x and M_y are not zero because the load case for cargo transfer creates a larger F_z, M_x and M_y than the dead load of the system. Also the force in y-direction has increased. When implementing this load case in equation 2-39, the forces of the Stewart platform cylinders can be calculated (Figure 6-12)

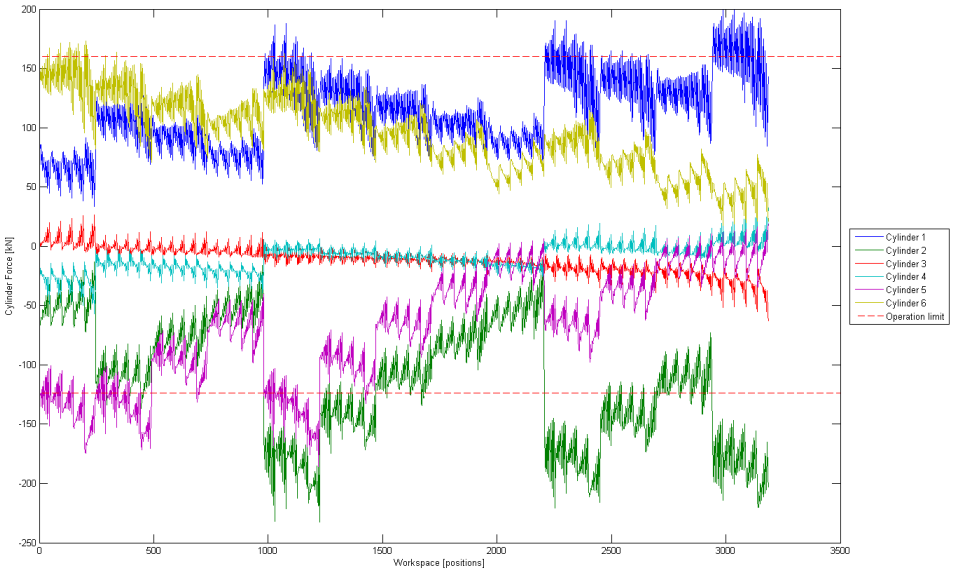

Figure 6-12: Stewart platform cylinder forces for reduced load case GXXL-CT

Evaluation: Method 1 Method 1 of the AFC was to counteract the dead load of the GXXL through the workspace of the system, leading to a reduced load case for the Stewart platform cylinders. This seemed not to be the case. The forces of the extra cylinders needed to counteract the dead load of the GXXL led to larger loads in other directions. For which the forces of the Stewart platform cylinders did not become constant through the workspace and even exceeded their operation limit. Even for a smaller load case (GXXL:NO-PT), the cylinders still exceed their maximum. This method does not has the outcome that was desired, so the second method of AFC will be used.

6-3-3 Method 2: Reduce maximum forces

In the previous section is was shown that applying a variable force, that counteracts the dead load of the GXXL with the use of a 3DoF model leads to large loads in other directions. This method did not had the desired outcome. The second method of the AFC is to determine the cylinder forces for all the possible positions of the platform and calculate which forces are needed to keep the forces below their operation limit. The pressure will be controlled with the use of a Look-up table per position, the same as for the motion control of the Stewart platform cylinders. In this report, not all positions are calculated but only the positions with the largest cylinder forces. This method contains the following 4 steps:

1. Find extreme forces of the Stewart platform cylinders for the load case excluding wind, with the constant force of the passive cylinders as determined in section 6-2-1.

2. Determine the position of the platform for the extreme cylinder forces.

3. Find the required forces of the extra cylinders to reduce the Stewart platform cylinder forces for these positions.

4. Determine the forces of the Stewart platform cylinders for the reduced load case obtained with the extra forces from step 3.

1. Extreme Stewart platform cylinder forces The first step is to determine the extreme cylinder forces. These forces are obtained for the reduced load case of the GXXL:NO-CT1000kg, without wind. The reduced load case means that the extra cylinders contribute a constant force (from section 6-2-1) to the system. Cylinder 1, 3, 4 and 6 exceed the operation limit for multiple positions. In this report only the largest forces per cylinder are used, to check the functioning of this AFC method. The largest forces are shown in Figure 6-13 with the red circle. The number next to the circle resembles the number of the Stewart platform cylinder.

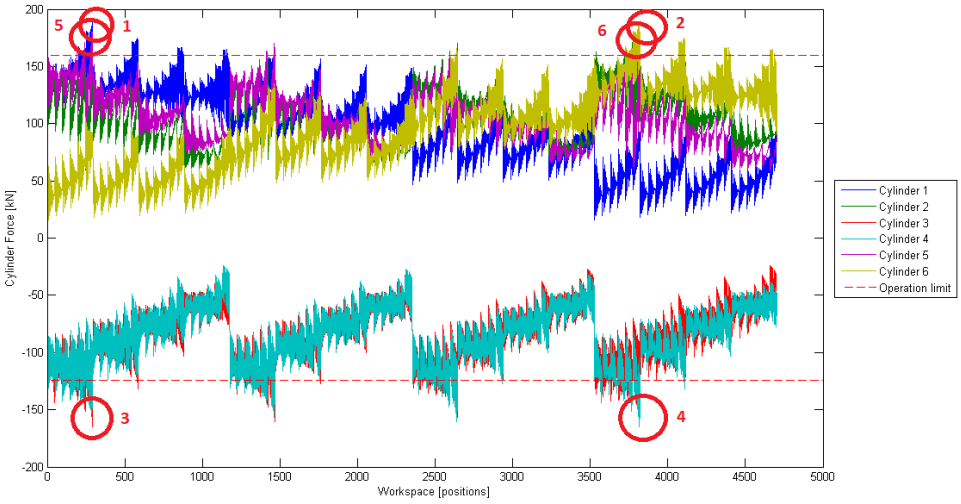

Figure 6-13: Largest forces over workspace

2. Extreme positions Stewart platform The extreme forces per cylinder occur for a certain position of the platform. It can be seen from Figure 6-13 that the extreme forces of cylinder 1, 3 and 5 occur nearly for the same position. The same holds for cylinder 2, 4 and 6. In fact, cylinder 1 and 3 and 4 and 6 have the extreme values at for the same position. This leads to a total of four extreme positions of the platform as shown in Figure 6-14. The positions are all at a point where the DoF (surge, sway, heave, pitch and roll) are minimum or maximum. For this reason not only these four positions are taken into account in the next step, but all the $2^5 = 32$ extreme positions.

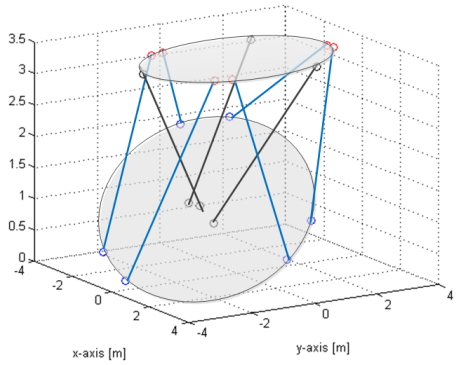

(a) Maximum force cylinder 1 and 3

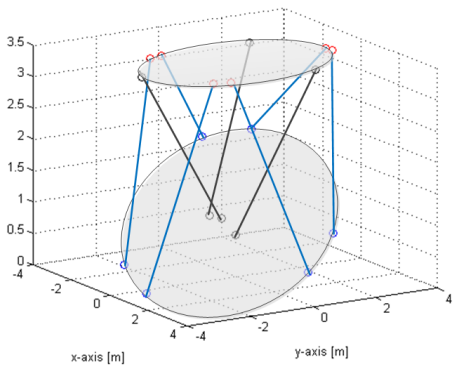

(b) Maximum force cylinder 2

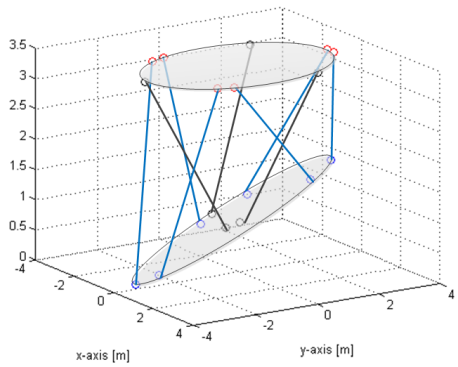

(c) Maximum force cylinder 4 and 6

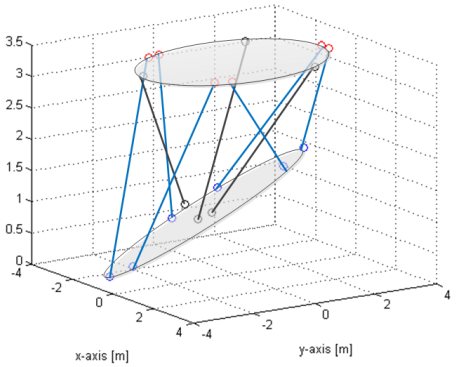

(d) Maximum force cylinder 5

Figure 6-14: Positions with largest cylinder forces

It must be stated that the axes of the four plots in Figure 6-14 are not equal. This results in a skewed representation of the positions.

3. Required extra cylinder forces For all these 32 positions, the required forces of the extra cylinders to counteract the dead and live load of the system are calculated. Per position the forces are obtained that will give the lowest forces for the Stewart platform cylinders. The difference with the previous method is that here, first the Stewart platform cylinder forces per position are calculated and then the extra cylinder forces are obtained that reduce these forces per position. In this calculated, the criteria is used that the cylinder forces may not exceed the pull limit. For the 32 position the forces of the extra cylinders are shown in Figure 6-15.

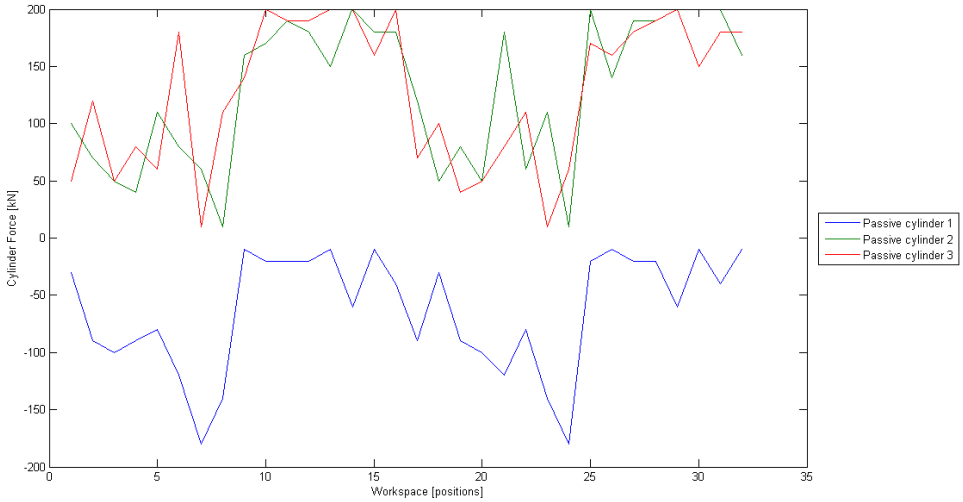

Figure 6-15: Forces extra cylinders for extreme positions

4. Stewart platform cylinder forces The forces of the extra cylinders cause a load case that can be subtracted from the critical load case of the platform. In the Figures 6-16 to 6-18 the forces of the Stewart platform cylinders are shown for the 3 different critical load cases: NO-CT-1000kg, NO-CT-500kg and NO-PT. Per load case, three different cylinder forces of the Stewart platform are shown. The top plot shows the cylinder forces with no passive forces, the middle plot shown the cylinder forces with the constant passive force and the bottom plot shows the cylinder forces with AFC. It can be seen that for all the load cases with AFC the cylinder forces are below the pull operation limit. At some extreme positions the forces exceed the push operation limit, however this is found acceptable.

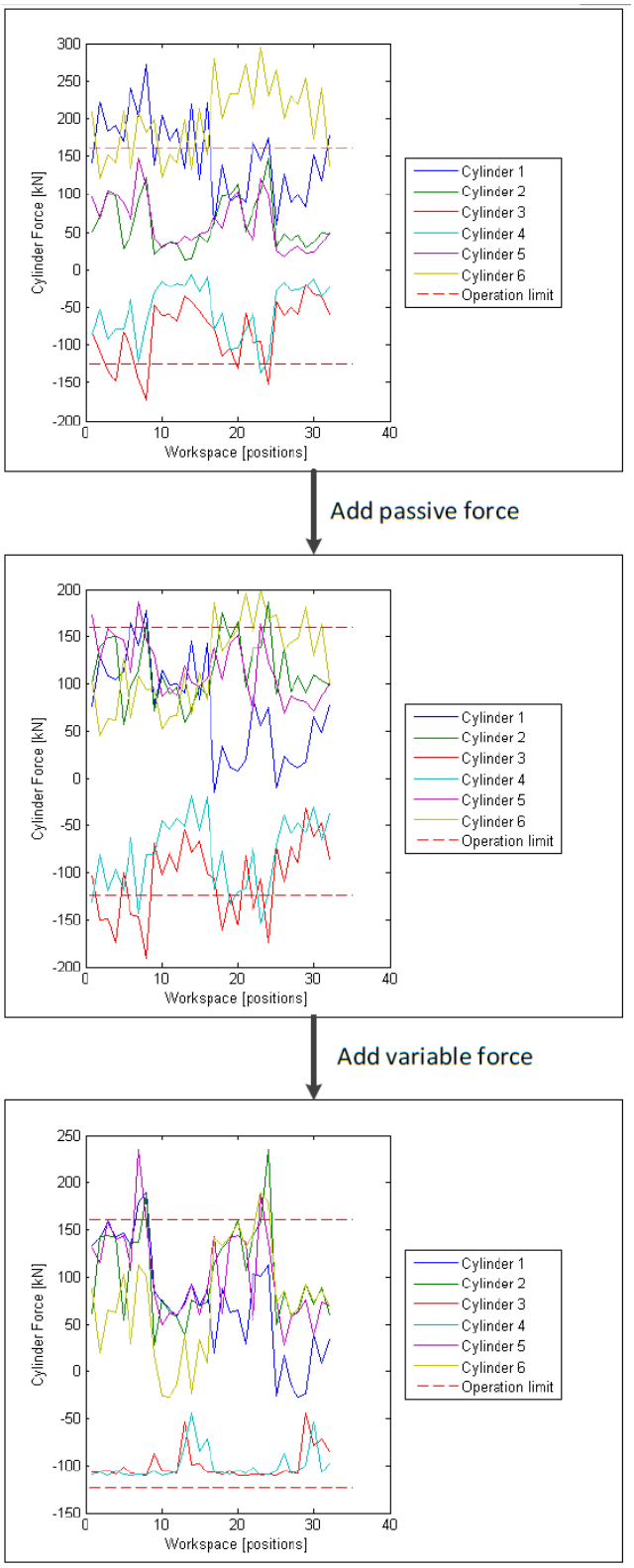

Figure 6-16: Stewart platform cylinder forces: GXXL:NO-CT1000kg

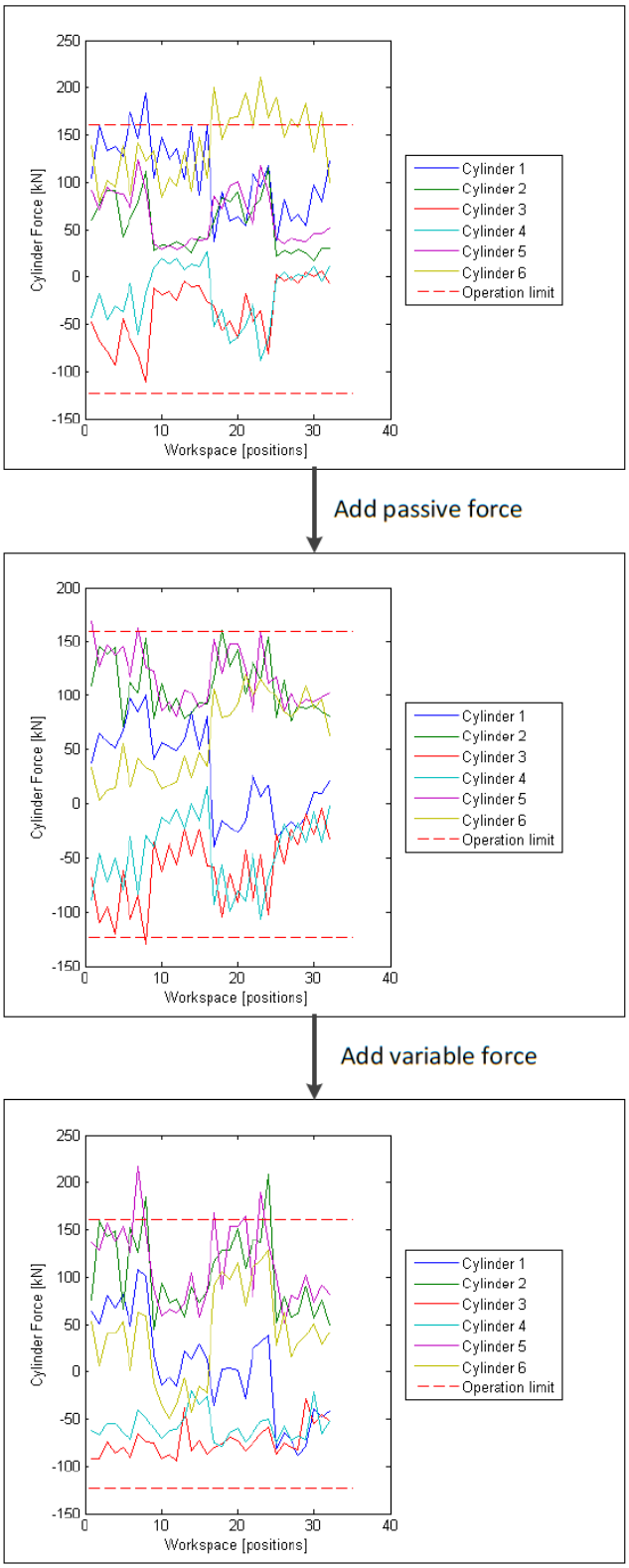

Figure 6-17: Stewart platform cylinder forces: GXXL:NO-CT500kg

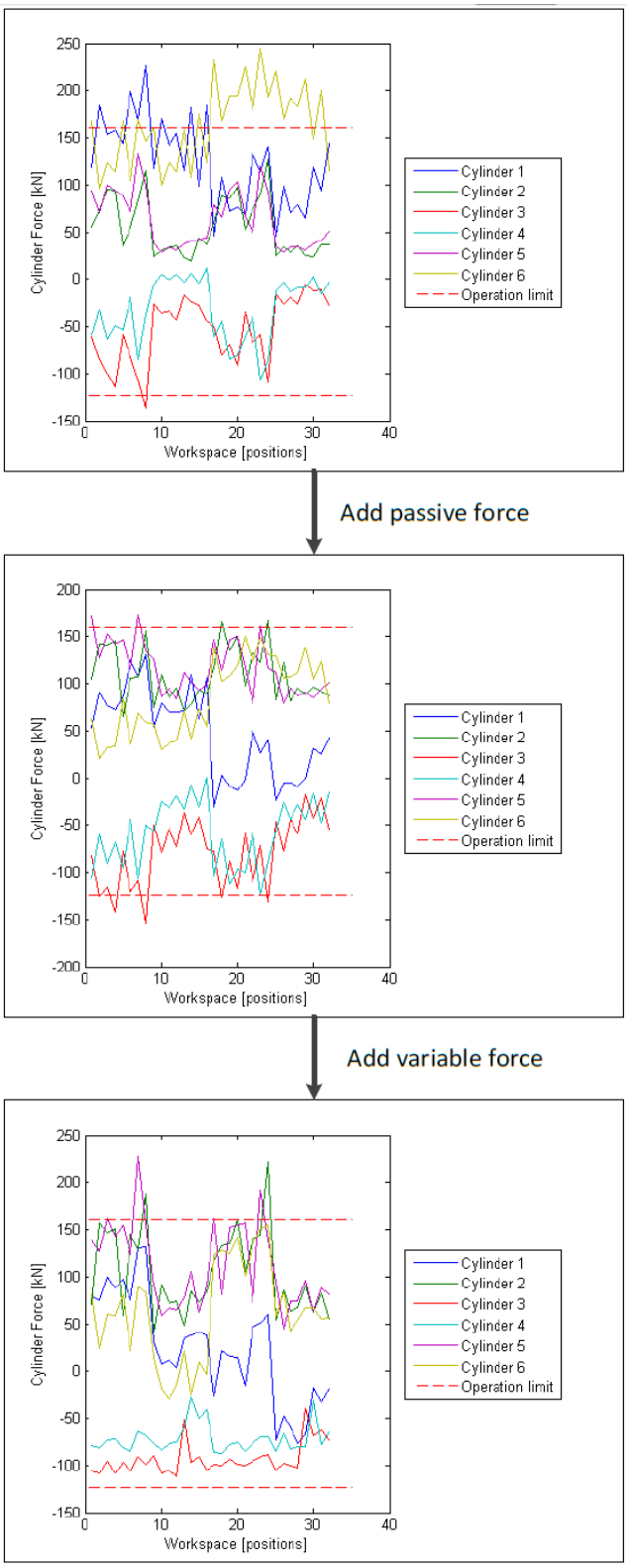

Figure 6-18: Stewart platform cylinder forces: GXXL:NO-PT

Evaluation: Method 2 After Method 1 of the AFC did not give the desired outcome, a second method was introduced. In Method 2, first the extreme forces of the Stewart platform cylinders were obtained. These extreme forces followed from the load case of the dead and live load of the system, excluding the wind load. Second, these extreme forces occurred for extreme positions of the platform, where the DoF of the platform were at their maximum. In the third step the forces of the extra cylinder were obtained for which the Stewart platform cylinders forces were reduced. The optimisation criteria that is used in this step is that the cylinders forces may not exceed their maximum pull force. For all the load cases the cylinder forces are indeed below their operational pull force. However, due to this criteria at some extreme positions the cylinder forces have larger push forces for the use of AFC than for the use of a constant passive force. It is recommended to investigate if this force criteria leads to the most even distributed Stewart platform cylinder forces or that it can be further optimised. This method shows that is possible to mount a GXXL on top of a Stewart platform with A-type dimensions and use it for both people transfer as cargo transfer.

It must be stated that the extreme positions that are used in this method can not be reached without the occurrence of residual motions (motions of the transfer deck). The model that is used in this method, does not include these motions, meaning that the cylinder lengths become smaller or larger than their maximum or minimum length. Due to this assumption the load case remains in the same direction. While in fact, when the transfer deck is rotated the load case on top of the platform should also be rotated. The effect of the rotated load case is assumed to be of minor importance, in comparison with the tipping moment and downward force. Second, the residual motions will have an effect on the direction of the axial forces. This variation in direction is not taken in to account and should be further investigated.

6-4 Concluding remarks

In this chapter, the model of the extra cylinder (Chapter 5) is implemented in the model of the optimised geometry (Chapter 4). Two possible configurations were considered, one with the top gimbals on either side of the gangway (configuration from 4) and one with two top gimbals below the gangway (configuration from 5). For both configurations the passive force were obtained for neutral position. For the cylinder forces over the workspace of the system, the second configuration led to the more even distributed cylinder forces. It was found that the two optimisation directions are complementary to each for the force distribution within the Stewart platform cylinders. For a constant force in neutral position, the forces remain well below their operation limit. The fluctuation due to the positions in the workspace remain. Apart from the workspace, the different load cases due to the change in live load and wind load also contribute to fluctuating cylinder forces.

The AFC method is introduced to counteract the dead load of the system for every position in the workspace. The live and wind loads are not constant and can not be counteracted with a predetermined force. The goal is that with the use of AFC, the only cylinder force fluctuations will appear due to the change of the load case. Two methods are presented to counteract the dead load of the system.

The first method uses a 3DoF model for the extra cylinder to calculate the required forces to counteract the dead load of the system. To calculate the forces of the 3 extra cylinders,

the Jacobian matrix should also be 3-by-3 matrix, otherwise it can not be inverted. Three cylinders have a 3DoF model in $z-$, ϕ- and θ-direction. For every position in the workspace, the forces of the extra cylinders are determined. As the 3 cylinders work in a 6DoF Stewart platform model, these forces also have to be transformed to a 6DoF model. This transformation leads to excessive large loads in the other 3DoF. Due to these large loads, the forces of the Stewart platform cylinders are also not reduced to below their operation limit with this method. This method did not had the desired outcome, so a seconf method was introduced.

The second method of AFC is to determine the required force of the extra cylinders per position to reduce the forces of the Stewart platform cylinders to below their operation limit. For this method both the dead and live load are taken into account for the prestressing force of the extra cylinders. Where in method 1, first the forces of the extra cylinders were determined, here the required force reduction is calculated first. This force reduction leads to different forces per position for the extra cylinders. These forces will be stored in a Look-up table, where a control program can link the position of the platform to a required pressure within the cylinders. The Stewart platform cylinder forces are then calculated for the reduced load case. The second method leads to a reduction of the cylinder forces to below their push operation limit. The force criteria was chosen so that the cylinder forces would not exceed the pull forces.

With the combination of the new found geometry of the Stewart platform, the extra cylinders and the use of AFC it is found possible to implement the GXXL on the Stewart platform with A-type dimensions. People transfer was already possible with only the implementation of the extra cylinders. With the use of AFC cargo transfer is now also found possible.

Chapter 7

Further research possibilities

In the previous chapters, two main directions have been presented to optimise the Stewart platform for the large asymmetric load cases of the GXXL. Both directions contained several assumptions and constraints that limited the outcome of the optimisation. The effects of some of these constraints are investigated in this chapter. For the geometry of the Stewart platform, the radius of the top and bottom frames are further investigated and for the extra cylinders, the dead and stroke length.

In this chapter also other further research possibilities are presented in the form of recommendations that can also lead to a reduction of the cylinder forces. These further research possibilities follow from the constraints set in the beginning of this research and are beyond the scope of this research. First, this research contains the improvements of the Stewart platform for the large asymmetric load case caused by the gangway. However, this problem could also be partly solved by a redesign of the gangway. Second, by creating another connection point between the platform and the gangway, the tipping moment can be reduced by creating an extra support.

[figure approach chapter]

7-1 Evaluation of constraints of optimisation directions

Both the optimisation directions from Chapter 4 and 5 had multiple constraints. These constraints limit the possibility of improvement. In this section some of these constraints are evaluated and investigated.

7-1-1 Maximum footprint

In Chapter 4, the geometry of the Stewart platform is optimised for the large asymmetric load case. A constraint of this optimisation direction was the maximum footprint of the Stewart

platform. However, from the local optima it was concluded that a larger radius has a positive effect on the cylinder force distribution. In this section the effects of a larger maximum footprint on the force distribution is investigated. The effect on the workspace is not taken into account.

In Figure 7-1 the cylinder forces are plotted for a top and bottom radius from 1 [m] to 6 [m], with a step size of 0.1 [m]. A top frame with a radius of 1 [m] will lead to two large push forces for cylinder 1 and 6 and to large pull forces for cylinder 2 and 5. This is caused by the small distance to the centre of the platform in y-direction. The forces become large to counteract the tipping moment. When the radius of the top frame is increased to 6 [m], to forces of cylinder 2 and 5 increase from a large pull force to a large push force. This is caused by the direction of the cylinders. Cylinder 1 and 6 have a push force below the gangway to counteract the tipping moment. These 2 cylinders will also have a large horizontal component, which is counteracted by the horizontal force component cylinder 2 and 5. Concluding, enlarging of the top frame is not efficient to lower the cylinder forces, only to reduce the pull forces. The same conclusions are drawn for the enlargement of the bottom radius.

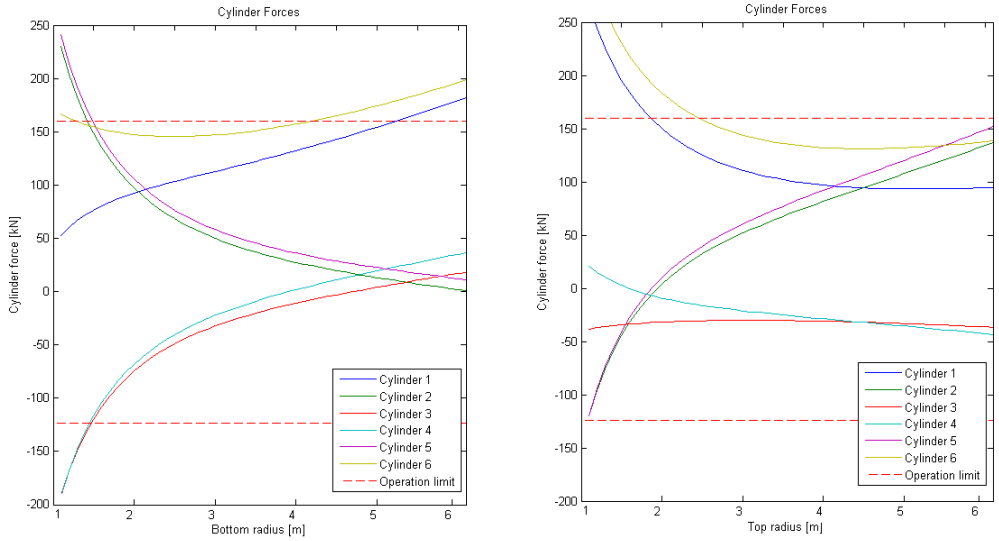

(a) Bottom radius from 1 to 6 [m] **(b)** Top radius from 1 to 6 [m]

Figure 7-1: Forces for variable top and bottom radii

When enlarging both frames simultaneously, the cylinder force distribution changes. The cylinder forces in neutral position are plotted for both frames with a radius of 3, 4, 5 and 6 [m] in Figure 7-2. The same holds as for enlarging only one of the two frames, for a larger radius the direction of the cylinders becomes more horizontal and the distance to the centre of the top frame becomes larger. A smaller vertical force component is required to counteract the tipping moment due to the larger distance, but the horizontal component becomes larger. This means that the horizontal forces in other direction also have to become larger. With two top gimbals below the gangway, the larger radius leads to smaller pull forces and larger push forces. It can be concluded that a larger radius does not result in an more even force distribution for the same size cylinders. If the length of the cylinders would increase and with that the neutral height of the system, the larger radius becomes favourable.

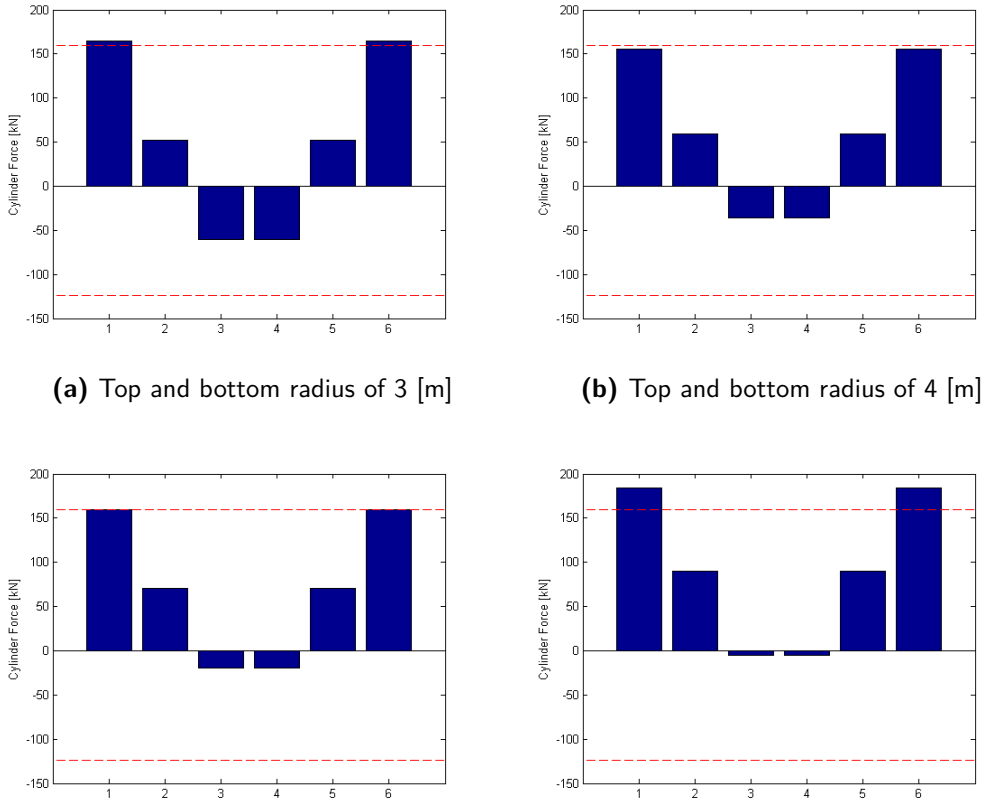

(a) Top and bottom radius of 3 [m]

(b) Top and bottom radius of 4 [m]

(c) Top and bottom radius of 5 [m]

(d) Top and bottom radius of 6 [m]

Figure 7-2: Forces in neutral position for different top and bottom radii

7-1-2 Dead and stroke length extra cylinders

In Chapter 5 it was assumed that the extra cylinders have the same dead and stroke length as the A-type cylinders. This assumption was made to obtain the same workspace as Stewart platform for the extra cylinders. The orientation of the extra cylinders has a horizontal distance of 2.45 [m], which leads to a large horizontal force component. To reduce the horizontal force component, the horizontal distance should be decreased. However, the cylinders should still be able to reach maximum and minimum height of the platform (2.15 and 4.65 [m]). For these two heights the stroke and dead length of the cylinders are obtained, with the use of equation 5-1. These lengths are plotted in Figure 7-3 for different Δ y.

A vertical orientation of the extra cylinders results in a negative dead length. This is not possible. A minimum dead length of the cylinder is necessary to give space for the gimbals and their connections to the cylinders. In the current A-type cylinders, not all of this length is used. It is possible to reduce the dead length of the cylinder with 0.25 meter, leading to $l_{dead} = 1.00$ [m]. To obtain the same minimum and maximum height of the platform, the stroke length becomes $l_{stroke} = 2.06$ [m]. The horizontal distance is reduced from 2.45 to 2.20 [m]. This is not a significant difference, however the effect on the force distribution is checked for the 3 cylinders model, configuration I.

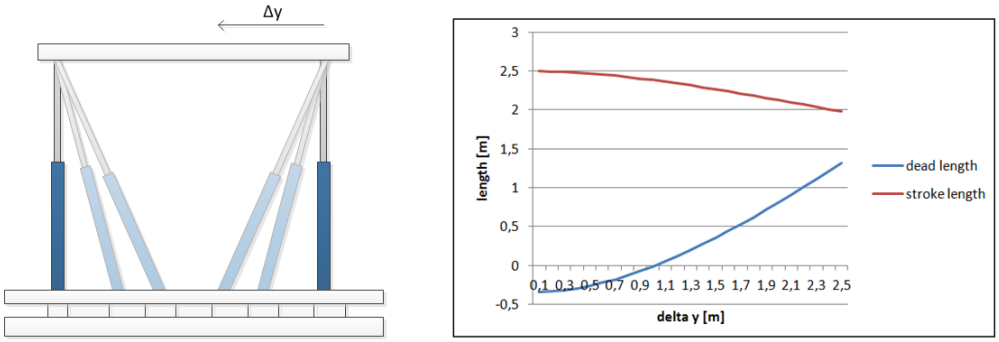

Figure 7-3: Variable stroke and dead length

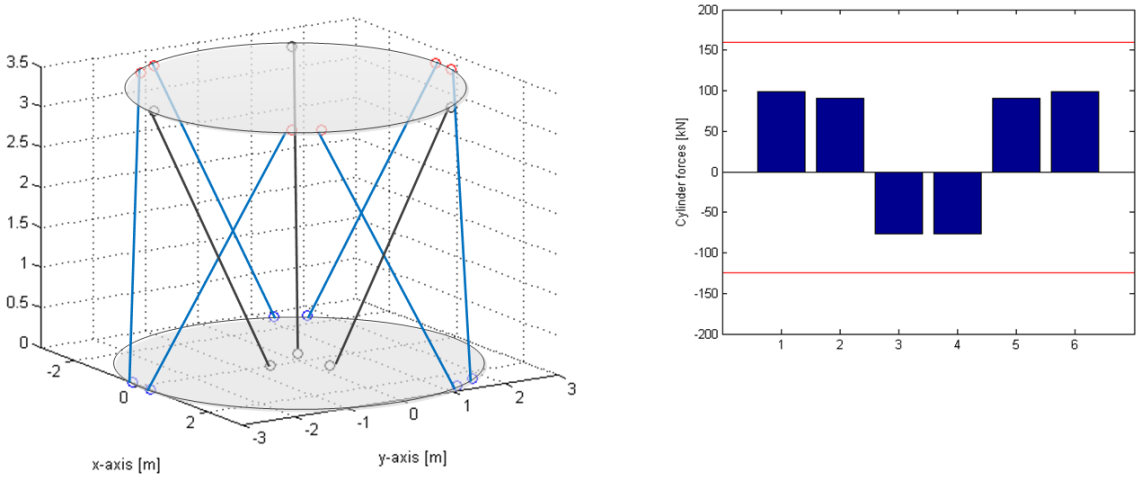

Figure 7-4: Stewart platform 3 cylinders I with smaller dead length

When comparing the forces from Figure 7-4 with A-4b, it can be concluded that the smaller dead length of the extra cylinders has only a minor influence on the force distribution over the six Stewart platform cylinders.

7-2 Other possible improvements

The purpose of this study was to make the A-type operable for larger gangways by improving the Stewart platform for the large asymmetric load case. Other possible improvements to make the A-type operable for the GXXL are considered in this section.

7-2-1 1. Reduction tipping moment

The first possible alternative is to reduce the tipping moment before it even reaches the top of the Stewart platform. This can be achieved by adding a superstructure on top of the gangway, in form of a crane like structure (see 1 in Figure 7-5). The super-structure is

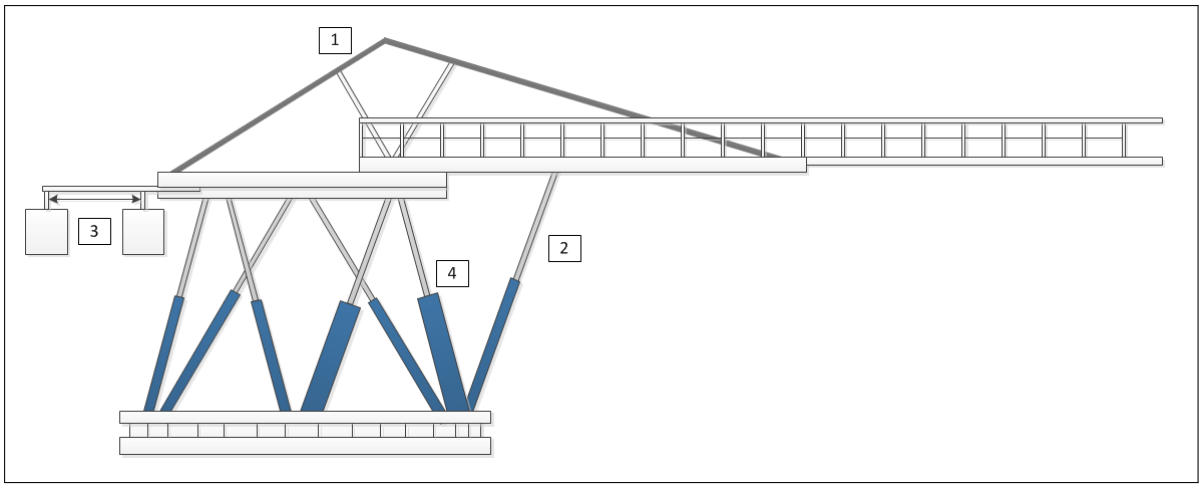

Figure 7-5: Possible solutions

connected to the gangway. This creates multiple challenges, as the gangway has 2 DoF (luffing and telescoping). The telescoping motion can be avoided for the structure by connecting it to the Main Boom, as also is shown in Figure 7-5. The luffing motion can be accounted for by using steel cables and connecting these to a winch. Attention points are:

- Force distribution cable and platform
- Strength and size steel cable
- Winch size and location
- Cable breaking hazard
- Control system winch

2. Support of the gangway

The second possible alternative is to counteract the tipping moment that works on the Stewart platform, reducing the total load case. This is also the starting idea for the passive cylinders method. This approach is to support the gangway by supporting cylinder(s), which are connected to the Main Boom and the bottom platform.

To see if this option is a useful, the cylinder lengths and the counteracting forces from the cylinders are investigated. In this stage the angle of the cylinders which is needed to make the +- 20 degrees angle of the gangway possible is not yet taken into account. Also the type of cylinders which is used is assumed the same as for the A-type, with a operational push force of 160 kN.

To reduce the external loads for the six cylinders of the Stewart platform, the forces of the gangway are partly reduced with the use of the extra cylinders. To make this possible these cylinders have to be connected to the bottom frame. The part of the force that will be reduced with the cylinders depends on the angle of the supporting cylinders and the force they can

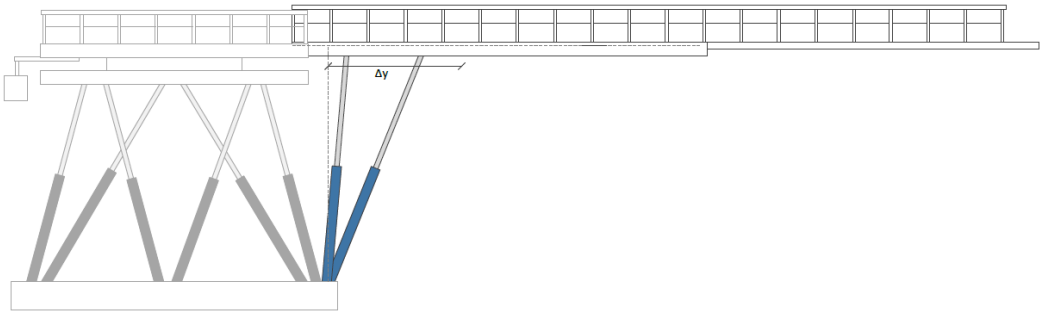

Figure 7-6: Supporting cylinders connections

contribute to the total system. For the first estimation the supporting cylinders are assumed to be the same as the A-type cylinders with a maximum push force during operation of 160 kN. With this assumption the part of the external force on the Stewart platform that can be reduced only depends on the angle of the extra cylinders (α). These cylinders make it possible for the gangway to make an angle of +/- 20 degrees, as shown in Figure 7-6. The angle of the cylinders depends on this angle and the connection point with the main boom.

Length supporting cylinders The supporting cylinders reach their maximum length when the Stewart platform is at its maximum height and the gangway has an angle of +20 degrees. The minimum length of the cylinders will occur when the Stewart platform is at its minimum height and the gangway has an angle of -20 degrees. The maximum and minimum length will be the limiting factor as the stroke of the cylinders can not be larger than 2 meters.

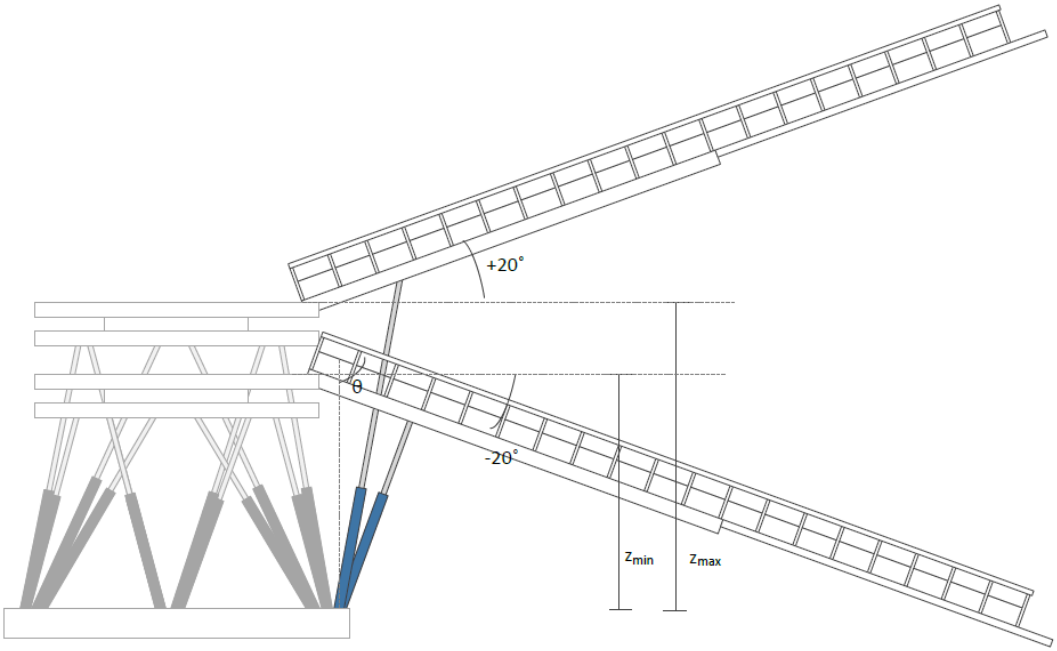

Figure 7-7: Supporting cylinders length

The bottom connection point is fixed at the bottom frame below the gangway. The top connection point is varied with a step size of 0.1 meter from 0 to 2 meter on the gangway. For every position of the gangway the length of the supporting cylinders can be determined with the use of the law of cosines:

$$l_{cyl}^2 = z^2 + l_{con}^2 - 2 \cdot z \cdot l_{con} \cdot \cos(\alpha) \tag{7-1}$$

Where,

l_{cyl}	Length supporting cylinder	[m]
z	Vertical distance from bottom frame to bottom gangway	[m]
l_{con}	Distance connecection point on gangway to start of gangway	[m]
θ	Angle of gangway (= 90 +/- 20)	[deg]

In the next section the lengths of the supporting cylinders are plotted in Figure 7-8 and 7-9. It must be stated that a l_{con} of 0 meter is not possible. The will not be able to make the supporting motion. Second, when l_{con} is small, a small difference in cylinder length will have a large influence on the position of the gangway.

Loads by supporting cylinders With the same law from equation 7-1, the angle of the supporting cylinder can be calculated for every position of the gangway. With the angle of the cylinders, the lever arm perpendicular to the cylinder to the centre of the top platform can be determined. This lever arm is used to calculate the external moment created by the supporting cylinder that works on the Stewart platform. The length of the supporting cylinders and the external moments created by these cylinders when they are connected to the gangway at a variable distance are plotted in Figure 7-8.

Max and min height is till top platform. distance to bottom gangway not yet included.

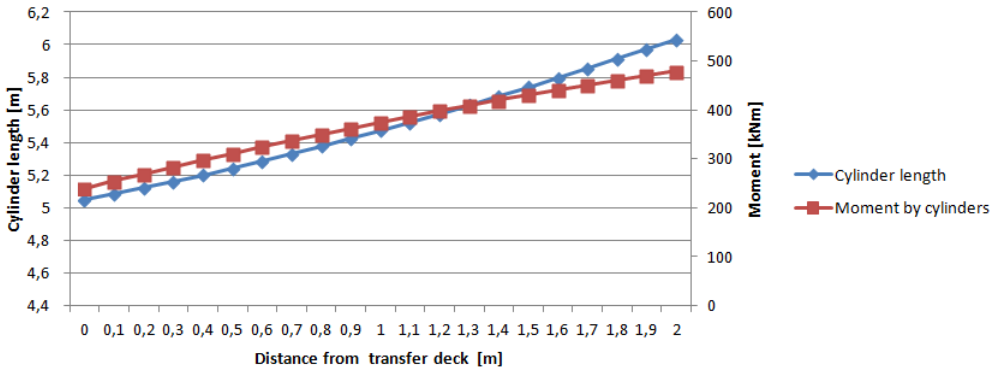

Figure 7-8: Cylinder length and contributing moment at maximum height with gangway at +20 degrees

When the Stewart platform is at maximum height with the gangway at +20 degrees, as shown in Figure 7-8, the length of the supporting cylinders increases from 5.05 to 6.03 meter when the distance of the top of the cylinders to the transfer deck increases from 0 to 2 meter. The almost linear increase can also be seen for the moment which the supporting cylinder

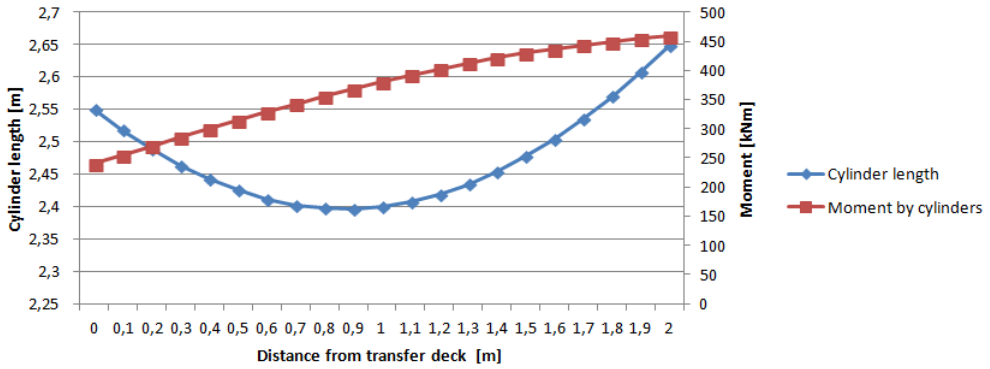

Figure 7-9: Cylinder length and contributing moment at minimum height with gangway at -20 degrees

contributes to the system. The larger the distance from the transfer deck the larger the contributing moment, which is positive for the total decrease of the tipping moment. The cylinder length however also increases. The maximum cylinder length of the A-type cylinder which are considered at the moment are 5.25 meter. This length is exceeded at a distance from the transfer deck of 0.6 meter. When the distance is 0.5 meter, the supporting cylinder length is 5.24 meter. The moment which is generated by one cylinder is 316 kNm. For two supporting cylinders, this will be 632 kNm.

Maximum cylinder stroke For hydraulic cylinders, the cylinder stroke equals the distance between l_{max} and l_{min}. For the A-type cylinders, the stroke length is 2 meters. The maximum cylinder length for the supporting cylinders occurs when the Stewart platform is at a maximum height and the gangway has an angle of +20 degrees. The minimum distance is when the Stewart platform is in settled position and the gangway is -20 degrees. When subtracting these values, the required stroke length is obtained and can be seen in Figure 7-10. When the supporting cylinder is vertical (top connection point is at beginning of the gangway), the stroke length already exceeds the 2.00 meter.

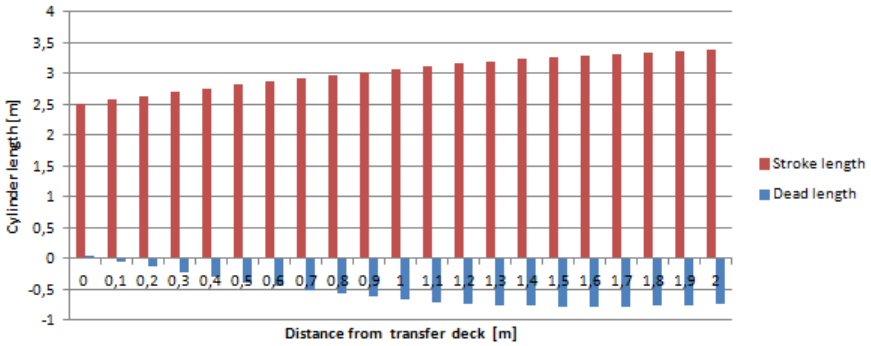

Figure 7-10: Difference in cylinder length between two critical positions

The stroke of the cylinder can not be enlarged that easily. This has also consequences for the dead length. When the stroke length is enlarged, the dead length will also increase. This

means that the minimum cylinder length will also be larger. The smallest required cylinder length for the supporting cylinder is already below the minimum cylinder length. A possible solution for this problem is to make use of double stroke cylinders.

Conclusion Luffing cylinders can reduce the external force and moment for the Stewart platform giving the cylinders multiple purposes. The advantage of this is that there is no need to add other super-structures to the system. However there are multiple disadvantages to this solution. First, the stroke length of the cylinders is not sufficient to

- Still cylinders are loaded that are primarily used to create a motion for the Ampelmann system
- The supporting cylinders do not have a sufficient stroke length to make the total supporting angle of 40 degrees.
- use of double stroke cylinders have two disadvantages:
  - only half of the operation force
  - lower buckling capacity
- Bottom frame is loaded asymmetrical

3. Movable counterweight

The current A-type system makes already use of a counterweight to counteract the tipping moment. A downside of this method is that in Stowed Condition, a tipping moment in the other direction is created. This tipping moment creates large forces for the seals and the connection points of the cylinders, which approach their maximum limit. A solution for this problem can be a moveable counterweight, which extract during operation (creating a large counter moment) and retracts during Stowed Condition (minimizing the counter moment).

When applying a movable counterweight, the effect when increasing the arm length of the counterweight with 1.00 meter will only reduce the moment in x-direction with about 50 kN. This reduction is only small compared to the total tipping moment. To make real improvement, the arm should be at least doubled. When doing so, a large block with a mass of over 4 tonnes will swing over the deck during the yaw motion in operation. This can cause dangerous situations where a large area behind the Ampelmann system should be free and not people should be able to be there during operation. Concluding, using a horizontal movable counterweight is not the solution to counteract the tipping moment, but can be used to reduce it.

4. Larger operation limits

The cylinder forces of the Stewart platform can be reduced by optimising the geometry of the system and by adding extra cylinders (see main report).

Chapter 8

Conclusion and recommendations

8-1 Conclusions

In this report it is investigated if it is possible to place the Gangway XXL on top of a motion compensating Stewart platform with A-type cylinders. For the current A-type, this leads to large cylinder forces that exceed their operation limit. The Stewart platform is optimised in this report to reduce the occurring cylinder forces.

The cylinder forces are calculated with the use of an expanded Jacobian matrix and cylinder dynamics. The first method includes the mass and position of the cylinders, leading to the axial and lateral cylinder forces per position of the platform. The second method includes also the motions of the cylinders, leading to the axial and lateral cylinder forces during vessel motion compensation. Both methods are compared to see what the impact of the lateral forces are on the total forces. The forces due to the motion of the cylinders is negligible in comparison with the external loads. In the report the expanded Jacobian matrix is used as calculation method for the cylinder forces.

The optimisation of the Stewart platform is made possible by relocating the slewing ring to below the bottom platform. In this way, the total system rotates during operation and the same cylinders are loaded in the same manner during operation. This relocation has also an impact on the load distribution, as the moment caused by the wind on the gangway can no longer be counteract by a slewing motion and will now have to be compensated by the Stewart platform.

The first optimisation step is the improvement of the Stewart platform geometry for its loading capacity. The asymmetric load case leads to a geometry which is also asymmetrical. The top frame becomes elliptical with a larger length than width and the bottom frame remains circular. The connection point at the bottom frame of the cylinder are as far from each other as is possible, for an allowable dexterity. This geometry leads to most equal force distribution within the system of the six cylinders. The maximum cylinder forces have been reduced in comparison with the current A-type system. This is however to the detriment of

the workspace, with is also reduced. The motion control limitations should be adapted to this geometry, to see the influence of this reduction on the workability of the system.

The second optimisation step is the reduction of the loads on top of the platform by adding extra cylinders with a constant counteracting force. In neutral position, the constant force of the extra cylinders leads to a reduction of the forces of the Stewart platform cylinders. However, when the system is placed in positions at the boundary of the workspace, these constant forces can lead to an amplification of the load case. Which again leads to larger the cylinder forces. A constant counteracting force for all position is not an option to reduce the cylinder forces.

With active fore control, the constant force of the extra cylinders becomes a variable force. For each position in the workspace of the system, the required forces of the extra cylinders are calculated. The extra cylinders can only counteract the dead load of the system, because the live and wind load are not constant during operation. The method for which the extra cylinder statically compensate the dead load of the system for every position also leads to an amplification of the load case due to the extra forces that are created in y-direction.

The only possible method to use active force control is to determine per position the Stewart platform cylinder forces and the required reduction of the dead load, to lower the cylinder forces below their operation limit. This method still leads to cylinder forces that exceed their operation limit.

The GXXL on top of a Stewart platform with A-type cylinders can not be used for cargo transfer. However, the main function of the gangway remains people transfer. This has been made possible by using active force control in a new geometry of the Stewart platform. The only adaption that has to be made is the workspace in x- and y-direction has to be lowered. This will cause some residual motion of the transfer deck but only in a horizontal manner and can be compensated with the slewing and telescoping motion of the gangway.

For the research objective of this report the following conclusion can be drawn:

> "Research how the Stewart Platform design of the A-type Ampelmann system can be improved for large asymmetric load cases, making it better suitable for higher loads"

The Stewart platform can be improved for the large assymetric load cases, but these improvements are marginal for the use of Cargo Transfer on the GXXL. The optimisation of the geometry of the platform including AFC makes People Transfer with the GXXL possible when the workspace of the system is limited in x- and y-direction.

8-2 Recommendations

- investigate dead and stroke length
- investigate possibility to reduce counterweight
- minimum dexterity of 0.12
- same neutral height for every condiguration

Appendix A

Configurations Passive cylinder models

In this appendix the 3d representation of all the twenty-two models of the passive cylinders are given. These models are used in Chapter 5 to determine the number of passive cylinders that is used to reduce the forces of the Stewart platform cylinders. First the Stewart platform cylinder forces are given for a model with a GXXL-NO-CT load case without passive cylinders. Two different directions of the load case are used, as shown by the gangway in Figure A-1. These two directions of the load case are also used for all the passive cylinder models, leading to two configurations for the 1, 2, 4, 5 and 6 cylinder model. Only the 3 cylinder model consists of ten separate configurations. All the passive cylinders have a axial push/pull force of 100 [kN], depending on their location with respect to the gangway.

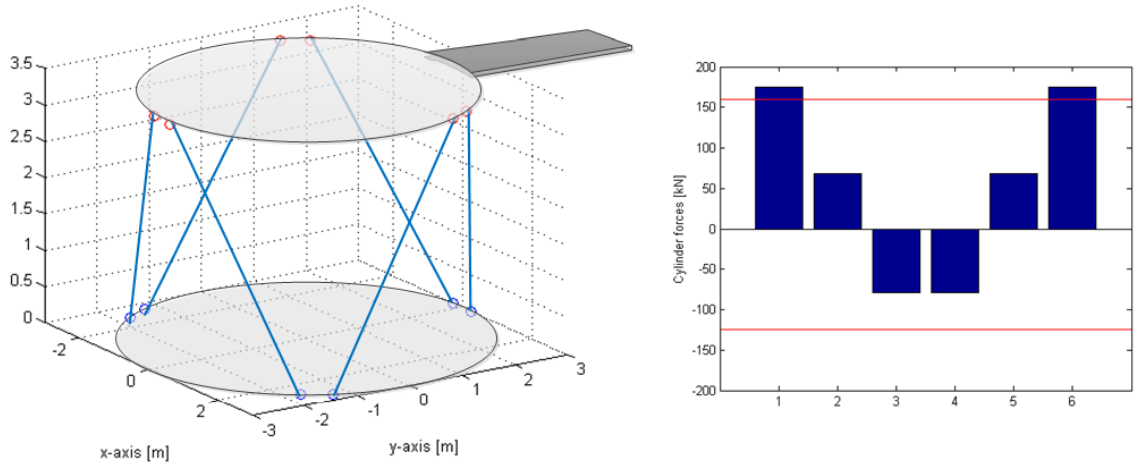

(a) Stewart platform configuration 1

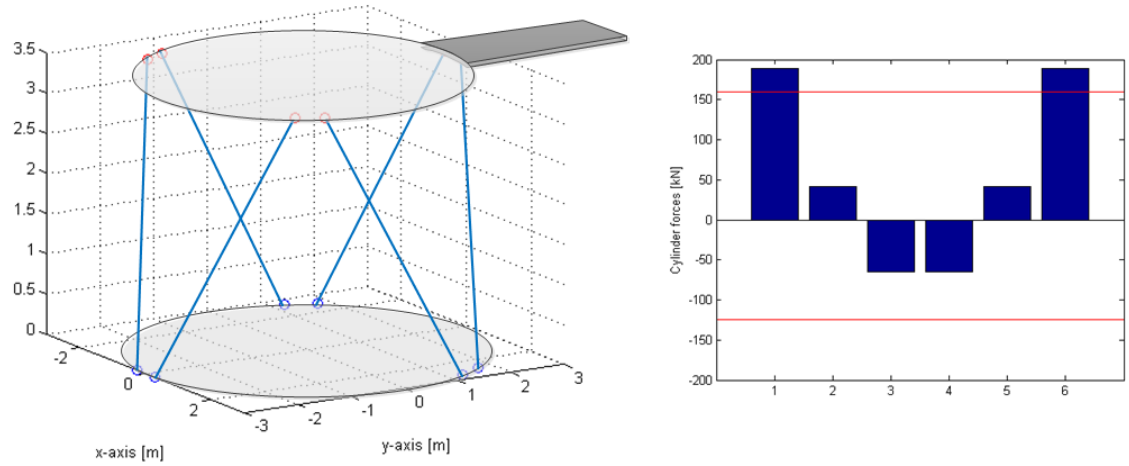

(b) Stewart platform configuration 2

Figure A-1: Stewart platform without passive cylinders

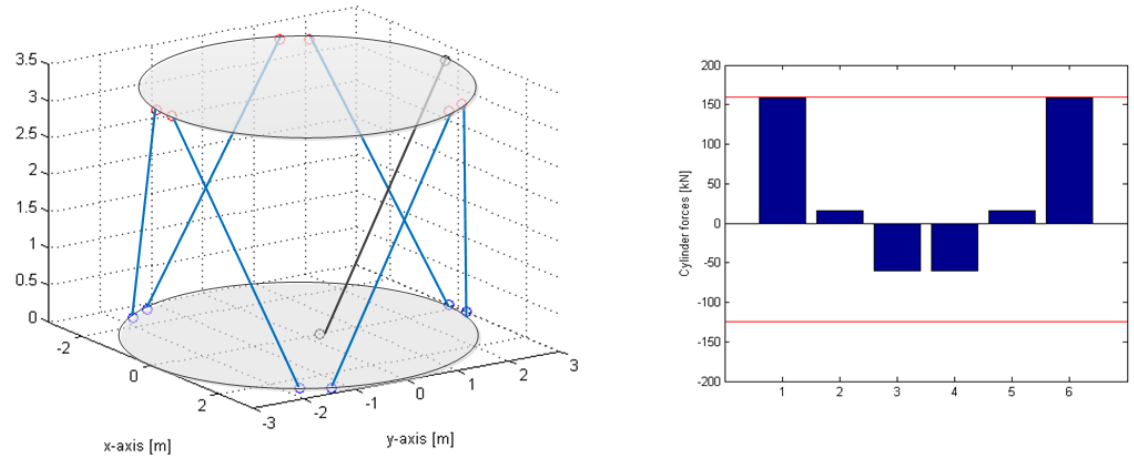

(a) Stewart platform configuration 1

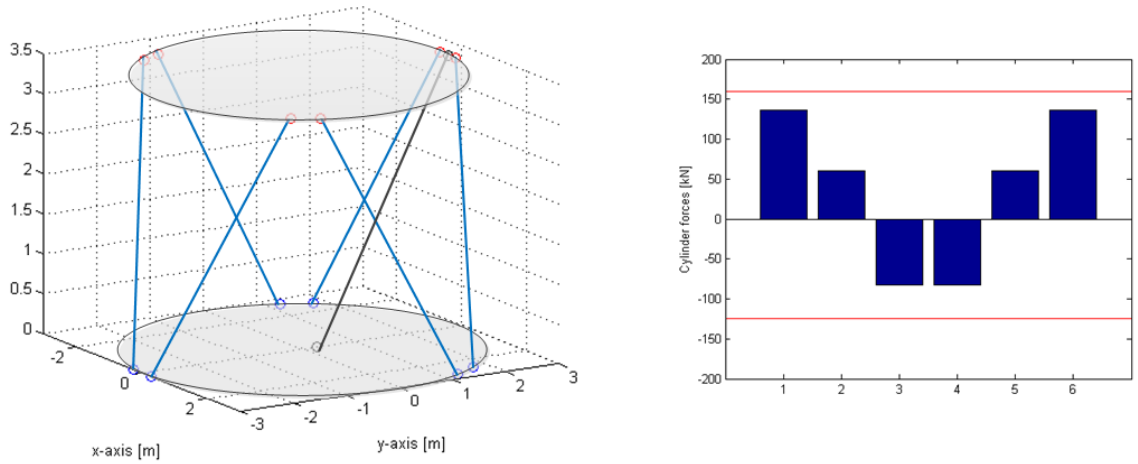

(b) Stewart platform configuration 2

Figure A-2: Stewart platform with 1 passive cylinder

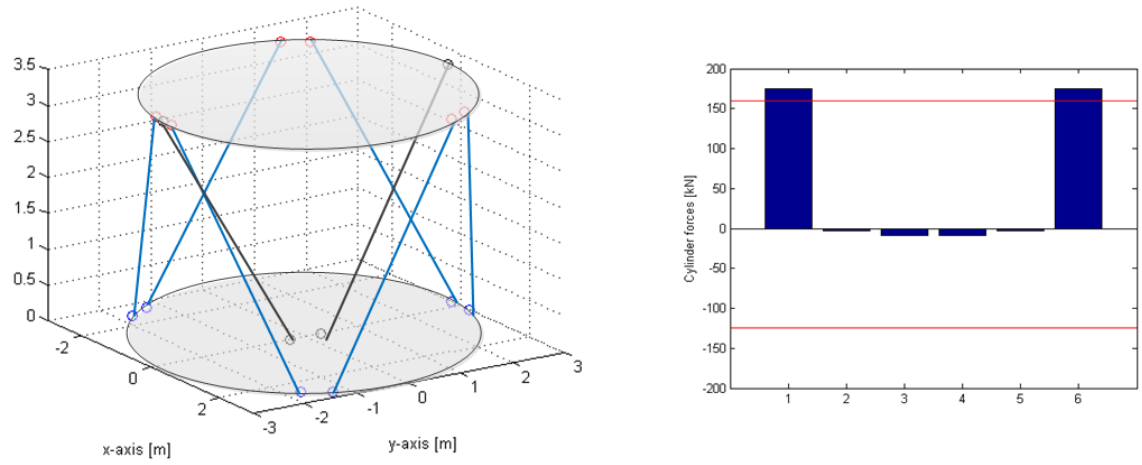

(a) Stewart platform configuration 1

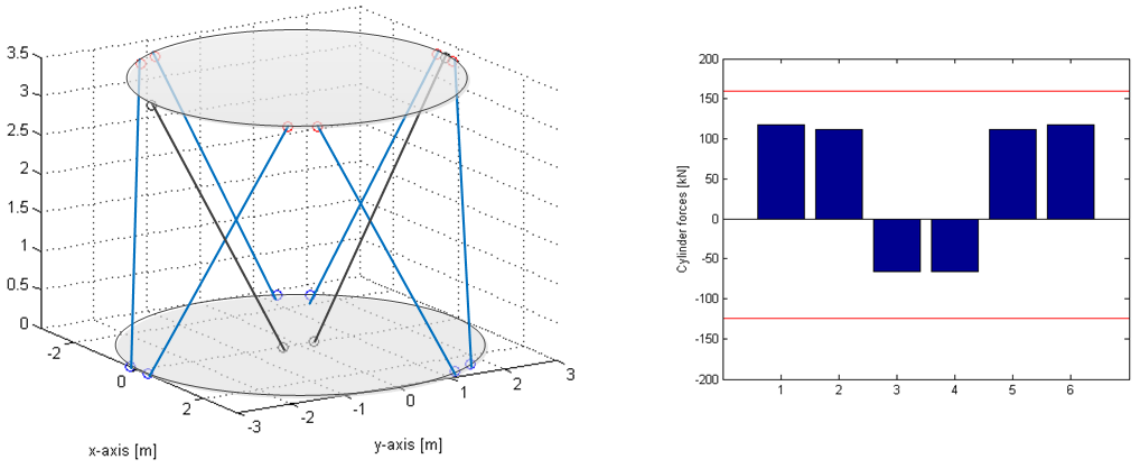

(b) Stewart platform configuration 2

Figure A-3: Stewart platform with 2 passive cylinders

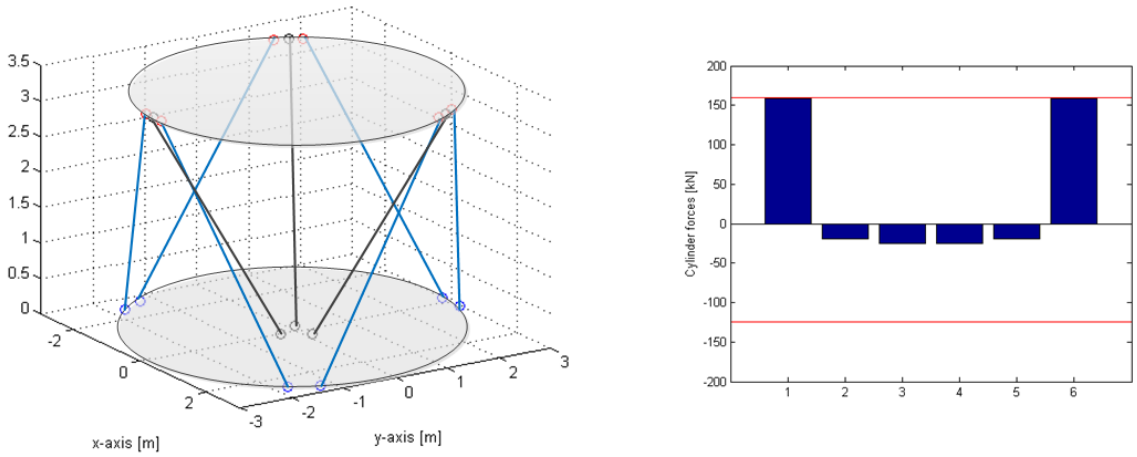

(a) Stewart platform configuration 1

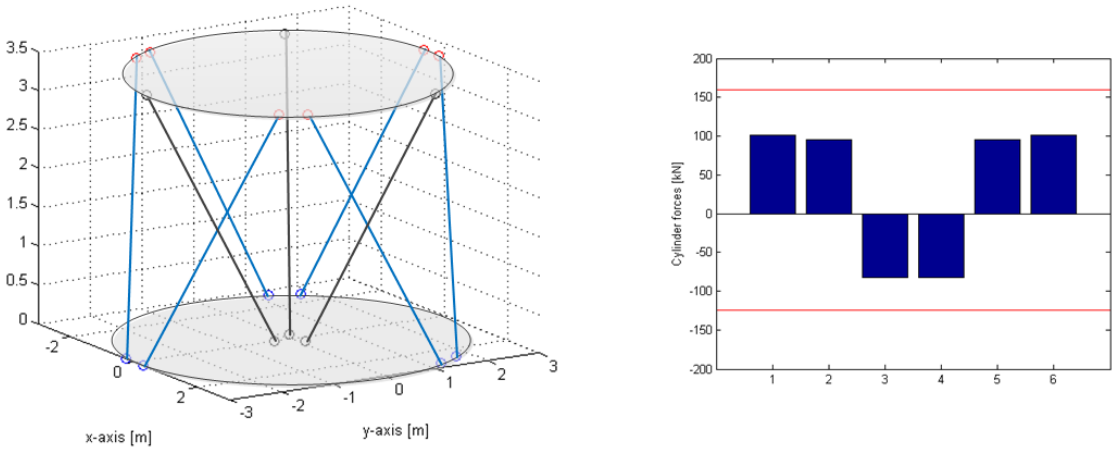

(b) Stewart platform configuration 2

Figure A-4: Stewart platform with 3 passive cylinders I

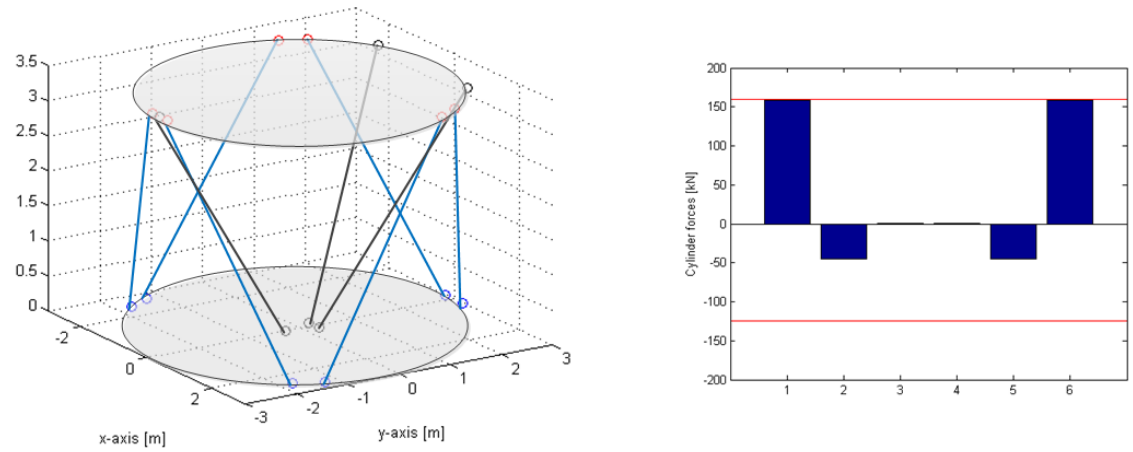

(a) Stewart platform configuration 1

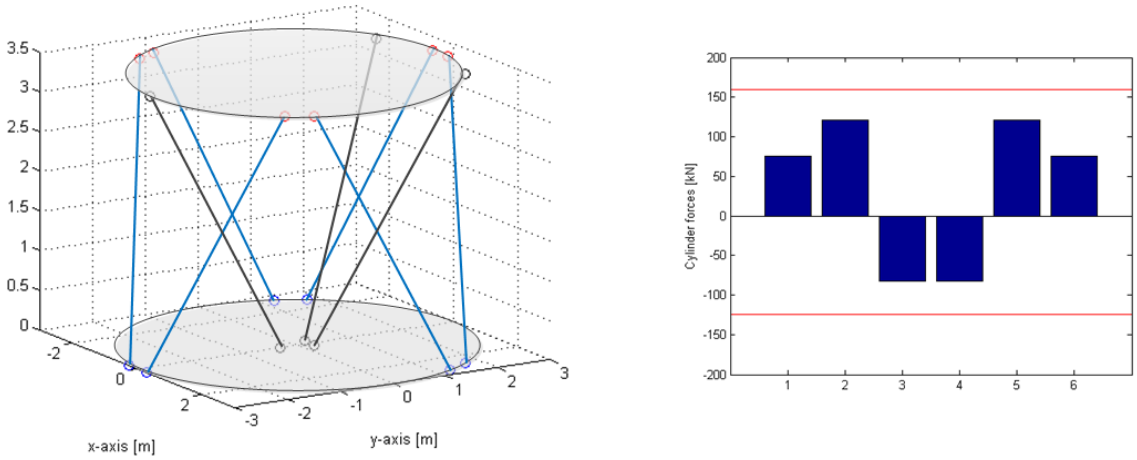

(b) Stewart platform configuration 2

Figure A-5: Stewart platform with 3 passive cylinders II

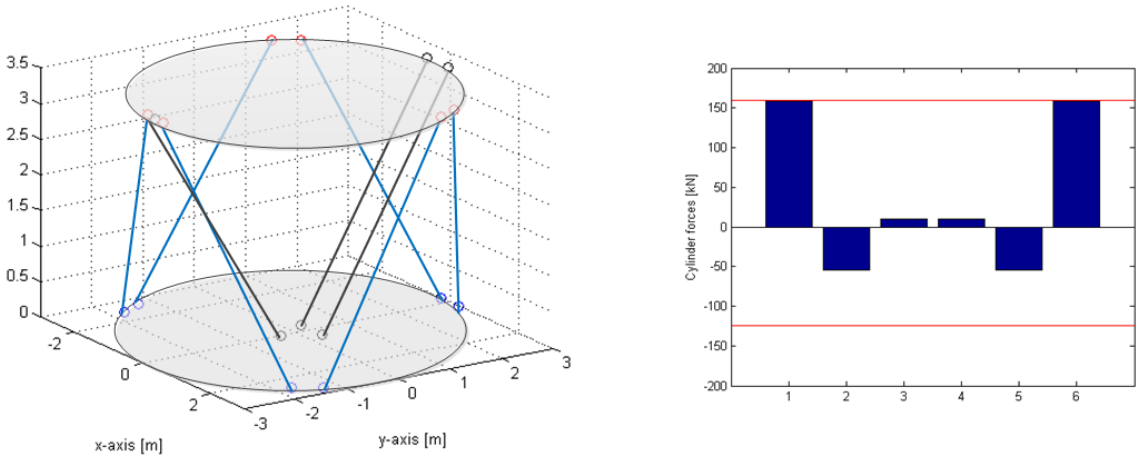

(a) Stewart platform configuration 1

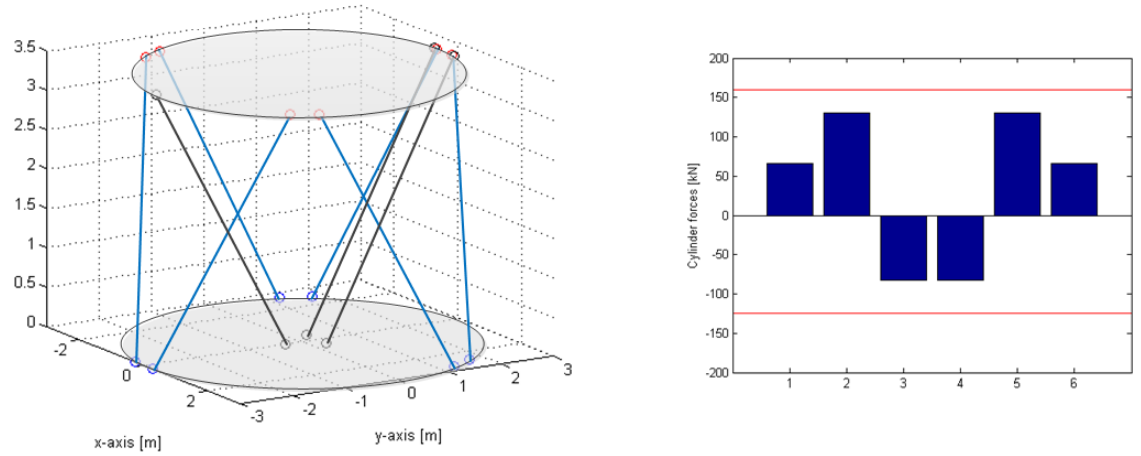

(b) Stewart platform configuration 2

Figure A-6: Stewart platform with 3 passive cylinders III

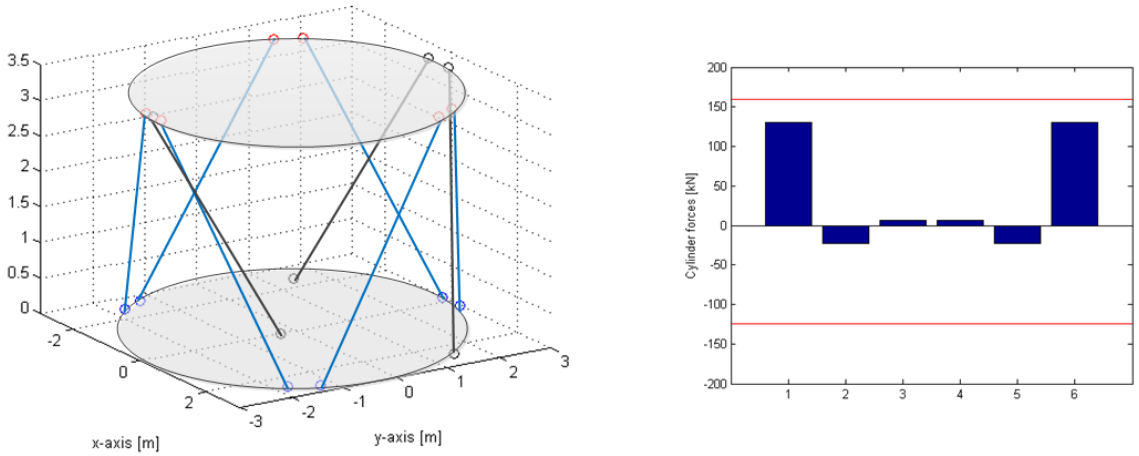

(a) Stewart platform configuration 1

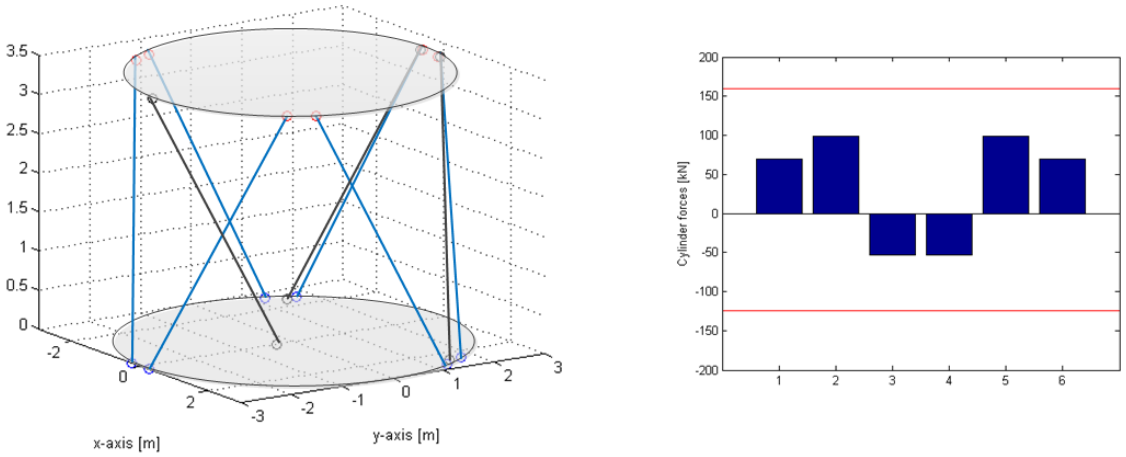

(b) Stewart platform configuration 2

Figure A-7: Stewart platform with 3 passive cylinders IV

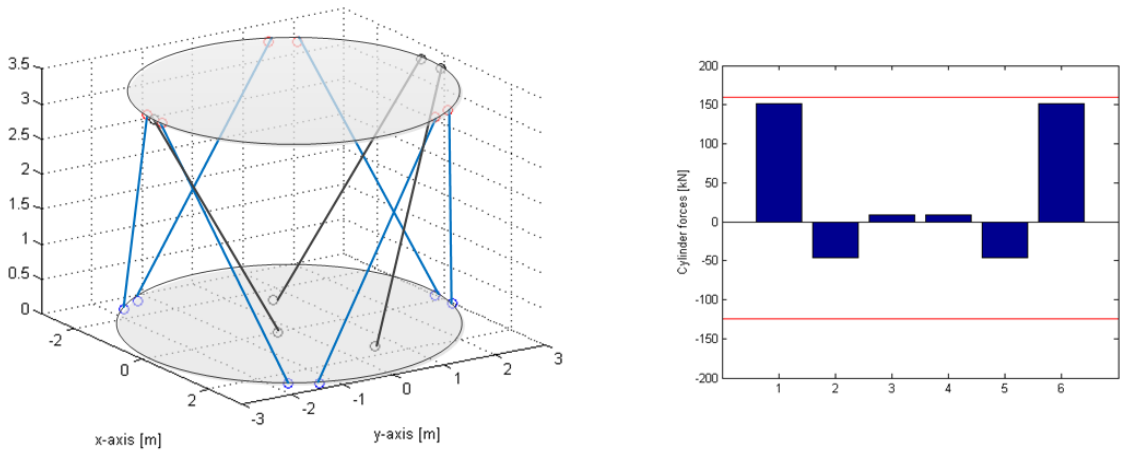

(a) Stewart platform configuration 1

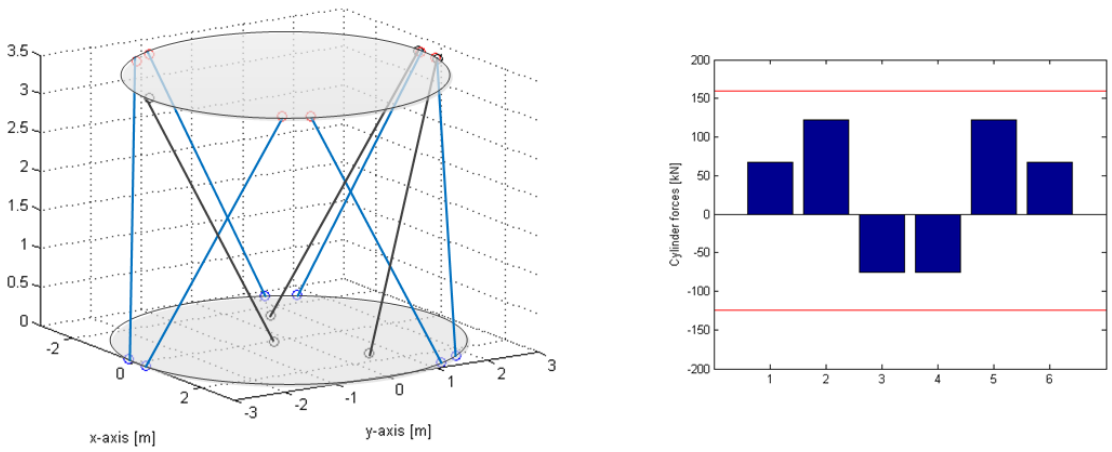

(b) Stewart platform configuration 2

Figure A-8: Stewart platform with 3 passive cylinders V

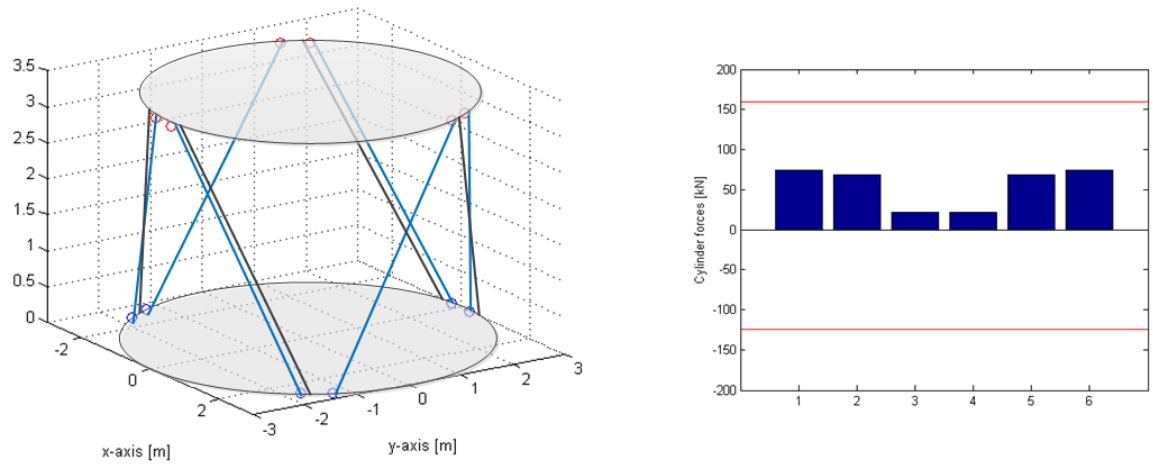

(a) Stewart platform configuration 1

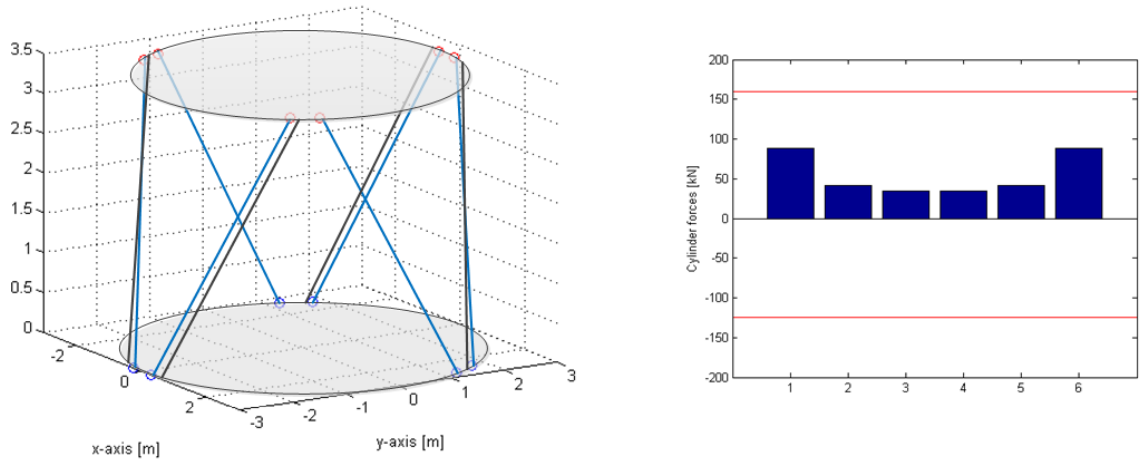

(b) Stewart platform configuration 2

Figure A-9: Stewart platform with 4 passive cylinders

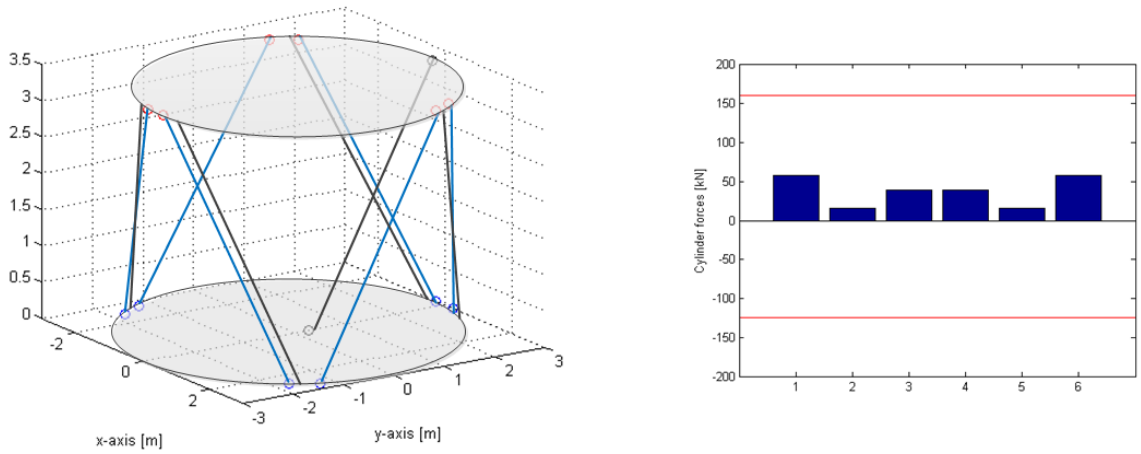

(a) Stewart platform configuration 1

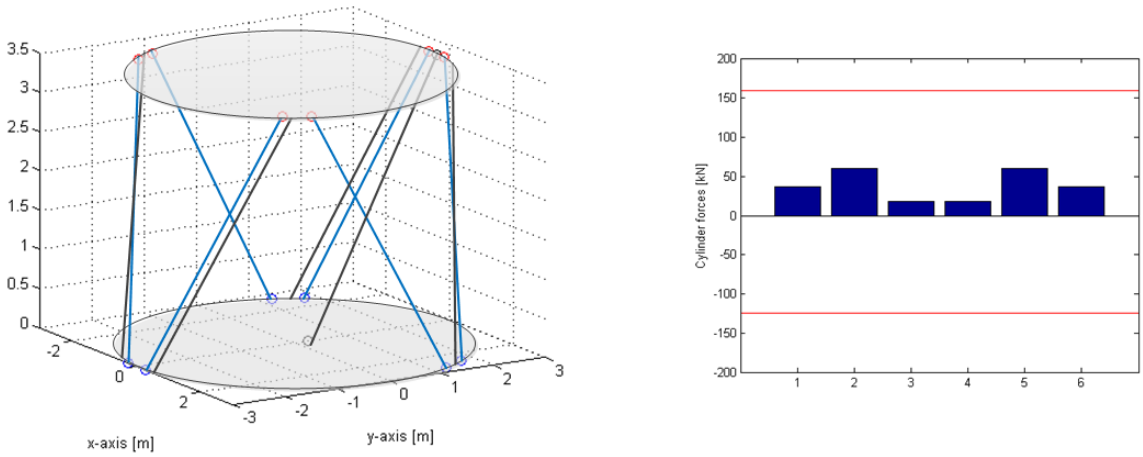

(b) Stewart platform configuration 2

Figure A-10: Stewart platform with 5 passive cylinders

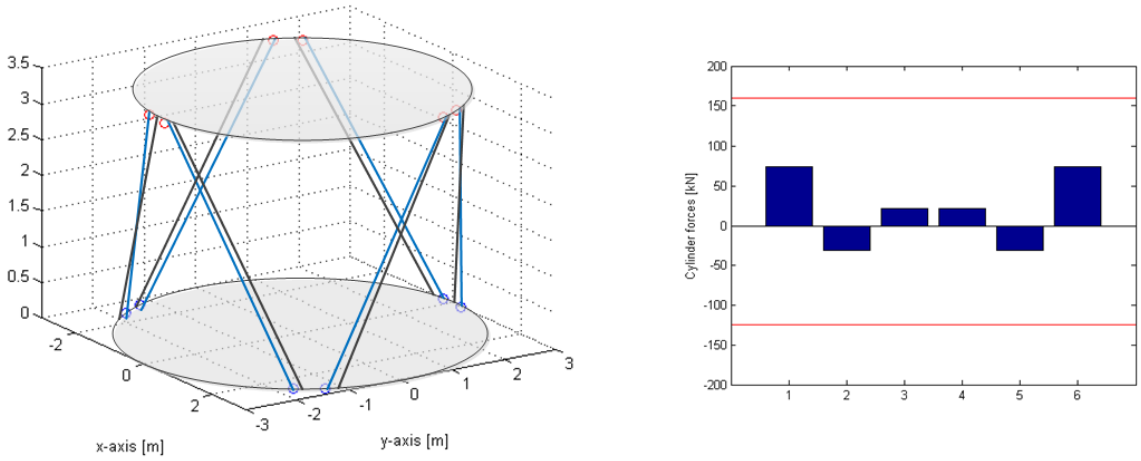

(a) Stewart platform configuration 1

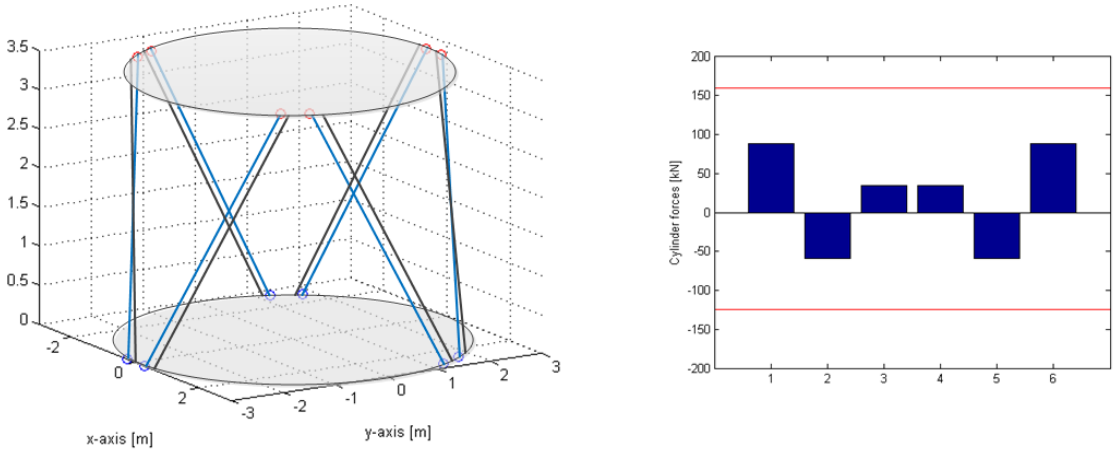

(b) Stewart platform configuration 2

Figure A-11: Stewart platform with 6 passive cylinders

Appendix B

Force reduction Passive cylinder models

In this appendix the Stewart platform cylinder force reduction for the selected passive cylinder models and configurations are given from Chapter 5. For each model and configuration the cylinder forces are obtained for the entire workspace of the system, with a constant passive force. Three external load cases are used: (1) GXXL:NO-CT1000kg, (2) GXXL:NO-CT500kg and (3) GXXL:NO-PT. The red dotted line shows the operation limit of the A-type cylinders. The passive forces are obtained from the force optimisation criteria from section 5-4.

B-0-1 2 Cylinder model

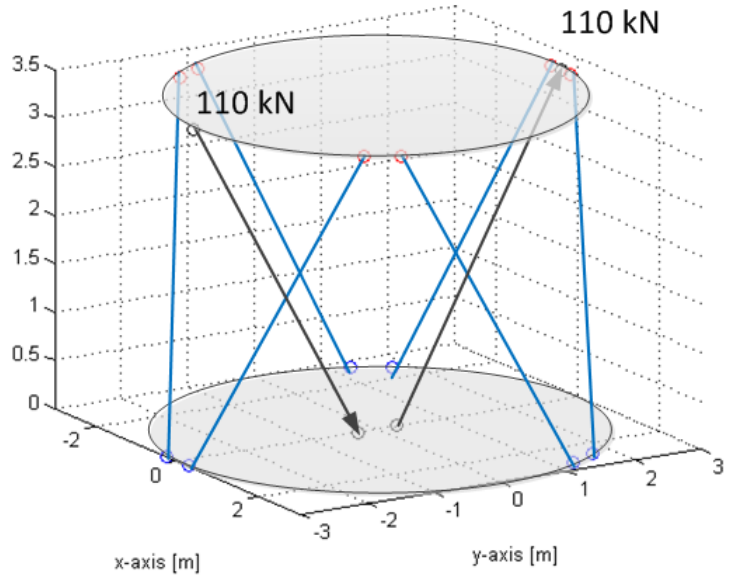

Figure B-1: 2 Cylinder model: Passive forces

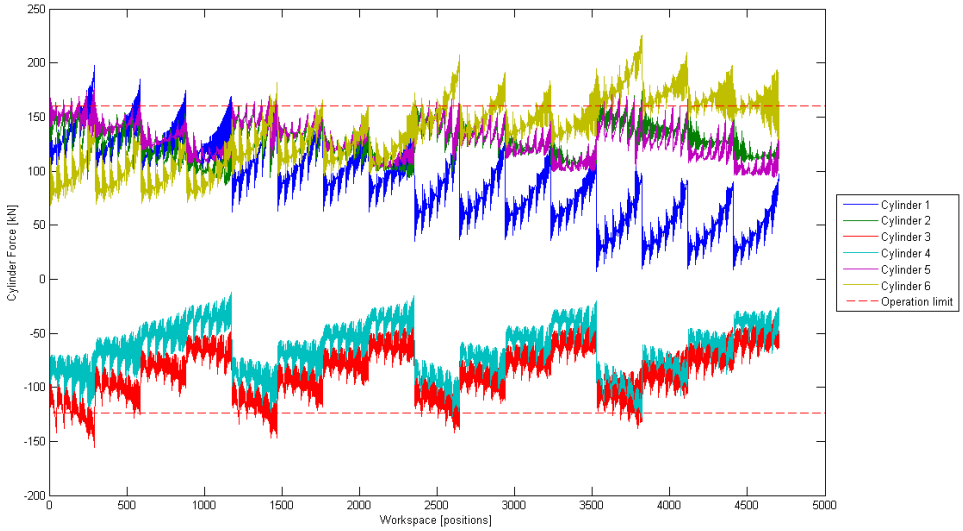

Figure B-2: 2 Cylinder model: load case GXXL:NO-CT1000kg

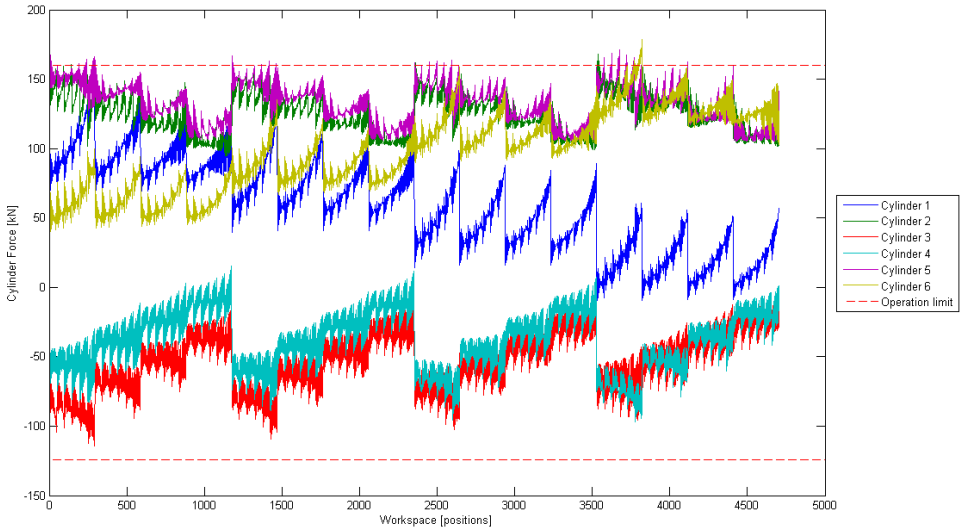

Figure B-3: 2 Cylinder model: load case GXXL:NO-CT500kg

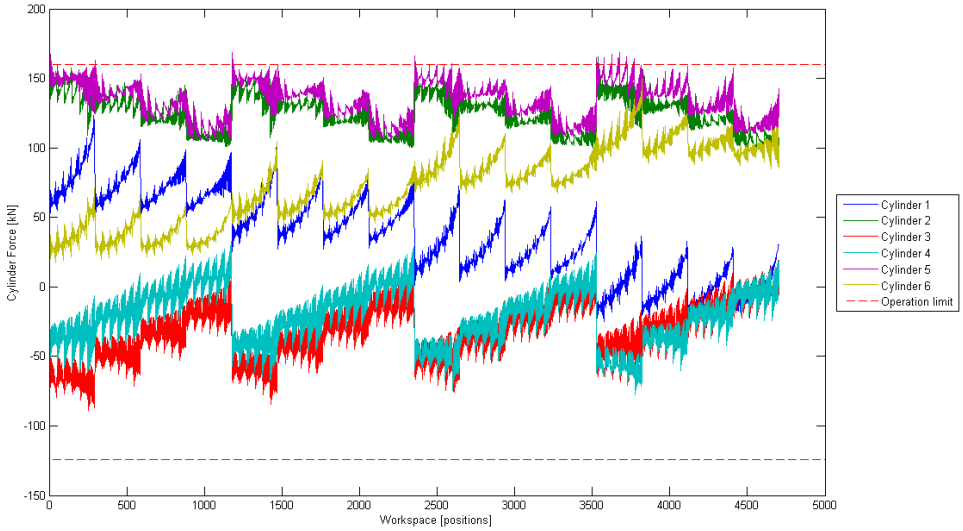

Figure B-4: 2 Cylinder model: load case GXXL:NO-PT

B-0-2 3 Cylinder model configuration I

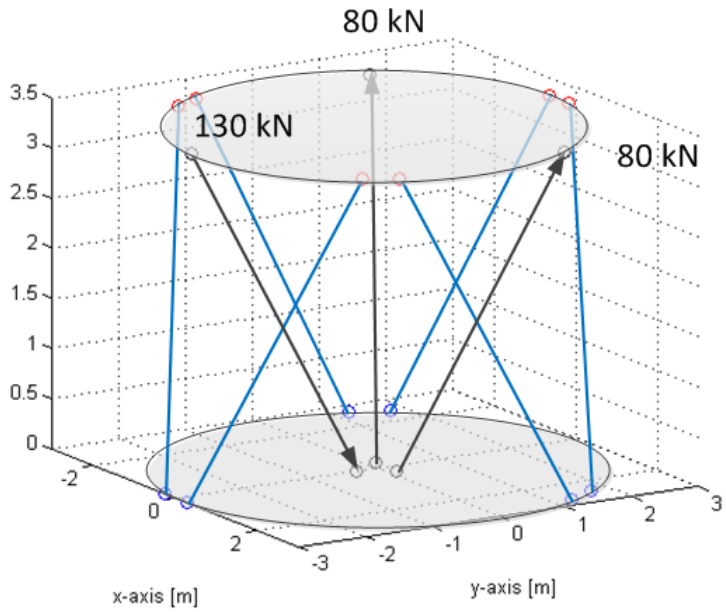

Figure B-5: 3 Cylinder model, configuration I: Passive forces

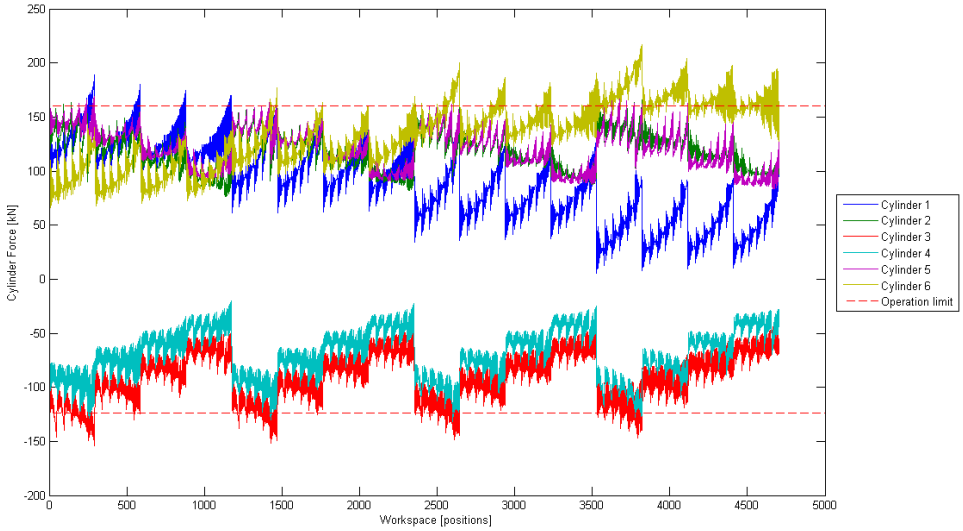

Figure B-6: 3 Cylinder model configuration I: load case GXXL:NO-CT1000kg

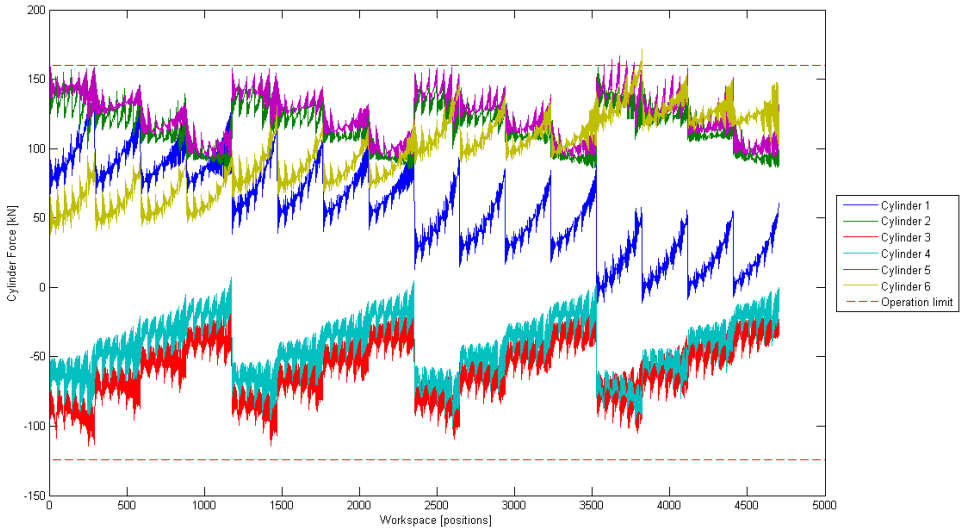

Figure B-7: 3 Cylinder model configuration I: load case GXXL:NO-CT500kg

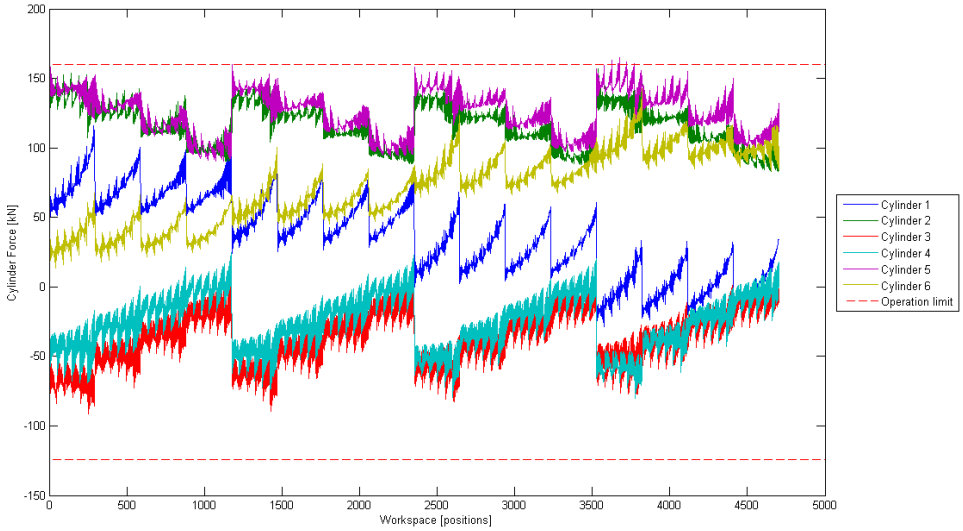

Figure B-8: 3 Cylinder model configuration I: load case GXXL:NO-PT

B-0-3 3 Cylinder model configuration IV

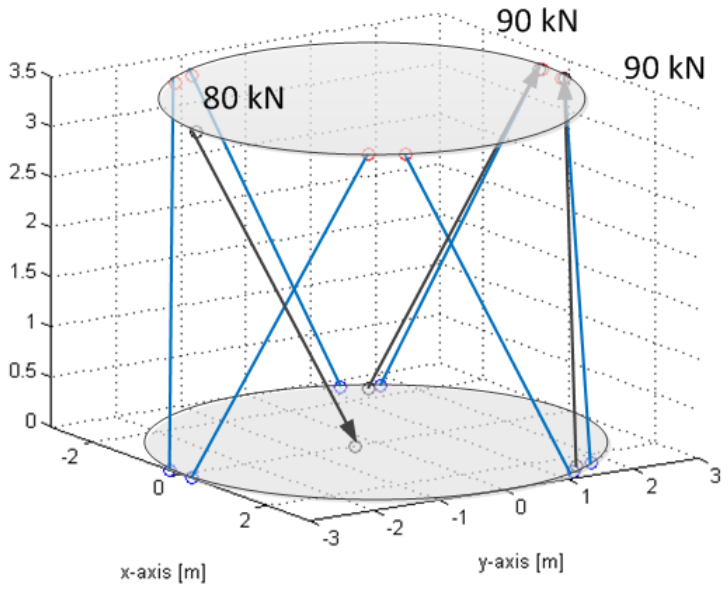

Figure B-9: 3 Cylinder model, configuration IV: Passive forces

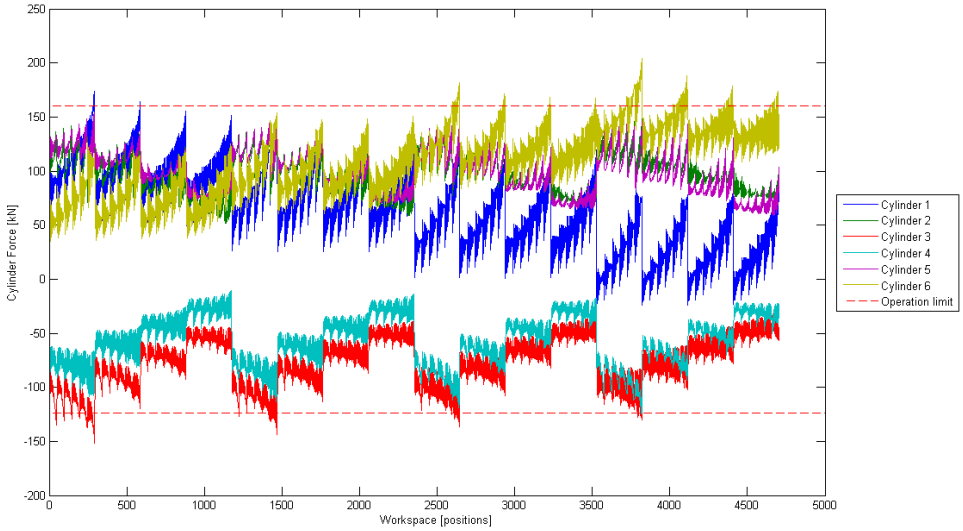

Figure B-10: 3 Cylinder model configuration IV: load case GXXL:NO-CT1000kg

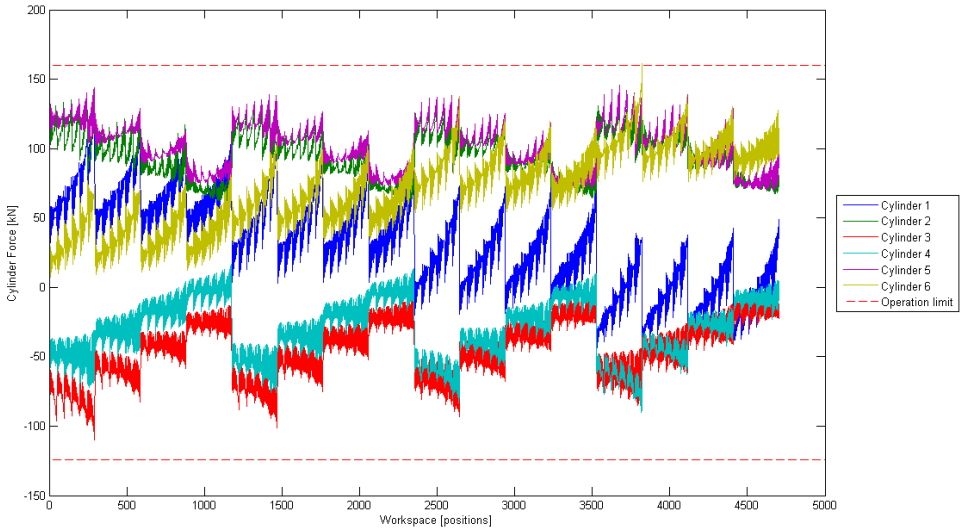

Figure B-11: 3 Cylinder model configuration IV: load case GXXL:NO-CT500kg

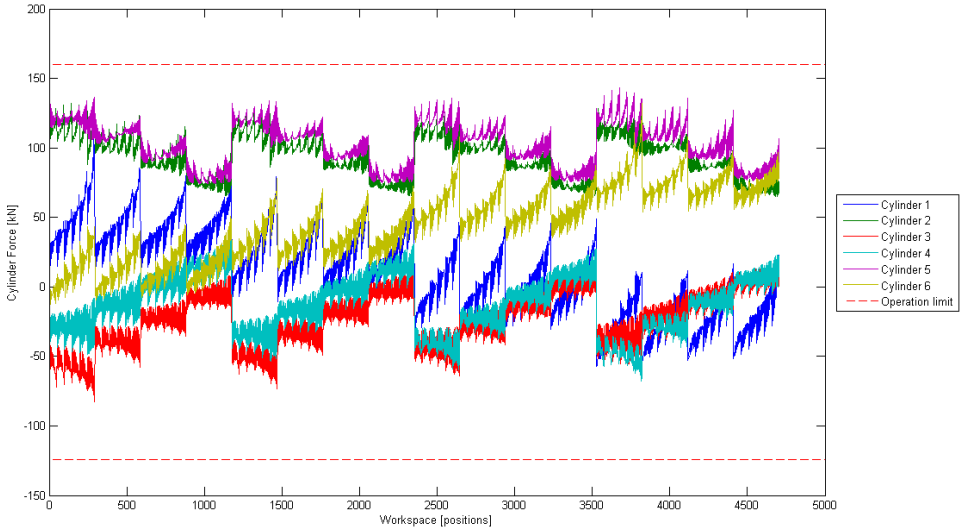

Figure B-12: 3 Cylinder model configuration IV: load case GXXL:NO-PT

B-0-4 4 Cylinder model

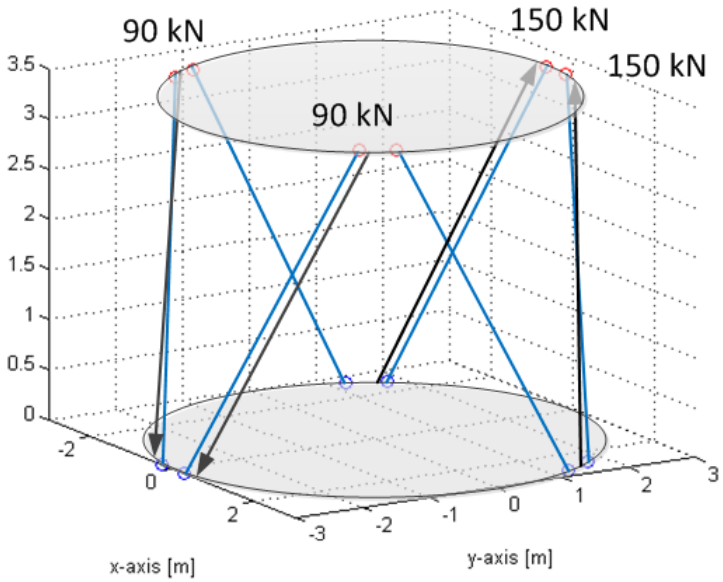

Figure B-13: 4 Cylinder model: Passive forces

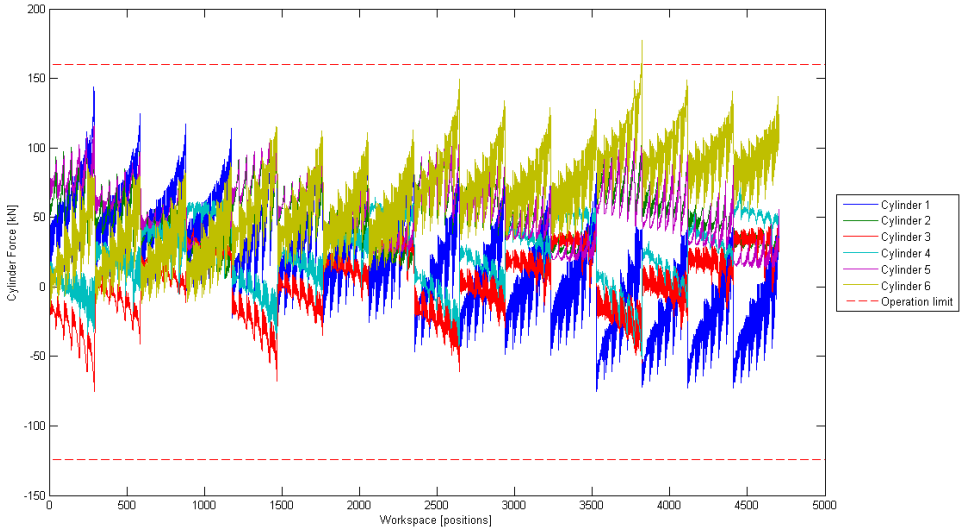

Figure B-14: 4 Cylinder model: load case GXXL:NO-CT1000kg

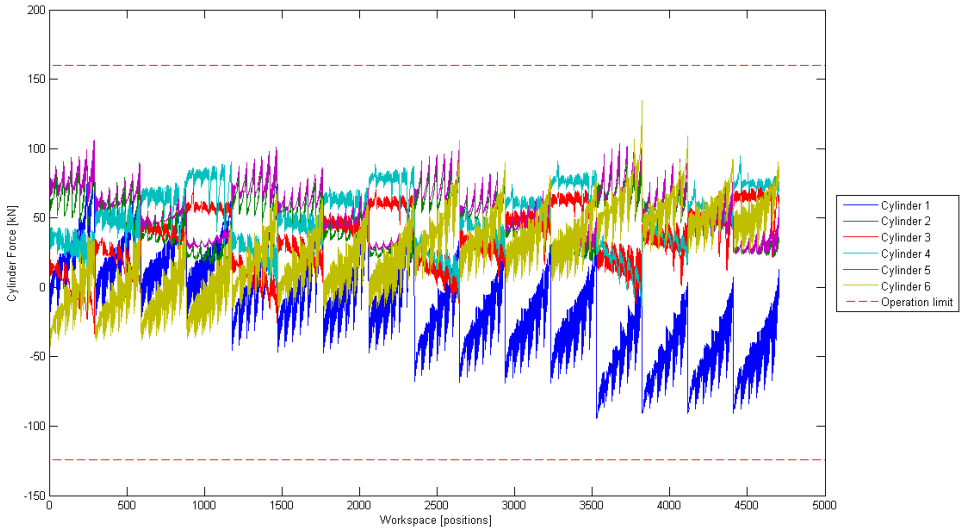

Figure B-15: 4 Cylinder model: load case GXXL:NO-CT500kg

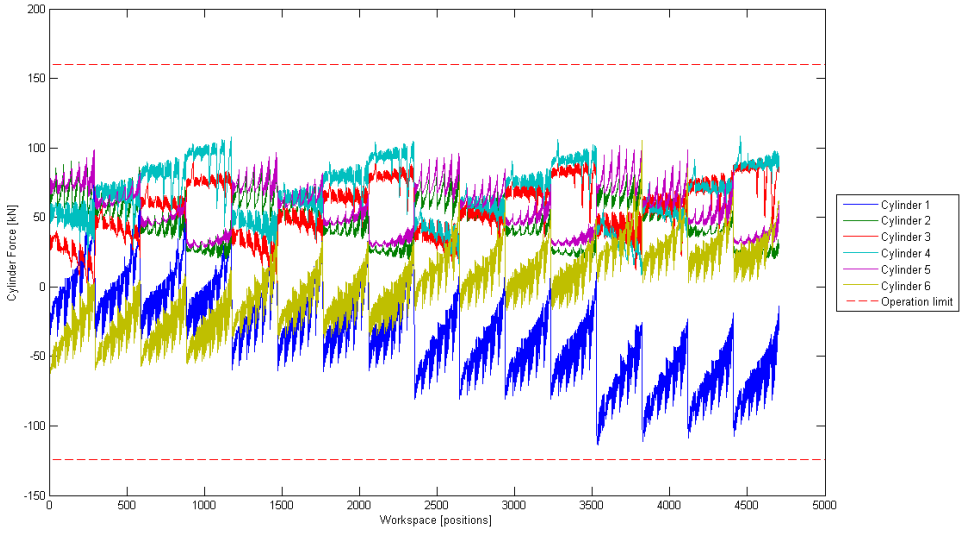

Figure B-16: 4 Cylinder model: load case GXXL:NO-PT

Appendix C

Hydraulic cylinder dynamics

The force control method is based on the pressure differences in the two chambers of the cylinder. The pressure in the upper chamber becomes variable, the same as for the lower chamber. With the force known per position, first the cylinder dynamics are derived. Followed by the pressure dynamics. The pressure can be maintained and controlled with the flow entering the chamber of the cylinder that is connected to the valve. This mass flow is derived from the valve dynamics. These dynamic equations can be used as input for a control model.

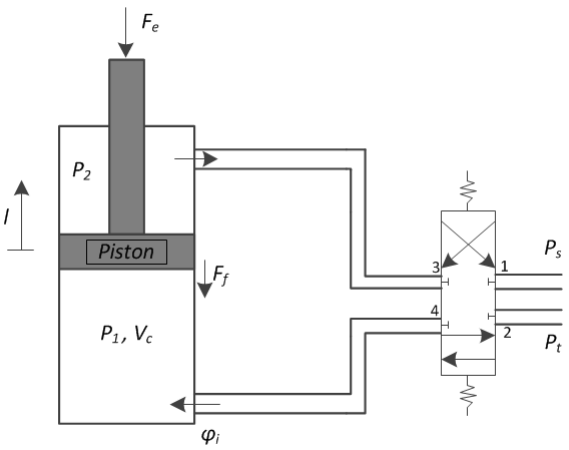

Figure C-1: Cylinder and valve with parameters

Cylinder Dynamics The first step to determine the inflow is to use the equation of motion for the piston of the cylinder:

$$M\ddot{l} = P_1 A_1 - P_2 A_2 - F_f - F_e - Mg \tag{C-1}$$

Where,

M	Mass of the cylinder rod	[kg]
$\ddot{l}$	Acceleration of the piston	[m/s^2]
$P_{1,2}$	Pressure in the lower,upper chamber	[N/m^2]
$A_{1,2}$	Piston area at lower,upper chamber side	[m^2]
F_f	Friction force	[N]
F_e	External force	[N]

The external forces are known from the Look-up table. For these forces the correct pressure is derived with the pressure dynamics.

Pressure dynamics The pressure in the chambers is determined with the inflow. Due to compressibility of the oil, the pressure dynamics are according to [18]:

$$\dot{P}_{1,2} = -E\frac{\dot{V}_{1,2}}{V_{1,2}} \tag{C-2}$$

Where,

E	Bulk Modulus of the oil	[kg]
$\dot{V}_{1,2}$	Rate of change of oil volume	[m^3/s]
$V_{1,2}$	Volume of the chamber	[m^3]

The rate of change of the oil volume is obtained from the change of volume of the chamber and the inflow:

$$\dot{V}_{1,2} = A_{1,2}\dot{l} - (\phi_{i1,2} + \phi_l) \tag{C-3}$$

From the inflow of oil the leakage flow has to be subtracted, which depends on the pressure difference between the upper and lower chamber [18]:

$$\phi_l = L_p(P_2 - P_2) \tag{C-4}$$

Where,

ϕ_l	Leakage flow	[m^3/s]
L_p	Laminar leakage flow coefficient	[-]

The total pressure dynamics becomes by implementing equation C-3 and C-4 into equation C-2:

$$\dot{P}_{1,2} = \frac{E}{V_c}\Big(- A_{1,2}\dot{l} + \phi_{i1,2} + L_p(P_2 - P_2)\Big) \tag{C-5}$$

With,

$$\begin{aligned} V_1 &= A_1 \cdot (l_{dead} + l_{stroke} - l) \\ V_2 &= A_2 \cdot (l_{dead} + l) \end{aligned} \tag{C-6}$$

Valve dynamics The inflow in the chambers depends on the opening of the valve ($u_{1,2}$) and the pressure difference between the two ports [18]:

$$\phi_i = C_d A_u(u) \sqrt{\frac{2(P_{o1} - P_{o2})}{\rho_0}} \tag{C-7}$$

Where,

$P_{o1,2}$	Pressure at open ports 1,2	[N/m^2]
C_d	Discharge coefficient	[-]
A_u	Valve area	[m^2]
ρ_0	Oil density	[kg/m^3]

The discharge coefficient and the oil density are assumed to be constant. The valve area is a non-linear function of the spool position u. These parameters are combined in one function (f_u) that contains the non-linearities of the valve. As stated, the inflow depends on the position of the valve openings:

$$\phi_{i,1} = \begin{cases} f_u(u)\sqrt{P_1 - P_t} & \text{if} \quad u > 0 \\ f_u(u)\sqrt{P_s - P_1} & \text{if} \quad u \leq 0 \end{cases} \tag{C-8}$$

$$\phi_{i,2} = \begin{cases} f_u(u)\sqrt{P_2 - P_t} & \text{if} \quad u > 0 \\ f_u(u)\sqrt{P_s - P_2} & \text{if} \quad u \leq 0 \end{cases} \tag{C-9}$$

Where,

P_t	Tank pressure	[N/m^2]
P_s	Supply pressure	[N/m^2]

State space representation The cylinder dynamics, pressure dynamics and valve dynamics can be included into one state space representation:

[nog verder uitwerken]

Bibliography

[1] T. Delft, "Motion thresholds and masking cues in flight simulation," 2014.

[2] A. O. B.V., "http://www.ampelmann.nl," 2014.

[3] A. van Leer, "Motion control enhancement for the ampelmann system," Master's thesis, Delft University of Technology, 2012.

[4] S. Advandi, *The Kinematic Design Of Flight Simulators Motion-Bases*. PhD thesis, Delft University of Technology, 1998.

[5] D. Stewart, "A platform with six degrees of freedom," *Proceedings of the Institution of Mechanical Engineers*, 1995.

[6] E. Fichter, "A stewart platform- based manipulator: General theory and practical construction," *The International Journal of Robotics Research*, 1986.

[7] T. M. B.Dasgupta, "Closed-from dynamic equations of the general stewart platform through the newton-euler approachl," *Mech. Mach. Theory Vol. 33, No. 7, pp. 993Âś1012,*, 1998.

[8] K. Harib and K. Srinivasan, "Kinematic and dynamic analysis of stewart platform-based machine tool structures," *Robotica, 21, pp 541-554 doi:10.1017/S0263574703005046*, 2003.

[9] T. M. B.Dasgupta, "A newton-euler formulation for the inverse dynamics of the stewart platform manipulator," *Mech. Mach. Theory Vol. 33, No. 8, pp.1135-1152,*, 1998.

[10] B. Dasgupta and T. Mruthyunjaya, "The stewart platform manipulator: a review," *Mechanism and Machine Theory*, 2000.

[11] J.-P. Merlet, "Jacobian, manipulability, condition number and accuracy of parallel robots," *Journal of Mechanical Design*, 2005.

[12] D. C. Salzmann, *Ampelmann, Development of the Access System for Offshore Wind Turbines*. PhD thesis, Delft University of Technology, 2010.

[13] "Inhouse document ampelmann," 2014.

[14] Lloyd's Register, *Code for Lifting Appliances in a Marine Environment*, February 2014.

[15] P. Albers, *Motion Control in Offshore and Dredging*. Springer, 2010.

[16] T. Popponen and T. Arai, "Accuracy analysis of a modified stewart platform manipulator," *Robotics and Automation, 1995. Proceedings., 1995 IEEE International Conference on*, 1995.

[17] D. L. C. M. D. J. S. V, Saxena, "A simulation study of the workspace and dexterity of a stewart platform based machine tool," *DSC-Vol. 61, Proceedings of the ASME Dynamic Systems and Control Division*, 1997.

[18] N. Manring, *Hydraulic Control Systems*. John Wiley and Sons, 2005.

Glossary

List of Acronyms

6DoF	Six Degrees of Freedom
FOG	Fibre Optic Gyroscopes
DSP	Digital Signal Processing
CoG	Centre of Gravity
HPU	Hydraulic Power Unit
HSC	High Speed Controller
GXXL	Gangway XXL
AFC	Active Force Control